THÈSE

présentée pour obtenir le titre de

DOCTEUR DE L'ÉCOLE CENTRALE DE LYON

Spécialité : Dynamique des structures

par

Dimitrios CHRONOPOULOS

PREDICTION OF THE VIBROACOUSTIC RESPONSE OF AEROSPACE COMPOSITE STRUCTURES IN A BROADBAND FREQUENCY RANGE

Soutenue publiquement le 29 novembre 2012 devant le jury

MM.	P. LADEVEZE	Professeur, École Normale Supérieure de Cachan	Président
	F. GAUTIER	Professeur, Université du Maine	Rapporteur
	D. DUHAMEL	Professeur, École Nationale des Ponts et Chaussées	Rapporteur
	B. TROCLET	Senior expert, EADS Astrium / Professeur, ENS Cachan	Examinateur
	M. MASSENZIO	Professeur, Université Claude Bernard Lyon 1	Examinateur
	O. BAREILLE	Maître de conférences, École Centrale de Lyon	Examinateur
	M. ICHCHOU	Professeur, École Centrale de Lyon	Directeur de thèse

Liste des personnes Habilitées à Diriger des Recherches en poste à l'Ecole Centrale de Lyon

Nom-Prénom	Corps grade	Laboratoire ou à défaut département ECL	Etablissement
BEROUAL Abderrahmane	professeur	AMPERE	ECL
BURET François	professeur	AMPERE	ECL
JAFFREZIC-RENAULT Nicole	directeur de recherche	AMPERE	CNRS/ECL
KRÄHENBÜHL Laurent	directeur de recherche	AMPERE	CNRS/ECL
NICOLAS Alain	professeur	AMPERE	ECL
NICOLAS Laurent	directeur de recherche	AMPERE	CNRS/ECL
SCORLETTI Gérard	professeur	AMPERE	ECL
SIMONET Pascal	directeur de recherche	AMPERE	CNRS/ECL
VOLLAIRE Christian	professeur	AMPERE	ECL

Nbre Ampère 9

HELLOUIN Yves	maître de conférences	DER EEA	ECL

Nbre DER EEA 1

GUIRALDENQ Pierre	professeur émérite	DER STMS	ECL
VINCENT Léo	professeur	DER STMS	ECL

Nbre DER STMS 2

LOHEAC Jean-Pierre	maître de conférences	ICJ	ECL
MAITRE Jean-François	professeur émérite	ICJ	ECL
MARION Martine	professeur	ICJ	ECL
MIRONESCU Elisabeth	professeur	ICJ	ECL
MOUSSAOUI Mohand	professeur	ICJ	ECL
MUSY François	maître de conférences	ICJ	ECL
ZINE Abdel-Malek	maître de conférences	ICJ	ECL

Nbre ICJ 7

CALLARD Anne-Ségolène	professeur	INL	ECL
CLOAREC Jean-Pierre	maître de conférences	INL	ECL
GAFFIOT Frédéric	professeur	INL	ECL
GAGNAIRE Alain	maître de conférences	INL	ECL
GARRIGUES Michel	directeur de recherche	INL	CNRS/ECL
GENDRY Michel	directeur de recherche	INL	CNRS/ECL
GRENET Geneviève	directeur de recherche	INL	CNRS/ECL
HOLLINGER Guy	directeur de recherche	INL	CNRS/ECL
KRAWCZYK Stanislas	directeur de recherche	INL	CNRS/ECL
LETARTRE Xavier	chargé de recherche	INL	CNRS/ECL
O'CONNOR Ian	professeur	INL	ECL
PHANER-GOUTORBE Magali	professeur	INL	ECL
ROBACH Yves	professeur	INL	ECL
SAINT-GIRONS Guillaume	chargé de recherche	INL	CNRS/ECL
SEASSAL Christian	directeur de recherche	INL	CNRS/ECL

SOUTEYRAND Eliane	directeur de recherche	INL	CNRS/ECL
TARDY Jacques	directeur de recherche	INL	CNRS/ECL
VIKTOROVITCH Pierre	directeur de recherche	INL	CNRS/ECL

Nbre INL 18

CHEN Liming	professeur	LIRIS	ECL
DAVID Bertrand	professeur	LIRIS	ECL

Nbre LIRIS 2

BAILLY Christophe	professeur	LMFA	ECL
BERTOGLIO Jean-Pierre	directeur de recherche	LMFA	CNRS/ECL
BLANC-BENON Philippe	directeur de recherche	LMFA	CNRS/ECL
BOGEY Christophe	chargé de recherche	LMFA	CNRS/ECL
CAMBON Claude	directeur de recherche	LMFA	CNRS/ECL
CARRIERE Philippe	directeur de recherche	LMFA	CNRS/ECL
CHAMPOUSSIN J-Claude	professeur émérite	LMFA	ECL
COMTE-BELLOT genevièvre	professeur émérite	LMFA	ECL
FERRAND Pascal	directeur de recherche	LMFA	CNRS/ECL
GALLAND Marie-Annick	professeur	LMFA	ECL
GODEFERD Fabien	directeur de recherche	LMFA	CNRS/ECL
GOROKHOVSKI Mikhail	professeur	LMFA	ECL
HENRY Daniel	directeur de recherche	LMFA	CNRS/ECL
JEANDEL Denis	professeur	LMFA	ECL
JUVE Daniel	professeur	LMFA	ECL
LE RIBAULT Catherine	chargée de recherche	LMFA	CNRS/ECL
LEBOEUF Francis	professeur	LMFA	ECL
PERKINS Richard	professeur	LMFA	ECL
ROGER Michel	professeur	LMFA	ECL
SCOTT Julian	professeur	LMFA	ECL
SHAO Liang	directeur de recherche	LMFA	CNRS/ECL
SIMOENS Serge	chargé de recherche	LMFA	CNRS/ECL
TREBINJAC Isabelle	maître de conférences	LMFA	ECL

Nbre LMFA 23

BENAYOUN Stéphane	professeur	LTDS	ECL
CAMBOU Bernard	professeur	LTDS	ECL
COQUILLET Bernard	maître de conférences	LTDS	ECL
DANESCU Alexandre	maître de conférences	LTDS	ECL
FOUVRY Siegfrid	chargé de recherche	LTDS	CNRS/ECL
GEORGES Jean-Marie	professeur émérite	LTDS	ECL
GUERRET Chrystelle	chargé de recherche	LTDS	CNRS/ECL
HERTZ Dominique	past	LTDS	ECL
ICHCHOU Mohamed	professeur	LTDS	ECL
JEZEQUEL Louis	professeur	LTDS	ECL
JUVE Denyse	ingénieur de recherche	LTDS	ECL
KAPSA Philippe	directeur de recherche	LTDS	CNRS/ECL
LE BOT Alain	directeur de recherche	LTDS	CNRS/ECL
LOUBET Jean-Luc	directeur de recherche	LTDS	CNRS/ECL
MARTIN Jean-Michel	professeur	LTDS	ECL
MATHIA Thomas	directeur de recherche	LTDS	CNRS/ECL
MAZUYER Denis	professeur	LTDS	ECL
PERRET-LIAUDET Joël	maître de conférences	LTDS	ECL
SALVIA Michelle	maître de conférences	LTDS	ECL
SIDOROFF François	professeur	LTDS	ECL
SINOU Jean-Jacques	professeur	LTDS	ECL
STREMSDOERFER Guy	professeur	LTDS	ECL

THOUVEREZ Fabrice	professeur	LTDS	ECL
TREHEUX Daniel	professeur	LTDS	ECL
VINCENS Eric	maître de conférences	LTDS	ECL

Nbre LTDS 25	
Total HdR ECL	91

Acknowledgments

I would firstly like to express my sincere gratefulness to my supervisors Prof. Bernard Troclet and Prof. Mohamed Ichchou. It is thanks to them that I spent three particularly constructive as well as enjoyable years completing this work. Our productive discussions and their guidances at a professional as well as at a personal level will always be in my mind.

A particular acknowledgement has to be made to all of my colleagues at EADS Astrium and the Ecole Centrale de Lyon, for the particularly useful discussions and the pleasant moments we spent together during all these years.

Last but not least, I would like to express my thankfulness to my parents and all of my friends, who stood by me throughout these years, throughout all the bad and the good times.

Preface - Industrial context

Launch vehicles are subject to a variety of aeroacoustic excitations, especially during lift-off and the first stages of their mission. These solicitations can particularly endanger parts that have their fist resonance modes within the excitation frequency bands, with the most important of them being the electronic equipment of the spacecraft and the payload. In order for the success of the mission not to be endangered, accurate and time efficient models for the vibroacoustic behaviour prediction of the spacecraft structures have to be available for a broadband frequency range.

This work was conducted in cooperation with EADS Astrium Space Transportation. EADS Astrium, responsible for a variety of parts integrated on the Ariane 5 launch vehicle has conducted a series of research projects on the vibroacoustic of aerospace structures since many years. In [Hiverniau, 2006], an SEA-like approach for the prediction of the dynamic behaviour of an ensemble of structures subject to realistic aerodynamic loads was proposed. Extending this work, in [de Rochambeau, 2010] the SEA-like approach was extended to coupled structural-acoustic systems based on analytic expressions of their modal data.

The methods typically used within EADS Astrium for the research, design and homologation of spacecraft structures and the payload are principally conventional deterministic methods for the low frequency range. For the prediction in the high frequency domain, an SEA software named SEALASCAR was recently developped in the Mureaux site. This software actually includes classical analytical models for the description of the energy characteristics of composite structures, which cannot always reflect with accuracy their vibrational behaviour. The work included in this thesis, is entirely oriented towards extending the SEALASCAR software or being implemented in a new mid-frequency software of EADS Astrium.

Part of the work presented in this thesis can be found in relevant publications. The reader is prompted to:

- The peer reviewed publications: [Chronopoulos et al., 2012f], [Chronopoulos et al., 2012e] and [Chronopoulos et al., 2012d]

- The international conference proceedings: [Chronopoulos et al., 2012a], [Chronopoulos et al., 2012c], [Chronopoulos et al., 2011b] and [Chronopoulos et al., 2012b]

- The national conference proceedings: [Chronopoulos et al., 2011a].

Abstract

During its mission, a launch vehicle is subject to broadband, severe, aeroacoustic and structure-borne excitations of various provenances, which can endanger the survivability of the payload and the vehicles electronic equipment, and consequently the success of the mission. Aerospace structures are generally characterized by the use of exotic composite materials of various configurations and thicknesses, as well as by their extensively complex geometries and connections between different subsystems. It is therefore of crucial importance for the modern aerospace industry, the development of analytical and numerical tools that can accurately predict the vibroacoustic response of large, composite structures of various geometries and subject to a combination of aeroacoustic excitations.

Recently, a lot of research has been conducted on the modelling of wave propagation characteristics within composite structures. In this study, the Wave Finite Element Method (WFEM) is used in order to predict the wave dispersion characteristics within orthotropic composite structures of various geometries, namely flat panels, singly curved panels, doubly curved panels and cylindrical shells. These characteristics are initially used for predicting the modal density and the coupling loss factor of the structures connected to the acoustic medium. Subsequently the broadband Transmission Loss (TL) of the modelled structures within a Statistical Energy Analysis (SEA) wave-context approach is calculated.

Mainly due to the extensive geometric complexity of structures, the use of Finite Element (FE) modelling within the aerospace industry is frequently inevitable. The use of such models is limited mainly because of the large computation time demanded even for calculations in the low frequency range. During the last years, a lot of researchers focus on the model reduction of large FE models, in order to make their application feasible. In this study, the Second Order ARnoldi (SOAR) reduction approach is adopted, in order to minimize the computation time for a fully coupled composite structural-acoustic system, while at the same time retaining a satisfactory accuracy of the prediction in a broadband sense. The system is modelled under various aeroacoustic excitations, namely a diffused acoustic field and a Turbulent Boundary Layer (TBL) excitation.

Experimental validation of the developed tools is conducted on a set of orthotropic sandwich composite structures. Initially, the wave propagation characteristics of a flat panel are measured and the experimental results are compared to the WFEM predictions. The later are used in order to formulate an Equivalent Single Layer (ESL) approach for the modelling of the spatial response of the panel within a dynamic stiffness matrix approach. The effect of the temperature of the structure as well as of the acoustic medium on the vibroacoustic response of the system is examined and analyzed. Subsequently, a model of the SYLDA structure, also made of an orthotropic sandwich material, is tested mainly in order to investigate the coupling nature between its various subsystems. The developed ESL modelling is used for an efficient calculation of the response of the structure in the lower frequency range, while for higher frequencies a hybrid WFEM/FEM formulation for modelling discontinuous structures is used.

Resumé

Pendant sa mission, un lanceur est soumis à des excitations large bande, sévères, aérodynamiques, de provenances diverses, qui peuvent mettre en danger la survivabilité de la charge utile et de l'équipement électronique du véhicule, et par conséquent le succès de la mission. Les structures aérospatiales sont généralement caractérisées par l'utilisation de matériaux composites exotiques des configurations et des épaisseurs variantes, ainsi que par leurs géométries largement complexes. Il est donc d'une importance cruciale pour l'industrie aérospatiale moderne, le développement d'outils analytiques et numériques qui peuvent prédire avec précision la réponse vibroacoustique des structures larges, composites de différentes géométries et soumis à une combinaison des excitations aéroacoustiques.

Récemment, un grand nombre de recherches ont été menées sur la modélisation des caractéristiques de propagation des ondes au sein des structures composites. Dans cette étude, la méthode des éléments finis ondulatoires (WFEM) est utilisée afin de prédire les caractéristiques de dispersion des ondes dans des structures composites orthotropes de géométries variables, nommément des plaques plates, des panneaux simplement courbés, des panneaux doublement courbés et des coques cylindriques. Ces caractéristiques sont initialement utilisées pour prédire la densité modale et le facteur de perte par couplage des structures connectées au milieu acoustique. Par la suite, la perte de transmission (TL) à large bande des structures modélisées dans le cadre dune analyse statistique énergétique (SEA) dans un contexte ondulatoire est calculée.

Principalement en raison de la complexité géométrique importante de structures, l'utilisation des éléments finis (FE) au sein de l'industrie aérospatiale est souvent inévitable. L'utilisation de ces modèles est limitée principalement à cause du temps de calcul exigé, même pour les calculs dans la bande basses fréquences. Au cours des dernières années, beaucoup de chercheurs travaillent sur la réduction de modèles FE, afin de rendre leur application possible pour des systèmes larges. Dans cette étude, lapproche de SOAR est adoptée, afin de minimiser le temps de calcul pour un système couplé de type structurel-acoustique, tout en conservant une précision satisfaisante de la prédiction dans un sens large bande. Le système est modélisé sous diverses excitations aéroacoustiques, nommément un champ acoustique diffus et une couche limite turbulente (TBL).

La validation expérimentale des outils développés est réalisée sur un ensemble de structures sandwich composites orthotropes. Ces derniers sont utilisés afin de formuler une approche couche équivalente unique (ESL) pour la modélisation de la réponse spatiale du panneau dans le contexte dune approche de matrice de raideur dynamique. L'effet de la température de la structure ainsi que du milieu acoustique sur la réponse du système vibroacoustique est examiné et analysé. Par la suite, un modèle de la structure SYLDA, également fait d'un matériau sandwich orthotrope, est testé principalement dans le but d'enquêter sur la nature de couplage entre ses divers sous-systèmes. La modélisation ESL précédemment développée est utilisé pour un calcul efficace de la réponse de la structure dans la gamme des basses et moyennes fréquences, tandis que pour des fréquences plus élevées, une hybridisation WFEM / FEM pour la modélisation des structures discontinues est utilisé.

Contents

List of Figures

List of Tables

Introduction

Scientific context

The research conducted in this work was aimed to extend the precedent work developed by the researchers of EADS Astrium and can be related to three main axes:

i) The peculiarities of composite structures and shell geometries: The vast majority of parts used on the Ariane 5 spacecraft are made of thick composite materials and have a great variety of geometries ranging from flat panels to curved, cylindrical and conical shells. Consequently, analytical modal and wave dispersion data are rarely available for such complicated structures, which makes the use of costly FE modelling inevitable. Therefore, efficient models that can take into account for the complex modelling of these materials and geometries are needed.

ii) A broadband frequency range modelling: In the low frequency range an FE modelling is typically used in order to model the dynamic behaviour of the structure. However as frequency increases, this approach quickly becomes extensively costly in terms of time and computational effort, especially for large aerospace structures. The application of FE modelling is also limited by pollution errors which also increase very fast with respect to frequency. Efficient models are therefore needed for reducing the duration and the intensity of the calculations. On the other side, in the high frequency range, when the variability of the response diminishes and the modal overlap is high, the SEA is used for predicting the average. However accurate modelling of composite structures having various geometries using the SEA is still under question and has to be examined. There is a category of systems, for which the FE and the SEA applicability ranges do not overlap. These systems present what is called as a mid-frequency range. It is therefore necessary to satisfy the predictions in this range, either by creating new models, or by extending the already developed ones.

iii) The modelling of aeroacoustic excitations: As aforementioned, a large variety of aeroacoustic excitations is applied on the upper part of launch vehicles. These can include a diffused sound field, a TBL noise, or a jet noise field. These types of excitation have to be taken into account. The previous researchers of EADS Astrium proposed an approach for including these excitations within FE, SEA and SEA-like models by using their equivalent coherence functions.

Outline of the thesis

In the first chapter, the results of the conducted literature survey are presented. The survey concerns the presentation of the existing approaches on the calculation of modal and wave propagation data in composite structures and for various geometries, on the modelling of the vibroacoustic behaviour of systems in a broadband frequency range, on the modelling of aerodynamic excitations and other aspects that will be helpful for the rest of the thesis.

In the second chapter of the thesis, the application of the WFEM for the modelling of flat composite panels in a broadband frequency range is presented. The results are used as an input to an SEA model. The calculation of the modal density, the radiation efficiency and eventually the TL of the structures is exhibited. Moreover, experimental results are presented for the mechanical characteristics and the dynamic behaviour of a sandwich panel with respect to temperature. The impact of the temperature factor on the vibroacoustic behaviour of the structure is subsequently examined.

In the third chapter the WFEM results for a sandwich structure are used in order to update a classical plate theory, resulting in an ESL modelling of the sandwich structure, through a dynamic stiffness approach. The wave dispersion characteristics of the structure are experimentally measured using the IWC method and are compared to the WFEM results. The application of the presented method in a cylindrical sandwich shell is also presented.

In the fourth chapter, the WFEM is applied to composite structures of curved geometries, such as singly curved shells, doubly curved shells and cylindrical shells. In a similar manner as done in the second chapter, the TL of the structures under a diffused acoustic excitation is calculated in an SEA wave-context, and is compared to experimental results.

In the fifth chapter of the thesis the SOAR method is used in order to reduce a fully coupled structural acoustic system in the low and medium frequency range under a variety of aeroacoustic excitations. The system can be of arbitrary geometry and mechanical properties and a stiffened double panel structure is also modelled. The results in terms of time efficiency and accuracy of the reduced model are presented.

In the sixth chapter an industrial validation case is presented. A model of the SYLDA structure comprising two conical and one cylindrical part is presented. The structure is made of an orthotropic sandwich material. Experimental analysis is conducted on the composite shell using point excitation shakers. For the numerical modelling, the ESL approach introduced in the third chapter is used in the low frequency range. In the higher frequency domain, a WFEM/FEM approach is exhibited, with the WFEM calculated wave propagation characteristics of the substructures being coupled to a FE model of the connecting structure.

Finally in the seventh chapter the main conclusions of the presented work, as well as some ideas on possible prospective work are presented.

Chapter 1

Literature survey

1.1   Introduction

The modelling of the vibroacoustic behaviour of aerospace composite structures presents a variety of peculiarities. In the low frequency range classical deterministic approaches such as the Finite Element (FE) or the Boundary Element (BE) method are used for modelling the system. The main advantage of such methods is their ability to accurately predict the response of complex systems having arbitrary geometrical and/or mechanical characteristics. However at higher frequency ranges where the vibrational wavelength becomes smaller, deterministic methods become computationally unaffordable and their interpolation and pollution errors affect the accuracy of the solution. A first challenge is therefore the development of new approaches which will extend the applicability of deterministic techniques to higher frequencies while maintaining their advantages. This mainly involves the use of reduction methods to retain the computational effort to realistic levels. The modelling of wave propagation characteristics within these composite structures of various geometries can offer a key to decode their vibrational behaviour.

On the other hand, in the high frequency range Statistical Energy Analysis (SEA) is the method typically used. However, taking into account for the peculiar characteristics of layered structures and their geometries as well as for the correlated aeroacoustic excitations applied on a launch vehicle within SEA is not always straightforward. It is again shown that calculating the SEA subsystem characteristics within a wave context can provide an interesting approach for an accurate modelling of the system and for extending the SEA method towards lower frequencies.

Throughout the rest of this chapter the results of a bibliographic survey are exhibited. The survey is based on three main axes:

- The modelling of wave propagation in layered structures.

- The modelling of the vibroacoustic behaviour of a structural acoustic system at frequencies where FEM is inefficient.

- The aeroacoustic excitations applied on a launch vehicle.

1.2   Wave dispersion in composite structures

1.2.1   Introduction

In this section the most important approaches on modelling the wave propagation in laminated composite panels will be summarised. It should be noted that during the last century there has been a significant amount of conducted research on the topic. Various 'exact' and approximate approaches have been developped for modelling the wave dispersion characteristics in the low as well as in the higher frequency ranges, for homogeneous, as well as for stratified structures. Citing and presenting all of these techniques is a particularly intensive task and beyond of the scope of this work. The most important and widely used methods will therefore be summarised. In sec.1.2.2 analytical laminated plate theories are presented, followed by an also analytical thin layer approach. Subsequently, in sec.1.2.4 and 1.2.5 more recently developed semi-analytical and numerical techniques are reviewed.

1.2.2   Laminated plate theories

1.2.2.1   Introduction

Towards the end of the 19th century, the work of Kirchhoff and Love, concluded in developping an elementary theory for the prediction of the dynamic behaviour of an isotropic plate. This approach, similar to the Euler-Bernoulli hypotheses for beams is limited in terms of frequency applicability because of its assumptions and can solely predict the principal transverse and longitudinal displacements in the low frequency range.

In 1917, Lamb suggested an exact theory for isotropic plates based on the study conducted in 1887 by Lord Rayleigh on surface waves (see [Graff, 1991]). The author analyzed guided waves (P, SV and SH) in a doubly bounded structural medium, that is to say a plate. To build his theory, Lamb used elastodynamic equations by imposing on the width of the plate a plane strain assumption and a hypothesis on the stress field to take into account for the free surfaces of the plate. From the proposed theory, it is observed that there exists an infinite number of waves that can be distinguished according to the distribution of their displacement fields in the thickness direction of the plate. The author distinguishes between longitudinal and transverse waves which have a displacement field symmetrically and antisymmetrically parallel to the direction of propagation. Moreover, there are also shear waves whose displacement field is perpendicular to the direction of propagation. To reflect the fact that there are several waves of the same type, the notations S_n, A_n and SH_n are used which denote respectively the longitudinal, transverse and shear waves. It is also noted that there exist primary and secondary waves. They can be identified simply through the notation system with the principal waves corresponding to waves for which the parameter n is zero.

After 1950, the researchers again tried to develop approximate theories in order to analyze the propagation of waves in plates. To do this, the general approach of Mindlin based on an approximation of the displacement field in Taylor series was successfully applied to isotropic plates. A first-order theory proposed in [Mindlin, 1951] was used to characterize high frequency transverse waves. Similarly, the authors in [Mindlin and Medick, 1959] developed a second-order theory to study S_n wave propagation. Compared to the Classical Plate Theory (CPT), it is observed that for the A_0 wave, the asymptotic value of the phase velocity is now finite and that the dispersion of the S_0 wave is now taken into account. Finally, it is noted that both theories account for secondary waves and two correction coefficients are introduced so that the predictions asymptotically approach the experimental values.

With respect to plates consisting of a laminated composite material, the first suggested approaches were essentially extensions of previous theories. It is noted as an example the Classical Laminate Plate Theory (CLPT) in [Stavsky, 1961] which reconsiders the basic assumptions of the Kirchhoff-Love theory and the First order Shear Deformation theory (FSDT) by [Whitney and Pagano, 1970] which is an extension of the first-order theory proposed by [Mindlin, 1951] to study the transverse waves. For each of these approximate theories, the composite laminate is completely homogenized and that is the reason for which they are often referred to as Equivalent Single Layer (ESL) theories. In this class of theories, there is also the Effective Modulus Theory introduced in [Sun and Liao, 1990] and whose predictions were compared with the exact theory in [Sun et al., 1996].

During the last thirty years, significant improvements were made to approximate theories so that they can more accurately predict the dynamic response in the thickness sense of a panel, that is to say the field distribution of stress, strain and displacement. As a first example the theories based on a Reissner-Heillinger type formulation are cited, such as the theory of [Muller and
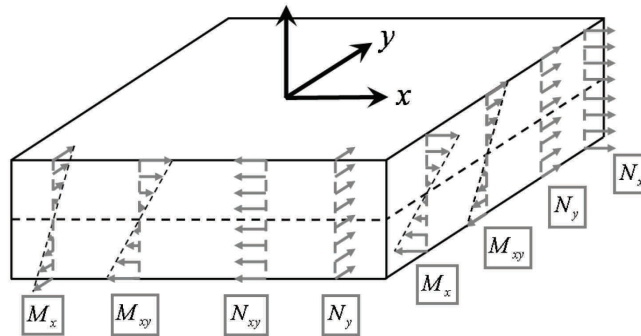
Figure 1.1: *Schematical representation of the considered forces and moments according to the CLPT*

Touratier, 1995]. These theories predict correctly the wave dispersion while avoiding the introduction of correction coefficients, as is the case for the FSDT. In addition, a second class of theories referred to as Layer-Wise (LW), eliminated the assumption of homogeneity and consider each layer independently [Reddy, 2004]. Unfortunately, these theories can, for certain stratifications, be very computationally intensive because the number of degrees of freedom needed, depends on the number of layers in contrast to ESL theories. To get an idea of the improvements introduced by these new theories, one can refer to the work exhibited in [Carrera, 2000], which shows that the global predictions (eigenmodes) as well as the local ones (field distribution of strain and stress in the thickness direction) are better predicted than by ESL theories such as the CLPT or FSDT. Finally, it is important to mention the exact theory developed by [Nayfeh, 1995] for layered structures, which generally adopts the same approach as Lamb, that is to say the reflection of waves in a medium bounded by several planes.

It is noted that each time, the appropriate theory has to be chosen in order to efficiently compromise between accuracy and computational effort.

1.2.2.2 The CLPT

The Classical Laminate Plate Theory (CLPT) presented in [Stavsky, 1961] is analogous to the Kirchhoff-Love theory, developed for isotropic plates, based on the assumptions used in conventional mechanics of materials, namely:

- The thickness h is small compared to the length and the width of the plate.

- The displacement along the thickness is assumed linear.

- The cross section perpendicular to the mid-plane of the plate remains perpendicular after deformation.

To account for these assumptions, the displacement field is formulated as follows:

$$u(x,y,z,t) = u_0(x,y,t) - z\frac{\vartheta w_0}{\vartheta x}$$

$$v(x,y,z,t) = v_0(x,y,t) - z\frac{\vartheta w_0}{\vartheta y} \tag{1.1}$$

$$w(x,y,z,t) = w_0(x,y,t)$$

with u_0,v_0,w_0 the displacements of the mid-plane of the plate.

From the above displacement field, the strain field can be deduced. The linear theory of elasticity is therefore used, resulting in:

$$
\left\{ \begin{array}{c} \epsilon_{xx} \\ \epsilon_{yy} \\ \epsilon_{zz} \\ \gamma_{xy} \\ \gamma_{xz} \\ \gamma_{yz} \end{array} \right\} = \left\{ \begin{array}{c} \frac{\vartheta u_0}{\vartheta x} + z\frac{\vartheta^2 w_0}{\vartheta x^2} \\ \frac{\vartheta v_0}{\vartheta y} + z\frac{\vartheta^2 w_0}{\vartheta y^2} \\ \frac{\vartheta w_0}{\vartheta z} \\ \frac{\vartheta u_0}{\vartheta y} + \frac{\vartheta v_0}{\vartheta x} - 2z\frac{\vartheta^2 w_0}{\vartheta x \vartheta y} \\ 2\epsilon_{xz} \\ 2\epsilon_{yz} \end{array} \right\} = \left\{ \begin{array}{c} \epsilon_{xx}^0 + z\kappa_x \\ \epsilon_{yy}^0 + z\kappa_y \\ 0 \\ \gamma_{xy}^0 + z\kappa_{xy} \\ 0 \\ 0 \end{array} \right\} \tag{1.2}
$$

with: ϵ_{xx}^0,ϵ_{yy}^0,γ_{xy}^0 the membrane deformations and $\kappa_x, \kappa_y, \kappa_{xy}$ standing for the curvatures. From the expressions of eq.(1.2), it is observed that the transverse shear strains γ_{xz}, γ_{yz} are neglected in the CLPT. Then the variational expressions of the kinetic and the potential energies of the plate are written as:

$$
\delta U = \int_v (\sigma_{xx}\delta\epsilon_{xx} + \sigma_{yy}\delta\epsilon_{yy} + \sigma_{xy}\delta\gamma_{xy})dv
$$
$$
\delta T = \int_v \rho(\dot{u}\delta\dot{u} + \dot{v}\delta\dot{v} + \dot{w}\delta\dot{w})dv \tag{1.3}
$$

By integrating in the sense of thickness the expressions (1.3), we obtain:

$$
\delta U = \int_s \left(\left(\frac{\vartheta N_{xx}}{\vartheta x} + \frac{\vartheta N_{xy}}{\vartheta y} \right)\delta u_0 + \left(\frac{\vartheta N_{xy}}{\vartheta x} + \frac{\vartheta N_{yy}}{\vartheta y} \right)\delta v_0 + \left(\frac{\vartheta^2 M_{xx}}{\vartheta x^2} + 2\frac{\vartheta^2 M_{xy}}{\vartheta x \vartheta y} + \frac{\vartheta^2 M_{yy}}{\vartheta y^2} \right)\delta w_0 \right) dS
$$

$$
\delta T = \int_s \rho_s(\ddot{u}_0\delta u_0 + \ddot{v}_0\delta v_0 + \ddot{w}_0\delta w_0)dS
$$
$$\tag{1.4}$$

with: N_{ij} the resulting membrane forces, M_{ij} the bending moments and ρ_s the surface density defined as:

$$
\left\{ \begin{array}{c} N_{xx} \\ N_{yy} \\ N_{xy} \end{array} \right\} = \sum_{k=1}^{n} \int_{h_{k-1}}^{h_k} \left\{ \begin{array}{c} \sigma_{xx} \\ \sigma_{yy} \\ \sigma_{xy} \end{array} \right\}_k dz, \left\{ \begin{array}{c} M_{xx} \\ M_{yy} \\ M_{xy} \end{array} \right\} = \sum_{k=1}^{n} \int_{h_{k-1}}^{h_k} \left\{ \begin{array}{c} \sigma_{xx} \\ \sigma_{yy} \\ \sigma_{xy} \end{array} \right\}_k zdz
$$
$$
\rho_s = \sum_{k=1}^{n} \int_{h_{k-1}}^{h_k} \rho_k dz \tag{1.5}
$$

where: h is the total thickness of the plate and n the total number of layers of a stratified structure (see fig.1.2). From the energy expressions (1.4), the equations of motion of the plate are determined via the Hamiltons principle. In the absence of external forces, these equations are expressed as:
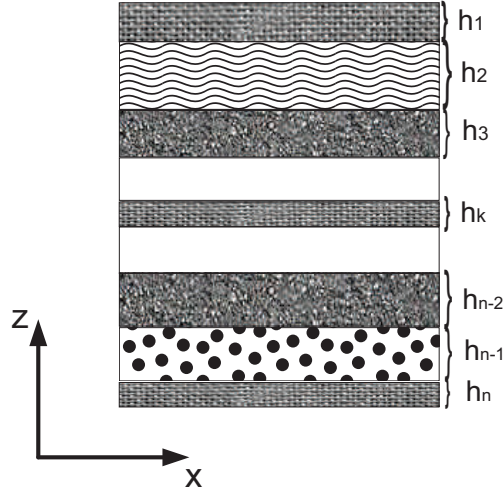
Figure 1.2: *Layer stacking within a stratified panel*

$$\delta u_0 : \frac{\vartheta N_{xx}}{\vartheta x} + \frac{\vartheta N_{xy}}{\vartheta y} = \rho_s \frac{\vartheta^2 u_0}{\vartheta t^2},$$

$$\delta v_0 : \frac{\vartheta N_{xy}}{\vartheta x} + \frac{\vartheta N_{yy}}{\vartheta y} = \rho_s \frac{\vartheta^2 v_0}{\vartheta t^2}, \tag{1.6}$$

$$\delta w_0 : \frac{\vartheta^2 M_{xx}}{\vartheta x^2} + 2\frac{\vartheta^2 M_{xy}}{\vartheta x \vartheta y} + \frac{\vartheta^2 M_{yy}}{\vartheta y^2} = \rho_s \frac{\vartheta^2 w_0}{\vartheta t^2}$$

The equations (1.6) depend on the forces N_{ij} and the moments M_{ij}. However, performing a dispersion analysis based on these equations means that they have to be expressed only in terms of the displacements u_0,v_0,w_0. For this reason, the expression of the forces and the moments as a function of the panel's displacements have to be introduced into eq.(1.5). Beginning with the laminar stress-strain relations:

$$\left\{ \begin{array}{c} \sigma_{xx} \\ \sigma_{yy} \\ \sigma_{xy} \end{array} \right\}_k = \left[\begin{array}{ccc} Q_{11} & Q_{12} & Q_{16} \\ Q_{12} & Q_{22} & Q_{26} \\ Q_{16} & Q_{26} & Q_{66} \end{array} \right] \left\{ \begin{array}{c} \epsilon_{xx} \\ \epsilon_{yy} \\ \gamma_{xy} \end{array} \right\} \tag{1.7}$$

and introducing eq.(1.7) into eq.(1.5) we get the desired expressions of the forces and moments as a function of the displacements and the so called **ABD** matrix written as:

$$\left\{ \begin{array}{c} N_{xx} \\ N_{yy} \\ N_{xy} \end{array} \right\} = \left[\begin{array}{ccc} A_{11} & A_{12} & A_{16} \\ A_{12} & A_{22} & A_{26} \\ A_{16} & A_{26} & A_{66} \end{array} \right] \left\{ \begin{array}{c} \epsilon_{xx}^0 \\ \epsilon_{yy}^0 \\ \gamma_{xy}^0 \end{array} \right\} + \left[\begin{array}{ccc} B_{11} & B_{12} & B_{16} \\ B_{12} & B_{22} & B_{26} \\ B_{16} & B_{26} & B_{66} \end{array} \right] \left\{ \begin{array}{c} \kappa_{xx} \\ \kappa_{yy} \\ \kappa_{xy} \end{array} \right\}$$

$$\left\{ \begin{array}{c} M_{xx} \\ M_{yy} \\ M_{xy} \end{array} \right\} = \left[\begin{array}{ccc} D_{11} & D_{12} & D_{16} \\ D_{12} & D_{22} & D_{26} \\ D_{16} & D_{26} & D_{66} \end{array} \right] \left\{ \begin{array}{c} \kappa_{xx} \\ \kappa_{yy} \\ \kappa_{xy} \end{array} \right\} \tag{1.8}$$

with **A** the membrane stiffness matrix, **B** the flexural/membrane coupling matrix and **D** the flexural stiffness matrix. The stiffness coefficients contained in the **A**, **B**, **D** matrices are related to

the stress-strain coefficients of eq.(1.7) through the relations:

$$
\begin{aligned}
A_{ij} &= \sum_{k=1}^{n} (h_k - h_{k-1})(Q_{ij})_k \\
B_{ij} &= \frac{1}{2} \sum_{k=1}^{n} (h_k^2 - h_{k-1}^2)(Q_{ij})_k \\
D_{ij} &= \frac{1}{3} \sum_{k=1}^{n} (h_k^3 - h_{k-1}^3)(Q_{ij})_k
\end{aligned}
\tag{1.9}
$$

It is now possible to study the scattering of waves by assuming the displacement field as a harmonic plane wave as follows:

$$
\left\{ \begin{array}{c} u_0 \\ v_0 \\ w_0 \end{array} \right\} = \left\{ \begin{array}{c} U \\ V \\ W \end{array} \right\} e^{ik(cos(\theta)+sin(\theta))\vec{r}} e^{-i\omega t}
\tag{1.10}
$$

By introducing the expression (1.10) in the equations of motion, a third order system is deduced whose determinant is equal to:

$$
\begin{vmatrix}
\alpha_1 k^2 + \alpha_2 & \alpha_3 k^2 & \alpha_4 k^3 \\
\alpha_3 k^2 & \alpha_5 k^2 + \alpha_2 & \alpha_6 k^3 \\
\alpha_4 k^3 & \alpha_6 k^3 & \alpha_7 k^4 - \alpha_2
\end{vmatrix} = 0
\tag{1.11}
$$

Finally, we calculate the characteristic polynomial of the determinant to obtain the desired dispersion relation. This relationship is expressed as:

$$
\begin{aligned}
&(\alpha_1\alpha_5\alpha_7 - \alpha_1\alpha_6^2 - \alpha_3^2\alpha_7 + 2\alpha_3\alpha_4\alpha_6 - \alpha_4^2\alpha_5)k^8 \\
&+(\alpha_2\alpha_5\alpha_7 + \alpha_1\alpha_2\alpha_7 - \alpha_2\alpha_6^2 - \alpha_4^2\alpha_2)k^6 \\
&+(\alpha_2^2\alpha_7 + \alpha_3^2\alpha_2 - \alpha_1\alpha_5\alpha_2)k^4 - (\alpha_5\alpha_2^2 + \alpha_1\alpha_2^2)k^2 - \alpha_2^3 = 0
\end{aligned}
\tag{1.12}
$$

with

$$
\alpha_1 = A_{11}(icos\theta)^2 + 2A_{16}(icos\theta)(isin\theta) + A_{66}(isin\theta)^2
$$

$$
\alpha_2 = -\rho_s(-i\omega)^2
$$

$$
\alpha_3 = A_{16}(icos\theta)^2 + (A_{12} + A_{66})(icos\theta)(isin\theta) + A_{26}(isin\theta)^2
$$

$$
\alpha_4 = -B_{11}(icos\theta)^3 - 3B_{16}(icos\theta)^2(isin\theta) - (B_{12} + 2B_{66})(icos\theta)(isin\theta)^2 - B_{26}(isin\theta)^3
$$

$$
\alpha_5 = A_{66}(icos\theta)^2 + 2A_{26}(icos\theta)(isin\theta) + A_{22}(isin\theta)^2
$$

$$
\alpha_6 = -B_{16}(icos\theta)^3 - 3B_{26}(icos\theta)(isin\theta)^2 - (B_{12} + 2B_{66})(icos\theta)^2(isin\theta) - B_{22}(isin\theta)^3
$$

$$
\begin{aligned}
\alpha_7 =\ & D_{11}(icos\theta)^4 + 4D_{16}(icos\theta)^3(isin\theta) \\
&+ 2(D_{12} + 2D_{66})(icos\theta)^2(isin\theta)^2 + 4D_{26}(icos\theta)(isin\theta)^3 + D_{22}(isin\theta)^4
\end{aligned}
$$

$$
\tag{1.13}
$$

The solutions of the relation (1.13) are eight in number and correspond to wavenumbers k_i associated with the principal waves S_0, A_0, SH_0 and the secondary wave A_1. In general, the

expressions of wavenumbers are complex because they reflect a variety of coupling effects existing within a laminated composite plate. However, as an illustration example we consider a laminated plate whose stacking sequence is symmetrical about the mid-plane of the plate, which will let us ignore the flexural/membrane coupling effect. Moreover for the S_n and SH_n waves, the expression of wavenumbers can become complicated depending on the direction of propagation. Indeed, according to [Prosser and Gorman, 1994], for S_n waves, the displacement field is purely longitudinal when the wave propagates along the axes of orthotropy of the material while in other directions the displacement field is quasi-longitudinal, that is to say mainly longitudinal with a transverse component. For SH_n waves, the properties are identical, except this time the displacement field is purely transverse to the axes of orthotropy and quasi-transverse everywhere else. Considering that 0° is the axis of orthotropy of the material, then the wavenumbers associated with the different waves S_0, A_0, SH_0 in this direction are expressed as follows:

$$c_1 = \sqrt{\frac{A_{11}}{\rho_s}}$$

$$c_2 = \sqrt{\frac{A_{22}}{\rho_s}}$$

$$c_3 = \sqrt{\sqrt{\frac{D_{11}}{\rho_s}}\omega}$$

(1.14)

1.2.2.3   FSDT

The CLPT theory is mainly used for the prediction of wave dispersion characteristics of thin plates and within the low frequency range. Another theory has to be utilized when someone needs to characterize the principal and secondary waves at higher frequencies. For this reason the FSDT proposed in [Whitney and Pagano, 1970] can be used, that reviews the assumption of the CLPT taking account of deformations associated with transverse shear and the rotational inertia of the cross section. Because of the new assumptions, the displacement field must be reformulated as follows:

$$u(x, y, z, t) = u_0(x, y, t) + z\phi_x(x, y, t)$$

$$v(x, y, z, t) = v_0(x, y, t) + z\phi_y(x, y, t)$$

(1.15)

$$w(x, y, z, t) = w_0(x, y, t)$$

As it can be seen, the displacement field now depends on five degrees of freedom. The two new degrees of freedom ϕ_x, ϕ_y correspond to the rotations along the axes O_x and O_y. From the displacement field in (1.15) and using linear elasticity theory, the new strain field of the plate is

calculated as follows:

$$
\left\{
\begin{array}{c}
\epsilon_{xx} \\
\epsilon_{yy} \\
\epsilon_{zz} \\
\gamma_{xy} \\
\gamma_{xz} \\
\gamma_{yz}
\end{array}
\right\}
=
\left\{
\begin{array}{c}
\frac{\vartheta u_0}{\vartheta x} + z\frac{\vartheta \phi_x}{\vartheta x} \\
\frac{\vartheta v_0}{\vartheta y} + z\frac{\vartheta \phi_y}{\vartheta y} \\
\frac{\vartheta w_0}{\vartheta z} \\
\frac{\vartheta u_0}{\vartheta y} + \frac{\vartheta v_0}{\vartheta x} + z(\frac{\vartheta \phi_x}{\vartheta y} + \frac{\vartheta \phi_y}{\vartheta x}) \\
\frac{\vartheta w_0}{\vartheta x} + \phi_x \\
\frac{\vartheta w_0}{\vartheta y} + \phi_y
\end{array}
\right\}
=
\left\{
\begin{array}{c}
\epsilon_{xx}^0 + z\kappa_x \\
\epsilon_{yy}^0 + z\kappa_y \\
0 \\
\gamma_{xy}^0 + z\kappa_{xy} \\
\frac{\vartheta w_0}{\vartheta x} + \phi_x \\
\frac{\vartheta w_0}{\vartheta y} + \phi_y
\end{array}
\right\}
\tag{1.16}
$$

From eq.(1.16), it is observed that, now strains γ_{xz}, γ_{yz} related to transverse shear deformation are taken into account by the FSDT. Subsequently, we can calculate the variational expressions of the kinetic and the potential energies as follows:

$$
\delta U = \int_v \left(\sigma_{xx}\delta\epsilon_{xx} + \sigma_{yy}\delta\epsilon_{yy} + \sigma_{xy}\delta\gamma_{xy} + \sigma_{yz}\delta\gamma_{yz} + \sigma_{xz}\delta\gamma_{xz} \right) dv
$$

$$
\delta T = \int_v \rho(\dot{u}\delta\dot{u} + \dot{v}\delta\dot{v} + \dot{w}\delta\dot{w})dv
\tag{1.17}
$$

and by integrating in the sense of thickness we have:

$$
\delta U = \int_s \left(\left(\frac{\vartheta N_{xx}}{\vartheta x} + \frac{\vartheta N_{xy}}{\vartheta y} \right) \delta u_0 + \left(\frac{\vartheta N_{xy}}{\vartheta x} + \frac{\vartheta N_{yy}}{\vartheta y} \right) \delta v_0 + \left(\frac{\vartheta Q_x}{\vartheta x} + \frac{\vartheta Q_y}{\vartheta y} \right) \delta w_0 \right.
$$

$$
\left. + \left(\frac{\vartheta M_{xx}}{\vartheta x} + \frac{\vartheta M_{xy}}{\vartheta x} - Q_x \right) \delta\phi_x + \left(\frac{\vartheta M_{xy}}{\vartheta x} + \frac{\vartheta M_{yy}}{\vartheta y} - Q_y \right) \delta\phi_y dS \right.
\tag{1.18}
$$

$$
\delta T = \int_s ((\rho_s\ddot{u}_0 + J_1\ddot{\phi}_x)\delta u_0 + (\rho_s\ddot{v}_0 + J_1\ddot{\phi}_y)\delta v_0
$$
$$
+ (J_1\ddot{u}_0 + J_2\ddot{\phi}_x)\delta\phi_x + (J_1\ddot{v}_0 + J_2\ddot{\phi}_y)\delta\phi_y + \rho_s\ddot{w}_0\delta w_0)dS
$$

with: Q_x, Q_y the forces associated to shear deformations and J_1, J_2 the first and second moments of inertia respectively defined as:

$$
\left\{
\begin{array}{c}
Q_x \\
Q_y
\end{array}
\right\}
= \sum_{k=1}^n \int_{h_{k-1}}^{h_k}
\left\{
\begin{array}{c}
\sigma_{xz} \\
\sigma_{yz}
\end{array}
\right\}_k
dz
$$

$$
\left\{
\begin{array}{c}
J_1 \\
J_2
\end{array}
\right\}
= \sum_{k=1}^n \int_{h_{k-1}}^{h_k}
\left\{
\begin{array}{c}
z \\
z^2
\end{array}
\right\} \rho_k dz
\tag{1.19}
$$

To determine the equations of motion, the Hamiltons principle is applied. In the absence of

external forces, eq.(1.19) takes the following form:

$$\delta u_0 : \frac{\vartheta N_{xx}}{\vartheta x} + \frac{\vartheta N_{xy}}{\vartheta y} = \rho_s \ddot{u}_0 + J_1 \ddot{\phi}_x,$$

$$\delta v_0 : \frac{\vartheta N_{xy}}{\vartheta x} + \frac{\vartheta N_{yy}}{\vartheta y} = \rho_s \ddot{v}_0 + J_1 \ddot{\phi}_y,$$

$$\delta w_0 : \frac{\vartheta Q_x}{\vartheta x} + \frac{\vartheta Q_y}{\vartheta y} = \rho_s \ddot{w}_0, \tag{1.20}$$

$$\delta \phi_x : \frac{\vartheta M_{xx}}{\vartheta x} + \frac{\vartheta M_{xy}}{\vartheta y} - Q_x = J_1 \ddot{u}_0 + J_2 \ddot{\phi}_x,$$

$$\delta \phi_y : \frac{\vartheta M_{yy}}{\vartheta y} + \frac{\vartheta M_{xy}}{\vartheta x} - Q_y = J_1 \ddot{v}_0 + J_2 \ddot{\phi}_y$$

The solution of the system is very similar to the one of the CLPT case, the major difference being that this time the system leads to a fifth order determinant, resulting in a solution set of S_0, A_0, SH_0 waves as with the CLPT, plus two secondary waves A_1, SH_1. The analytical expression of the plate wavenumbers involves a large algebraic effort and the presentation of the system's solution is outside the scope of this thesis.

1.2.2.4   Higher order theories

When a thick layered panel, with its layers having significantly different mechanical characteristics is to be modelled, FSDT may result in erroneous predictions, especially in the higher frequency range. Sandwich panels comprising stiff facesheets and a softer compressible core is a typical example. For these cases, Higher Shear Order Deformation (HSDT) theories were developed by adding higher order terms to account for the shear deformation within the panel. Description and application of such HSDT approaches can be found in [Reddy, 1997, Meunier and Shenoi, 2001].

In [Frostig and Thomsen, 2004], the Higher-Order Sandwich Panel Theory (HSAPT) was derived to model the behaviour of sandwich plates with a flexible core based on the assumption of a nonlinear through-the-thickness displacement field of the core in both longitudinal and vertical directions. The corresponding acceleration field in the core is however assumed to vary linearly with height, a fact that introduces inconsistency in the formulation. To overcome this disadvantage, in [Sokolinsky and Nutt, 2004, Wang et al., 2008] a consistent higher-order theory was proposed for modelling the free vibration of beams and plates having a compressible core. This approach was also used in [Wang et al., 2010] to model the vibroacoustic behaviour of flat plates in an SEA approach.

1.2.2.5   Shell structures

A summary of the general form of the strain displacement equations, the stress strain equations and the equations of motion for layered shell structures is given in [Leissa, 1969, Soedel, 1993, Qatu, 2004]. The analogous of both the Kirchhoff-Love and the Mindlin type theories (usually named after Donnell-Mushtari and Flügge respectively) are presented.

In their general form the strain displacement relations contain shape dependent coefficients, also referred as the Lamé coefficients. The general fundamental form of a shell of revolution is

written as in [Qatu, 2004]:

$$(ds)^2 = (R_a d\phi)^2 + sin^2(\phi)(R_b d\theta) \tag{1.21}$$

with R_a and R_b the curvatures of the shell in the directions ϕ and *theta* respectively. The Lamé coefficients as well as the specific fundamental forms for various shell geometries are also given in [Soedel, 1993, Qatu, 2004].

The extraction of the wave propagation characteristics of shell structures from their equations of motion is analogous to the process followed for the flat panels, however forming the wavenumber determinant and solving for the possible wavenumbers propagating within the shell is usually a much more complicated process. Rationally accurate approximations of the Flügge equations of motion for cylindrical shells have been given in [Karczub, 2006]. Other works that have studied the problem of wave propagation in composite cylindrical shells using the exact threedimensional elasticity theory include [Armenakas, 1970, Markus and Mead, 1995, Yuan and Hsieh, 1998], however wave propagation in layered shells of arbitrary geometries is still a subject of intensive research.

1.2.3   Discrete laminate approach

Introduced in [Lysmer, 1970] and usually referred to as the Thin Layered Method (TLM) this approach involves the discretization of the panel in the sense of lamination. The motion within each sublayer is assumed to be in the form of harmonic wave propagation. The interlaminar equilibrium is preserved by applying appropriate conditions to each layer. A variational approach is then generally used to derive the governing equations of the cross section.

In [Ghinet and Atalla, 2006, Ghinet et al., 2005] the authors introduced a discrete laminate method for the prediction of wave propagation characteristics in flat and singly curved panels. The core of a sandwich panel as well as the layers of a stratified structure are considered to be homogeneous and are modelled using a Mindlin type theory. The facesheets of sandwich structures are considered to be thin and vibrating in a bending motion; therefore a Kirchhoff-Love theory was used for describing their displacement fields. The interlayer stress continuity relations are then applied to acquire the dynamic equilibrium relations along each direction of propagation. Assuming time harmonic wave propagation within the laminate eventually results in a fourth order polynomial eigenvalue problem, which can either be solved by linearization or numerical manipulation. In [Ghinet and Atalla, 2011] the same authors developed a similar model of equations to account for the symmetric vibrational motion of the core within a sandwich panel.

1.2.4   The SAFE method

The Semi-Analytical Finite Element (SAFE) method first appeared in [Dong and Nelson, 1972] and [Shah and Datta, 1982] under the name 'Ritz extended technique' or 'Infinite Layer method'. These relationships have since then been used for the calculation of modes in multilayer plates, in particular in [Liu et al., 1991]. Then a method derived by the 'Strip Element method' was developed in [Liu and Achenbach, 1994] and was also applied to the case of laminate structures. This method was then renamed to SAFE and has been studied for applications on various structures.

In the SAFE approach, the displacement field is formulated following a decomposition into plane waves (sinusoidal interpolation functions) in the direction of propagation, and using finite elements (piecewise polynomial interpolation functions) in the directions perpendicular to propagation one. Therefore, it can approximate the exact field where the wavelengths are small without having to use a large amount of elements.

More precisely if a semi-analytical element i is considered, for which the displacement at a point P is:

$$u_i(x, y, z, t) = \mathbf{N}(y, z)\mathbf{q_i}(t)e^{i(kx - \omega t)} \tag{1.22}$$

with N the polynomial interpolation functions matrix, q_i the vector of nodal displacements associated with the element i and k is the wavenumber. Then one proceeds as with the FEM, that is to say the elastodynamic equations will be transformed in a matrix system. If the external forces applied to the system are ignored, the obtained system matrix is as follows:

$$\left(\mathbf{K}_1 - ik\mathbf{K}_2 + k^2\mathbf{K}_3 - \omega^2\mathbf{M}\right)\mathbf{U} = 0 \tag{1.23}$$

where $\mathbf{K}_1,\mathbf{K}_2,\mathbf{K}_3$ and $\mathbf{M}$ are respectively the global stiffness and mass matrices. The vector $\mathbf{U}$ stands for the displacement of the ensemble of the mesh. Generally, the system is transformed as follows:

$$(\mathbf{A} - k\mathbf{B})\{\mathbf{Q}\} = 0 \tag{1.24}$$

with:

$$\mathbf{A} = \begin{bmatrix} \mathbf{0} & \mathbf{K}_1 - \omega^2\mathbf{M} \\ \mathbf{K}_1 - \omega^2\mathbf{M} & -i\mathbf{K}_2 \end{bmatrix}, \mathbf{B} = \begin{bmatrix} \mathbf{K}_1 - \omega^2\mathbf{M} & \mathbf{0} \\ \mathbf{0} & -\mathbf{K}_3 \end{bmatrix}, \{\mathbf{Q}\} = \begin{bmatrix} \mathbf{U} \\ k\mathbf{U} \end{bmatrix} \tag{1.25}$$

The above system can be solved using simple numerical methods since it is an eigenvalue problem. The solutions of this system allow for the determination of phase velocities (eigenvalues) and deformations (eigenvectors) of the different waves that can propagate in the x direction. The number of these waves depends directly on the number of elements used for meshing the system. The numerical model can therefore be adapted, based on the expected number of waves propagating in the structure for the studied frequency bands.

1.2.5 The 2D WFEM method

As aforementioned, in the SAFE method, the displacement field is formulated using sinusoidal functions in the direction of propagation. Furthermore it is necessary to develop semi-analytical elements, which greatly limits its use. A numerical method will be presented hereby, the Wave Finite Element Method (WFEM) which attempts to overcome these limitations by combining the Periodic Structural Theory (PST) introduced in [Mead, 1973] to the FEM.

1.2.5.1 Formulation of the problem

A rectangular composite panel is considered hereby (see fig.1.3) with L_x, L_y its dimensions and h its thickness. A periodic segment of the panel with dimensions dx and dy (see fig.1.4) is modelled using FE.

Initially, the mass and stiffness matrices of the segment $\mathbf{M}$ and $\mathbf{K}$ are extracted using classical FEM algorithms. The entries for each Degree of Freedom (DoF), of every node laying on the same edge of the segment, say edges Q, R, S and T, are placed in the mass and stiffness matrices so that the vector of displacements can be written as: $\mathbf{u} = \{\mathbf{u_Q}\ \mathbf{u_R}\ \mathbf{u_S}\ \mathbf{u_T}\}^T$. Following the analysis
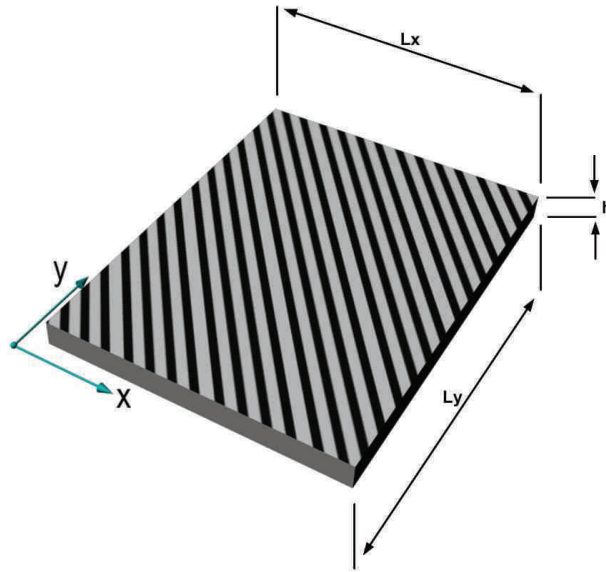
Figure 1.3: *A composite panel modelled within the present approach*

presented in [Manconi and Mace, 2007, Inquiété, 2008] the time-harmonic equation of motion of the segment assuming uniform and structural damping for all the DoF can be written as:

$$\left(\mathbf{K}\left(1 + \eta \mathrm{i}\right) - \omega^2 \mathbf{M}\right) \mathbf{u} = \mathbf{F} \tag{1.26}$$

where η is the structural damping coefficient, ω is the angular frequency and $\mathbf{F}$ the vector of the nodal forces. Then the dynamic stiffness matrix can be written as:

$$\mathbf{D} = \mathbf{K}\left(1 + \eta \mathrm{i}\right) - \omega^2 \mathbf{M} \tag{1.27}$$

therefore eq.(1.26) may be written as:

$$\begin{bmatrix} \mathbf{D_{QQ}} & \mathbf{D_{QR}} & \mathbf{D_{QS}} & \mathbf{D_{QT}} \\ \mathbf{D_{RQ}} & \mathbf{D_{RR}} & \mathbf{D_{RS}} & \mathbf{D_{RT}} \\ \mathbf{D_{SQ}} & \mathbf{D_{SR}} & \mathbf{D_{SS}} & \mathbf{D_{ST}} \\ \mathbf{D_{TQ}} & \mathbf{D_{TR}} & \mathbf{D_{TS}} & \mathbf{D_{TT}} \end{bmatrix} \begin{Bmatrix} \mathbf{u_Q} \\ \mathbf{u_R} \\ \mathbf{u_S} \\ \mathbf{u_T} \end{Bmatrix} = \begin{Bmatrix} \mathbf{F_Q} \\ \mathbf{F_R} \\ \mathbf{F_S} \\ \mathbf{F_T} \end{Bmatrix}$$

Using the Floquet theory for a rectangular segment and assuming a time-harmonic response the displacements of each edge can be written as a function of the displacements at one single edge. Taking edge Q as the edge of reference we have:

$$\mathbf{u_R} = \lambda_x \mathbf{u_Q}, \ \mathbf{u_S} = \lambda_y \mathbf{u_Q}, \ \mathbf{u_T} = \lambda_x \lambda_y \mathbf{u_Q} \tag{1.29}$$

Using the same theory, the force vectors can be written as:

$$\mathbf{F_R} = \lambda_x \mathbf{F_Q}, \ \mathbf{F_S} = \lambda_y \mathbf{F_Q}, \ \mathbf{F_T} = \lambda_x \lambda_y \mathbf{F_Q} \tag{1.30}$$

With λ_x and λ_y the phase constants which are related to the wavenumbers κ_x and κ_y through
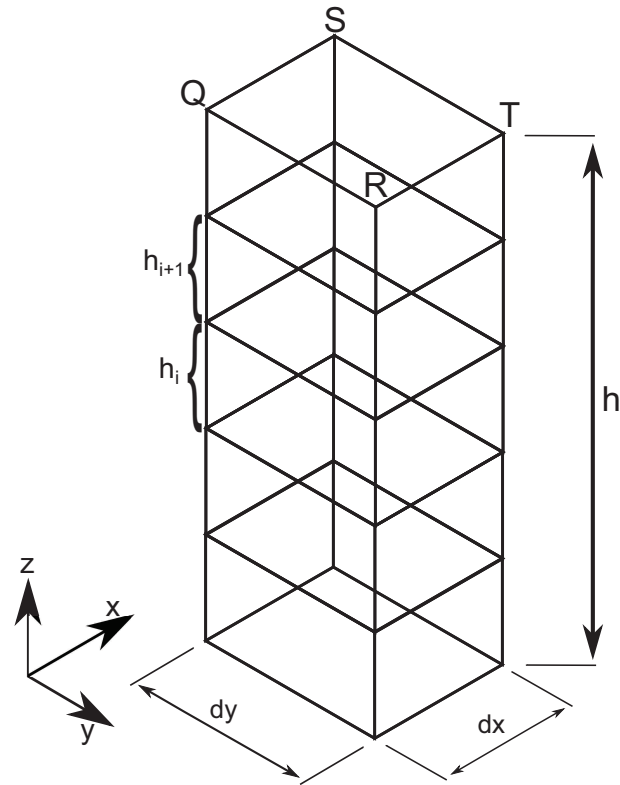
Figure 1.4: *View of the modeled periodic segment with its edges Q, R, S and T*

the relation:

$$\lambda_x = \mathrm{e}^{-\mathbf{i}\kappa_x d_x}, \ \lambda_y = \mathrm{e}^{-\mathbf{i}\kappa_y d_y} \tag{1.31}$$

The displacement vector can therefore be written as:

$$\left\{ \begin{array}{c} \mathbf{u_Q} \\ \mathbf{u_R} \\ \mathbf{u_S} \\ \mathbf{u_T} \end{array} \right\} = \left\{ \begin{array}{c} \mathbf{I} \\ \lambda_x \mathbf{I} \\ \lambda_y \mathbf{I} \\ \lambda_x \lambda_y \mathbf{I} \end{array} \right\} \mathbf{u_Q}$$

Assuming no external excitation, equilibrium along edge Q implies that:

$$\left\{ \begin{array}{cccc} \mathbf{I} & \lambda_y^{-1}\mathbf{I} & \lambda_x^{-1}\mathbf{I} & \lambda_x^{-1}\lambda_y^{-1}\mathbf{I} \end{array} \right\} \left\{ \begin{array}{c} \mathbf{F_Q} \\ \mathbf{F_R} \\ \mathbf{F_S} \\ \mathbf{F_T} \end{array} \right\} = \mathbf{0}$$

Eventually, substituting eq.(1.32,1.33) in eq.(1.26) we end up with the eigenproblem:

$$\left\{ \begin{array}{cccc} \mathbf{I} & \lambda_y^{-1}\mathbf{I} & \lambda_x^{-1}\mathbf{I} & \lambda_x^{-1}\lambda_y^{-1}\mathbf{I} \end{array} \right\} \mathbf{D} \left\{ \begin{array}{c} \mathbf{I} \\ \lambda_x \mathbf{I} \\ \lambda_y \mathbf{I} \\ \lambda_x \lambda_y \mathbf{I} \end{array} \right\} \mathbf{u_Q} = \mathbf{0}$$

which can be written in the form:

$$
\left(
\begin{array}{c}
(\mathbf{D_{QQ}} + \mathbf{D_{RR}} + \mathbf{D_{SS}} + \mathbf{D_{TT}}) + (\mathbf{D_{QR}} + \mathbf{D_{ST}})\,\lambda_x + (\mathbf{D_{RQ}} + \mathbf{D_{TS}})\,\lambda_x^{-1} \\
+ (\mathbf{D_{QS}} + \mathbf{D_{RT}})\,\lambda_y + (\mathbf{D_{SQ}} + \mathbf{D_{TR}})\,\lambda_y^{-1} + \mathbf{D_{QT}}\lambda_x\lambda_y + \\
\mathbf{D_{TQ}}\lambda_x^{-1}\lambda_y^{-1} + \mathbf{D_{SR}}\lambda_x\lambda_y^{-1} + \mathbf{D_{RS}}\lambda_x^{-1}\lambda_y
\end{array}
\right) \mathbf{u_Q} = \mathbf{0}
$$

1.2.5.2 Solving the eigenproblem

Various methods exist for the solution of the eigenproblem and are discussed extensively in [Manconi and Mace, 2007, Inquiété, 2008]. For the particular case where the frequency and the wavenumber towards y direction are considered as fixed or known (e.g wavenumber corresponding to a mode of the full panel) the non-linear eigenproblem of eq.(1.35) is reduced to:

$$
\left(\mathbf{A_2}\lambda_x^2 + \mathbf{A_1}\lambda_x + \mathbf{A_0}\right)\mathbf{u_Q} = \mathbf{0} \tag{1.36}
$$

where:

$$
\mathbf{A_i} =
\begin{cases}
\mathbf{D_{QT}}\lambda_y^2 + (\mathbf{D_{QR}} + \mathbf{D_{ST}})\lambda_y + \mathbf{D_{SR}} & ,\ \text{i=2} \\[2mm]
(\mathbf{D_{QQ}} + \mathbf{D_{RR}} + \mathbf{D_{SS}} + \mathbf{D_{TT}} + \mathbf{D_{QS}} + \mathbf{D_{RT}})\lambda_y + \mathbf{D_{SQ}} + \mathbf{D_{TR}} & ,\ \text{i=1} \\[2mm]
\mathbf{D_{RS}}\lambda_y^2 + (\mathbf{D_{RQ}} + \mathbf{D_{TS}})\lambda_y + \mathbf{D_{TQ}} & ,\ \text{i=0}
\end{cases}
\tag{1.37}
$$

The above quadratic eigenproblem can also be converted as shown in [Tisseur and Meerbergen, 2001] into an ordinary linear generalized eigenproblem of twice the size, by defining a new vector $\mathbf{z} = \lambda_y\mathbf{u_Q}$:

$$
\begin{bmatrix} -\mathbf{A_0} & \mathbf{0} \\ \mathbf{0} & \mathbf{I} \end{bmatrix}
\left\{ \begin{array}{c} \mathbf{u_Q} \\ \mathbf{z} \end{array} \right\}
= \lambda_y
\begin{bmatrix} \mathbf{A_1} & \mathbf{A_2} \\ \mathbf{I} & \mathbf{0} \end{bmatrix}
\left\{ \begin{array}{c} \mathbf{u_Q} \\ \mathbf{z} \end{array} \right\}
$$

with $\mathbf{I}$ the identity matrix. The propagating wavenumbers are then calculated as:

$$
\kappa_x = \frac{\log\left(\lambda_x\right)}{-\mathrm{i}d_x} \quad \text{and} \quad \kappa_y = \frac{\log\left(\lambda_y\right)}{-\mathrm{i}d_y} \tag{1.39}
$$

Throughout the applications of the WFEM, simplicity is exhibited as its main advantage compared to other semi-analytical methods such as SAFE or the Spectral Element Method (SEM). Indeed, it suffices to develop the numerical model of the cell using a computer code capable of extracting the mass and stiffness matrices of the model and then exploit them using an ordinary mathematical software. On the other hand, the use of a finite element discretization of a cell can lead to numerical errors. Recently, an amount of research has been conducted (see [Akrout, 2005], [Waki et al., 2009] for the 1D-periodic structures and [Manconi and Mace, 2007] for 2D-periodic structures) on the prediction of these numerical errors.
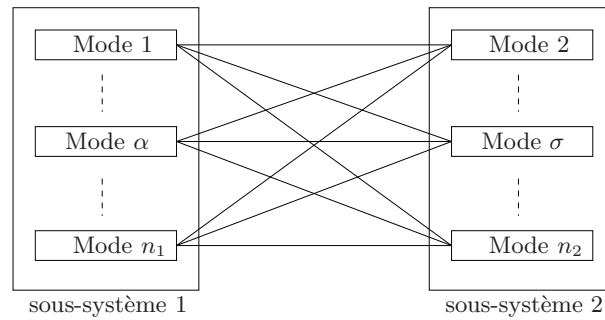
Figure 1.5: *Modal coupling between two SEA subsystems*

1.3 Predicting the vibroacoustic response in the high and the mid-frequency range

1.3.1 Introduction

In this section the principal approaches for modelling a structural-acoustic system at frequencies where deterministic numerical methods are inefficient are presented. A frequency-wise inverse sequence is adopted, with the SEA method firstly presented as the most classical and developped one. Subsequently more recently developped approaches aiming at covering the so called 'mid-frequency' gap are presented.

1.3.2 The SEA method

1.3.2.1 Introduction

The Statistical Energy Analysis (SEA) method (see [Lyon and DeJong, 1995]), is an energy method commonly used in the high frequency domain. A its name implies it is not a deterministic method which describes precisely the characteristics of a particular system. The SEA is applied to subsystems whose frequency averaged parameters serve as an input to the model. The subsystems are not described by their spatial response which becomes complicated to manage in high frequencies but by their energies.

In [Lyon and DeJong, 1995], the authors made an exhaustive description of the SEA method, starting with the energy equation between two coupled systems with one degree of freedom and which forms the basis of the SEA, and concluding with industrial applications.

In the low frequency domain, the first modes of a system are sufficient to describe its dynamic behaviour. For years, studies of mechanical systems have attempted to describe the low frequency behaviour of complicated systems. The SEA method was developed in the early 60's when large sized structures subjected to random excitations at high frequencies were to be studied, mainly in the aeronautical field. At high frequencies, the modes become very sensitive to parametric uncertainties. Moreover, the large number of degrees of freedom to be considered when modelling this type of systems makes the calculation cost prohibitive. Thus, a new method was introduced, whose characteristics could overcome the disadvantages mentioned above.

The SEA is based on a simple principle: the power exchanged between two oscillators with one degree of freedom is proportional to the energy difference between the two subsystems. This principle is established in [Lyon and DeJong, 1995] and is exhibited when certain specified conditions
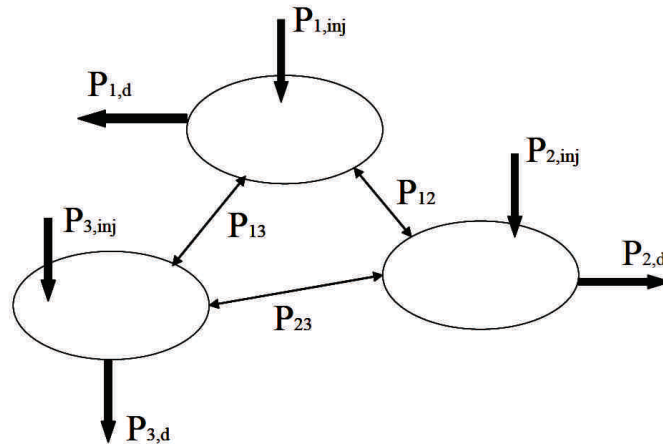
Figure 1.6: *Graphical representation of the energy exchange between three SEA subsystems*

are established.

1.3.2.2   SEA parameters

The SEA is based on an analogy frequently used in the study of heat transfer between systems. It consists in decomposing a complex structure into coupled substructures or subsystems and in performing a power balance between these subsystems. The expression of this power balance requires the estimation of the power injected in the sub-systems, the power exchanged between the subsystems and the power dissipated by them. The power injected in a subsystem is equal to the power dissipated by the subsystem plus the sum of powers exchanged with subsystems that are coupled to it.

In schematic form, the power balance between the subsystems is illustrated in fig.1.6, with $P_{i,inj}$ the injected power in subsystem i, P_{ij} the power exchanged between subsystem i and subsystem j and P_i the power dissipated by subsystem i.

Writing the power balance, allows for introducing the SEA parameters, such as the Dissipation Loss Factors (DLF) and the Coupling Loss Factors (CLF) to express the various power exchanges. The characterization of these parameters as well as the knowledge of the injected power within the subsystems allow for the solution of the power balance system, and thus the estimation of the averaged vibrational energies of the SEA subsystems.

The powers needed to write the SEA equilibrium are expressed in terms of average total energies of the considered subsystems. The benefit of this approach when studying a large system is the reduction of the DOF of the system to the energy variables, whose number is equal to the number of subsystems. The resolution is therefore less computationally intense compared to conventional methods such as the FEM.

1.3.2.3   The Dissipation Loss Factor

The DLF is involved in writing the power dissipated by a subsystem. The dissipated power can be written as:

$$P_{diss,i} = \omega \eta_i E_i \tag{1.40}$$

where ω is the central angular frequency of the frequency band under consideration and η_i is the DLF of subsystem i.

This factor characterizes the different sources of dissipation of energy within the subsystem such as structural damping or the effects of internal friction and the effect of radiation in the case of a structural subsystem surrounded by an acoustic fluid.

1.3.2.4 The Coupling Loss Factor

The relationship between the exchanged power and the average total energies of the subsystems can be written so as to introduce the couplings terms:

$$P_{ij} = \omega \eta_{ij}(E_i - n_i/n_j E_j) \tag{1.41}$$

The terms η_{ij} and η_{ji} are the CLF between the two subsystems i and j, and n_i, n_j are the modal densities of the subsystems. This form allows us to introduce the reciprocal relationship linking the CLF between subsystems, provided that the necessary assumptions are satisfied:

$$n_i \eta_{ij} = n_j \eta_{ji} \tag{1.42}$$

This reciprocal relationship is of practical interest because it allows for a complex system to determine one sole part of the coupling loss factors. The parameters introduced can allow for expressing the SEA power balance. In the simple case of two subsystems, the system is written as follows:

$$\begin{cases} P_{i,inj} = P_{i,diss} + P_{ij} \\ P_{j,inj} = P_{j,diss} + P_{ji} \end{cases} \tag{1.43}$$

Using the previous relations the system in now written as:

$$\begin{bmatrix} \eta_i + \eta_{ij} & -\eta_{ji} \\ -\eta_{ij} & \eta_j + \eta_{ji} \end{bmatrix} \begin{Bmatrix} E_{i,tot} \\ E_{j,tot} \end{Bmatrix} = \begin{Bmatrix} P_{i,inj}/\omega \\ P_{j,inj}/\omega \end{Bmatrix} \tag{1.44}$$

The total energies are obtained by a matrix inversion. The presented approach can be generalized to the case of n subsystems and the SEA factors matrix will be now of dimension n^2:

$$\begin{bmatrix} \eta_1 + \sum\limits_{i=2}^{n} \eta_{1i} & -\eta_{21} & \cdots & -\eta_{n1} \\ -\eta_{12} & \eta_2 + \sum\limits_{i=1,i\neq 2}^{n} \eta_{2i} & \cdots & -\eta_{n2} \\ \cdots & \cdots & \cdots & \cdots \\ -\eta_{1n} & \cdots & \cdots & \eta_n + \sum\limits_{i=1}^{n-1} \eta_{ni} \end{bmatrix} \begin{Bmatrix} E_1 \\ E_2 \\ \cdots \\ E_n \end{Bmatrix} = \begin{Bmatrix} P_{1,inj}/\omega \\ P_{2,inj}/\omega \\ \cdots \\ P_{n,inj}/\omega \end{Bmatrix} \tag{1.45}$$

The SEA matrix is symmetric if we consider the verified reciprocal relationships. Solving an SEA system thus requires knowledge of the CLF and the DLF for each subsystem. These factors can be obtained in various ways which will be detailed later in this thesis. A summary of the main quantities essential to the calculation of the SEA matrix is presented below.

1.3.2.5   The modal density

The SEA method involves frequency averaged characteristics of the subsystems in order to calculate the vibrational response at high frequencies. The natural frequencies of the modes are assumed equi-probable within the frequency band considered. This assumption implies that we consider that the number of modes within the band is quite large and that the modal overlap is high. It is often assumed that a sufficient number of modes within the frequency band justifies the proper application of the SEA method. In practice, most researchers assume that a number of five modes per frequency band is enough.

The estimated number of modes per band generally requires the concept of modal density. This concept is used in the law of reciprocity and a poor estimate of the modal density may cause great discrepancies in the coupling loss factors calculated for the subsystems.

The calculation of the analytical modal density is done by considering the resonance frequencies of the subsystems in the case where the edges are simply supported, in order to simplify the mathematical formulations. It is usually considered that the modal density obtained using this assumption on the boundary conditions can be applied in the high frequency range. The calculation of the modal density for various composite structural components is exhibited in the following chapters of this thesis.

1.3.2.6   Fluid/structure interaction in SEA

To apply the SEA method for a system presenting a fluid/structure coupling nature, we should study especially the phenomena governing the coupling between the acoustic fluid and the structure in the high frequency domain. Two representative cases are considered: i) an academic one where an infinite panel is radiating in a semi-infinite acoustic cavity and ii) a realistic case where two finite rooms are separated by a finite panel.

1.3.2.7   Radiation from an infinite panel in an acoustic cavity

The radiation of a plate in a semi-infinite fluid is a phenomenon which depends on the frequency of the wave incident on the panel and which involves the notion of the coincidence frequency of the plate. This frequency depends on the properties of the plate and the ones of the surrounding fluid.

An infinite panel is considered situated on the plane $z = 0$, having a surface mass of ρ_s, connected to a rigid baffle for $z < 0$, and connected to an acoustic fluid having a sound velocity equal to c_0 for $z > 0$. The plate is subject to a harmonic excitation of $\omega = \dfrac{f}{2\pi}$. The structural wavenumber of the panel can be calculated following the approaches described in sec.1.2.

The acoustic pressure within the fluid is described by the Helmholtz equation:

$$\Delta p + k^2 p = 0 \tag{1.46}$$

where $k = \omega/c_0$. The boundary condition at $z = 0$ is :

$$\frac{\partial p}{\partial z} = -\rho_0 \omega^2 w \tag{1.47}$$

The normal displacement of the plate is written as $w = w_0 exp(ik_x x + ik_y y)$ with the wavenumbers verifying the relation $k_x^2 + k_y^2 = k_s^2$. Thus, according to eq.(1.46) and eq.(1.47), the pressure
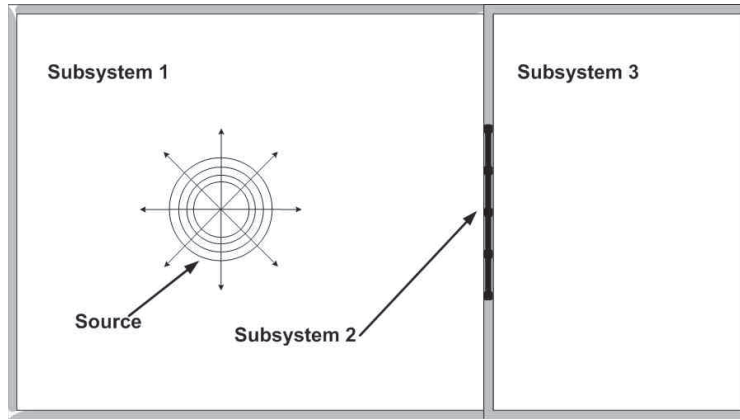
Figure 1.7: *The configuration to be modelled by SEA analysis.*

inside the cavity is written as:

$$p = \frac{i\omega^2}{\gamma} w_0 e^{i} \left(k_x x + k_y y + \gamma z \right) \tag{1.48}$$

with γ the wavenumber towards z in the cavity, given by the equation:

$$\gamma = \begin{cases} \left(k^2 - k_s^2 \right)^{1/2} & \text{si} \quad k > k_s \\ i \left(k_s^2 - k^2 \right)^{1/2} & \text{si} \quad k < k_s \end{cases} \tag{1.49}$$

Three possible cases are distinguished with respect to the value of k_s:

a) if $k > k_s$, p is described by a propagating wave towards z and the panel radiates,

b) if $k < k_s$, p is described by an evanescent wave towards z, and the panel does not radiate,

c) if $k = k_s$, the pressure becomes infinite and the phenomenon is called coincidence.

The acoustic wavenumber is equal to the structural wavenumber when the excitation frequency f becomes equal to the coincidence frequency.

1.3.2.8 SEA formulation for the finite system

In the case of a finite plate, when the excitation frequency is below the critical frequency, there is acoustic radiation from the edges of the panel. From a modal point of view, this reflects the fact that the modes of the plate radiate beyond a frequency, whose value depends on their resonance frequency. Therefore, even below the coincidence frequency, some modes having a resonance frequency below the excitation frequency will radiate.

The considered system now consists of two cavities separated by a plate. One of the cavities is acoustically excited. The objective is to calculate the power transmitted to the other cavity through the plate. To do this, the system is modelled using an SEA approach and is divided in: i)the excited cavity (subsystem 1), ii) the plate (subsystem 2) and iii) the second cavity (subsystem 3) (see fig.1.7).

The transmission of energy between the two cavities involves the phenomenon of acoustic transmission. There exist two types of transmission: the resonant and the non-resonant ones.

Resonant transmission involves the resonant modes of the plate. In this case, the plate stores energy from the excited cavity and then radiates this energy in subsystem 3. This phenomenon greatly depends on the characteristics of the panel.

Non-resonant transmission involves the non-resonant modes of the plate. These modes do not accumulate energy, thus in SEA modelling, the plate is not involved in energy exchange between the two cavities.

If the excitation frequency is greater than the coincidence frequency of the plate, the dominant contribution in the calculation of the transmission coefficient is the one of resonant modes (for which the frequency is close to the excitation frequency) since these modes have a significant radiation efficiency. This phenomenon is called resonant transmission. On the other hand, if the excitation frequency is below the coincidence frequency, the radiation efficiency of resonant modes is negligible. Therefore the contribution of non-resonant modes has to be taken into account.

The SEA matrix of the cavity-plate-cavity system is then written as follows:

$$
\left\{ \begin{array}{c} \langle P_{1,inj} \rangle \\ \langle P_{2,inj} \rangle \\ \langle P_{3,inj} \rangle \end{array} \right\} = \omega \left[\begin{array}{ccc} \eta_1 + \eta_{12} & -\eta_{21} & -\eta_{31} \\ -\eta_{12} & \eta_2 + \eta_{21} + \eta_{23} & -\eta_{32} \\ -\eta_{13} & -\eta_{23} & \eta_3 + \eta_{32} \end{array} \right] \left\{ \begin{array}{c} \langle E_1 \rangle \\ \langle E_2 \rangle \\ \langle E_3 \rangle \end{array} \right\}
\tag{1.50}
$$

η_{12} and η_{23} stand for the resonant transmission coefficients between the cavities and the plate and η_{13} corresponds to the non-resonant transmission coefficient.

The CLF η_{12} is expressed in terms of the radiation efficiency of the panel:

$$
\eta_{sa} = \frac{\rho_0 c_0}{\omega \rho_s h_s} \sigma
\tag{1.51}
$$

where ρ_0 and c_0 stand for the density and the acoustic velocity inside the medium, ρ_s and h_s are the area density and the thickness of the plate and ω is the central angular frequency of the studied frequency band.

The radiated power from a structure can be calculated through its radiation efficiency, which takes into account for the radiation of each mode of the structure:

$$
\sigma = \frac{P_{rad}}{\rho_0 c_0 A_s \langle v^2 \rangle}
\tag{1.52}
$$

where P_{rad} is the radiated power, A_s is the radiation area and $\langle v^2 \rangle$ is the averaged square vibrational velocity.

Some of the most classical and important studies on the calculation of the radiation efficiency of plates are exhibited in [Maidanik, 1962], [Crocker and Price, 1969] and [Leppington, 1988].

1.3.2.9 Limitations of the SEA applicability

The principal SEA hypotheses are reviewed in [Soize, 1987]:

- The method is applied in a permanent regime.

- The system under study is partitioned into subsystems. Each subsystem considered separately is weak-dissipating and it has a countable number of modes.

- The subsystems are considered weakly coupled, meaning that no global modes are present in the studied frequency range. Indirect coupling between subsystems is also ignored.

- The coupling between two subsystems is conservative. It is performed by mass, stiffness and gyroscopic bahaviours. Coupling losses are not taken into account. This means that damping is small.

- The excitations are statistically independent (uncorrelated) and randomly stationary.

- The mean number of resonant modes of each subsystem must be large for a given frequency band. This guarantees the statistical representation of the mean computed values. The main assumption is that any subsystem has to be reverberant.

- The averaged total energy in a frequency band is due to the contributions of the resonant modes in the band.

- The energy transmission between two coupled subsystems in a frequency band is performed only by the resonant modes of the two subsystems in this frequency band.

- The behaviour of a group of modes of a subsystem may be described by an average mode. These modes have the same energy level and have sensibly the same behaviour.

The assumptions of the SEA method are verified only under the above conditions. These conditions strongly depend on two parameters: the diffuseness of the vibrational field within each subsystem (spatial modal overlap) and the number of modes in the frequency band considered (spectral modal overlap). High modal overlap serves in validating the hypothesis of equal probability of natural frequencies of the modes within the frequency band considered.

Another important hypothesis to consider when applying the SEA method, which also depends on the modal overlap, is the assumption of weak coupling. Several criteria were presented in order to define the weak coupling between the subsystems:

- In [Chandiramini, 1978] it is considered that the coupling is weak if the DLF of the subsystem is much larger than the coupling loss factor.

- In [Wester and Mace, 1996] the authors introduced two parameters that depend on the coefficients of reflection and transmission at the junction between the two subsystems and on the modal overlap, and which allow for determining the strength of coupling between two subsystems.

- Fahy indicated that the coupling is weak between two subsystems if the modes of the coupled system present similar characteristics compared to the modes of the decoupled subsystems.

- The coupling is also considered as weak if the coupling of two modes of the same subsystem via a mode of the coupled subsystem is negligible compared to the direct coupling between the modes of the same subsystem.

When the coupling is strong, it is necessary to study the indirect coupling between two subsystems not physically connected. When applying an SEA modelling, the indirect coupling is neglected (except for some special cases such as the study of coupling between two cavities separated by a plate). In [Langley, 1989, Langley, 1990] Langley shows that for weakly coupled and reverberant systems the indirect coupling can be neglected. In [Finnveden, 1995], Finnveden exhibits similar conclusions for a system comprising three subsystems.

1.3.3 The EIC method

The Energy Influence Coefficient approach (EIC) was introduced in [Lesueur et al., 1988]. It is a deterministic energy method, based on a modal analysis of the studied system. The SEA tends to overestimate the structural coupling in the low and medium frequency ranges. The EIC method was therefore developed to provide a more accurate modelling of structural coupled systems in these frequency domains. The use of modal analysis allows the reduction of calculation times with respect to an FE modelling. However, the modal data are difficult to obtain for certain complex structures, which limits the use of the method.

We consider several coupled linear vibrating systems, whose characteristics are time independent. No assumptions are made on the nature or the coupling of the systems, which can be structural or acoustic. These systems are subject to excitations which are assumed:

- decorrelated for two different systems,

- separable in space and time,

- in steady-state.

The EIC C_{ij} gives the kinetic energy in the system i when the system j is excited with an excitation PSD equal to $S_j(\omega)$. This coefficient is expressed in terms of the function of spatial dependence $\beta_j(M'_j, M''_j)$ of the forces exciting the system j and of the frequency response function $H_{ij}(M_i, M'_j, \omega)$ between the point M_i of system i and the point M'_j of system j. H_{ij} is the Fourier transform of the velocity response at point M_i for a unit impulse force at point M'_j. The coefficient C_{ij} corresponding to the frequency band $\Delta\omega$ is given as:

$$C_{ij}(\Delta\omega) = \frac{1}{2} \int_{\Delta\omega} \int_{\Omega_i} \iint_{\Omega_j} \rho_i(M_i) H_{ij}(M_i, M'_j, \omega) H_{ij}^*(M_i, M''_j, \omega) \beta_j(M'_j, M''_j) \mathrm{d}M'_j \mathrm{d}M''_j \mathrm{d}M_i \mathrm{d}\omega \tag{1.53}$$

where ρ_i is the density of system i. If system j is subject to an excitation of PSD S_j and constant throughout $\Delta\omega$, the energy of system i averaged in $\Delta\omega$ is written as :

$$\langle E_{ci} \rangle = C_{ij} S_j \tag{1.54}$$

Because of the presence of the term β_j in the expression of C_{ij}, the EIC depends on the energy applied to the excitation system j. For a δ-correlated excitation applied on system j, the spatial correlation function of the excitation can be written:

$$\beta_j(M'_j, M''_j) = \delta(M'_j - M''_j) \tag{1.55}$$

The expression of the EIC is simplified:

$$C_{ij}(\Delta\omega) = \int_{\Delta\omega} \int_{\omega_i} \int_{\omega_j} \rho_i |H_{ij}(M_i, M_j, \omega)|^2 \mathrm{d}M_i \mathrm{d}M_j \mathrm{d}\omega \tag{1.56}$$

A symmetrical relationship relates then the coefficients C_{ij} and C_{ji}, with the hypothesis that densities ρ_i et ρ_j are constants throughout the systems i and j :

$$\frac{C_{ij}}{\rho_i} = \frac{C_{ji}}{\rho_j} \tag{1.57}$$

The frequency response functions H_{ij} are calculated by conducting a modal analysis on the ensemble of the coupled systems. With the introduction of ω_k, Φ_k and m_k, the resonance frequency, the deformation and the modal mass respectively for mode k, the EIC are written as :

$$C_{ij} = \sum_{k,p} \Psi_{kp}^{(i)} \frac{B_{kp}}{m_k m_p} G_{kp}^{(j)} \tag{1.58}$$

$\Psi_{k,p}^{(i)}$ is expressed in terms of mode shapes k and p of system i and represents the spatial coupling between modes k and p within system i. B_{kp} is expressed in terms of the resonance frequencies and the damping of modes k and p and represents the spectral coupling between modes k and p. Finally $G_{kp}^{(j)}$ represents the spatial coupling between modes k and p of system j and depends on the excitation. This formulation allows separating the different mechanisms of energy transfer. These mechanisms are discussed in more detail in the case of the SEA-like method in sec.1.3.6.2.

In [Boisson et al., 1985], [Boisson et al., 1982] and [Guyader et al., 1982], the EIC method is applied to various plate configurations. Notably in [Boisson et al., 1982], the EIC method is applied to two coupled plates in L shape, one of which is subject to a δ-correlated excitation. The model is then compared to the SEA. It is observed that the SEA overestimates the energy transfer between the two plates relative to the EIC method. This discrepancy occurs when the two plates are different. In this case, the difference decreases as the frequency increases and the SEA modelling is again correct in the high frequency domain.

1.3.4   The Wave Based Method

More recently, a Wave Based prediction Method (WBM) adopting an indirect Trefftz approach has been presented in [Desmet, 1998, Desmet et al., 2001, Desmet et al., 2002] and has received a lot of attention. The WBM is a deterministic technique, however in contrast to the element based approaches, this technique expands the dynamic response variables in terms of selected wave functions which are exact solutions of the governing differential equations. Thus, no fine discretization of the considered domains is required resulting in much smaller model sizes and an increased computational efficiency. For instance, within an acoustic cavity the steady-state pressure $p(x, y, z)$ can be approximated as a solution expansion:

$$p(x, y, z) \approx \hat{p}(x, y, z) = \sum_{a=1}^{n_a} p_a \Phi_a(x, y, z) \tag{1.59}$$

with each function $\Phi_a(x, y, z)$ being an acoustic wave function satisfying the Helmholtz equation and having the general form:

$$\Phi_a(x, y, z) = \begin{cases} \Phi_{a_r}(x, y, z) = cos(k_{xa_r} x) cos(k_{ya_r} y) e^{-jk_{za_r} z} \\ \\ \Phi_{a_s}(x, y, z) = cos(k_{xa_s} x) e^{-jk_{ya_s} y} cos(k_{za_s} z) \\ \\ \Phi_{a_t}(x, y, z) = e^{-jk_{xa_t} x} cos(k_{ya_t} y) cos(k_{za_t} z) \end{cases} \tag{1.60}$$

In the same sense, for a structural subsystem the steady-state normal displacement $w(x, y)$ can

be approximated as an expansion:

$$w(x,y) \approx \hat{w}(x,y) = \sum_{b=1}^{n_s} w_s \Psi_s(x,y) + \hat{w}_{Fi}(x,y) \tag{1.61}$$

with the wave functions $\Psi_s(x,y)$ having the general form:

$$\Psi_s(x,y) = e^{-j(k_{xs}x + k_{ys}y)} \tag{1.62}$$

The sole requirement for the selection of the acoustic wavenumbers k_{xa_i} , k_{ya_i} and k_{za_i} with $(i = r, s, t)$ is that:

$$k_{x_i}^2 + k_{y_i}^2 + k_{z_i}^2 = k^2 \tag{1.63}$$

with $k = \omega/c$. Respectively, for the selection of the structural wavenumbers the condition that has to be fulfilled is:

$$(k_{xs}^2 + k_{ys}^2)^2 = k_b^2 \tag{1.64}$$

with k_b the bending wavenumber of the structural panel. Therefore, an infinite number of wave functions can be found for applying them to the expansions in eq.(1.59),(1.61). However, as proposed in [Desmet, 1998] the following wavenumber components are usually selected for an acoustic system:

$$(k_{xa_r}, k_{ya_r}, k_{za_r}) = (a_1\pi/L_x, a_2\pi/L_y, \pm\sqrt{k^2 - (a_1\pi/L_x)^2 - (a_2\pi/L_y)^2})$$

$$(k_{xa_s}, k_{ya_s}, k_{za_s}) = (a_3\pi/L_x, \pm\sqrt{k^2 - (a_3\pi/L_x)^2 - (a_4\pi/L_z)^2}, a_4\pi/L_z) \tag{1.65}$$

$$(k_{xa_t}, k_{ya_t}, k_{za_t}) = (\pm\sqrt{k^2 - (a_5\pi/L_y)^2 - (a_6\pi/L_z)^2}, a_5\pi/L_y, a_6\pi/L_z)$$

and for a structural system:

$$(k_{xs}, k_{ys}) = \left\{ \begin{array}{c} (s_1\pi/L_{xs}, \pm\sqrt{k_b^2 - (s_1\pi/L_{xs})^2}) \\[2mm] (s_1\pi/L_{xs}, \pm j\sqrt{k_b^2 + (s_1\pi/L_{xs})^2}) \\[2mm] (\pm\sqrt{k_b^2 - (s_2\pi/L_{ys})^2}, s_2\pi/L_{ys}) \\[2mm] (\pm j\sqrt{k_b^2 + (s_2\pi/L_{ys})^2}, s_2\pi/L_{ys}) \end{array} \right\} \tag{1.66}$$

with L_i the dimensions of the smallest bounding surface or volume enclosing the considered convex domain. It is shown in [Desmet, 1998] that the convexity of the considered domains is a sufficient condition for the proposed expansions in eq.(1.59),(1.61) to converge in their limits for $a_{1,2,3,4,5,6} \to \infty$ and $s_{1,2} \to \infty$ respectively, towards the exact solution. The WBM has already been successfully applied to a variety of systems including two and three dimensional bounded and unbounded acoustic domains [Desmet et al., 2001, Desmet et al., 2000] as well as flat,curved and acoustically coupled structural panels [Desmet, 2002, Van Genechten et al., 2011].

1.3.5   The PIM method

The SEA coefficients are usually calculated using wave-context approaches, which can generally be applied only on simple systems with high modal overlaps. For more complex systems, methods based on FE modelling of the studied systems or on experimental measurements can be used to calculate the SEA coefficients [Bies and Hamid, 1980, Shorter and Mace, 1998, Mace and Shorter, 2000, Cotoni et al., 2008].

The Power Injected Method (PIM) allows for the calculation of the SEA coefficients, either by an FE low frequency modelling, or by experimental measurements. In all cases, the system is subjected to an ROR excitation, that is to say a set of forces reproducing a white noise, by being randomly placed on the system and randomly phase-shifted relative to each other. In [Bies and Hamid, 1980], it is exhibited that five forces are generally sufficient to reproduce an ROR excitation. In [Troclet et al., 2009], the Influence Circle Method (ICM) was used in order to decide the number of applied loads, while an OLH (Optimal Latin Hypercube) approach was adopted to place the forces on the subsystems. The ROR excitation allows also for the decorrelation of modes of the excited system, a necessary condition for the application of SEA.

The coupling loss factors can be determined by the PIM method, by inverting the system of energy equations under the desired excitations. In [Hiverniau, 2006] the author measured the SEA coefficients of two coupled plates using the PIM method. The measurement of the internal loss factor of the decoupled plates was performed using the injected power method as well as the reverberation time method [Bies and Hamid, 1980], which gave similar results. He also studied the influence of the number of excitation points and the number of measurement points on the results. The coupling loss factor was then calculated by three different methods: i)the PIM method applied to experimental measurements, ii) the same method applied to aN FEM, and iii) a wave approach. The values of the experimentally measured coefficients presented many discrepancies compared to the FE approach and the wave approach when the intrinsic loss factors of the plates introduced to the numerical models did not match the experimental ones. When the experimental damping loss factors were introduced into the FE model, the coupling loss factors calculated by the two approaches conforms well to the experimental values.

The PIM is more accurate than the wave approaches in the frequency domain [Hiverniau, 2006] where the SEA assumptions are no longer verified e.g. in the case of low modal overlap. However, outside the SEA validity domain, the coefficients obtained by this method can present inconsistencies, such as the dependence of coupling loss factors to subsystems damping.

The SEA-like method, presented below, is also based on low-frequency methods. However unlike the PIM, the SEA-like approach is not an inverse energy method, being closer to the EIC approach.

1.3.6   The SEA-like method

The SEA-like method is a modal based energy method; as the EIC method it relates the energy vector to the injected power vector by the SEA-like coefficient matrix (see the approach proposed by Mace in [Mace, 2003, Mace, 2005a]).

1.3.6.1   Presentation of the SEA-like approach

The SEA provides a statistical modelling of the system pertinent in the high frequency domain, where the modal overlap is high in the various subsystems and when the coupling between the

subsystems is weak. However, the assumptions of SEA - including loose coupling - are no longer verified for lower frequencies. In this case, the system's behaviour is sensitive to the characteristics of each mode. It is therefore no longer pertinent to model a particular system with a statistical method.

Frëdo in [Fredö, 1997] introduced an energy method relaxing some of the restrictive conditions of SEA. The method was named SEA-Like. The assumptions used in SEA are not necessarily verified during the application of the SEA-like. In SEA, the modal energy is assumed equi-distributed between the modes and entirely contained within the frequency band considered. The non-resonant modes are neglected. The modal energies of resonant modes are considered incoherent to each other and of spatially homogeneous density within the subsystem.

These assumptions are suitable to describe a set of systems in the high frequency domain. But when the modal overlap of a system is low, the system has a more intense modal behaviour. It can no longer be described as a sum of equi-energized modes. The SEA-like method, developped from the analytical modal data or by an FE modelling of the system, is used to describe this particular modal behaviour of the system.

In [Fredö, 1997] it is shown that the coefficients of the energy flow may be negative, indicating that the power flow is directed from a low energy subsystem to a subsystem of higher energy. This is the case for example when the excited subsystem has a non-resonant behaviour, while an attached subsystem contains a resonant mode. In SEA, only the resonant behaviour of the subsystems is taken into account and such a phenomenon can not be modelled. In the same reference a criterion of validity of the use of SEA is also presented: the modal densities should verify the reciprocity condition, which relates the modal densities to the CLF:

$$n_1 \eta_{12} = n_2 \eta_{21} \tag{1.67}$$

In [Mace, 2005a] Mace used a similar approach for deriving the SEA-like method.

He introduced the SEA equation, which expresses the injected power vectors as a function of the energy vectors for each of the subsystems :

$$\mathbf{P}_{inj} = \mathbf{LE} \tag{1.68}$$

where the SEA coefficients can be rewritten as:

$$L_{ii} = \omega(\eta_i + \sum_{j \neq i} \eta_{ij}) \tag{1.69}$$

$$L_{ij, i \neq j} = -\omega \eta_{ji} \tag{1.70}$$

with η_i and η_{ij} the DLF and the CLF of the subsystems respectively.

Generally, matrix L is considered as an SEA matrix if it verifies two conditions:

1. The energy conservation condition : $\sum_i L_{ij} = \omega \eta_j$

2. The reciprocity condition: $n_i \eta_{ij} = n_j \eta_{ji}$

There is a third condition, which is validated in most cases, but is not required for the matrix to be considered as an SEA one: this is that the CLF are positive and independent of the damping of subsystems, and that they are equal to zero between subsystems that are not physically connected.

There are some cases where the third hypothesis is not verified, especially when the modal overlap is low. When all three conditions are verified, the matrix $\mathbf{X} = \mathbf{A}^{-1}$ is an SEA matrix. We can therefore write the proportionality relation as given by Lyon which relates the energy flow between two subsystems.

If only the first two conditions are satisfied the matrix is called a 'quasi-SEA matrix'. The system therefore has to be modelled with an SEA-like approach. The energy flow between two subsystems no longer depends solely on the energies of the two subsystems considered but may also depend on the energy of a third subsystem.

The SEA-like matrix coefficients are calculated in the same way as with the PIM method, using the expression:

$$A_{rs} = \frac{\langle E_r \rangle}{\langle P_{inj,s} \rangle} \tag{1.71}$$

where $\langle \rangle$ stands for the spatial average.

The calculation of subsystem energies and of injected powers is made with methods such as classic modal analysis or FE analysis. As aforementioned, we can model a coupled problem in two ways: either by using the modes of the entire system or by using the modes of each subsystem considered as decoupled.

1.3.6.2   Projection on the coupled system modes

Hereby, the SEA-like coefficient between a subsystem r and a subsystem s is calculated based on the coupled system modes. This approach, presented in [Mace, 2003, Mace, 2005a], allows for highlighting two modal coupling phenomena: the spatial coupling and the spectral coupling. After presenting the calculations leading to the expression of the SEA-like coefficient, the influence of these coupling phenomena on the SEA-like coefficients calculation will be studied.

1.3.6.3   Calculation of the energy influence coefficients

We consider a system divided in various subsystems with the subsystem s being excited by a ROR pressure field p_{ext}. With Φ_j standing for the j-th mode of the complete system, the associated response function α_j is given by the following expression:

$$\alpha_j(\omega) = \frac{1}{\omega_j^2(1 + i\eta) - \omega^2} \tag{1.72}$$

The velocity field of subsystem r is therefore written in the following way:

$$v(\mathbf{x_r}; \omega) = i\omega \sum_j \Phi_j(\mathbf{x_r})\alpha_j(\omega) \int_{V_s} \Phi_j(\mathbf{x_s})p_{ext}(\mathbf{x_s}; \omega)\mathrm{d}\mathbf{x_s} \tag{1.73}$$

which allows for the expression of the total energy density at point $\mathbf{x_r}$ of the subsystem r:

$$\delta E(\mathbf{x_r}; \omega) = \frac{1}{2}\rho(\mathbf{x_r})v(\mathbf{x_r}; \omega)v^*(\mathbf{x_r}; \omega) \tag{1.74}$$

being:

$$\delta E(\mathbf{x_r};\omega) = \frac{1}{2}\rho(\mathbf{x_r})\omega^2 \sum_j \sum_k \Phi_j(\mathbf{x_r})\Phi_k(\mathbf{x_r})\alpha_j(\omega)\alpha_k^*(\omega)$$

$$\iint_{V_s} \Phi_j(\mathbf{x_s})p_{ext}(\mathbf{x_s};\omega)\Phi_j(\mathbf{x_s'})p_{ext}^*(\mathbf{x_s'};\omega)\mathrm{d}\mathbf{x_s}\mathrm{d}\mathbf{x_s'} \quad (1.75)$$

The joint-acceptance is therefore introduced in the expression of the energy density of subsystem r as:

$$\delta E(\mathbf{x_r};\omega) = \frac{1}{2}\rho(\mathbf{x_r})\omega^2 \sum_j \sum_k \Phi_j(\mathbf{x_r})\Phi_k(\mathbf{x_r})\alpha_j(\omega)\alpha_k^*(\omega)S_{p_{ext}}(\omega)j_{jk}^{(s)}(\omega) \quad (1.76)$$

Considering:

$$\Psi_{jk}^{(r)} = \int_{V_r} \rho(\mathbf{x_r})\Phi_j(\mathbf{x_r})\Phi_k(\mathbf{x_r})\mathrm{d}\mathbf{x_r} \quad (1.77)$$

The frequency averaged energy of subsystem r is written as:

$$\langle E_r \rangle = \frac{1}{2}\frac{1}{\Delta\omega} \sum_j \sum_k \Psi_{jk}^{(r)} \int_{\Delta\omega} \omega^2\alpha_j(\omega)\alpha_k^*(\omega)S_{p_{ext}}(\omega)j_{jk}^{(s)}(\omega)\mathrm{d}\omega \quad (1.78)$$

Considering an ROR excitation, the joint-acceptance expression verifies the eq.(1.93), therefore using a variable change:

$$\Gamma_{jk} = \frac{1}{\Delta\omega} \int_{\Delta\omega} \omega^2\alpha_j(\omega)\alpha_k^*(\omega)S_{p_{ext}}(\omega)\mathrm{d}\omega \quad (1.79)$$

we can eventually write:

$$\langle E_r \rangle = \frac{1}{2} \sum_j \sum_k \Gamma_{jk}\Psi_{jk}^{(r)}\Psi_{jk}^{(s)} \quad (1.80)$$

The injected power in subsystem s is written as:

$$P_{inj,s}(\omega) = \Re\left(\frac{1}{2}\int_{V_s} p_{ext}(\mathbf{x_s};\omega)v^*(\mathbf{x_s};\omega)\mathrm{d}\mathbf{x_s}\right) \quad (1.81)$$

and substituting for the velocity field we have:

$$P_{inj,s}(\omega) = \Re\left(\frac{1}{2}i\omega \int_{V_s} p_{ext}(\mathbf{x_s};\omega)\int_{V_s}\sum_j \Phi_j(\mathbf{x_s})\alpha_j(\omega)\Phi_j(\mathbf{x_s'})p_{ext}^*(\mathbf{x_s'};\omega)\mathrm{d}\mathbf{x_s}\mathrm{d}\mathbf{x_s'}\right) \quad (1.82)$$

Assuming a constant modal damping factor we can write:

$$P_{inj,s}(\omega) = \frac{1}{2}\omega \sum_j \eta\omega_j^2\|\alpha_j(\omega)\|^2 \iint_{V_s} \Phi_j(\mathbf{x_s})\Phi_j(\mathbf{x_s'})p_{ext}(\mathbf{x_s};\omega)p_{ext}^*(\mathbf{x_s'};\omega)\mathrm{d}\mathbf{x_s}\mathrm{d}\mathbf{x_s'} \quad (1.83)$$

and taking into account for the joint-acceptance term as before we have:

$$P_{inj,s}(\omega) = \frac{1}{2}\omega \sum_j \eta\omega_j^2 \|\alpha_j(\omega)\|^2 S_{p_{ext}}(\omega) j_{jj}^{(s)}(\omega) \tag{1.84}$$

Eventually the frequency averaged expression of the injected power in system s becomes:

$$P_{inj,s}(\omega) = \frac{1}{2}\sum_j \eta\omega_j^2 \frac{1}{\Delta\omega}\int_{\Delta\omega} \omega \|\alpha_j(\omega)\|^2 S_{p_{ext}}(\omega) j_{jj}^{(s)}(\omega)\mathrm{d}\omega \tag{1.85}$$

Considering ω_c as the central frequency of the studied frequency band we have:

$$P_{inj,s}(\omega) = \frac{1}{2}\eta\omega_c \sum_j \Gamma_{jj}\Psi_{jj}^{(s)} \tag{1.86}$$

Combination of eq.(1.80) and eq.(1.86) provides the expression of the EIC as a function of the modes of the system:

$$A_{rs} = \frac{1}{\eta\omega_c}\frac{\sum_j \sum_k \Gamma_{jk}\Psi_{jk}^{(r)}\Psi_{jk}^{(s)}}{\sum_j \Gamma_{jj}\Psi_{jj}^{(s)}} \tag{1.87}$$

Spectral coupling term Γ_{jk}

The term Γ_{jk} describes the spectral coupling between modes j and k. It depends on the transfer functions of modes j and k, therefore on the natural frequencies and the damping of the two modes and provides information on the resonant character and the overlap between them. Thus if one of the modes j or k is non resonant the Γ_{jk} term is negligible. If both modes are resonant, Γ_{jk} is high as the two modes become superposed when their natural frequencies come closer.

Spatial coupling term $\Psi_{jk}^{(r)}$

The term $\Psi_{jk}^{(r)}$ indicates the spatial correlation between modes j and k. It can be observed from eq.(1.87) that when the terms $\Psi_{jj}^{(r)}$ and $\Psi_{jj}^{(s)}$ become important the modes are well coupled between subsystems r and s. More precisely, the term $\Psi_{jj}^{(r)}$ indicates the proportion of kinetic energy of mode j in the subsystem r. We can therefore distinguish two types of modes: the local modes and the global ones. A mode j is considered as global when the term $\Psi_{jj}^{(r)}$ is of same order in every subsystem. The kinetic energy is therefore distributed throughout the system. On the other hand a mode j is considered as a local mode when the term $\Psi_{jj}^{(r)}$ is considerable in subsystem r and negligible for the rest of the subsystems. In this case the kinetic energy is localized in subsystem r.

1.3.6.4   Modal coupling approach

Using the modes of the complete system can give a simple expression of the SEA-like matrix coefficients. However, when the studied system is complex, these modes can be particularly expensive to calculate. Then it is better to use a more local approach and to decompose the equations of the system on the modes of the decoupled subsystems.

Calculating the SEA-like coefficients depends on the characteristics of the studied system and will therefore not be exhibited here. The reader is referred to Chapter 3 in [de Rochambeau, 2010] for calculating the SEA-like coefficients of a plate-cavity coupled system by a modal coupling method.

1.4   Aeroacoustic excitations on a launch vehicle

1.4.1   Introduction

Launch vehicles are subject to aeroacoustic excitations of broadband random nature during the lift-off phase and their flight within the atmosphere. There are three main types of aeroacoustic excitations [Troclet, 2006a, Troclet, 2007]:

- A jet noise, produced and propagating along the launcher when the kinetic energy of the exhaust jet is converted into acoustic energy while mixing with the atmospheric air.

- A diffused noise field due to the reverberation of the produced sound waves around the launch pad.

- An aerodynamic Turbulent Boundary Layer (TBL) noise that occurs during the transonic and supersonic phases of the flight. This excitation is produced by turbulence in the boundary layers formed around the launcher. During the transonic phase, the discontinuities in the external structures of the launch vehicle induce detachments of the flow and turbulence can be particularly high. This turbulence produces strong pressure fluctuations perceived as noise in the payload cavity.

Hereby the principles of a δ-correlated Rain On the Roof (ROR) excitation will be exhibited. Then two aeroacoustic random excitations assumed to be stationary ergodic will be presented: i) a diffused noise field and ii) a TBL excitation.

These excitations are random and broadband. They are therefore statistically modelled by the product of a spatial correlation function (which describes the spatial distribution of the excitation spectrum) and of the spectral density (which describes the intensity of the excitation as a function of frequency). The spatial correlation functions are generally obtained in a semi-empirical way.

1.4.2   Rain On the Roof excitation

It is assumed that the system is subject to a particular type of excitation, called Rain On the Roof (ROR). This excitation is of random nature, ergodic broadband and spatially uncorrelated. To characterize this excitation, it is necessary to introduce the term of joint-acceptance.

We consider a structural-acoustic system subject to a pressure p of a Power Spectral Density (PSD) S_{pp}. We call Φ_p the p_{th} mode shape of the system and α_p the associated transfer function.

The velocity at a point $\mathbf{x}$ of the structure is therefore written as:

$$v(\mathbf{x};\omega) = i\omega \sum_p \Phi_p(\mathbf{x})\alpha_p(\omega) \int_{sys} \Phi_p(\mathbf{x}')p(\mathbf{x}';\omega)\mathrm{d}\mathbf{x}' \qquad (1.88)$$

We can therefore write the velocity spectral density as:

$$S_{vv}(\mathbf{x};\omega) = \omega^2 \sum_p \sum_q \Phi_p(\mathbf{x})\Phi_q(\mathbf{x})\Re\left(\alpha_p(\omega)\alpha_q(\omega)^*\right)$$

$$\iint_{sys} \Phi_p(\mathbf{x}')\Phi_q(\mathbf{x}'')S_{pp'}(\mathbf{x}'-\mathbf{x}'';\omega)\mathrm{d}\mathbf{x}'\mathrm{d}\mathbf{x}'' \quad (1.89)$$

The term $S_{pp'}$ in eq.(1.89) is the interspectral density of the excitation and is commonly used to describe the aeroacoustic excitation. It can be decomposed into a frequency term S_p called PSD and a spatial term C called correlation function, which depends on ω and the distance between the points $\mathbf{x}$ and $\mathbf{x}'$:

$$S_{pp'}(\mathbf{x}-\mathbf{x}';\omega) = S_p(\omega)C(\mathbf{x}-\mathbf{x}';\omega) \qquad (1.90)$$

The double integration in eq.(1.89) can then be expressed in terms of the spectrum of pressure and of a term that describes the spatial distribution depending on the modes of the system, the so-called joint-acceptance. The latter term is defined as follows:

$$j_{pq}(\omega) = \iint_{sys} \Phi_p(\mathbf{x}')\Phi_q(\mathbf{x}'')C(\mathbf{x}'-\mathbf{x}'';\omega)d\mathbf{x}'d\mathbf{x}'' \qquad (1.91)$$

The velocity spectral density is therefore written as:

$$S_{vv}(\mathbf{x};\omega) = \omega^2 \sum_p \sum_q \Phi_p(\mathbf{x})\Phi_q(\mathbf{x})\Re\left(\alpha_p(\omega)\alpha_q(\omega)^*\right)j_{pq}(\omega)S_p(\omega) \qquad (1.92)$$

The main characteristic and advantage of an ROR excitation is that it causes the joint-acceptance function to become independent of ω and can therefore be expressed in the following way:

$$j_{pq}^{(s)} = \int_{V_s} \rho(\mathbf{x_s})\Phi_p(\mathbf{x_s})\Phi_q(\mathbf{x_s})\mathrm{d}\mathbf{x_s} \qquad (1.93)$$

with $j_{pq}^{(s)}$ not dependent on ω. The ROR excitation is ergodic. Moreover, the integral in eq.(1.93) depends only on one spatial variable. The spatial correlation function $C(\mathbf{x}-\mathbf{x}')$ is therefore equal to zero if $\mathbf{x} \neq \mathbf{x}'$. The ROR excitation in therefore spatially uncorrelated.

1.4.3 Diffused sound field excitation

1.4.3.1 Description of the excitation

The diffused noise field is a pressure field where at a given point the pressure waves have a direction of incidence of equal probability. In a Cartesian coordinate system, the spatial correlation function

corresponding to a diffused noise is written as follows:

$$C(\zeta, \eta; \omega) = \frac{\sin(k_0\zeta)}{k_0\zeta} \frac{\sin(k_0\eta)}{k_0\eta} \tag{1.94}$$

where $\zeta = x - x'$ and $\eta = y - y'$ are the distances separating the two points in x and y directions respectively and k_0 is the acoustic wavenumber defined by the excitation.

This function can also be expressed in the wavenumber space using a Fourrier transform $\mathcal{F}$ given as:

$$\mathcal{F}(k_x, k_y; \omega) = \iint_\infty f(\zeta, \eta; \omega) e^{-ik_x\zeta - ik_y\eta} \mathrm{d}\zeta \mathrm{d}\eta \tag{1.95}$$

The result is a low-pass function:

$$C(k_x, k_y) = \begin{cases} \dfrac{\pi^2}{k_0^2}, & \text{if } \|k_x\| < k_0 \text{ and } \|k_y\| < k_0 \\ 0, & \text{otherwise} \end{cases} \tag{1.96}$$

From eq.(1.96) it can be deduced that the modes that respond well to the diffused noise excitation are the modes whose wavenumbers are inferior to k_0, called acoustically fast modes and whose radiation area occupies the whole surface of the structure. Modes whose wavenumbers are greater than k_0 are called acoustically slow modes and respond less efficiently to the excitation.

When studying a rectangular plate excited by a diffuse noise, Maidanik distinguished three categories in [Maidanik, 1962]: i) acoustically fast modes, ii) edge modes and iii) corner modes. The acoustically slow modes having a wavenumber component greater than k_0 are called edge modes. These modes radiate at the edges of the structure. Modes whose both components of the wavenumber are inferior to k_0 only radiate at the corners of the structure and respond very inefficiently. The later are also called corner modes.

1.4.3.2 Equivalent coherence function

The equivalent coherence functions for various aeroacoustic excitations were presented in [Ichchou et al., 2009]. The aerodynamic excitations are of random broadband nature and spatially correlated. A term commonly used to describe them is the spectral density, which is written for a pressure field $p(x, y; \omega)$ as:

$$S_{pp}(x - x', y - y'; \omega) = S_p(\omega) C(x - x', y - y'; \omega) \tag{1.97}$$

where S_p is the frequency spectrum of the excitation and C a spatial term describing the correlation of the excitation between two points of coordinates (x, y) and (x', y').

The aerodynamic excitations applied to the structure modify the modal equations describing the system, namely the term joint-acceptance which describes the interaction between the excitation and the structural modes. We recall that the general expression of the joint-acceptance term corresponding to modes m and n of the structure is written as:

$$j_{m,n}(\omega) = \iint_{A_s} \Phi_m^s(x, y) \Phi_n^s(x', y') C(x - x', y - y'; \omega) \mathrm{d}x\mathrm{d}x'\mathrm{d}y\mathrm{d}y' \tag{1.98}$$

For an ROR excitation, which is δ-correlated, the expression of joint acceptance is simplified:

$$j_{m,n}^{ror} = \iint_{A_s} \rho_s h_s \Phi_m^s(x,y) \Phi_n^s(x',y') \delta(x-x') \delta(y-y') \mathrm{d}x \mathrm{d}x' \mathrm{d}y \mathrm{d}y' \tag{1.99}$$

This expression leads to simplifications in the calculation of averaged energies and injected powers, which simplifies the calculation of SEA and SEA-like coefficients. In the case of aerodynamic excitations, the expression of joint-acceptance terms is generally complicated. The calculation of averaged energy in the system must be simplified, hence the need to develop a model of equivalent excitations.

An equivalent spatial correlation function C_{eq} is therefore introduced, verifying the expression:

$$C(x-x', y-y'; \omega) \approx C_{eq}(\omega) \delta(x-x') \delta(y-y') \tag{1.100}$$

The expression of the equivalent joint-acceptance, $j_{m,n}^{aero}$ is then related to the term $j_{m,n}^{ror}$ as:

$$j_{m,n}^{aero} = \delta_{m,n} \frac{C_{eq}(\omega)}{h_s \rho_s} j_{m,n}^{ror} \tag{1.101}$$

In [Hiverniau, 2006] two main approaches are adopted in order to calculate the equivalent spatial coherence function. The 'spatial extent' approach originally developped in [Maidanik, 1961], and the equivalence in the wavenumber space presented in [Ichchou et al., 2009]. For a diffused field excitation, both approaches lead to the same results. Using eq.(1.94) or the equivalent eq.(1.96), the equivalent correlation function for a diffused sound field is written as:

$$C_{eq,diff}(\omega) = \frac{\pi^2}{k_0^2} \tag{1.102}$$

1.4.4   Turbulent Boundary Layer excitation

1.4.4.1   Description of the excitation

This type of excitation is produced by the airflow along the launch vehicle during its atmospheric flight. The fluid forms a boundary layer in the vicinity of the structure, where the velocity of the flow varies and induces a pressure field that excites the structure.

The relative fluid velocity in the turbulent boundary layer has a profile variation which depends on the characteristics of the fluid. This velocity is equal to zero in the vicinity of the structure and equal to U_∞ outside the TBL (see fig.1.8). The TBL is characterized by its thickness δ and its convection velocity U_c, which is the average flow velocity within the TBL.

The most commonly used model to describe the pressure field induced by a TBL is the Corcos model [Corcos, 1964]. It gives the spatial correlation function of the pressure field in the form of a product of two functions between the spatial variables x and y describing the structure:

$$C(\zeta, \eta; \omega) = e^{-\alpha_x \omega \frac{|\zeta|}{U_c}} e^{-\alpha_y \omega \frac{|\eta|}{U_c}} e^{i\omega \frac{(\zeta)}{U_c}} \tag{1.103}$$

where α_x and α_y are correlation coefficients along the directions e_x and e_y, and $\zeta = x - x'$ and $\eta = y - y'$ are the distances separating the two points in the propagation and the perpendicular
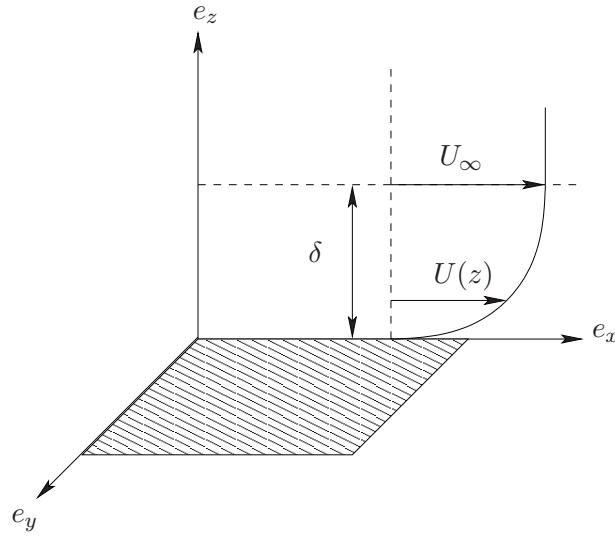
Figure 1.8: *Representation of a TBL excited panel*

directions respectively. The values of α_x and α_y can be found in the open literature as in [Blake, 1986].

Applying the same Fourrier transform as with the diffused sound field, the spatial coherence function can be expressed in the wavenumber space as:

$$C(k_x, k_y; \omega) = \frac{4\alpha_x\alpha_y}{(\alpha_x^2 + (k_x/k_c - 1)^2)(\alpha_y^2 + k_y^2/k_c^2)} \tag{1.104}$$

where $k_c = \omega/U_c$ is the convection wavenumber.

The high frequency range is characterized by surface interactions between the structure and the acoustic medium. In the low frequency range, also referred to as viscous range, the energy exchange between the fluid and the structure is mainly due to edge interactions. In the viscous domain, the modal receptance function which characterizes the energy exchange between the plate and the cavity is highly dependent on the boundary conditions of the panel [Hambric et al., 2004].

1.4.4.2 Equivalent coherence function in the wavenumber space

The spatial correlation function expressed in the wavenumber space and the calculation of the equivalent function is based on the equality of the integration of the functions in a finite wavenumber space:

$$\int_{k_1}^{k_2} \int_0^{2\pi} C_{eq,tbl}(k\cos(\theta), k\sin(\theta), \omega) \, dk \, d\omega = \int_{k_1}^{k_2} \int_0^{2\pi} C_{tbl}(k\cos(\theta), k\sin(\theta), \omega) \, dk \, d\omega \tag{1.105}$$

with $C_{eq,tbl}$ being spatially δ-correlated, eq.(1.105) becomes:

$$C_{eq,tbl}(\omega) = \frac{4\pi}{k_2^2 - k_1^2} \int_{k_1}^{k_2} \int_0^{2\pi} C_{tbl}(k\cos(\theta), k\sin(\theta), \omega) \, dk \, d\omega \tag{1.106}$$

in which the expression of the correlation function in the wavenumber space as exhibited in eq.(1.104) can be replaced.

Chapter 2

On the transmission loss of layered structures by a two-dimensional Wave Finite Element modelling

2.1 Abstract

A robust model for the prediction of the dynamic response of layered panels within a Statistical Energy Analysis (SEA) wave-context approach is proposed hereby. The dispersion characteristics of composite orthotropic structures are predicted using a Wave Finite Element (WFE) method. By manipulating the mass and stiffness matrices of the modelled structural segment a polynomial eigenvalue problem is formed, the solutions of which correspond to the propagation constants of the waves travelling within the structure. The wavenumbers and group velocities for waves comprising out of plane structural displacements can then be calculated. Using the numerically extracted wave propagation data the most important SEA quantities of the structure, namely the modal density and the radiation efficiency of each wave type are calculated. The vibroacoustic response of the structure under a broadband diffused excitation is then computed within an SEA approach. The impact of the symmetric and the antisymmetric vibrational motion of the panel on its sound transmission loss is exhibited and the approach proves robust enough for thin as well as for thick layered structures.

2.2 Introduction

Complex, non-isotropic stratified and sandwich type constructions are widely used in engineering applications such as in the aerospace and automotive industries, mainly because of their high stiffness-to-mass ratio and the fact that their mechanical characteristics can be designed to suit the particular purposes. Unluckily this high stiffness-to-mass ratio being responsible for the increased mechanical efficiency, imparts as well efficient vibration transmission and acoustic radiation. The modelling of the vibrational behaviour of complex composite structures has been a field of extensive study in modern mechanical engineering. The knowledge of the wave propagation characteristics within a structure seems to provide a key to decode and model its vibrational behaviour.

Analytic formulas for the dispersion characteristics in orthotropic thin plates can be found in classical books [Graff, 1991, Reddy, 2004] starting with the Classical Laminate Plate Theory (CLPT) [Stavsky, 1961], developed as an extension of the Kirchoff-Love theory for isotropic plates and suitable for thin panels. Furthermore, the First-order Shear Deformation theory (FSDT) [Whitney and Pagano, 1970] takes into account the transverse shear deformation of the panel and can be used for predicting the dispersion characteristics at higher frequencies. Such classical theories have been successfully used by many authors, as in [Leppington et al., 1982] in order to model the radiation efficiency and the vibroacoustic response under a reverberant field [Leppington et al., 2002] of thin orthotropic panels.

Kurtze and Watters [Kurtze and Watters, 1959] were the first to develop an asymptotic model for the wave dispersion into symmetric flat thick sandwich structures. They divided the flexural wave speed of a sandwich panel (frequency-wise) into three sections, the first characterized by the panel vibrating as a whole, the second by the core's shear wave speed and the third by each of the two facesheets vibrating separately and loaded with half of the core mass. Nevertheless, the model assumed the core to be incompressible, and the deformation of the panel in the thickness sense could not be modelled. Dym and Lang [Dym and Lang, 1974] were the first to develop a structural model for an infinite sandwich panel by using the kinematic assumptions of [Ford et al., 1967] and derived the five equations of motion corresponding to the symmetric and antisymmetric motion of the panel. Moore and Lyon [Moore and Lyon, 1991] extended this structural model to symmetric sandwiches with an orthotropic core. A consistent Higher-order Shear Deformation Theory (HSDT) taking into account the core's shear deformation was developed in [Sokolinsky

and Nutt, 2004] and used in [Wang et al., 2010,Wang et al., 2005] to construct a structural model of an infinitely long sandwich panel and calculate its vibroacoustic response within an SEA context.

In [Cotoni et al., 2008], the authors calculated the phase constant surfaces of periodic composite and stiffened structures using FE and periodic structure theory (PST). The authors gave an expression of the radiation efficiency of the panels based on the calculated wave displacement shapes. The STL of the panels was expressed through the radiation and mechanical impedances of the structures. An insight to the calculation of the same quantities by a modal approach was also given. In [Renji et al., 1997] the authors have used the Mindlin plate theory to derive the flexural wave speed and modal density of composite sandwich panels. The authors in [Ghinet and Atalla, 2006,Ghinet et al., 2005] used a multi-layer analytical model based on Mindlin theory to compute the dispersion characteristics within layered structures. They also computed the vibroacoustic response of layered panels under a diffused sound field using SEA.

A variety of applications of the Wave Finite Element Method (WFEM) has been conducted to predict the wave speeds of one-dimensional [Mencik and Ichchou, 2005,Mace et al., 2005] and two-dimensional structures [Inquiété, 2008,Manconi and Mace, 2007]. Introduced by in [Mead, 1973] the main underlying assumption of the method is the periodicity of the structure to be modelled. The PST is then coupled to the FEM. A set of structures including a vehicle's chassis [Houillon, 1999], and a stiffened plate [Ichchou et al., 2008b,Ichchou et al., 2008c] has been modelled using the WFE method. The two-dimensional technique was successfully used in [Manconi and Mace, 2007] and [Inquiété, 2008] to model the wave propagation in orthotropic thin panels and sandwich structures.

In this chapter the two-dimensional WFEM is employed in order to compute the Sound Transmission Loss (STL) of thick layered structures by accounting for their symmetric and antisymmetric wave motion. Anisotropic, multi-layered panels can be accurately modelled using this generic approach for a broadband frequency range. The resonant transmission coefficient of the panels is directly expressed in relation to the SEA quantities. A way for computing the reverberant field STL of the structures directly derived by their SEA properties is also exhibited. The results are successfully compared to experimental measurements encountered in the open bibliography. A parametric study considering the vibroacoustic behaviour of layered panels as a function of temperature is also conducted. Results from experiments conducted on a honeycomb sandwich panel are used within the developed SEA approach in order to calculate the temperature and altitude dependent STL of the layered panel.

The work presented in this paper is part of a research project first started in 2000 by EADS Astrium. To tackle the problem of the prediction of the response of composite structures within the mid-frequency range, an SEA-Like method was chosen (see [Troclet et al., 1999]). Taking into account for the energy transmission and dissipation characteristics of composite structures within the mid-frequency domain, is an important challenge. At first, the work was focused on structure-borne transmission [Troclet et al., 2009,Ichchou et al., 2009]. Then, the fluid/structure interaction was investigated [Rochambeau et al., 2008]. The results of the current approach will eventually be used to improve the predictions of the developed models.

The paper is organized as follows: In sec.2.3 the process of solving the resulting polynomial eigenproblem as well as the post-processing of the occurring solutions is discussed. In sec.2.4 the calculation of the main SEA quantities, namely the modal density and the radiation efficiency of the layered panels is presented. In sec.2.5 some numerical applications are exhibited in order to validate the conducted work. In sec.2.6 the temperature and altitude dependent STL of a sandwich honeycomb panel is computed. The conclusions are eventually given in sec.2.7.

2.3   The WFE method

2.3.1   The Wave Finite Element method

A rectangular layered panel is considered hereby. A periodic segment of the panel with dimensions dx and dy is modelled using conventional FE. Using the dynamic stiffness matrix of the segment, a nonlinear eigenvalue problem is formulated whose eigenvalues correspond to propagation constants of the various structural wave types. The formulation and the solution of the eigenproblem is discussed in sec.1.2.5.

2.3.2   Post-processing the results of the solution

Once the eigenproblem is resolved the results corresponding to real and propagating waves in the structure have to be distinguished from the ones being computational artifacts or corresponding to evanescent waves. A second task is correlating the eigenvalues corresponding to the same wave type for each frequency and for each direction of propagation. The direction dependent wave mode shapes are mainly caused when coupling highly orthotropic materials (e.g. in sandwich constructions) together. This causes different proportions between the layer deflections (different wave mode shapes) for each direction of propagation, making correlation of wave types sometimes delicate.

In order to distinguish the propagating from evanescent waves an evanescent wave rejection criterion is used. Supposing that a calculated wavenumber is in the form $\kappa = \alpha + \beta i$, we consider that under the condition: $|\alpha|/|\beta| > p$ the wave is propagating, with p a parameter chosen according to the characteristics of each structure. Typical empirical values of p for composites are between 3 and 10. The selection attempt generally starts with a low p value. If all eigenvalues are categorized into wave types through the correlation process (see below), the attempt is considered successful. Otherwise a higher p value is used until all the selected eigenvalues correspond to a set of wave types.

In order to categorize the eigenvalues and eigenvectors corresponding to the same wave type together, in the present study each propagating wave mode shapes was compared to the whole set of wave mode shapes for each angle and frequency. The Modal Assurance Criterion (MAC) criterion which expresses the correlation of two vectors $\mathbf{\Phi_i}$ and $\mathbf{\Phi_j}$ was used for this purpose and can be written as:

$$\text{MAC} = \frac{\left(\mathbf{\Phi}_i^T \bar{\mathbf{\Phi}}_j\right)\left(\mathbf{\Phi}_j^T \bar{\mathbf{\Phi}}_i\right)}{\left(\mathbf{\Phi}_i^T \bar{\mathbf{\Phi}}_i\right)\left(\mathbf{\Phi}_j^T \bar{\mathbf{\Phi}}_j\right)} \tag{2.1}$$

where T stands for the transpose and $-$ for the conjugate of each vector. Typical empirical values for the MAC criterion for orthotropic sandwich structures are between 0.4 and 0.8. On the other hand for isotropic structures, correlation can be achieved with values as high as 0.99. Contrary to p parameter, a high MAC value should firstly be attempted. If no correlated wave modes are found, a lower MAC value is used until all selected eigenvalues are correlated to a set of wave types. A schematic representation of the process followed in order to select the propagating wavenumbers for each frequency and direction is shown in fig.2.1.

As already stated, for some configurations (e.g. coupling a highly orthotropic layer to an isotropic one in a sandwich construction) the wave mode shapes can be strongly direction dependent, making correlation of wave types difficult. In these cases a particularly small angular step has
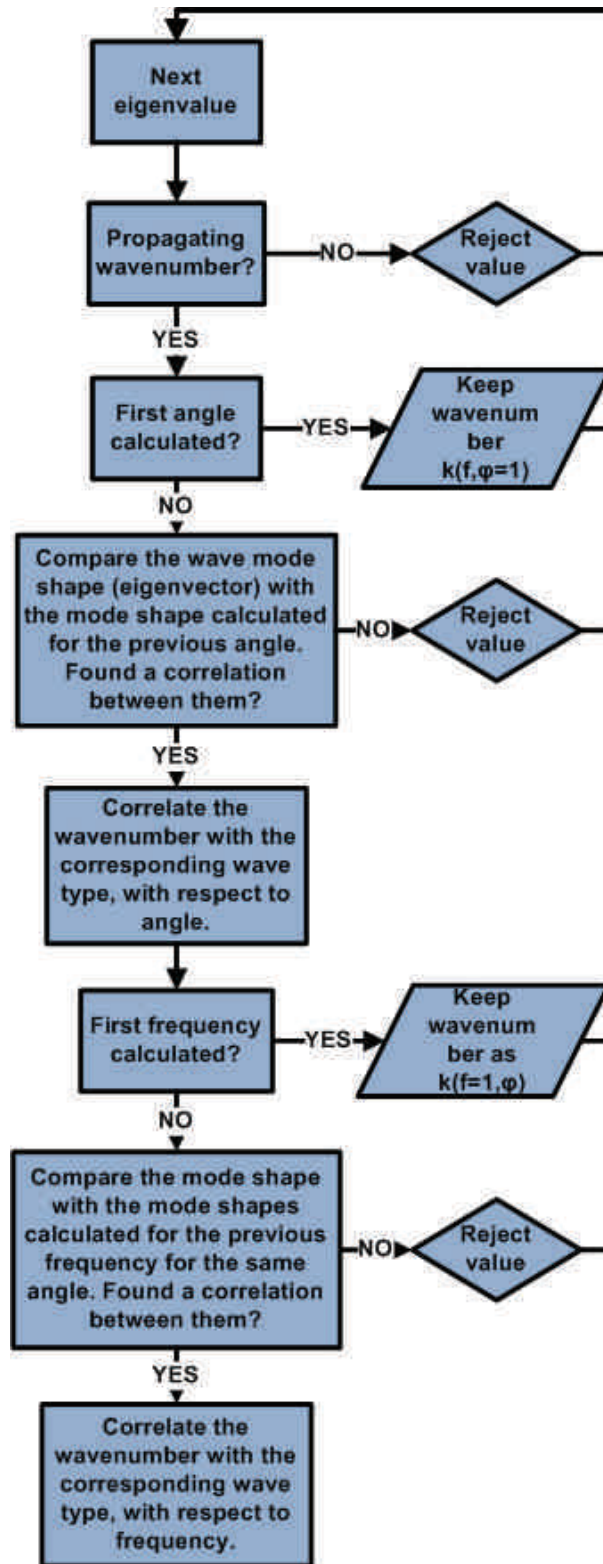
Figure 2.1: *A schematic representation of the algorithmic procedure of correlating the wave types with respect to frequency and direction of propagation.*

to be used, in order to minimize the difference of wave mode shapes between consecutive calculated angles.

2.4 Computation of the energy analysis quantities

2.4.1 Calculation of the modal density

Using the Courant's formula [Courant and Hilbert, 1989], the modal density of each propagating wave type w can be written for each angle ϕ as a function of the propagating wavenumber and its corresponding group velocity c_g:

$$n_w\left(\omega, \phi\right) = \frac{A\ \kappa_w\left(\omega, \phi\right)}{2\pi^2\ \left|c_{g,w}\left(\omega, \phi\right)\right|} \tag{2.2}$$

where A is the area of the panel and the group velocity is expressed as:

$$c_g\left(\omega, \phi\right) = \frac{\mathrm{d}\omega}{\mathrm{d}\kappa\left(\omega, \phi\right)} \tag{2.3}$$

The angularly averaged modal density of the structure is eventually given as a function of frequency:

$$n_w\left(\omega\right) = \int_0^\pi n_w\left(\omega, \phi\right)\mathrm{d}\phi \tag{2.4}$$

2.4.2 Calculation of the radiation efficiency

In order to calculate the radiation efficiency $\sigma\left(\kappa\left(\omega\right)\right)$ for each propagating wave type w, relations presented in the open bibliography are employed. For continuous structures mode shapes of sinusoidal form can be assumed in order to avoid any FE discretization errors in the solution. After employing the Rayleigh's formula for calculating the induced pressure and the time-averaged power flow radiated from the vibrating panel, $\sigma\left(\kappa\left(\omega\right)\right)$ can be written as in [Leppington et al., 1982]:

$$\sigma_{rad,w} = \frac{2\omega^2}{c^2\pi A}\int_0^{L_x}\int_0^{L_x}\int_0^{L_y}\int_0^{L_y}sin(\kappa_{x,w}x)sin(\kappa_{x,w}x')sin(\kappa_{y,w}y)sin(\kappa_{y,w}y')\frac{sin(k_0 r)}{k_0 r}\mathrm{d}y\mathrm{d}y'\mathrm{d}x\mathrm{d}x' \tag{2.5}$$

with $r = \sqrt{(x-x')^2 + (y-y')^2}$. For a periodic discontinuous structure the assumption of sinusoidal mode shapes is no longer valid, therefore the radiation efficiency should be calculated directly from the WFEM derived wave mode shapes. The radiation efficiency expression given in [Cotoni et al., 2008] can therefore be employed.

2.4.3 Calculation of the Sound Transmission Loss (STL) of a panel by an SEA approach

The STL (or TL) is one of the most important indices of the vibroacoustic performance of a structure. The system to be modelled comprises two reverberant chambers separated by the modelled composite panel attached to a rigid baffle. No flanking transmission is considered in the
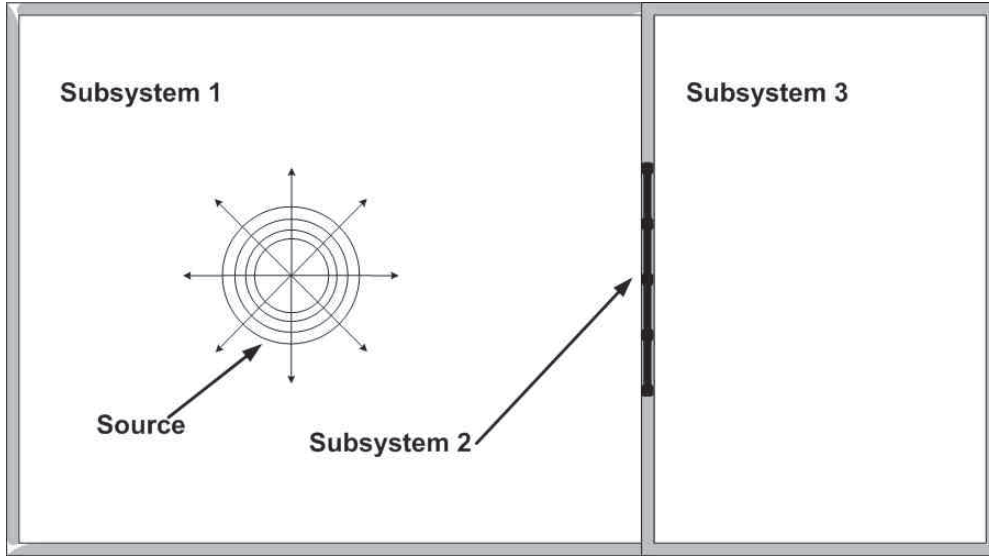
Figure 2.2: *The configuration to be modelled by SEA analysis.*

SEA model. A graphical representation of the modelled subsystems is given in fig.2.2. The energy balance of the subsystems as it is considered within an SEA approach (see [Lyon and DeJong, 1995]) is illustrated in fig.2.3, in which E_1, E_3 stand for the acoustic energy of the source room and the receiving room respectively and E_3 for the vibrational energy of the composite panel. Moreover P_{in} is the injected power in the source room, P_{1d}, P_{2d} and P_{3d} stand for the power dissipated by each subsystem and P_{13} is the non-resonant transmitted power between the rooms. Considering each wave type $w = a, b, c...n$ propagating within the composite panel as a separate SEA subsystem we have:

$$P_{12} = \sum_{w=a}^{n} P_{12,w}$$

$$P_{23} = \sum_{w=a}^{n} P_{23,w}$$

(2.6)

where P_{12} and P_{23} stand for the power flow between the rooms and the panel.

The STL is defined as:

$$\text{STL} = 10 \log_{10} \left(\frac{1}{\tau} \right)$$

(2.7)

where τ is the transmission coefficient which represents the ratio between the transmitted and the incident sound powers. It can be written as the sum of the resonant and the non-resonant transmission coefficient:

$$\tau = \frac{P_{23} + P_{13}}{P_{inc}} = \sum_{w=a}^{n} \frac{P_{23,w}}{P_{inc}} + \frac{P_{13}}{P_{inc}}$$

(2.8)

where P_{inc} stands for the acoustic power incident on the layered panel, which for a reverberant
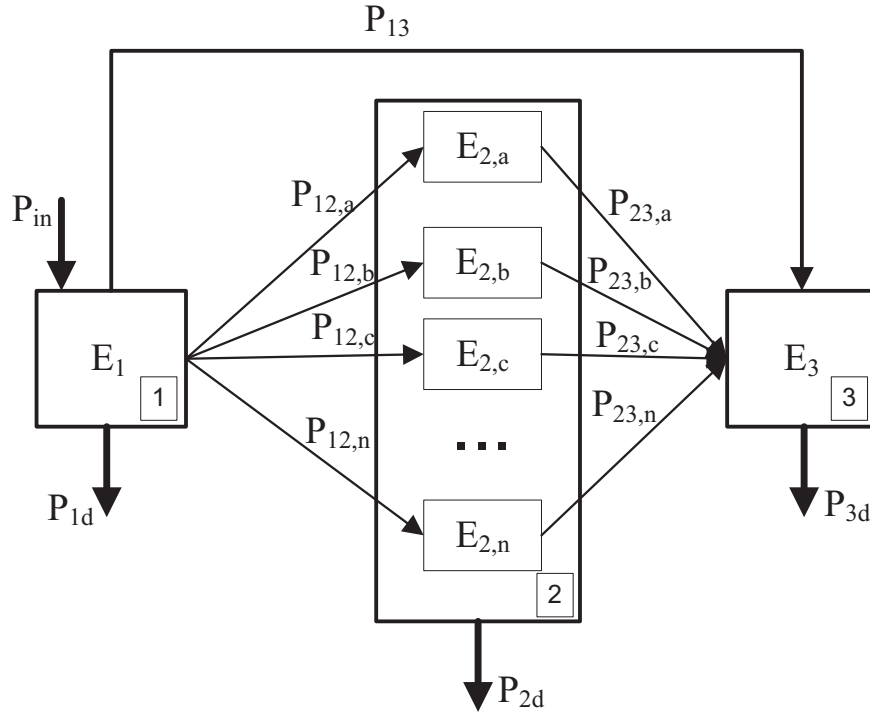
Figure 2.3: *A schematic representation of the SEA power exchanges and energies for the modelled system.*

sound field can be written as:

$$P_{inc} = \frac{\langle p_1^2 \rangle A}{4\rho c} \tag{2.9}$$

where $\langle p_1^2 \rangle$ the mean-square sound pressure. An attempt to calculate the resonant coefficient for each wave type w is hereby made. Assuming no energy exchanges between different wave types within the structure, the energy balance of a structural wave subsystem can be written as:

$$P_{12,w} = P_{2d,w} + P_{23,w} \tag{2.10}$$

The power dissipated can be written as:

$$P_{2d,w} = E_{2,w}\omega\eta_{2,w} \tag{2.11}$$

with $\eta_{2,w}$ the structural loss factor of the wave type w. The vibrational energy of the panel due to wave type w can be written as:

$$E_{2,w} = \rho_s A \langle v_w^2 \rangle \tag{2.12}$$

where ρ_s is the mass per unit of area, A is the total area of the panel and $\langle v_w^2 \rangle$ is the mean-square panel vibration velocity due to wave type w.

The power flow $P_{12,w}$ can be written using the SEA reciprocity rule, as:

$$P_{12,w} = \omega\eta_{12,w}n_1\left(\frac{E_1}{n_1} - \frac{E_{2,w}}{n_{2,w}}\right) = \omega\eta_{21,w}n_{2,w}\left(\frac{E_1}{n_1} - \frac{E_{2,w}}{n_{2,w}}\right) \tag{2.13}$$

where $n_1, n_{2,w}$ are the modal density of the source room and of the wave type w respectively and $\eta_{21,w}$ the coupling loss factor between the receiving room and the wave type w which can be written as:

$$\eta_{21,w} = \eta_{23,w} = \frac{\rho c\sigma_{rad,w}}{\rho_s\omega} \tag{2.14}$$

Where ρ is the acoustic medium density of the room. The total acoustic energy of the source room can be written as:

$$E_1 = \frac{\langle p_1^2\rangle V}{\rho c^2} \tag{2.15}$$

A generally acceptable approximation for the modal density of the source room is made as:

$$n_1 = \frac{V_1\omega^2}{2\pi^2c^3} \tag{2.16}$$

then the modal energy of the source room can be written as:

$$\frac{E_1}{n_1} = \frac{2\pi^2c\langle p_1^2\rangle}{\rho\omega^2} \tag{2.17}$$

Using the SEA reciprocity rule again, the power flow from the composite panel to the receiving room can be written as:

$$P_{23,w} = \omega\eta_{23,w}n_{2,w}\left(\frac{E_{2,w}}{n_{2,w}} - \frac{E_3}{n_3}\right) = \omega\eta_{23,w}\left(E_{2,w} - \frac{E_3n_{2,w}}{n_3}\right) \tag{2.18}$$

It is hereby assumed that $n_3 >> n_{2,w}$ (reasonable for typically sized cavities and especially for medium and high frequencies) and it is also logical that $E_{2,w} > E_3$ for an acoustically efficient, out of plane wave. Therefore presuming that $E_{2,w} >> \frac{E_3n_{2,w}}{n_3}$, eq.(2.18) can be written as:

$$P_{23,w} = E_{2,w}\omega\eta_{23,w} \tag{2.19}$$

Eventually, after manipulating eq.(2.9) and eq.(2.11)-(2.19) and substituting them into eq.(2.10) we get:

$$\frac{\langle v_w^2\rangle}{\langle p_1^2\rangle} = \frac{2\pi c^2\sigma_{rad,w}n_{2,w}}{\rho_s\omega^2A(\rho_s\omega\eta_{2,w} + 2\rho c\sigma_{rad,w})} \tag{2.20}$$

Using eq.(2.12),(2.14),(2.19),(2.20),(2.9) and substituting them into eq.(2.8) we get the expression for the transmission coefficient of the wave type w:

$$\tau_w = \frac{8\rho^2c^4\pi\sigma_{rad,w}^2n_{2,w}}{\rho_s\omega^2A(\rho_s\omega\eta_{2,w} + 2\rho c\sigma_{rad,w})} \tag{2.21}$$

Table 2.1: *Mechanical properties of materials*

Material I	Material II	Material III	Material IV	Material V	Material VI	Material VII
$\rho = 9740$ kg/m^3	$\rho = 1600$ kg/m^3	$\rho = 160$ kg/m^3	$\rho = 1550$ kg/m^3	$\rho = 110.44$ kg/m^3	$\rho = 629.9$ kg/m^3	$\rho = 16$ kg/m^3
$v_{xy} = 0.028$	$v_{xy} = 0.15$	$v_{xy} = 0.15$	$v_{xy} = 0.3$	$v_{xy} = 0.45$	$v_{xy} = 0.15$	-
$E_x = 2023.7$ GPa	$E_x = 49$ GPa	–	$E_x = 48$ GPa	$E_x = 0.1448$ GPa	$E_x = 8.3$ GPa	$E_x = 0.0083$ GPa
$E_y = 31375$ GPa	$E_y = 49$ GPa	–	$E_y = 48$ GPa	$E_y = 0.1448$ GPa	$E_y = 8.3$ GPa	$E_y = 0.0083$ GPa
$G_{xy} = 888.79$ GPa	–	–	$G_{xy} = 18.1$ GPa	$G_{xy} = 0.05$ GPa	-	$G_{xy} = 0.0031$ GPa
$G_{yz} = 888.79$ GPa	–	$G_{yz} = 0.09$ GPa	$G_{yz} = 2.76$ GPa	$G_{yz} = 0.05$ GPa	-	$G_{yz} = 0.0031$ GPa
$G_{xz} = 888.79$ GPa	–	$G_{xz} = 0.14$ GPa	$G_{xz} = 2.76$ GPa	$G_{xz} = 0.05$ GPa	-	$G_{xz} = 0.0031$ GPa

The total transmission coefficient of the panel τ can now be written as:

$$\tau = \sum_{w=a}^{n} \tau_w + \frac{P_{13}}{P_{inc}} \qquad (2.22)$$

The non resonant transmission coefficient $\tau_{nr} = P_{13}/P_{inc}$ for a diffused acoustic field can be written as in [Ghinet and Atalla, 2006]:

$$\frac{P_{13}}{P_{inc}} = \frac{\int_0^{2\pi} \int_0^{\theta_{max}} \dfrac{4Z_0^2 \sigma(\theta,\phi,\omega)\sin\theta\cos^2\theta}{|i\omega\rho_s + 2Z_0|^2} \mathrm{d}\theta \mathrm{d}\phi}{\pi(1 - \cos^2\theta_{max})} \qquad (2.23)$$

in which θ and ϕ are the incidence angle and the direction angle of the acoustic wave respectively, and $Z_0 = \rho c / \cos\theta$ is the acoustic impedance of the medium. The term θ_{max} stands for the maximum incidence angle, accounting for the diffuseness of the incident field. It is considered that $\theta_{max} = pi/2$ for all the results presented in the current work. The term $\sigma(\theta,\phi,\omega)$ is the corrected radiation efficiency term. It is used in order to account for the finite dimensions of the panel by accounting for the radiation of the mass controlled non-resonant modes, and it is calculated using a spatial windowing correction technique presented in [Allard, 1993]. In eq.(2.22) the total transmission coefficient of the layered panel is expressed merely as a function of its SEA quantities and independently of the room dimensions and modal energies.

2.5   Numerical examples

In this section numerical applications of the approach described above will be presented. In order to validate the proposed models, four structures were chosen to be computed; the first being a thin stratified orthotropic composite panel. Subsequently, two honeycomb sandwich structures as well as a particularly thick sandwich panel comprising a soft core are modelled. It should be noted that experimental results for the response of layered panels under a reverberant acoustic field are rare to find in the open bibliography. Consequently, the available options of composite structures to be modelled while concurrently having test data to compare with were not a lot. The mechanical static characteristics of each material used for the validation process are mentioned in Table 2.1, in which ρ is the density of the material, E_i the Young modulus in direction i, G_{ij} stands for the shear modulus in direction j on the plane whose normal is in direction i and v_{ij} for the Poisson's ratio that corresponds to a contraction in direction j when an extension is applied in direction i. The extraction of the FE matrices for each structural segment was carried out using a commercial FE software package, the eigenproblems were solved within a commercial mathematics software package and the results were then post processed as described in sec.2.3.2.
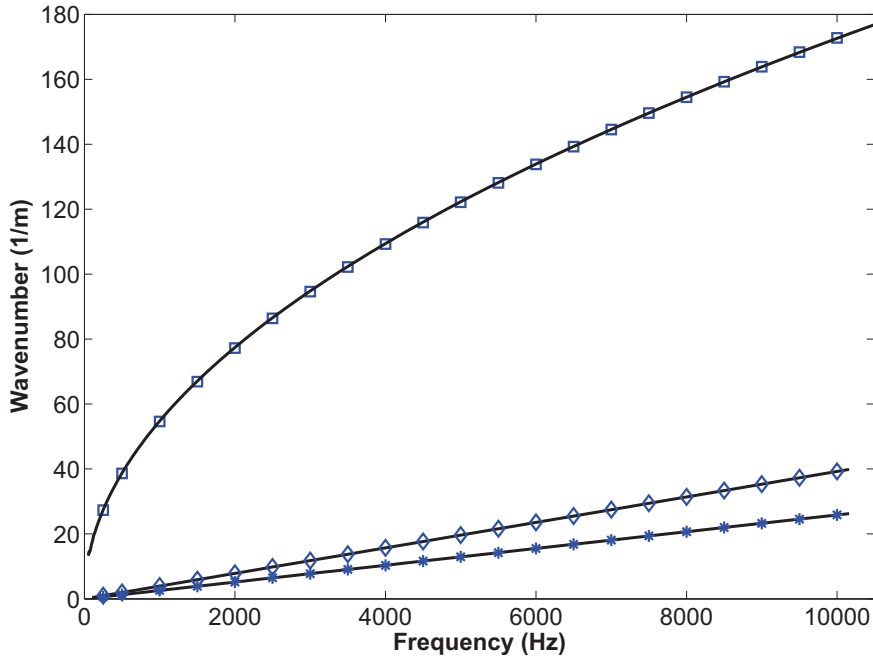
Figure 2.4: *Comparison of the WFEM calculated dispersion curves (–) with CPT analytical formulas for: flexural (□), shear (◇) and membrane (∗) propagating wavenumbers for a thin orthotropic panel*

2.5.1 Validation on an orthotropic thin monolithic structure

The wavenumbers for the bending, shear and membrane wave types were identified for a thin, stratified type structure for propagation towards x direction. The panel is made of material I. Its thickness is equal to h=0.5mm and its dimensions are 1.4m x 0.9m. The resulting dispersion curves are presented in fig.2.4, and the results are compared with the CPT analytic solutions (see [Graff, 1991]). Excellent accordance is observed for the shear and the membrane wave types. Concerning the flexural wave type, the WFE predictions are very much in agreement with the analytical formula even for the high frequency range. To give an idea for the discrepancy between the two models, a difference of 0.09% is observed at $10kHz$. Under an acoustic excitation, antisymmetric wave modes are responsible for the transmission of the vast majority of energy through the structure, therefore they will be the main wave type to be considered in the SEA analysis.

The flexural wavenumbers are presented as a function of direction and frequency in fig.2.5. The directional dependence of the wavenumber within a highly orthotropic panel is observed. It is known that each mode of the panel corresponds to an exact set of wavenumbers depending on the panels boundary conditions. For a simply supported panel this set is: $k_x = m\pi/L_x$ and $k_y = n\pi/L_y$ where m, n are integers and L_i the length and width of the panel. Eventually, with the dispersion characteristics of the structure known for every direction of propagation, the frequency of occurrence and the corresponding wavenumbers for each mode can be found by interpolating the values in fig.2.5.

The modal density of the monolithic orthotropic panel is subsequently calculated using the antisymmetric wave propagation characteristics presented in fig.2.5 and eq.(2.4). Small discrepancies are observed between the values calculated using the WFEM and the CPT because of the fact that the latter approach does not account for the shear effects within the laminate. As expected, the two predictions are very similar for the low frequency range. The largest divergence for the
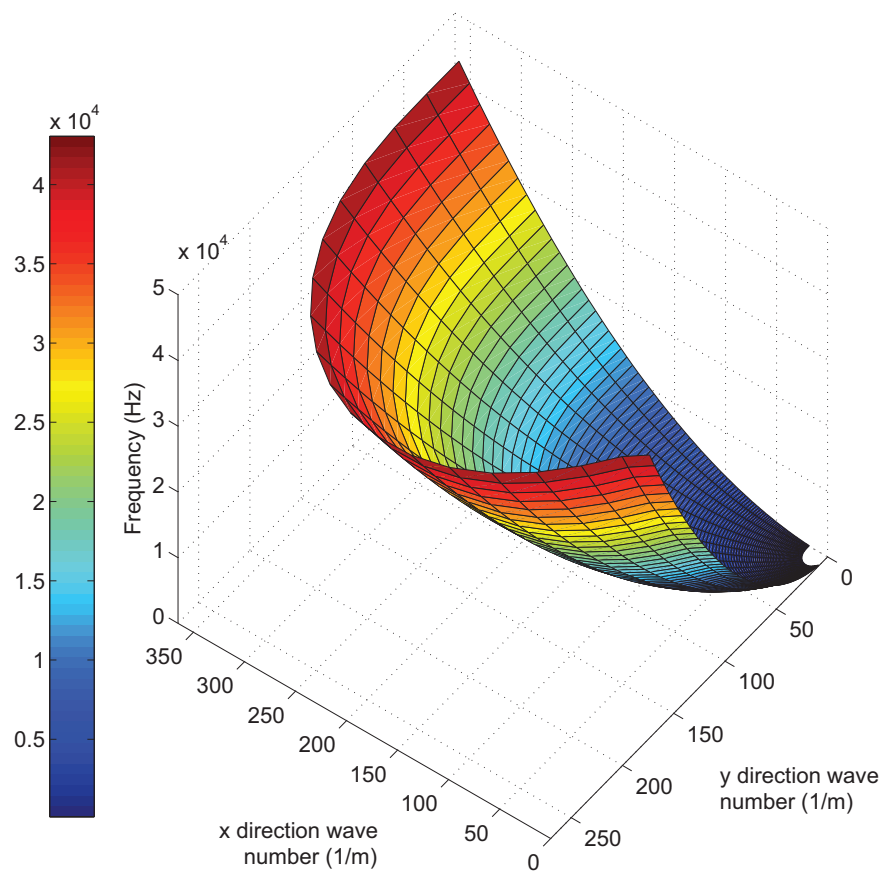
Figure 2.5: *3-dimensional view of the bending propagating wavenumbers within the stratified structure as a function to direction of propagation and frequency*
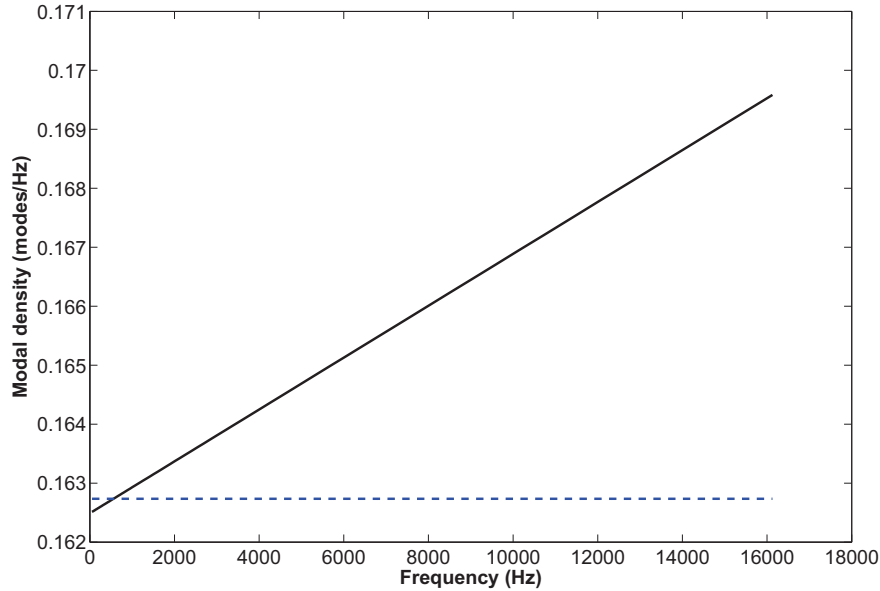
Figure 2.6: *Comparison of the predicted modal density for a monolithic panel: present approach (–), CPT (- -)*

two predictions is 4.1% and is observed at the highest frequency range of the analysis. It is seen that taking into account for the shear effects within the laminate becomes important as frequency increases.

The radiation efficiency of the monolithic orthotropic panel is calculated using the Leppington's asymptotic and transition formulas. The results are shown in fig.2.7. The beginning of the coincidence range (approximately 2kHz) is marked by an intensive increase of the radiation efficiency, which continues rising steadily throughout the coincidence region. The end of the coincidence range (approximately 9.5kHz) is marked with a peak of the radiation efficiency curve. Fluctuations of the curve throughout the coincidence range were expected and are discussed in [Leppington et al., 1982]. The individual modal radiation efficiencies are also calculated using the formulas given in [Wallace, 1972] and presented in the same figure. Each mode is separately attributed to a different category depending on its individual characteristics namely the directional wavenumbers k_x and k_y and its occurrence frequency. It can be clearly observed that the corner modes are the less radiating ones, while the surface modes are the most efficient with regard to sound radiation. The frequency average of the modal radiation values is calculated using the relations presented in [Anderson and Bratos-Anderson, 2005]. The result is presented in the same figure. Very good agreement is observed comparing with the calculations.

The STL of the orthotropic thin panel under a reverberant acoustic field is presented in fig.2.8. On the same figure experimental data for the same quantity, published in [Leppington et al., 2002] are shown. The results of an asymptotic TL calculation model presented in [Leppington et al., 2002] are also compared in the same figure. Excellent agreement between the experimental and predicted results is observed for the sub-coincident frequency range as well as for the whole coincidence range. The radiation efficiency is not overestimated -in contrast to the asymptotic model- at the beginning of the coincidence area. The fluctuations of the TL curve throughout the coincidence range are due to the radiation efficiency formulas used and are discussed in [Leppington et al., 1982]. A structural loss factor equal to 0.01 is used. The discrepancy between the numerical prediction and the experimental results at the end of the coincidence range can either be attributed to an overestimation of the radiation efficiency or to a higher structural damping coefficient (probably
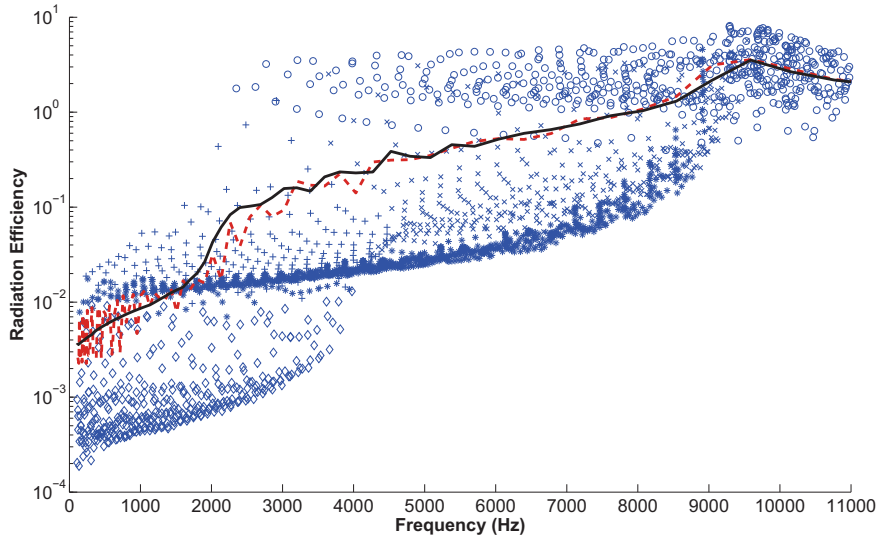
Figure 2.7: *Comparison of the radiation efficiency of a monolithic orthotropic panel using: the present methodology (−), modal radiation formulas in [Wallace, 1972] (surface modes 'o', x-edge modes '+', y-edge modes '*', x-y edge modes 'x', corner modes '⋄'), frequency averaged radiation efficiency according to [Anderson and Bratos-Anderson, 2005] (- -)*

due to large deflections) for the panel in this frequency range. Fast convergence of the predicted values towards the experimental data is observed in the post-coincident frequency range.

2.5.2   Validation on honeycomb sandwich panels

A sandwich panel is subsequently considered. It comprises a core made of material V and facesheets made of material IV. The thickness of the core is equal to 12.7mm while the thickness of the facesheets is equal to 1.2mm. The dimensions of the panel are equal to 1.37m x 1.65m. The calculated antisymmetric wavenumbers of the panel in x direction are presented in fig.2.9. The results in [Ghinet and Atalla, 2006] for the same panel using a LW approach are exhibited in the same figure and are in excellent agreement with the presented approach. The frequency ranges of the dynamic behaviour of the sandwich panel are clearly distinguished (see also [Wang et al., 2010]). A low-frequency region where the panel vibrates as a whole, an intermediate region where the shear stiffness of the panel dominates its vibrational behaviour and a high-frequency region where the flexural wavenumber for the panel is converging to the wavenumber of each facesheet vibrating separately, loaded with half of the core mass. The dispersion relation predicted by a Mindlin type model proposed for thick sandwich panels in [Renji et al., 1997] which takes into account the shear deformation of the panel is depicted in the same figure. The Mindlin theory diverges quickly when the sandwich panel enters the shear deformation dominated region. As a result a misguiding coincidence frequency for the antisymmetric wave ($f_{c1} = 560$Hz) is predicted, which is far from the one predicted by the WFEM ($f_{c1} = 1190$Hz). At higher frequencies the Mindlin model further diverges, having a difference of 250% at 40kHz. The asymptotic Kurtze and Watters (KW) model implemented as presented in [Davis, 1999] is also shown in the same figure. It is seen that the KW prediction agrees asymptotically with the WFEM model, with the three regions of the panel clearly distinguished. However discrepancies between the two models occur at the transition regions of the KW model.

In order to validate the WFEM predicted values for the modal density of a sandwich panel, a structure presented in [Zhou and Crocker, 2010] was modelled. It comprises a honeycomb foam
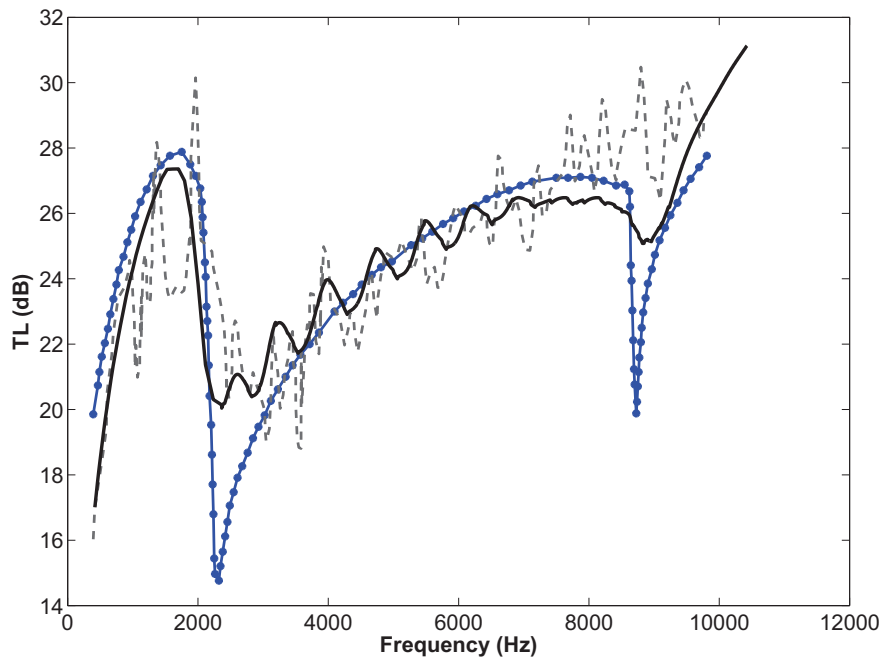
Figure 2.8: *Comparison of the diffused field TL of an orthotropic thin panel: present methodology (−), model in [Leppington et al., 2002] (∗), experimental results in [Leppington et al., 2002] (--)*
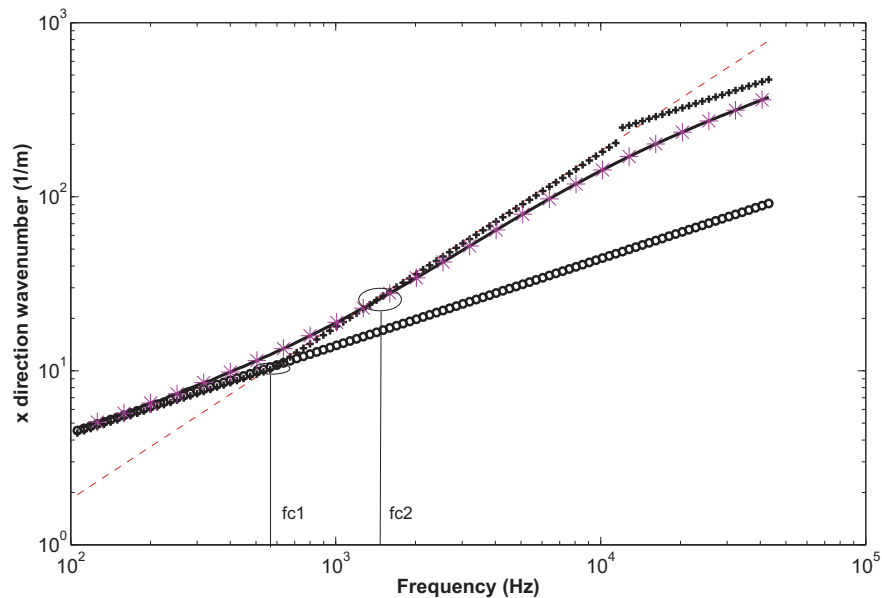
Figure 2.9: *Comparison of the wavenumber in x direction for a sandwich panel: present methodology (−), results in [Ghinet and Atalla, 2006] (∗), a Mindlin type model (o), Kurtze-Watters model (+), acoustic wavenumber (--)*
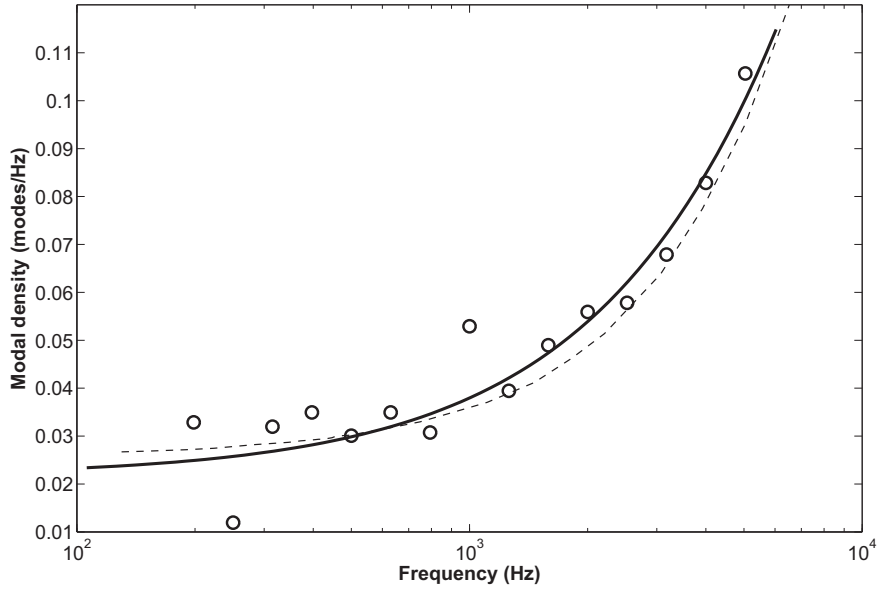
Figure 2.10: *Comparison of the predicted modal density for a sandwich panel: present approach (−), model in [Clarkson and Ranky, 1983] (- -), experimental results in [Zhou and Crocker, 2010] (o)*

core made of material III and facesheets made of material II. The thickness of the core is equal to 6.35mm while the thickness of the facesheets is equal to 0.5mm. The dimensions of the panel are equal to 1.12m x 0.62m, but were reduced to 0.84m x 0.42m when the panel was fixed to the baffle. The results of the modal density are shown in fig.2.10. An excellent agreement between the calculations and the experimental measurements is observed. Within the lower frequency range the present approach seems to correctly predict the mean value around which the measured modal density is dispersed.

The radiation efficiency of the honeycomb foam core sandwich is calculated using the same set of asymptotic formulas as before and is compared to the predictions of the Crocker's model and the experimental data presented in [Zhou and Crocker, 2010]. It is observed that the Leppington's formula combined with the WFEM predictions leads to more accurate results in a broadband frequency range. Furthermore, the used set of formulas does not overestimate the radiation efficiency of the panel at the coincidence range.

Furthermore, the diffused field STL of the foam filled honeycomb sandwich structure is calculated. The result is depicted in fig.2.12 along with experimental data presented in [Zhou and Crocker, 2010]. The results demonstrate a very good correlation. The low-frequency response seems to be very well simulated. The coincidence frequency band is very well predicted and above coincidence discrepancies of less than 2dB are observed between the experimental results and the SEA models. Higher experimental STL values around the coincidence frequency are probably due to an increase of damping for the panel. In the same figure the results of the SEA model presented in [Zhou and Crocker, 2010] are also shown. The discrepancies between the two SEA models are due to the better prediction of the radiation efficiency by the current approach and the spatial windowing correction hereby used. Above coincidence, the results of the two SEA models are very well correlated.
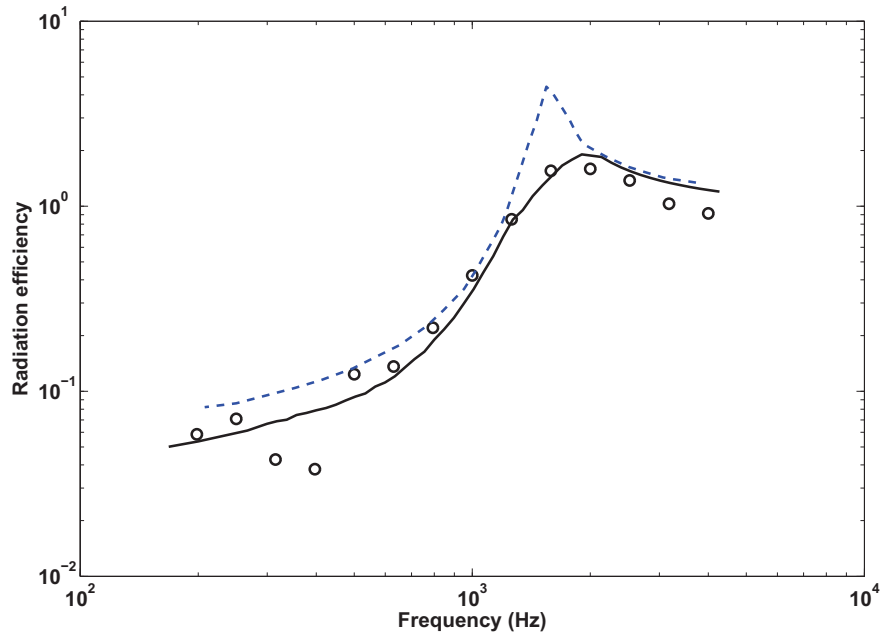
Figure 2.11: *Comparison of the predicted radiation efficiency for a sandwich panel: Leppington's set of formulas (−), model in [Zhou and Crocker, 2010] (- -), experimental results in [Zhou and Crocker, 2010] (o)*
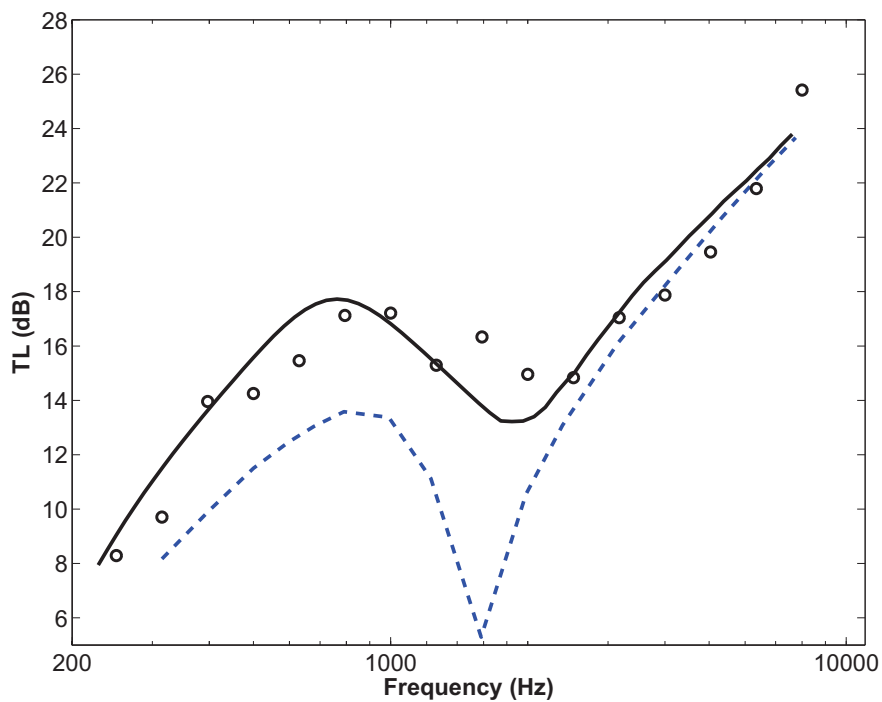
Figure 2.12: *Comparison of the diffused field TL of a sandwich panel: present methodology (−), model in [Zhou and Crocker, 2010] (- -), experimental results in [Zhou and Crocker, 2010] (o)*
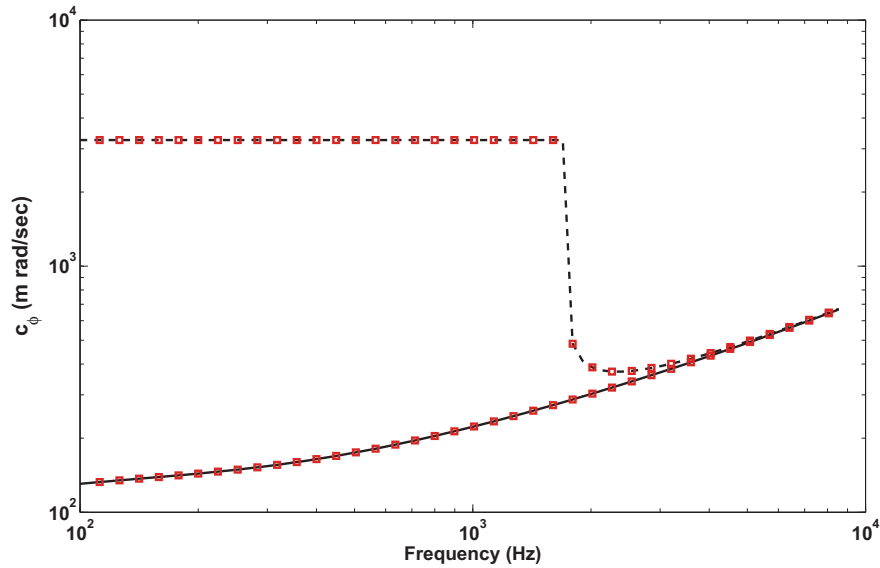
Figure 2.13: *Predicted wavenumbers for the out of plane motion of the thick panel: WFEM anti-symmetric (–), WFEM symmetric (- -), results in [Wang et al., 2010] (□)*

2.5.3   Validation on a thick layered panel

For layered panels comprising a thick and soft core, the dilatational motion of the soft layer (also referred to as symmetric motion) can contribute significantly to the resonant acoustic transmission of the panel (see [Dym and Lang, 1974]). In order to exhibit the robustness of the presented approach considering the modelling of arbitrarily thick panels a sandwich structure comprising a 38.1mm core made of material VII, coupled to 6.35mm thick facesheets made of material VI is hereby modelled. The WFEM computed phase velocities for the propagating, out of plane wave motions are shown in fig.2.13 and are compared to predictions of an analytic HSDT derived model, presented in [Wang et al., 2010]. Excellent correlation is observed between the two predictions.

A cut on frequency is observed for the symmetric motion above which the wave starts propagating within the panel. Below this cut on frequency the dilatational motion is not expected to influence the transmission coefficient of the panel due to the particularly low modal density of the wave mode. A lock-up of the symmetric and the antisymmetric wave motion is observed for higher frequencies. The total transmission coefficient of the panel is calculated using eq.(2.22) and the STL of the structure is exhibited in fig.2.14 along with experimental results provided in [Wang et al., 2010].

Very good correlation between the computed values and the measurements is observed below the coincidence range. It is noted that the acoustic coincidence frequency for the antisymmetric motion of the panel occurs at 2900Hz. At 2000Hz the impact of the dilatational motion of the panel on its TL becomes evident with the values presenting a sudden decrease of 14dB at the cut on frequency of the symmetric wave. The coincidence range is extended up to 3000Hz because of the antisymmetric coincidence phenomenon and because of the fact that the symmetric phase velocity remains very close to the one of the acoustic medium. A closer look to the contribution of each acoustic transmission path to the total transmission coefficient is shown in fig.2.15.

The mass controlled phenomena dominate the low frequency range of the total transmission coefficient. Approaching the coincidence range, the resonant contribution becomes the most important one. The symmetric motion of the panel dominates its acoustic transmission at the dilata-
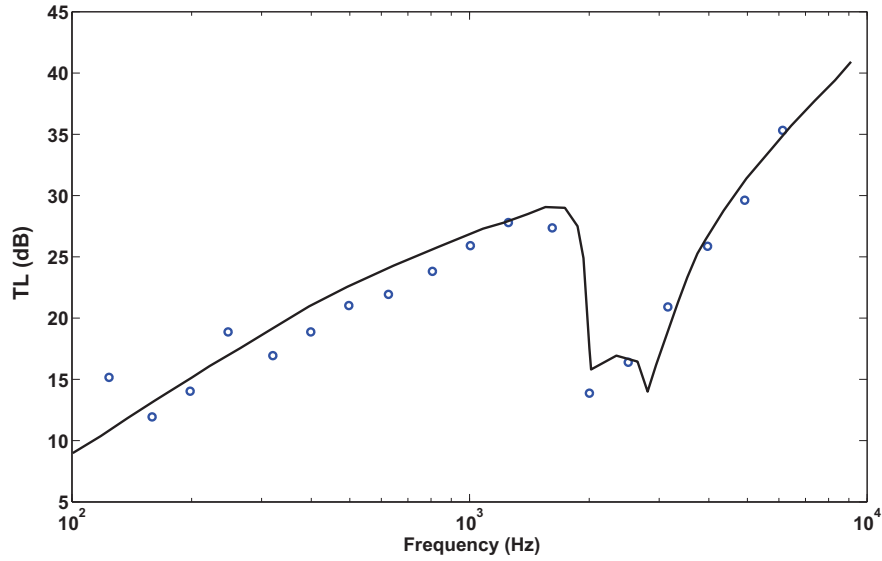
Figure 2.14: *Comparison of the diffused field TL of the thick sandwich panel: present approach (−), experimental results in [Wang et al., 2010, Narayanan and Shanbhag, 1982] (o)*
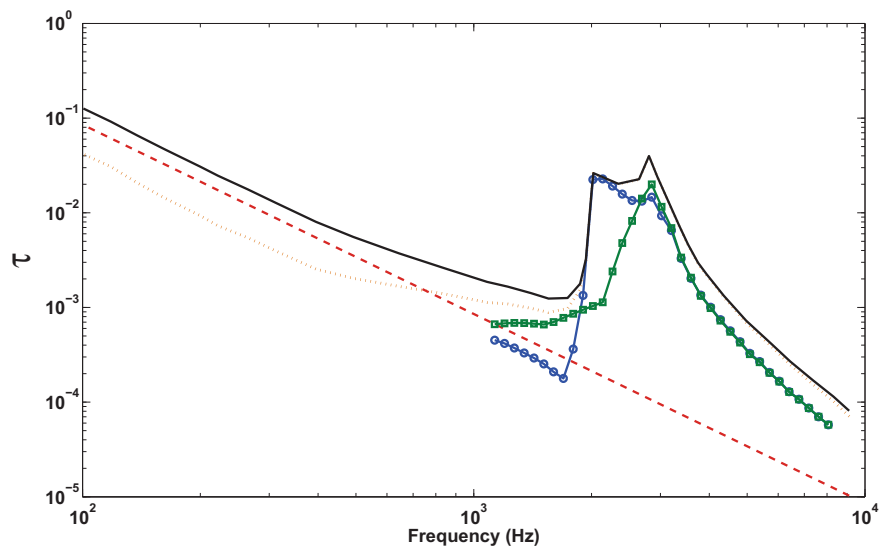
Figure 2.15: *Contribution of each transmission path to the transmission coefficient of the panel: total transmission coefficient (−), non-resonant transmission coefficient (- -), resonant transmission coefficient (· · ·), symmetric motion transmission coefficient (o), antisymmetric motion transmission coefficient (□)*
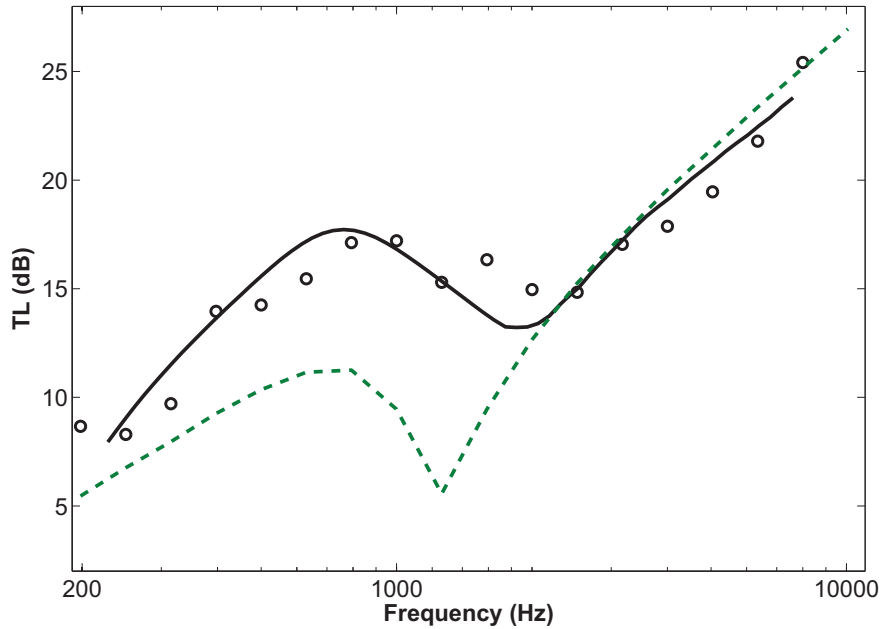
Figure 2.16: *Comparison of the diffused field TL of a sandwich panel: present methodology (–), SEALASCAR prediction (--), experimental results in [Zhou and Crocker, 2010] (o)*

tional motion cut on, while close to the antisymmetric coincidence frequency both wave motions contribute to the transmission. In the post coincidence frequency range the contribution of the two wave motions is almost equal due to fact that the corresponding phace velocities are very close. It is therefore shown that thick and heavy layers do not always reduce the acoustic transmission of a panel because of the fact that they also reduce its dilatational cut on frequency. It is observed that the effect of the symmetric motion on the acoustic transparence of a panel may not be neglected. Care has to be taken therefore when designing an insulating structure for the existence of more than one out of plane propagating wave modes.

2.5.4   Comparison to SEALASCAR predictions

The software daily used for high frequency vibroacoustic computations within EADS Astrium is SEALASCAR. It makes use of analytical formulas for the calculation of the SEA CLF of thin and layered panels. The STL of the sandwich panel presented above is modelled using SEALASCAR and the predictions are compared to the presented approach and to experimental results in fig.2.16.

It is observed that in the high frequency range the response of the panel is correctly modelled. Slight discrepancies are due to the different estimations on the modal density of the panel. It is clear however that the coincidence frequency of the structure is not well predicted using classic analytic formulas. As in fig.2.12, the Crocker radiation efficiency model overestimates the radiation efficiency of the panel in the acoustic coincidence range, resulting in very low STL values. In the lower frequency range SEALASCAR again underestimates the STL of the panel mainly because it does not take into account for the panel's finite dimensions.

2.6 The impact of temperature on the vibroacoustic response of layered panels

2.6.1 Introduction

An aerospace structure operates within a broad temperature range, typically varying between -100 ^oC to 200 ^oC for launch vehicles. With regard to aircrafts, their mission usually involves narrower temperature ranges (typically -60 ^oC to +50 ^oC) as is the case for automotive structures. A very little amount of research (to the best of the author's knowledge) has been conducted on predicting the effect of temperature on the vibrational behaviour of layered structures. Hereby an attempt is made in order to exhibit the sensitivity of the vibroacoustic behaviour of the previously considered system to the ambient flight temperature.

The mechanical characteristics of a sandwich panel are experimentally measured using a Thermal Mechanical Analysis (TMA) configuration. The TMA measured modula are injected in a WFEM model in order to predict the temperature dependent wave propagation characteristics of the sandwich panel. These characteristics are validated by the results of an experimental FRF analysis of the entire sandwich panel for various temperatures. Initially the system will be considered to be laying on the sea level. In this case temperature has significant influence on the mechanical characteristics of the panel, the density of the acoustic medium and the celerity of sound. The effect of the modification of these parameters on the TL of the structure will be investigated. Subsequently the structure will be considered to operate at an altitude greater than zero. In this case the modified system parameters have to be expressed as a function of altitude, in order to compute the altitude dependent TL of the layered panel.

2.6.2 Accounting for temperature dependent parameters

An orthotropic sandwich panel is hereby considered. Its facesheets are made of a 1mm thick carbon epoxy composite comprising four layers of 1-1 twilled weaves. Its core is made of an orthotropic 12.7mm thick Nomex honeycomb material. The technique used for the panel's fabrication is to impregnate the carbon fabric within the resin, then drape it over the mold, add the honeycomb and then put the system in vacuum. The polymerization takes place at all parts at the same time and the honeycomb absorbs some of the resin included in the tissues and thus adheres thereto. The same kind of resin therefore serves as the facesheets matrix and as an adhesion agent. The mechanical characteristics of the panel are exhibited in Table 2.2. Its facesheets are made of material I, while its core is made of material II.

Table 2.2: *Mechanical properties of materials*

Material I	Material II
$\rho = 1410$ kg/m^3	$\rho = 48$ kg/m^3
$E_x = 54$ GPa	$E_x = 85$ MPa
$E_y = 54$ GPa	$E_y = 85$ MPa
$v_{xy} = 0.09$	$v_{xy} = 0.23$
$G_{xy} = 8.5$ GPa	$-$
$-$	$G_{yz} = 44$ MPa
$-$	$G_{xz} = 24$ MPa

A segment of the panel is used to measure its temperature dependent characteristics at the TMA device. A constant 1Hz motion is selected for all the TMA measurements. A 0.1% deformation
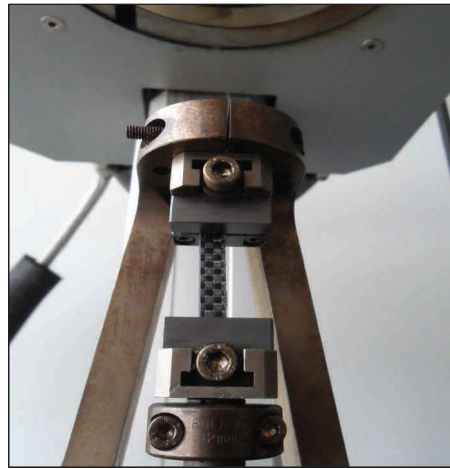
Figure 2.17: *Aspect of the facesheet clamped in the TMA machine*

was imposed as displacement to the segment during the tests. Initially a longitudinal traction test of the facesheet of the structure was conducted (see fig.2.17). The dissipation of the segment is measured by the phase lag between stress and strain δ for which we have $\tan \delta = E''/E'$, with E'' the Loss modulus and E' the Storage modulus. The results are shown in fig.2.18. It is noted that the measurements were conducted in a temperature range of -10 ^{o}C to 160 ^{o}C due to the limits of the apparatus used. Results for temperatures below -10 ^{o}C are extrapolated assuming smooth quadratic expansion of the curves which is generally acceptable for composite materials having no significant transitions (e.g crystallization) in their structure at low temperatures. It is observed that a smooth nearly linear behaviour with regard to both the Young modulus and the $\tan(\delta)$ is observed up until 90 ^{o}C. Thereafter the resin included in the structure enters its glass transition region (see [Angell, 1988]). A high peak is observed for the dissipation of the material, typical for most materials in the glass transition range. The Young modulus is also decreased by 45% in the range of 90 ^{o}C to 110 ^{o}C. After the glass transition region the Young modulus keeps decreasing with a steady rate, while the $\tan(\delta)$ quantity after a short decrease starts increasing again due to the high viscosity of the melting resin.

In order to measure the temperature dependent shear modulus of the honeycomb core the configuration shown in fig.2.19 was adopted. An aluminium layer was adhered to the facesheets of the segment in order for the elasticity of the later (especially after the glass transition range) not to affect the measured results on the shear deformation of the segment. Traction forces were applied to opposite facesheets of the panel, allowing for deforming the core shear-wise. The obtained results are shown in fig.2.20. A similar behaviour is observed as with the facesheet measurements. As aforementioned the same type of resin is used for forming the facesheets and as an adhesive agent between the facesheets and the core, therefore the glass transition of the resin is responsible for the decrease of the shear modulus of the core. An overall decrease of 38% of the shear modulus is observed throughout the glass transition range.

Temperature has a severe impact on the characteristics of the acoustic medium which directly influences the radiation efficiency and therefore the TL of the panel. A constant 50% humidity factor is considered. The system is initially considered at a sea level altitude. Relations between temperature and the density ρ_0 as well as the celerity c_0 of the acoustic medium can be found in the open bibliography such as in [Everest, 1994]. The temperature dependent characteristics of the acoustic medium that will be taken into account during the following calculations are exhibited in fig.2.21
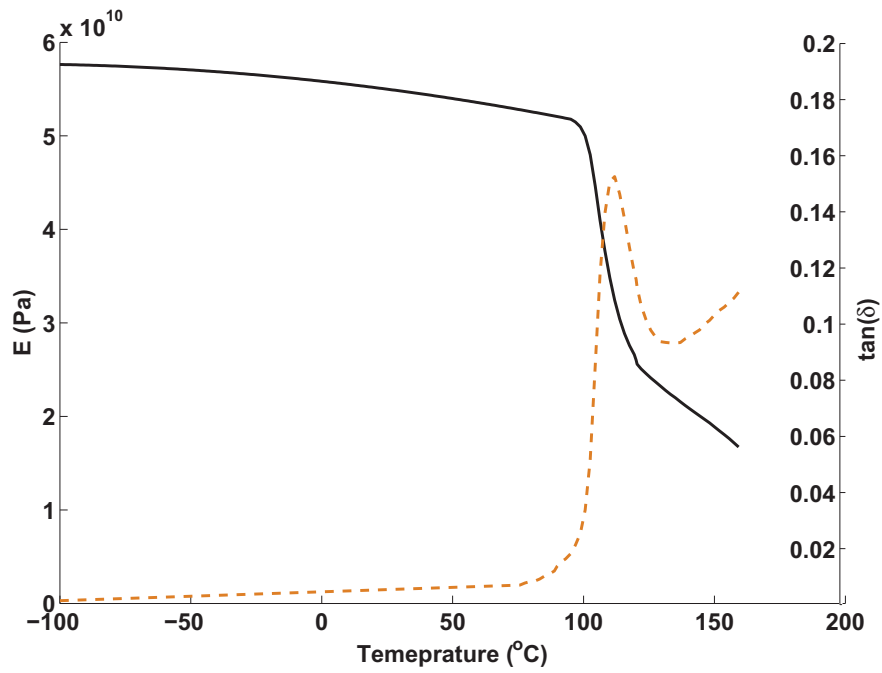
Figure 2.18: *Experimentally obtained temperature dependent Young modulus and the corresponding tan(δ) for the facesheet of the sandwich panel: Young modulus (–), tan(δ) (--)*

Figure 2.19: *Aspect of the core shearing configuration clamped in the TMA machine*
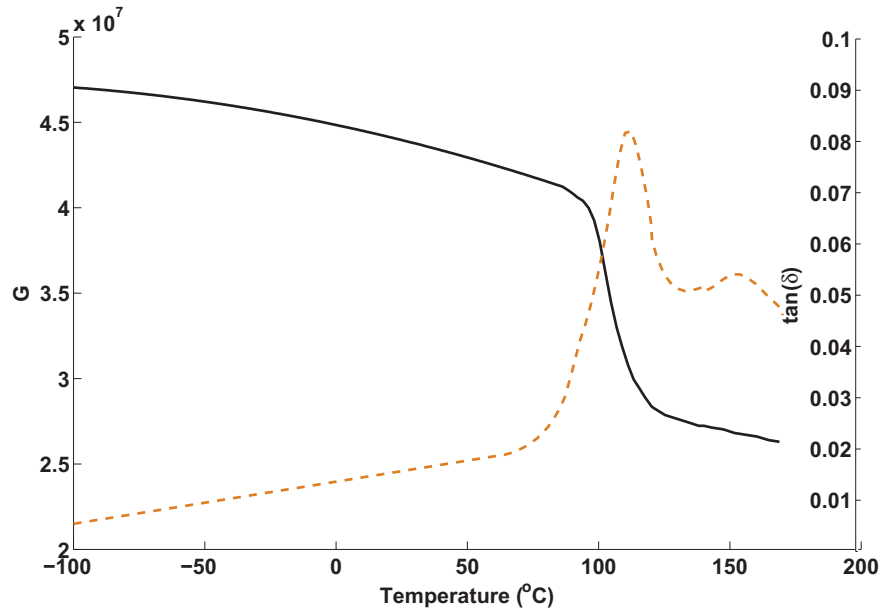
Figure 2.20: *Experimentally obtained temperature dependent shear modulus and the corresponding tan(δ) for the core of the sandwich panel: shear modulus (−), tan(δ) (--)*
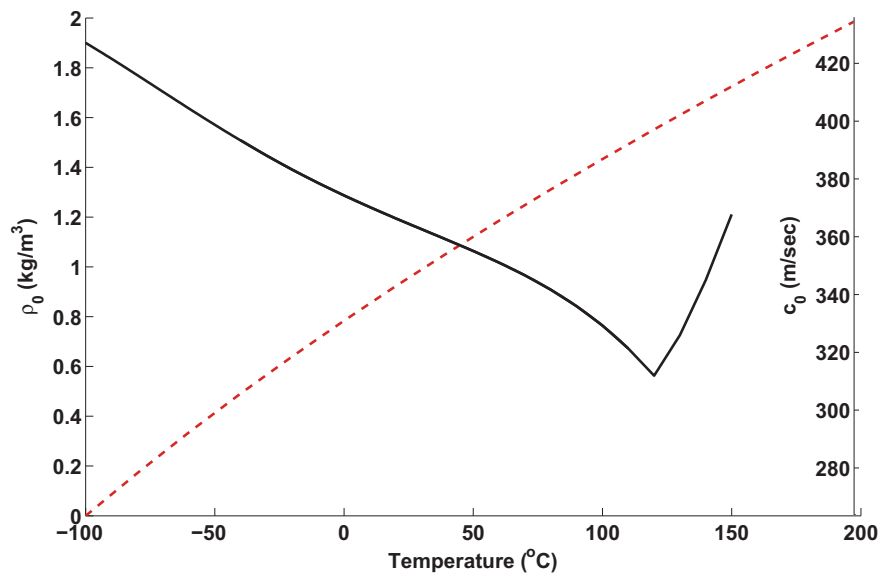
Figure 2.21: *The temperature dependent density and celerity of the acoustic medium: ρ_0 (−), c_0 (--)*
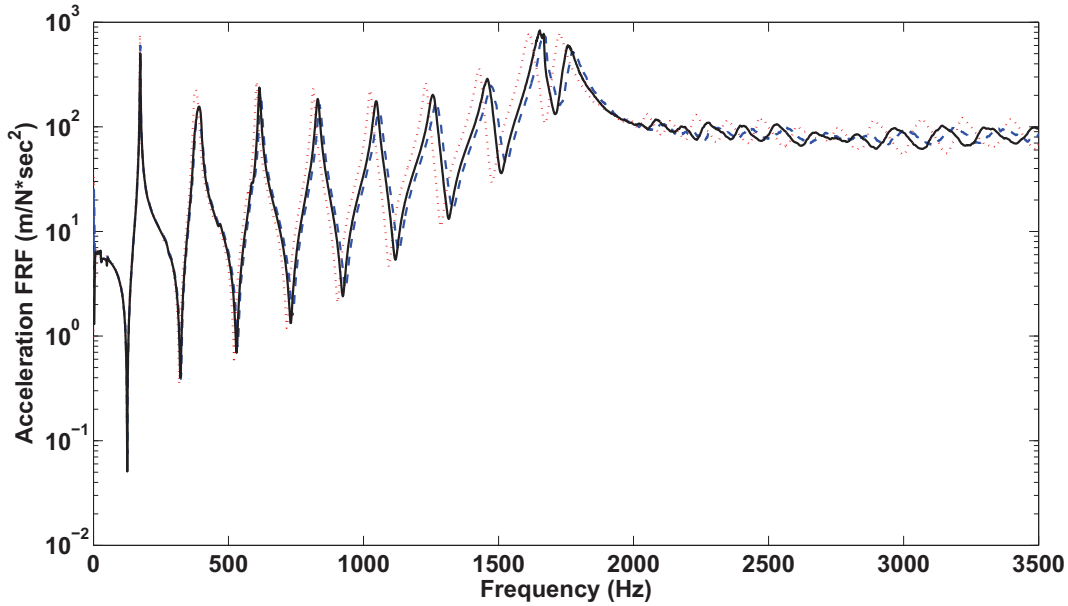
Figure 2.22: *Experimentally obtained acceleration FRF of the sandwich panel for different temperatures: 10 ºC (--), 25 ºC (–), 47 ºC (···)*

2.6.3   Experimental validation of the WFEM predictions

The TMA measured quantities can be injected in a WFE model of the sandwich panel in order to predict its temperature dependent wave dispersion characteristics. In order to validate the WFEM results the sandwich panel is freely suspended in a climatic test chamber and is excited with a pseudo-random broadband noise. Further details on the experimental procedure as well as the calculation of the experimental structural wavenumbers through the measured natural frequencies of the panel in discussed in sec.3.5. The temperature in the test chamber is initially regulated at its extreme low at 10 ºC, then at 25 ºC and finally at its upper limit at 47 ºC. The results of the acceleration FRF at the excitation point for the three different temperatures are shown in fig.2.22.

It is observed that for the very low frequency range, the results are very similar and the flexural stiffness presents no significant differences with respect to temperature. For higher order modes however, it seems that the 'cold' panel presents a greater damping coefficient compared to the 'hot' one. It is also observed that the same modes occur at lower frequencies for the 'hot' panel, suggesting a lower flexural stiffness as proposed by the TMA results. It is noted as an example that the seventh flexural mode occurs at 1470Hz with a damping ratio equal to 2.1% for the panel at 10 ºC, while the same mode occurs at 1425Hz with a damping ratio equal to 1.4% for the panel at 47 ºC. The growing damping difference of the 'hot' and the 'cold' panel with respect to frequency, suggests a higher radiation efficiency for the 'cold' panel, which will be verified later in this section. The same observations are valid for the higher frequency range. It is evident that these differences will be even greater for real aerospace structures which are exposed to larger temperature variations during their operation cycle.

Subsequently, the WFEM results calculated using the TMA measured values are compared to the experimental flexural wavenumbers as derived by fig.2.22. The comparison is exhibited in fig.2.23. A very good correlation is observed between the WFEM and the experimentally measured wavenumbers for all the three temperatures. It is clearly shown that the difference between the wavenumbers increases with frequency reaching 3.3% at 1800Hz between 10 ºC and 47 ºC. It is evident that this difference will be much greater for higher frequencies and larger temperature
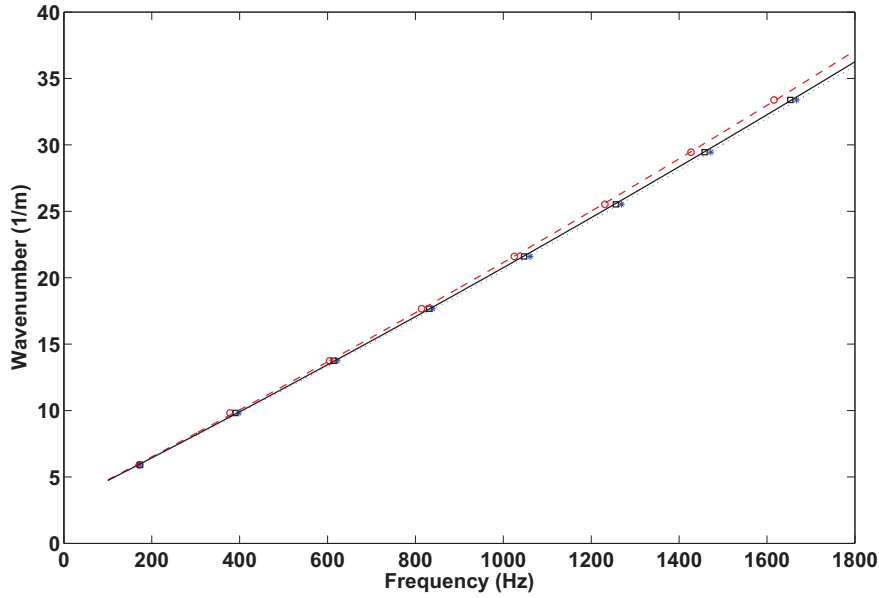
Figure 2.23: *Comparison between the experimental and the WFEM predicted wavenumbers of the sandwich panel: experimental 10 ºC (∗), 25 ºC (□), 47 ºC (O), WFEM 10 ºC (⋯), 25 ºC (–), 47 ºC (--)*

ranges.

In order to more accurately exhibit the correlation between the experimental and the WFEM results, the predicted resonance frequencies for the (7,0) and the (8,0) modes of the panel are shown in fig.2.24 for the three tested temperatures. The observed divergencies between the WFEM and the experimental results vary from 0.2% to 0.3%. Very good agreement is therefore observed.

2.6.4 The influence of temperature on the modal density of the panel

In order to exhibit the effect of ambient temperature on the SEA quantities of a panel, the already calculated sandwich panel used in sec.2.5.2 is hereby considered. The same panel will be used for calculating its temperature dependent loss factor, radiation efficiency and TL. The evolution of the mechanical characteristics of its facesheets and core with respect to temperature is considered to be analogous to the TMA measurements shown in fig.2.18, 2.20. The wave dispersion characteristics of the panel are calculated using the WFEM for five temperatures: -100 ºC, 25 ºC, 90 ºC, 110 ºC and 160 ºC. The modal density for the flexural modes of the panel is computed using eq.(2.4) and the results are presented in fig.2.25.

It is observed as expected that the modal density increases when stiffness decreases and the panel softens. Before the glass transition relatively small differences are observed e.g the modal density between -100 ºC and 90 ºC presents a constant discrepancy of 7.5%. However when it comes to glass transition the modal density of the panel rapidly increases resulting in a difference of 46% between -100 ºC and 160 ºC. Such discrepancies can have an important impact on the TL calculation of the panel.
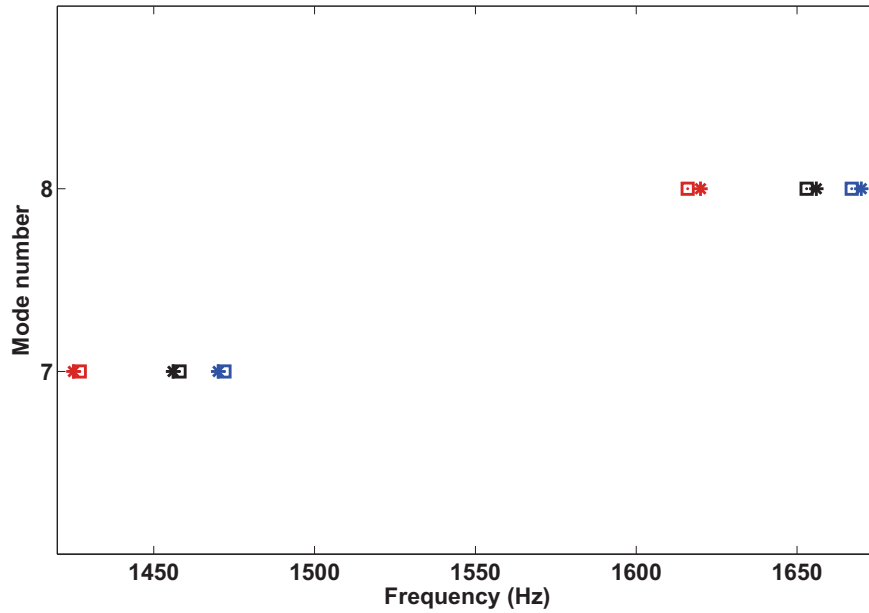
Figure 2.24: *Comparison of the predicted (7,0) and (8,0) modes of the panel for the three testing temperatures: experimental predictions (□) and WFEM (∗)*
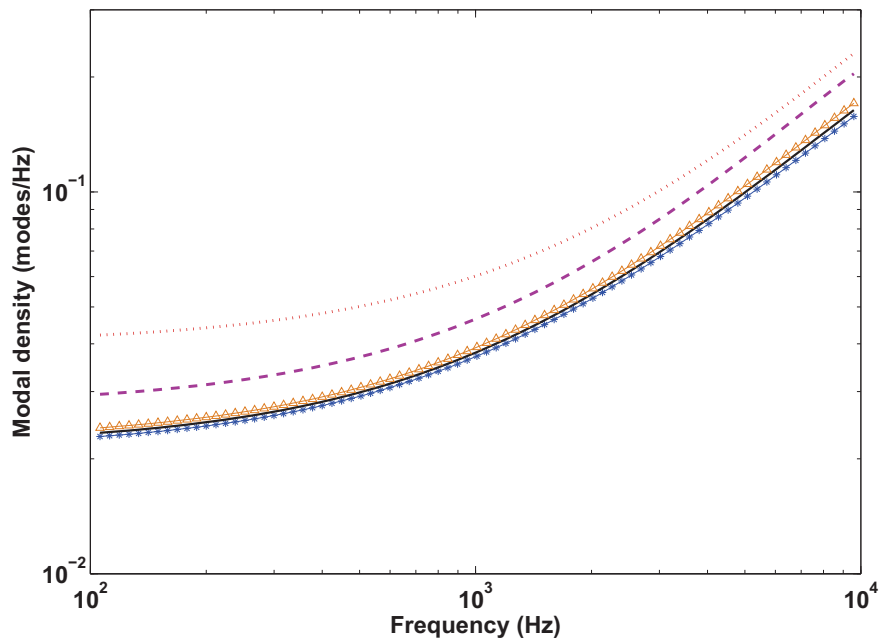
Figure 2.25: *Temperature dependent modal density of the sandwich panel: -100 ºC (∗), 25 ºC (−), 90 ºC (△), 110 ºC (--), 160 ºC (⋯)*

2.6.5   The influence of temperature on the loss factor of the panel

The measurement of the $\tan(\delta)$ quantity allows for expressing the stiffness matrix of the facesheets and the core $\mathbf{K}_f$,$\mathbf{K}_c$, as well as the global stiffness matrix of the panel $\mathbf{K}$ as:

$$\mathbf{K}_f = \mathbf{K}_f' + i\mathbf{K}_f''$$

$$\mathbf{K}_c = \mathbf{K}_c' + i\mathbf{K}_c'' \qquad\qquad (2.24)$$

$$\mathbf{K} = \mathbf{K}' + i\mathbf{K}'' = \sum_{n=1}^{3} \mathbf{K}_n' + i\sum_{n=1}^{3} \mathbf{K}_n''$$

In order to compute the global intrinsic loss factor of the sandwich panel, a similar approach as the one presented in [Manconi and Mace, 2010] is hereby adopted. It is assumed that the shear modulus of the facesheets retains the same proportion to the Young modulus throughout the temperature range. The same assumption is made for the mechanical characteristics of the core. Using WFEM analysis, the loss factor at each direction of propagation can be expressed as:

$$\eta(\omega, T, \theta) = \frac{\mathbf{Q}^*(\omega, T, \theta)\mathbf{K}''(T)\mathbf{Q}(\omega, T, \theta)}{\mathbf{Q}^*(\omega, T, \theta)\mathbf{K}'(T)\mathbf{Q}(\omega, T, \theta)} \qquad\qquad (2.25)$$

with η the loss factor for the flexural wave motion, $\mathbf{Q} = [\boldsymbol{\Phi}_Q^T \ \ \boldsymbol{\Phi}_Q^T e^{-ik_x L_x} \ \ \boldsymbol{\Phi}_Q^T e^{-ik_y L_y} \ \ \boldsymbol{\Phi}_Q^T e^{-ik_x L_x} e^{-ik_y L_y}]^T$ the modal displacements of the segment's nodes for the flexural wave mode, $\mathbf{K}'$ the real part of the segment's stiffness matrix and $\mathbf{K}''$ its imaginary part. The expression of the global loss factor is eventually given by averaging over all directions of propagation and taking into account for the mode count of the panel in each direction as:

$$\eta(\omega, T) = \frac{\int_0^\pi \eta(\omega, T, \theta)dN(\omega, T, \theta)}{\int_0^\pi dN(\omega, T, \theta)} = \frac{\int_0^\pi \eta(\omega, T, \theta)k(\omega, T, \theta)\dfrac{\partial k(\omega, T, \theta)}{\partial \omega}d\theta}{\int_0^\pi k(\omega, T, \theta)\dfrac{\partial k(\omega, T, \theta)}{\partial \omega}d\theta} \qquad\qquad (2.26)$$

The calculated global loss factors of the sandwich panel for each temperature are shown in fig.2.26. As expected, very high values of the loss factor are observed at 110 ^{o}C where the glass transition takes place. It is also observed that the loss factor is much more affected by the local loss factor of the facesheets. This was expected as the facesheets are the ones that offer the greatest part of the panel's rigidity and therefore influence much more the formulation of the stiffness matrix.

2.6.6   Influence on the acoustic radiation efficiency of the panel

The Leppington's formula is used hereby in order to calculate the radiation efficiency of the sandwich panel for each considered temperature. The flexural wavenumbers, as well as the acoustic medium characteristics of fig.2.21 are injected in the model. The resulting radiation efficiencies are presented in fig.2.27.

It is observed that temperature has a significant impact on the radiation efficiency of the structure. The coincidence frequency utterly depends on the wave phase velocity inside the acoustic medium and the the structure. When temperature increases, phase velocity in the acoustic medium increases, while the one of the waves propagating inside the layered panel decreases, which results in a higher coincidence frequency. The observation made in sec.2.6.3 on the radiation damping
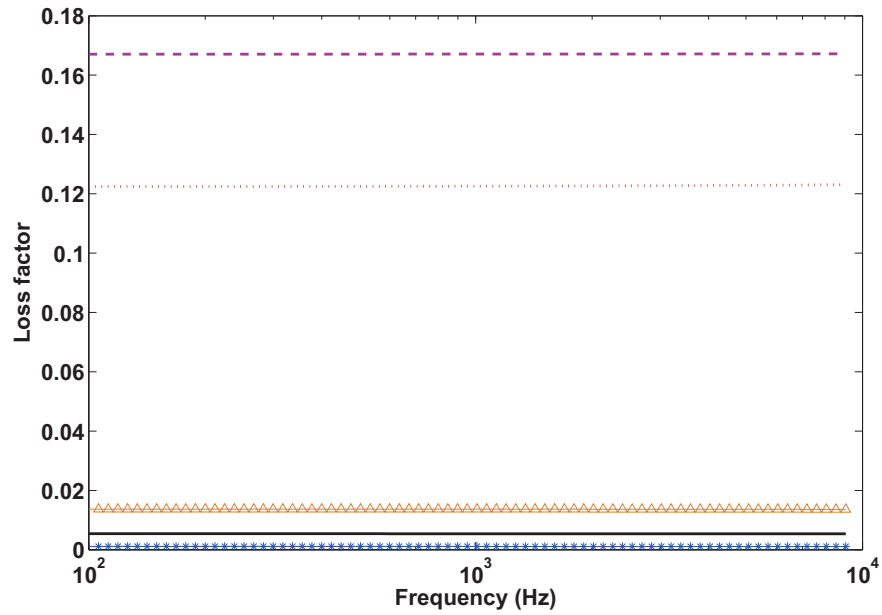
Figure 2.26: *Temperature dependent intrinsic loss factor of the sandwich panel: -100 $^o C$ ($*$), 25 $^o C$ (–), 90 $^o C$ ($\triangle$), 110 $^o C$ (--), 160 $^o C$ ($\cdots$)*
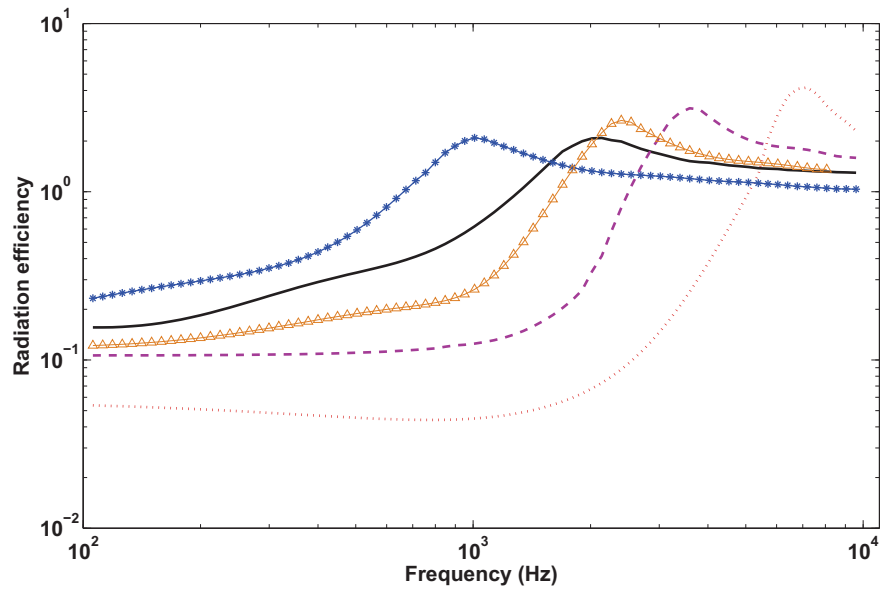
Figure 2.27: *Temperature dependent acoustic radiation efficiency of the sandwich panel: -100 $^o C$ ($*$), 25 $^o C$ (–), 90 $^o C$ ($\triangle$), 110 $^o C$ (--), 160 $^o C$ ($\cdots$)*
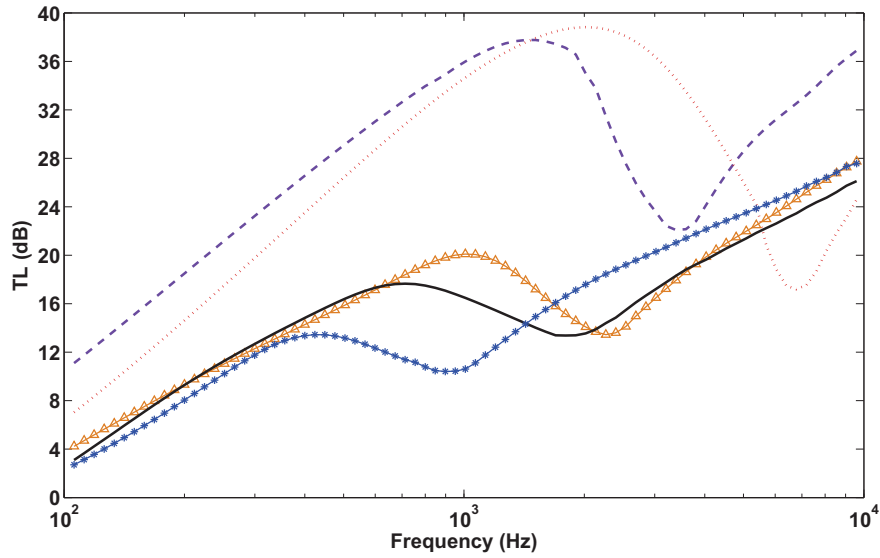
Figure 2.28: *Temperature dependent Transmission Loss of the sandwich panel at sea level: -100 ºC (∗), 25 ºC (–), 90 ºC (△), 110 ºC (--), 160 ºC (···)*

is therefore verified; at lower frequencies, a 'cold' panel has a higher radiation efficiency as its coincidence frequency is closer than the one for a 'hot' panel.

2.6.7 Influence on the TL of the panel

The TL of the panel, is calculated using the approach presented in sec.2.4.3, and the results computed for each temperature are compared to the ones of fig.2.12. The temperature dependent TL is shown in fig.2.28.

As was expected, the first noticeable difference between the compared temperatures is regarding to the coincidence frequency of the panel, which ranges from 850Hz at -100 ºC up to 7500Hz at 160 ºC. For results below the glass transition temperature, the TL is generally divided into three ranges. The sub-coincident range where the non-resonant transmission dominates and the results are close, the coincidence range where the TL mainly depends on the radiation efficiency prediction and the damping loss factor and the post-coincident damping controlled range where the inclination of the TL curve mainly depends on the damping of the panel. When it comes to the results for the panel within the glass transition region, the TL values are much greater throughout these three bands. This is principally due to the much greater loss factor of the panel in those temperatures. In the sub-coincident range, lower radiation efficiency also contributes to the higher TL. It can generally be concluded that operation in or after the glass transition temperature of the panel can result is improved acoustic insulation performance. Once more it is observed that the mechanical and acoustic performances of the structure need to be compromised. It seems finally that the higher modal density values of the panel at higher temperatures cannot counterbalance the effect of radiation efficiency and damping.

2.6.8 The impact of altitude on the TL of the panel

In the previous section it was verified that the impact of the operating and ambient temperature on the TL of a layered panel can be significant. The operation of aerospace structures however is not only conducted at sea level. Therefore in this section, the TL will be expressed as a function of
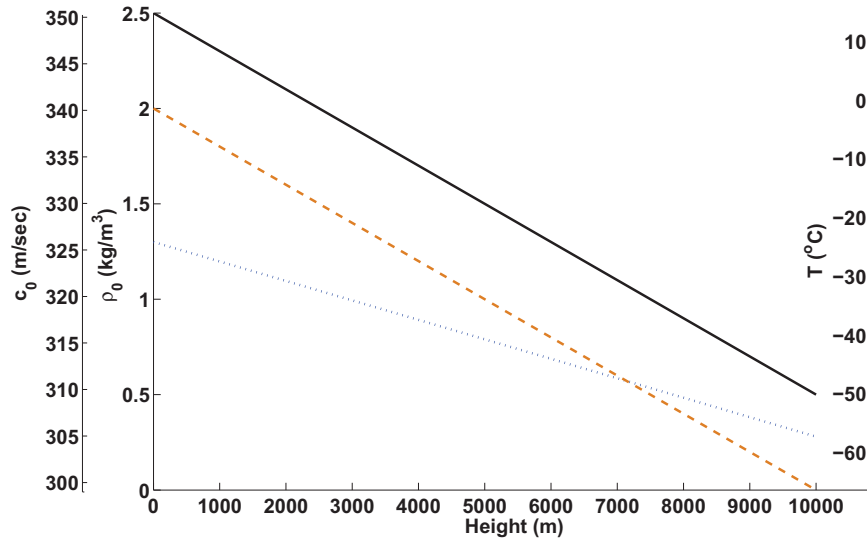
Figure 2.29: *Altitude dependent parameters: Ambient temperature (–), density (· · ·) and celerity (--) of the acoustic medium*

altitude. The temperature, the air density and the sound speed inside the troposphere are shown as a function of altitude in fig.2.29.

It is noted that in order to get a global idea of the operating conditions for a launch vehicle the whole atmospheric range should be verified. However outside the troposphere the relation of temperature and air pressure to altitude becomes more complicated. The resulting TL of the sandwich panel at 0m, 5000m and 10000m is shown in fig.2.30.

It is observed that at 10000 meters the panel has a higher TL with a difference approaching 9dB compared to the same panel at sea level. This divergence is mainly attributed to the lower atmospheric air density at higher altitudes which radically reduces the resonant transmission contribution. The effect on the radiation efficiency is also noticeable, with the coincidence frequency varying from 1800Hz at sea level to 1100Hz at 10000m.

2.7 Conclusions

The modelling of the vibroacoustic behaviour of composite layered structures with orthotropic material characteristics, was accomplished through a wave-context SEA approach. Summarizing the most important points of the presented work: 1) A description of the formulation of the WFE approach was given. The process followed for post-processing the results of the resulting eigenproblem was described. 2) The WFEM was applied to composite, arbitrarily layered panels in order to predict their dispersion characteristics. The predicted dispersion characteristics were successfully compared to bibliographic results. The advantage of the WFEM with respect to classical analytical models, especially with regard to predicting the correct coincidence frequency of composite structures is of great importance for a proper vibroacoustic analysis. 3) The main SEA quantities, namely the modal density and the radiation efficiency of the panels were computed following the calculation of their dispersion characteristics. The calculation was done using analytic formulas in a wave context. The results showed an excellent correlation between a variety of bibliographic models and the current approach. 4) For the calculation of the STL of the panels a classic SEA approach was adopted. A formula for computing the STL derived directly by the
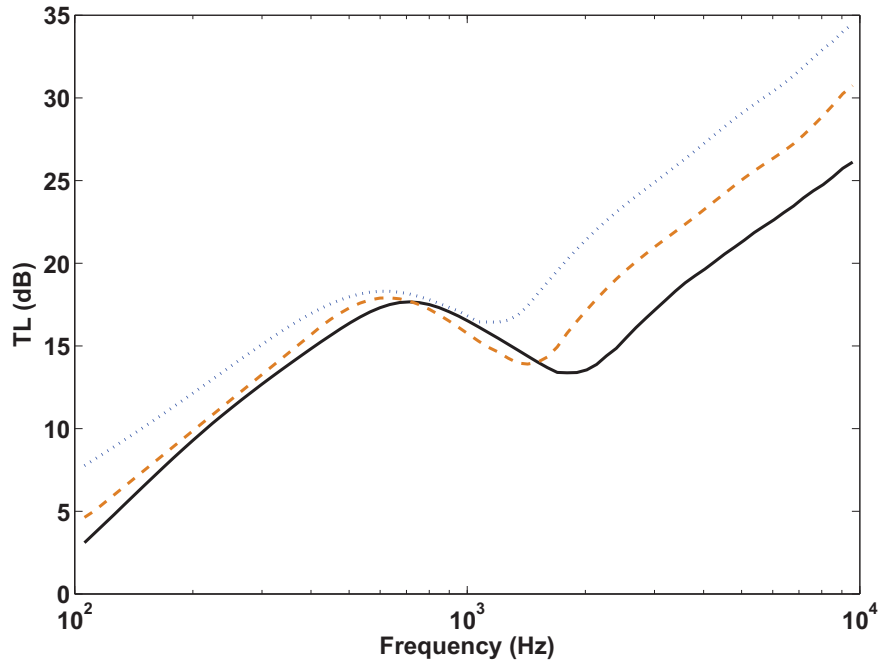
Figure 2.30:   *Altitude dependent Transmission Loss of the sandwich panel: sea level (–), 5000 meters (--), 10000 meters (···)*

characteristics of the structures, with no dependence on the room properties was given. A generally very good agreement between the experimental measurements and the STL predictions of the presented method was observed throughout the frequency band, validating the effectiveness and the robustness of the later. 5) Care has to be taken when modelling the dissipation characteristics of composite structures especially around the coincidence frequency, as it can be increased enough to cause misleading STL predictions. 6) The symmetric and the antisymmetric wave motion within a thick layered panel was well predicted. It was shown that adding mass to a panel does not always reduce its acoustic transmission and that the effect of the symmetric motion on the STL especially during its cut-on frequency range should not be neglected. 7) The temperature and altitude dependent STL of a sandwich orthotropic panel was also investingating following the measurement of its temperature dependent characteristics within a TMA. It can generally be concluded that operation within or beyond the glass transition temperature of the panel can result is improved acoustic insulation performance.

Chapter 3

Modelling the response of composite panels by a dynamic stiffness approach

3.1 Abstract

A dynamic stiffness approach for the prediction of the vibratory response of thick laminates and sandwich panels is hereby proposed. Initially, the wave dispersion characteristics of a two dimensional periodic medium are numerically predicted using a Wave Finite Element Method (WFEM). The effects of layer coupling on wave propagation within the laminate are therefore captured through a full three dimensional Finite Element (FE) modelling for a wide frequency range. The computed dispersion characteristics are used in order to update classical plate theories and calculate a dynamic stiffness matrix for the modelled laminate. The resulting updated Equivalent Single Layer (ESL) modelling proves to be time efficient and accurate for a wide frequency range. An experimental validation of the presented approach is also conducted. The response of a honeycomb orthotropic sandwich panel is measured and is successfully compared to the prediction of the ESL model. The WFEM computed wavenumbers are also validated by experimental measurements. The accuracy and the computational efficiency of the approach are discussed and compared to the ones of modern refined shell theories.

3.2 Introduction

Composite structures are widely used in the aerospace and automobile industry [Prel, 1999]. These often include anisotropic layered constructions which further complicate the prediction of the dynamic response of the industrial product. Moreover, the extensive use of layered structures implies a reduced acoustic performance at higher frequencies where composites have higher modal densities [Ghinet and Atalla, 2006]. Thus, the modelling of the vibroacoustic response for layered structures of arbitrary anisotropy is of great importance for the modern industry. The options offered within Finite Element (FE) software packages for the simulation of layered structures are usually limited. They typically include Classical Laminated Plate Theory (CLPT) or First-order Shear Deformation Theory (FSDT) modelling options, which result in fast, nevertheless inaccurate results for frequencies higher than the first resonance of the structure. On the other hand, modelling each layer of the structure separately using solid FE may offer good quality results even for higher frequencies; it implies however great calculation costs, especially when very thin layers are to be modelled. Thus, introducing a very fine mesh to maintain interpolation [Desmet, 2002] and pollution [Babuska et al., 1997] errors to acceptable levels can be prohibitive. It is hereby shown that calculating the wave propagation characteristics for composite structures provides a key for modelling their dynamic response.

The prediction of the vibratory response of thick layered panels has been a popular field of research. The CLPT is based on the Kirchhoff-Love theory, neglecting the transverse shear deformation and the transverse normal effects of the structure. This hypothesis usually leads to poor results for thick laminates, for which the ratio of the shear modulus to the in-plane elastic modula is sometimes very low. The shear deformation effect must therefore be taken into account in the analysis. This was firstly attempted by [Mindlin, 1951] who introduced the panels shear effect in the kinematic assumptions. The work in [Whitney and Pagano, 1970] presented an extension of the Mindlin's theory, the FSDT. More recently, Higher-order Shear Deformation Theories (HSDT) have been developed in the literature [Vinson and Sierakowski, 2002] introducing refined kinematic assumptions which render more accurate predictions. The higher order of the theory however also increases the mathematical complexity and computational cost of the solution. The aforementioned theories are also referred as Equivalent Single Layer (ESL) approaches, or global approaches, which aim to reduce a 3D structural model into a 2D one. More accurate predictions for a multilayered structure can be provided by a Layer-Wise (LW) modelling, which considers the

individual displacement field of each lamina separately allowing for a discontinuous strain field and a continuous transverse stress field at the interfaces of different materials [Reddy, 2004]. LW modelling usually results in very accurate predictions, however it also implies significant computational effort, as each lamina is modelled through a separate mathematical layer. A good compromise between accuracy and computational effort is achieved through the so called zig-zag or partially layer-wise theories [Carrera, 2003], in which an expansion of the displacement field is conducted using a zig-zag variation through the thickness. Higher order zig-zag theories have also been introduced [Lee et al., 1990]. Moreover, hybridization between zig-zag and LW methods [Aitharaju and Averill, 1999], as well as between zig-zag and ESL methods [Sulmoni et al., 2008] seem to offer superior features over the individual models.

The authors in [Kurtze and Watters, 1959] were the first to develop an asymptotic set of equations to model the wave propagation into symmetric flat thick sandwich structures. The authors in [Ghinet and Atalla, 2006, Ghinet et al., 2005] used a multi-layer analytical model based on Midlin theory to compute the dispersion characteristics of layered structures. A consistent HSDT was developed in [Wang et al., 2008] and used in [Wang et al., 2005] to predict the wave propagation characteristics within an infinitely long sandwich panel. Lately, the Wave Finite Element Method (WFEM) has received great attention. The method was introduced by Mead [Mead, 1973] and was derived as an expansion of the Bloch's theorem. Its main underlying assumption is the periodicity of the structure to be modelled. The Periodic Structure Theory (PST) is then coupled to the FEM. The WFEM has been applied to one-dimensional [Mace et al., 2005, Mencik and Ichchou, 2005] and two-dimensional structures [Mace and Manconi, 2008, Chronopoulos et al., 2012f]. A similar approach was also used in [Cotoni et al., 2008] to model the wave propagation in arbitrary periodic structures. The work of [Finnveden, 2004] provided an FE approach for the evaluation of wave propagation within structural waveguides.

Experimental identification of wave propagation characteristics has proved to be a complicated task for two dimensional structures. The methods most often used to measure the propagating flexural wavenumbers within a structure include least squares methods [McDaniel and Shepard Jr., 2000], discrete Fourier Transforms [Bolton et al., 1998] and Prony series [Grosh and Williams, 1993]. The authors in [Ferguson et al., 2002] proposed a method dealing with a windowed field of the normal displacement of a plate. The Inhomogeneous Wave correlation (IWC) method was lately proposed [Berthaut et al., 2005, Ichchou et al., 2008a], extending the two-dimensional spatial Fourier transform methods by including the structural loss factor in the inhomogeneous wave.

In the work presented hereby, the wave propagation characteristics of a composite panel are numerically calculated for a wide frequency range and subsequently validated through experimental measurements. The panel can be of arbitrary layering and anisotropy. The wave propagation characteristics are subsequently used through a dynamic stiffness approach for updating classic shell theories in order to predict the dynamic response of the structure. A new ESL approach is therefore proposed for a computationally efficient and accurate calculation of the dynamic response of composite structures for a wide frequency range. The approach is capable of taking into account for the complex shear deformation effects of the layers of the structures while avoiding the complicated kinematic assumptions of higher order theories. In the presented validation case, an orthotropic sandwich panel comprising a honeycomb core is considered. Experimental validation of the computed wave propagation characteristics and the spatial response of the panel is provided. The accuracy and the computational efficiency of the approach are also discussed and compared to the ones of modern refined shell theories. It is shown that while the presented approach can provide accurate results compared to higher order refined theories, it is also significantly more efficient than them.

The chapter is organized as follows: In sec.3.3 a numerical as well as an experimental method
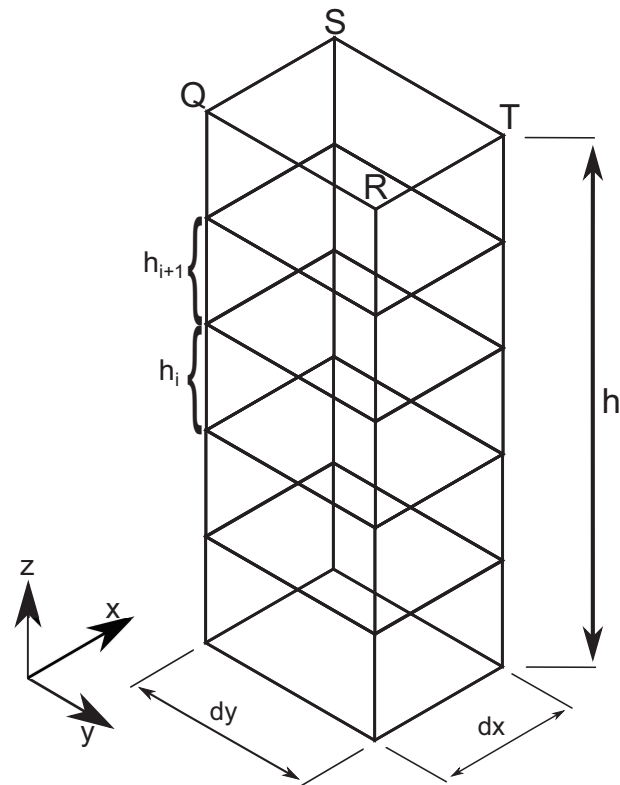
Figure 3.1: *View of the modeled periodic segment with its edges Q, R, S and T*

for estimating and measuring the propagation of flexural waves within a laminate are described. In sec.3.4 the dynamic stiffness approach for the calculation of the response of a layered panel is formulated. In sec.3.5 the experimental configuration used to validate the presented approach is exhibited along with comparative results and comments. In sec.3.6 and sec.3.7 respectively, the accuracy and the computational efficiency of the presented approach is discussed and compared to a variety of refined shell theories. In sec.3.8 the application of the approach to a layered cylindrical shell is described. Finally, in sec.3.9 conclusions on the presented work are given.

3.3 Wave propagation in layered structures

3.3.1 The Wave Finite Element method

A rectangular layered panel is considered hereby. A periodic segment of the panel with dimensions dx and dy (see fig.3.1) is modelled using conventional FE. Using the dynamic stiffness matrix of the segment, a nonlinear eigenvalue problem is formulated whose eigenvalues correspond to propagation constants of the various structural wave types. The formulation and the solution of the eigenproblem is discussed in sec.1.2.5.

For every wave type, a set of two wavenumbers $k(\theta)^+$, $k(\theta)^-$ are calculated, propagating respectively towards the positives and the negatives of the direction θ under consideration. It has been exhibited [Zhong and Williams, 1995] that: $k(\theta)^+ = -k(\theta)^-$. The corresponding wave modes (eigenvectors corresponding to each eigenvalue) are written as: Φ^+, Φ^-. For the sake of conciseness, only the positive propagating waves will be taken into account throughout the work presented below. By using a full 3D FE modelling, the effects of layer coupling on wave propagation within

the laminate are therefore captured for a very wide frequency range.

3.3.2   The Inhomogeneous Wave Correlation method

The IWC method was presented and validated for the measurement of the flexural propagating wavenumber of two-dimensional structures in [Berthaut et al., 2005, Ichchou et al., 2008a]. An inhomogeneous wave $\hat{o}_{k_f,\gamma,\theta}$ is introduced with k_f the apparent flexural wavenumber of the wave, θ its direction of propagation and γ its attenuation which according to [Lyon and DeJong, 1995] is related to the structural loss factor as: $\gamma = \eta c_\phi / 2 c_g$, with c_ϕ, c_g the phase and group velocities respectively. The propagating wave is therefore defined as:

$$\hat{o}_{k_f,\gamma,\theta}(x,y) = e^{-ik_f(\theta)(1+i\gamma(\theta))(x\cdot cos(\theta)+y\cdot sin(\theta))} \tag{3.1}$$

Subsequently, the correlation between the inhomogeneous wave of eq.(3.1) and the measured wave field $\hat{w}(x,y)$ which is considered to be known at arbitrary points of the structure can be calculated with a MAC type [Ewins, 2000] criterion:

$$IWC_{k_f,\gamma,\theta} = \frac{\left| \sum_1^m \hat{w} \cdot \hat{o}^*_{k_f,\gamma,\theta} S_i \right|}{\sqrt{\sum_1^m |\hat{w}|^2 \, S_i \cdot \sum_1^m \left| \hat{o}_{k_f,\gamma,\theta} \right|^2 S_i}} \tag{3.2}$$

where $\hat{}$ signifies the ω dependence, $*$ the complex conjugate, S_i is the surface of the structure that corresponds to the measurement point, and m is the number of measurement points on the structure. Using an algorithmic procedure, the angle of propagation θ can be discretized and the targeted wavenumbers $k_f(\theta)$ for which the maximum of the IWC criterion occurs can be found.

3.4   Calculating the dynamic response of composite panels

Following classic or modern plate theories, the propagating flexural $(k_{f,x}, \, k_{f,y})$, and shear $(k_{s,xy})$ wavenumbers can be expressed as a function of the mechanical characteristics of the structure. Since the values of these propagating wavenumbers are numerically calculated for a wide frequency range using the WFEM, expressions for the equivalent dynamic mechanical characteristics of the structures can be derived. If the CLPT is used, these expressions can be written as:

$$\hat{D}_{eq,i} = \frac{\omega^2 \rho_s}{k_{f,i}^4}$$

$$\hat{B}_{eq,xy} = \frac{\omega^2 \rho_s}{k_{s,xy}^2} \tag{3.3}$$

with ρ_s the mass per unit of area, $\hat{D}_{eq,i}$ the equivalent flexural stiffness of the structure towards direction i, and $\hat{B}_{eq,xy}$ its equivalent shear stiffness in the x,y plane. The response of the panel can then be computed using classic methods such as the h- or p- version of the FEM [Schwab, 1998], or by a modal expansion approach. It is evident that the theory used for the calculation of the response of the structure should be same theory as the one used for the calculation of the equivalent dynamic
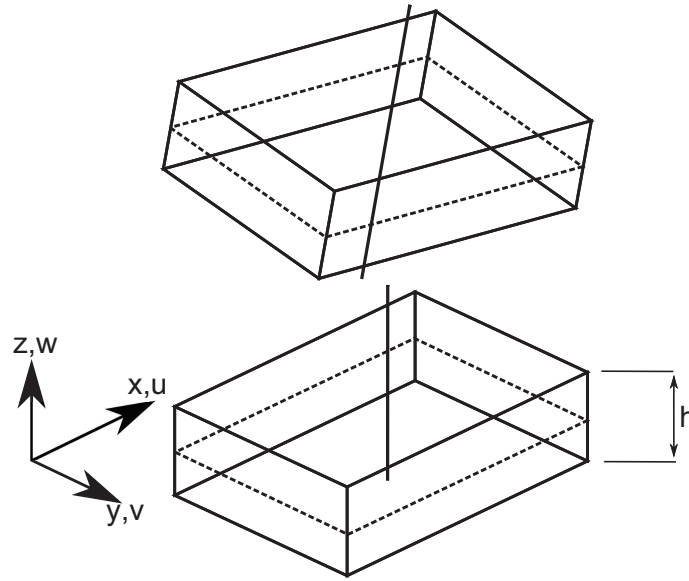
Figure 3.2: *Deformation of a plate, modelled with the CPT. The mid-surface (---) is highlighted, while the normal to the mid-surface remains normal after the deformation.*

characteristics. For the sake of versatility with respect to geometry and boundary conditions, an h-version of the FE method is hereby used. A deformed element modelled with the CPT is depicted in fig.(3.2). The normal to the mid-surface remains normal after deformation, in contrast to higher order theories. The modelled, equivalent thin panel should have the same ρ_s as the original composite one. The energy functions for an element governed by the CPT theory can be derived by its strain-displacement relation:

$$
\left\{
\begin{array}{c}
\epsilon_x \\
\epsilon_y \\
\gamma_{xy} \\
\gamma_{xz} \\
\gamma_{yz}
\end{array}
\right\}
=
\left\{
\begin{array}{c}
\dfrac{\vartheta u}{\vartheta x} \\
\dfrac{\vartheta v}{\vartheta y} \\
\dfrac{\vartheta u}{\vartheta y} + \dfrac{\vartheta v}{\vartheta x} \\
\dfrac{\vartheta u}{\vartheta z} + \dfrac{\vartheta w}{\vartheta x} \\
\dfrac{\vartheta v}{\vartheta z} + \dfrac{\vartheta w}{\vartheta y}
\end{array}
\right\}
=
\left\{
\begin{array}{c}
-z\dfrac{\vartheta^2 w}{\vartheta x^2} \\
-z\dfrac{\vartheta^2 w}{\vartheta y^2} \\
-2z\dfrac{\vartheta^2 w}{\vartheta x \cdot \vartheta y} \\
0 \\
0
\end{array}
\right\}
\tag{3.4}
$$

Then the strain and kinetic energies of the element [Petyt, 1990] are written as:

$$
\hat{U} = \frac{1}{2}\int_A \mathbf{q}^T \hat{\mathbf{D}}\mathbf{q}\,\mathrm{d}A
$$
$$
T = \frac{1}{2}\int_A \rho h \dot{w}^2\,\mathrm{d}A
\tag{3.5}
$$

with A the surface of the element, ρ its density, and:

$$\mathbf{q} = \left\{ \begin{array}{c} -z\dfrac{\vartheta^2 w}{\vartheta x^2} \\ -z\dfrac{\vartheta^2 w}{\vartheta y^2} \\ -2z\dfrac{\vartheta^2 w}{\vartheta x \cdot \vartheta y} \end{array} \right\} \tag{3.6}$$

Using the equivalence relations, the frequency dependent matrix $\hat{\mathbf{D}}$ is written as:

$$\hat{\mathbf{D}} = \mathbf{R}^T \begin{bmatrix} \hat{D}_{eq,x} & \hat{D}_{eq,x} \cdot \mathrm{v}_{xy} & 0 \\ \hat{D}_{eq,y} \cdot \mathrm{v}_{yx} & \hat{D}_{eq,y} & 0 \\ 0 & 0 & \hat{D}_{eq,xy} \end{bmatrix} \mathbf{R} \tag{3.7}$$

where $\hat{D}_{eq,xy} = \hat{B}_{eq,xy} \cdot h_{eq}^2/12$ with h_{eq} the thickness of the ESL, $\mathbf{R}$ the transformation matrix depending on the selected coordinate system and $\mathrm{v}_{xy}, \mathrm{v}_{xy}$ the Poisson's ratios of the panel in the x,y plane.

With the energy functions known, it is straightforward to apply the Hamilton's principle and build the FE matrices of the equivalent thin panel. Eventually, the solution of the system under a harmonic excitation is written as:

$$\mathbf{x} = \left[\omega^2 \mathbf{M} + \omega\hat{\mathbf{C}} + \hat{\mathbf{K}} \right]^{-1} \mathbf{F} \tag{3.8}$$

It is noted that in eq.(3.8) frequency dependent damping is assumed. The means by which damping can be modelled will be exhibited in the following section. The fact that the FE matrices are formulated in the frequency domain restrains the applicability of the approach to harmonic analysis. Nevertheless, when the applied loads have fixed coordinates, transient analysis is possible through an inverse Fourier transform. Moreover, modal analysis for systems having frequency-dependent stiffness has already been investigated in the literature [Remillat, 1997]. The resulting accuracy and computational efficiency for other types of analysis using the presented approach is a current subject of research.

It is evident that all the complex shear deformation effects are accounted for in the dynamic stiffness matrix through the WFEM homogenization procedure, however they are not included in the kinematic field of the shell model. To investigate possible inconsistencies caused by the assumption of a dynamic stiffness matrix, the expression of the response of a one-dimensional structure formulated in the wave context (very similar to the one formulated in the modal context) and given in [Langley, 1997] is mentioned:

$$\dot{u}_{x=x_1}(\omega) = (i\omega/\rho\gamma) \sum_r \frac{F\cos(k_r x_0 - \phi_r/2)\cos(k_r x_1 - \phi_r/2)}{\omega_{nr}^2(1+i\eta) - \omega^2} \tag{3.9}$$

with F the force applied at position x_0, and r the considered mode. This wave-mode duality assures that close to resonance frequencies the predictions of the presented approach will be accurate as the response is dominated by the wave motion associated to the resonant mode. For a broadband excitation however, if the response is dominated by non-resonant modes, the accuracy of the prediction is expected to present inconsistencies. It is noted that the objective of this work is not the prediction of the 'exact' response of a layered structure, but the development of an approach combining efficiency, accuracy and numerical simplicity.
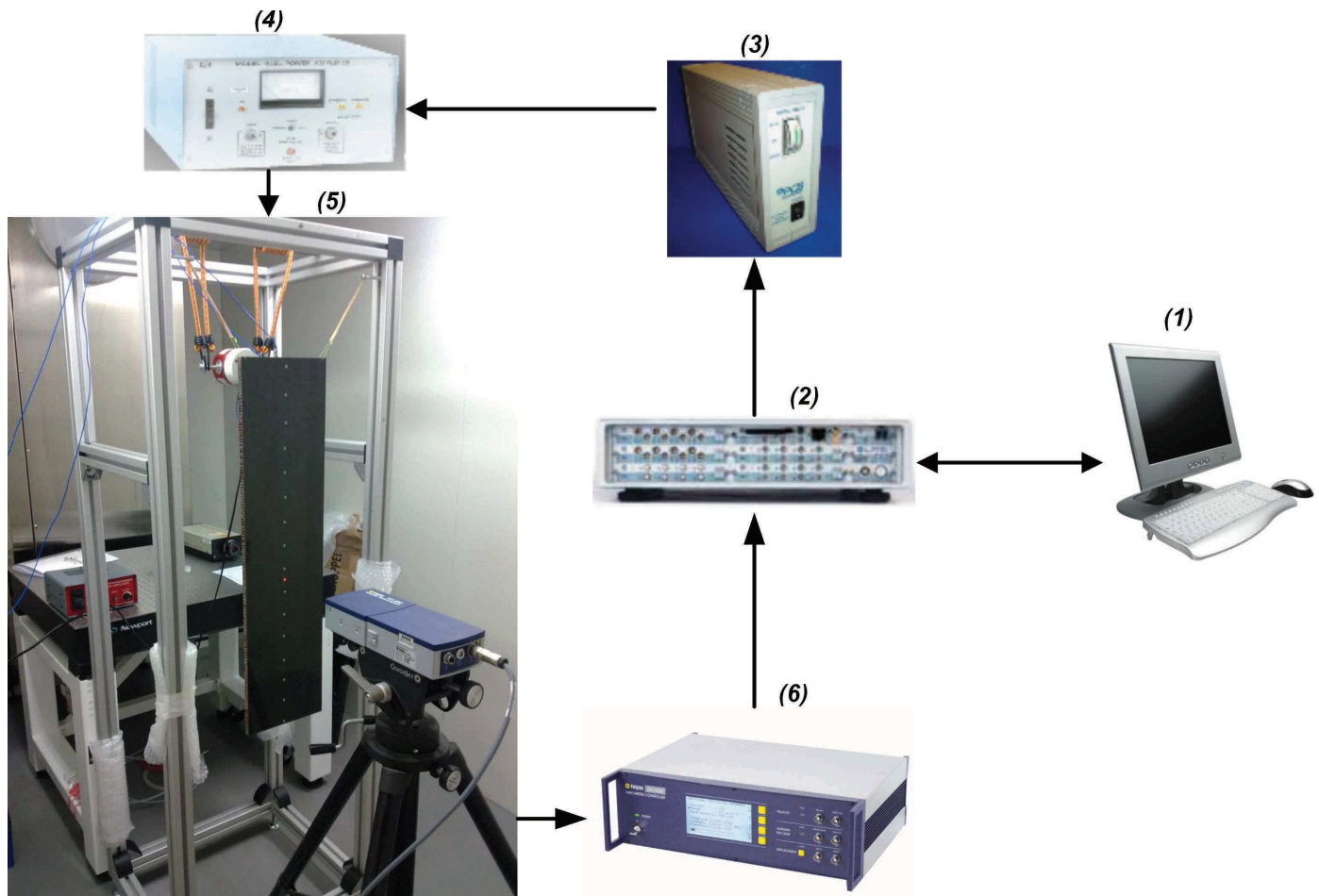
Figure 3.3: *A caption of the experimental configuration, depicting the intermediate sensors and signal processing devices.*

3.5 Experimental validation

3.5.1 Experimental configuration

The tested structure is a sandwich panel with its facesheets made of a carbon epoxy composite (Material I), and its core made of a Nomex type honeycomb (Material II). The mechanical characteristics of the materials as given by the manufacturer are shown in Table 3.1. The dimensions of the panel are L_x=0.8m and L_y=0.2m. The thickness of the facesheets is equal to h_f=1mm while the one of the core is equal to h_c=12.7mm. Each facesheet comprises four layers of plain weaved carbon fibres, resulting in a quasi-isotropic lamina. The mass ratio of carbon fibres to resin is 1.083. The experimental configuration is depicted in fig.3.3.

The panel is suspended by two corners so as to simulate free boundary conditions (FFFF) around its edges. The test was conducted in a climatic test chamber within which the temperature and the humidity are kept steady. An LMS data acquisition system (2) was used for the signal processing. The panel was excited using a PCB exciter (5) adhered to the structure through a force sensor. An ICP signal conditioner (3), along with a 30W dP power amplifier (4) were used for the conditioning of the excitation signal. The structural response is measured using a Polytec laser

Table 3.1: *Mechanical properties of materials*

Material I	Material II	Material III	Material IV	Material V	Material VI	Material VII
$\rho = 1410$ kg/m^3	$\rho = 48$ kg/m^3	$\rho = 1578$ kg/m^3	$\rho = 1578$ kg/m^3	$\rho = 1578$ kg/m^3	$\rho = 1500$ kg/m^3	$\rho = 58$ kg/m^3
$E_x = 54$ GPa	$E_x = 85$ MPa	$E_x = 6.9$ GPa	$E_x = 224.25$ GPa	$E_x = 172.5$ GPa	$E_x = 55$ GPa	$E_x = 78$ MPa
$E_y = 54$ GPa	$E_y = 85$ MPa	$E_y = 6.9$ GPa	$E_y = 6.9$ GPa	$E_y = 6.9$ GPa	$E_y = 55$ GPa	$E_y = 78$ MPa
$v_{xy} = 0.09$	$v_{xy} = 0.23$	$v_{xy} = 0.25$	$v_{xy} = 0.25$	$v_{xy} = 0.25$	$v_{xy} = 0.10$	$v_{xy} = 0.20$
$G_{xy} = 8.5$ GPa	–	$G_{xy} = 1.38$ GPa	$G_{xy} = 56.58$ GPa	$G_{xy} = 3.45$ GPa	$G_{xy} = 8.7$ GPa	-
–	$G_{yz} = 44$ MPa	$G_{yz} = 1.38$ GPa	$G_{yz} = 1.38$ GPa	$G_{yz} = 1.38$ GPa	–	$G_{yz} = 40.6$ MPa
–	$G_{xz} = 24$ MPa	$G_{xz} = 1.38$ GPa	$G_{xz} = 56.58$ GPa	$G_{xz} = 3.45$ GPa	–	$G_{xz} = 40.6$ MPa

vibrometer (5,6) and is transmitted to the acquisition system in order to compute the structural impedance at various points of the panel.

3.5.2   Validation of the computed natural frequencies

A first validation between various modelling approaches for thick layered structures will be conducted by computing the first natural frequencies of the suspended panel. The results are compared to the experimental outcomes in fig.3.4. It is noted that in order to keep a maximal aspect ratio of 5:5:1 for the solid mesh of the panel, an FE model comprising 246024 DoF was obtained. The ESL theories were applied using the ANSYS 12.1 FE software. Analytic solutions relating the structural wavenumber of a panel to its natural frequencies have been given in classical textbooks [Leissa, 1969] for a variety of boundary conditions of the panel. For an FFFF configuration, one can consider the general solution for two-dimensional panel as:

$$
\begin{aligned}
w(x,y) = &A sin(k_x x) \cdot sin(k_y y) + B sin(k_x x) \cdot cos(k_y y) \\
&+ C cos(k_x x) \cdot sin(k_y y) + D cos(k_x x) \cdot cos(k_y y) \\
&+ E sinh(k_x x) \cdot sinh(k_y y) + F sinh(k_x x) \cdot cosh(k_y y) \\
&+ G cosh(k_x x) \cdot sinh(k_y y) + H cosh(k_x x) \cdot cosh(k_y y)
\end{aligned}
\tag{3.10}
$$

By applying the appropriate boundary conditions to eq.(3.10) it is derived that the natural frequencies of the panel correspond to the wavenumber values that satisfy the relations:

$$
\begin{aligned}
cosh(k_x L_x) \cdot cos(k_x L_x) = 1 \\
cosh(k_y L_y) \cdot cos(k_y L_y) = 1
\end{aligned}
\tag{3.11}
$$

which has the asymptotic solution [Xie et al., 2004] of:

$$
\begin{aligned}
k_x L_x = (m - \frac{3}{2})\pi \\
k_y L_y = (n - \frac{3}{2})\pi \quad \text{for} \quad \text{m,n=3,4...}
\end{aligned}
\tag{3.12}
$$

With the structural wavenumbers known, the exact natural frequencies of the panel can be calculated.

It is observed that the WFEM results are in very good agreement for all the computed natural frequencies. Slight divergence from the experimental results are due to parametric uncertainties of the structure with respect to the exact mechanical characteristics of each structural and adhesive layer. The solid mesh model exhibits the ability of a precise FE model to predict the natural frequencies of the panel. The large number of DoF needed, as well as the excessive computation time would however be prohibitive for the application of such an approach to large industrial
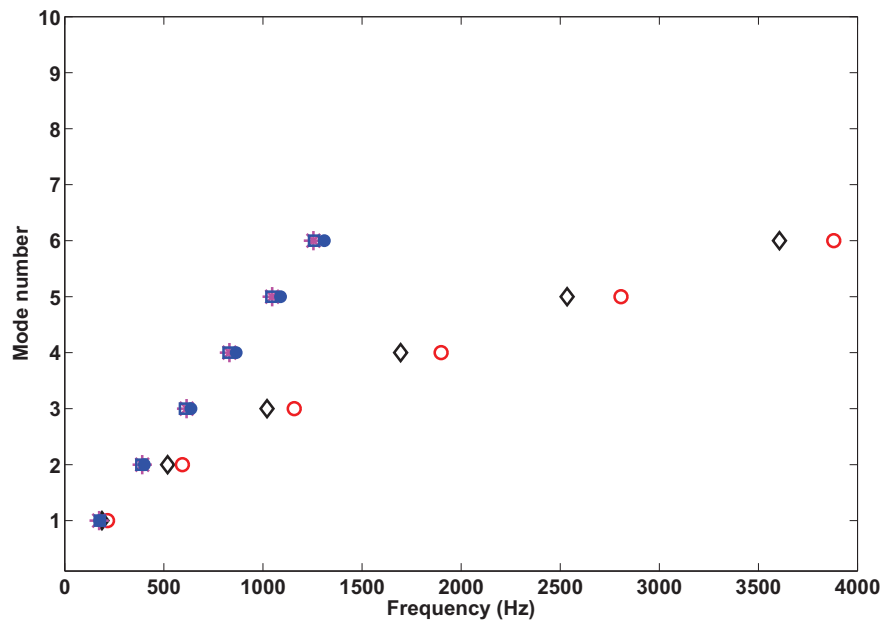
Figure 3.4: *The first six flexural natural frequencies of the panel as predicted by: experimental results (∗), WFEM results (□), solid mesh (•), Mindlin ESL (◇), FSDT ESL (o)*

system. Moreover, pollution errors are already visible in the calculation after the third flexural mode. The failure of the FSDT and Mindlin ESL theories to accurately predict the dynamic behaviour of the panel higher than its first resonance is exhibited.

3.5.3   Validation of the computed structural wavenumbers

The wave propagation characteristics of the sandwich panel are initially calculated for every frequency and direction of propagation by the WFEM. The solutions corresponding to propagating flexural waves are distinguished by evanescent waves [Chronopoulos et al., 2012f] and computational artifacts and are presented in fig.3.5.

The natural frequencies of the panel corresponding to out-of-plane modes can be found by interpolating on fig.3.5 for each determined set of values k_x and k_y which are solutions of eq.(3.11). The IWC approach is then applied on the vibratory data measured by the experimental configuration. The grid of measured data points comprises 30 points along the x axis and 5 along the y axis. The response of the structure is measured under a white noise excitation using the laser vibrometer. The FRF is then obtained through an inverse Fourier transform. The comparison of the experimentally measured wavenumbers towards x direction versus the WFEM estimation are presented in fig.3.6.

Oscillations around the WFEM estimation are observed for the experimental results. The largest divergences are observed in the low-frequency range, where the maximum error between the results is equal to 17,9% at approximately 450Hz. Fast convergence is observed at higher frequencies, where the results are in very good agreement.

Following the validation of the calculated flexural wavenumbers, the equivalent dynamic structural stiffness can then be calculated using eq.(3.3). The results for $\hat{D}_{eq,x}$ are shown in fig.3.7. As expected, large fluctuations are observed in the low frequency range, while the results converge fast for higher frequencies. It is noted that comparing the values for 100Hz and 3000Hz, it is observed that the equivalent flexural stiffness for the CPT has been reduced by 97,2%.
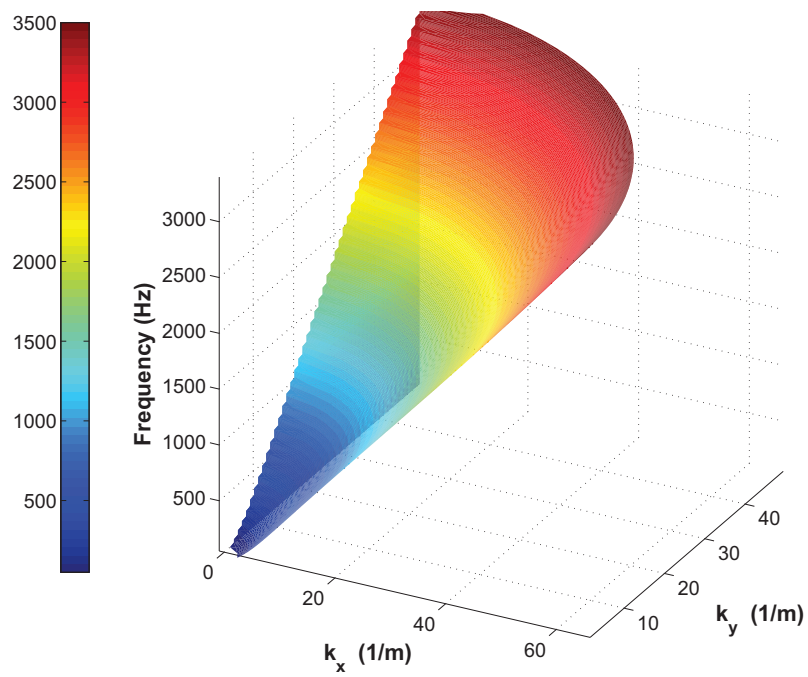
Figure 3.5: *3-dimensional view of the flexural wavenumbers propagating within the layered structure as a function of the direction of propagation and frequency.*
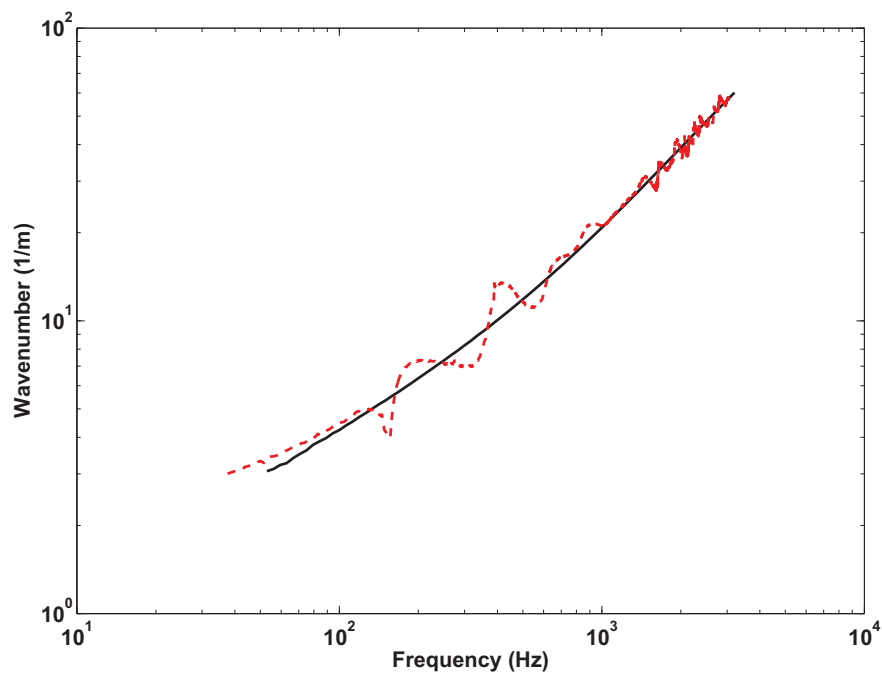
Figure 3.6: *Comparison between the flexural wavenumbers predicted by the WFEM (−) and the experimentally obtained ones (--).*
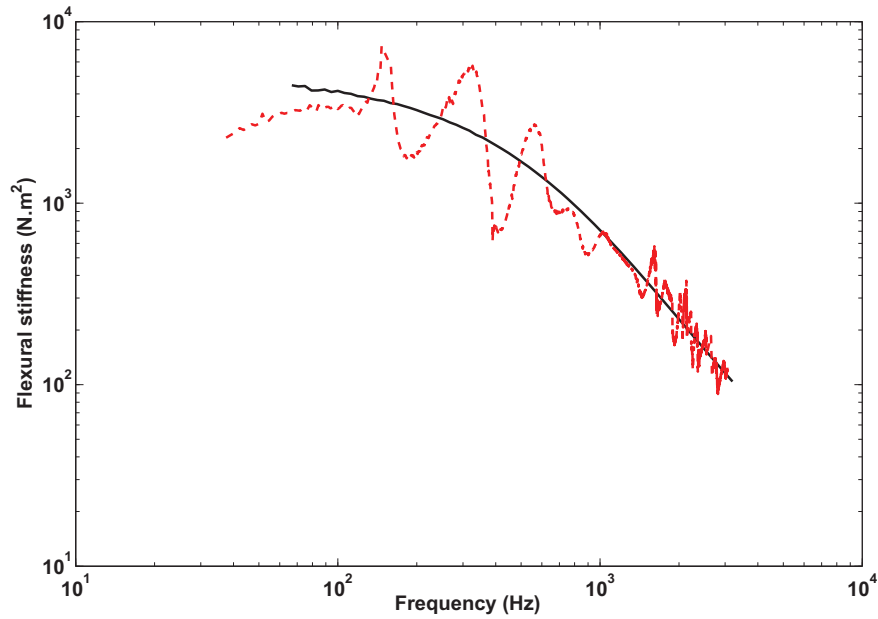
Figure 3.7: *Comparison between the dynamic flexural stiffness predicted by the WFEM (–) and the IWC approach (--).*

3.5.4   Structural damping modelling

When the resonance peaks of the response of a structure are clearly distinguished, the modal damping ratio of a linear system can be estimated by the half-power method [Torvik, 2011], through the relation:

$$\zeta_r = \frac{\omega_a^2 - \omega_b^2}{4\omega_r^2} \tag{3.13}$$

with ω_r the resonance frequency and ω_a, ω_b the frequencies around resonance for which the response is reduced by 3dB. The modal damping ratios of the first modes of the sandwich panel as calculated by eq.(3.13) are shown in fig.3.8. It is noted that the increase of damping with respect to frequency is mostly due to additional radiation damping which is included in the overall damping estimation.

A linear least square fitting curve is shown in fig.3.8 along with the experimental results, in order to extrapolate the prediction of the structural damping values up to 3kHz. Obviously, more complicated fitting functions can be applied in the case of a more accurate representation of the structural dissipation properties being desired. A range of choices exists for implementing these values in an FE model. Assuming a frequency dependent damping matrix as in eq.(3.8), the coefficients a,b of a Rayleigh damping model can be chosen for every frequency band, so that the following relation between the damping ratio and the coefficients is satisfied:

$$\zeta_r = \frac{1}{2}\left(\frac{a}{\omega_r} + b \cdot \omega_r\right) \tag{3.14}$$

Moreover, the approach presented in [Adhikari, 2000] can be implemented for any type of fitting
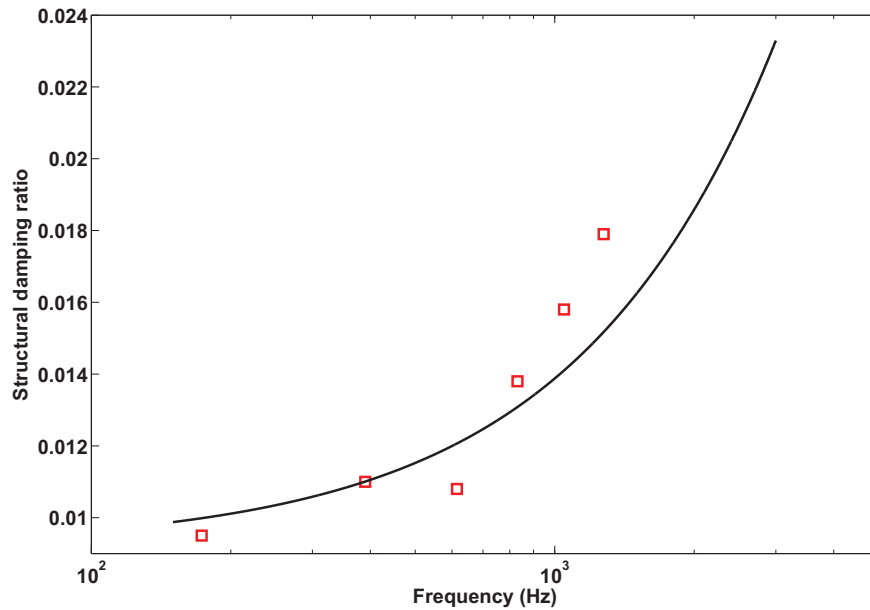
Figure 3.8: *The modal damping ratio values ($\square$) and a fitted linear curve ($-$).*

function. Assuming a linear fitting function which is written as a function of frequency as:

$$f(\omega) = \alpha_1 \omega + \alpha_2 \tag{3.15}$$

the damping matrix satisfying the desired modal damping values can be expressed as:

$$\begin{aligned}
\hat{\mathbf{C}} &= 2\mathbf{M}\sqrt{\mathbf{M}^{-1}\hat{\mathbf{K}}}f(\omega) \\
&= 2\mathbf{M}\sqrt{\mathbf{M}^{-1}\hat{\mathbf{K}}}\left(\alpha_1\sqrt{\mathbf{M}^{-1}\hat{\mathbf{K}}} + \alpha_2\right)
\end{aligned} \tag{3.16}$$

with the coefficients α_1, α_2 for the present case being equal to $4.7078 \cdot 10^{-6}$ and 0.00917 respectively. The second approach was the one adopted throughout the presented results.

3.5.5   Structural response validation

In order to validate the dynamic stiffness approach predictions, the experimentally obtained dynamic response of the sandwich panel is compared to the FE results at arbitrary coordinates of the panel. The results are exhibited in fig.3.9 and fig.3.10. The reference displacement is equal to $d_{ref} = 5e^{-8}$m.

A very good correlation is observed between the results. Intense fluctuations of the experimental results are due to low coherence of the laser velocimeter's signal for those frequencies. The resonance frequencies, the response amplitude, and the modal damping ratios seem to be very well simulated up to 1,5kHz. Higher order resonances are very sensitive to parametric uncertainties [Ichchou et al., 2011] of the structural characteristics. The exact response becomes therefore particularly difficult to predict at higher frequencies, especially for sandwich structures whose precise density and material characteristics are highly uncertain. The updated ESL model seems however to be accurately predicting the medium of the structural response even for the higher frequency range. It is noted that care should be taken when applying the FEM at high frequencies as its accuracy can be dramatically limited by the induced pollution errors.
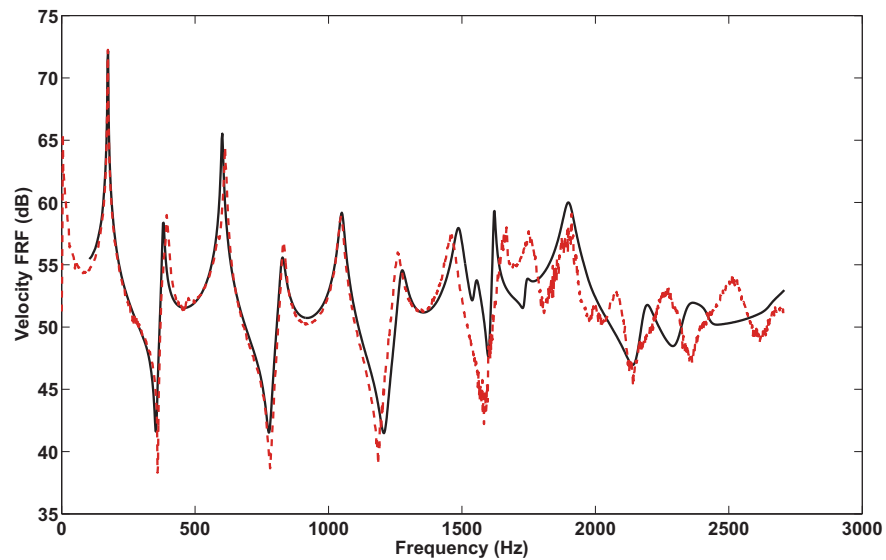
Figure 3.9: *Velocity FRF at (0.40,0.12): FEM updated by WFEM results (–) and experimental measurements (--)*
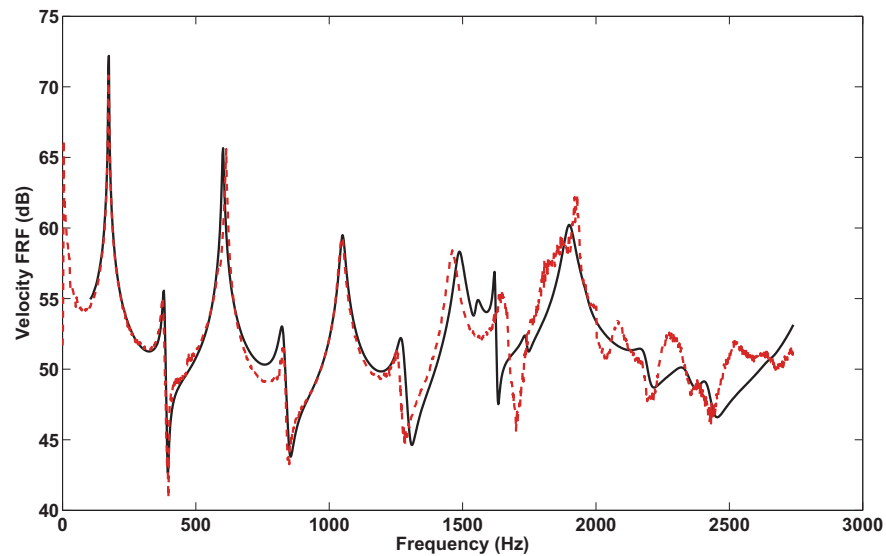
Figure 3.10: *Velocity FRF at (0.77,0.07): FEM updated by WFEM results (–) and experimental measurements (--)*

3.6   Comparison to refined shell theories

In order to compare the accuracy of the presented method to refined shell theories, a layered beam having an arbitrary lamina layout is used in order to compute its natural frequencies through various methods. The characteristics of the beam as well as the predictions of the refined theories are extracted from [Zhen and Wanji, 2008]. The beam is made of materials I, II and III presented in Table 3.1. The structure is a five-ply beam having a layer stacking of type $(0^o/0^o/0^o/0^o/0^o)$. The layer thickness proportions are $(0.1h/0.25h/0.15h/0.2h/0.3h)$ with h the total thickness and the material sequence is $(I/II/III/I/III)$. The predicted natural frequencies are normalized by $\Omega = \omega_n L^2 \sqrt{\rho/E_o}/h$ with $E_o = 6.9e9$, and L the length of the beam. A variety of L/h ratios is studied, from a very thick beam with L/h=5 up to L/h=20. An analytical solution for the free vibration of the layered beam as given in [Kapuria et al., 2004] is hereby used as reference. The predictions of a series of refined shell theories are compared to the presented approach:

- A Global/Local Higher-Order theory (GLHT); initially presented in [Li and Liu, 1997], the method satisfies displacements and transverse shear stresses continuity conditions at lamina interfaces with a displacement field expression comprising 6 unknowns.

- A Zig-zag theory (ZZT) proposed in [Cho and Parmerter, 1993] comprising a displacement field with 3 unknowns.

- A global HSDT presented in [Matsunaga, 2001] assuming a displacement field with 19 unknowns.

- A HSDT also published in [Matsunaga, 2001] comprising a displacement field having 11 unknowns.

- A HSDT proposed in [Kant and Swaminathan, 2001] assuming a displacement field with 8 unknowns.

- A HSDT presented in [Reddy, 1984] which can satisfy the transverse shear stress free boundary conditions and assuming a displacement field having 3 unknowns.

The predictions for each approach are given in Table 3.2. A comparison of the error of the predictions with respect to the reference values is also exhibited in fig.3.11. It is observed that as the L/h ratio of the beam increases, the ZZT along with the WFEM homogenization tend to be the most accurate methods, while all HSDT approaches present a greater error for the entirety of the predicted natural frequencies. On the other hand, when the beam becomes particularly thick with an $L/h \leq 5$, it seems that the errors of the ZZT, GLHT and WFEM approaches rapidly increase with frequency, leaving global high order HSDT methods as the most suitable ones for modelling the laminate. It can therefore be observed that the WFEM homogenization provides fairly accurate results compared to global HSDT, zig-zag and global-local approaches, especially for panels having a large L/h ratio.

3.7   Discussion on the computational efficiency of the approach

In order to compare the computational efficiency of the presented dynamic stiffness approach to classical and refined theories the processing time for each solution step is presented in Table 3 for three different FE model sizes. All calculations were done using a server of two quadruple core Xeon E5343 processors with 8Gb of RAM memory available. The WFEM analysis was performed using

Table 3.2: *Comparison between predictions of the current approach and of some refined shell theories on the first four natural frequencies of the layered beam. Brackets include the error compared to the reference values.*

Mode number	L/h	Reference	Present approach	GLHT	ZZT	HSDT-19	HSDT-11	HSDT-8	HSDT-3
	5	7.2551	7.3893	7.4686	7.2876	7.5005	7.9849	9.0526	10.7705
			(1.82)	(2.94)	(0.45)	(3.38)	(10.06)	(24.78)	(48.45)
1	10	10.152	10.2480	10.3694	10.1828	10.3415	10.7376	11.4181	12.1924
			(0.94)	(2.14)	(0.30)	(1.87)	(5.77)	(12.47)	(20.10)
	20	11.924	11.9772	12.0327	11.9510	12.0153	12.1764	12.4189	12.6548
			(0.44)	(0.91)	(0.23)	(0.77)	(2.12)	(4.15)	(6.13)
	5	18.837	19.7118	19.2328	19.4374	19.8072	20.8615	23.8353	31.7068
			(4.44)	(2.10)	(3.19)	(5.15)	(10.75)	(26.53)	(68.32)
2	10	29.020	29.5574	29.8747	29.1505	30.0022	31.9398	36.2106	43.0823
			(1.82)	(2.95)	(0.45)	(3.38)	(10.06)	(24.77)	(48.46)
	20	40.606	40.9920	41.4776	40.7315	41.3661	42.9505	45.6726	48.7696
			(0.94)	(2.14)	(0.30)	(1.87)	(5.77)	(12.48)	(20.10)
	5	32.769	35.9144	33.9995	36.2256	34.9223	36.3173	39.8386	54.1257
			(8.76)	(3.76)	(10.55)	(6.57)	(10.83)	(21.57)	(65.17)
3	10	50.832	52.3341	52.0734	51.4644	53.0128	56.3359	64.9560	83.215
			(2.87)	(2.44)	(1.24)	(4.29)	(10.83)	(27.79)	(63.71)
	20	76.577	77.6602	78.7483	76.8460	78.6932	83.1366	91.8751	103.771
			(1.39)	(2.84)	(0.35)	(2.76)	(8.56)	(19.97)	(35.51)
	5	47.602	54.7183	52.1422	58.2790	50.7929	52.6974	55.7109	76.7002
			(13.01)	(9.54)	(22.43)	(6.70)	(10.70)	(17.03)	(61.13)
4	10	75.349	78.8472	76.9313	77.7496	79.2289	83.4460	95.3414	126.827
			(4.44)	(2.10)	(3.19)	(5.15)	(10.75)	(26.53)	(68.32)
	20	116.08	118.2295	119.499	116.602	120.008	127.759	144.842	172.329
			(1.82)	(2.95)	(0.45)	(3.38)	(10.06)	(24.78)	(48.46)

MATLAB 7.9.0, while the FE matrices calculation and solution for the structure was done using ANSYS 12.1. The WFEM analysis is independent of the size of the structure, thus it has a constant processing burden. It is observed that as the size of the FE model increases, the percentage of the extra processing time needed for the WFEM analysis and the dynamic calculation of the FE matrices decreases fast, so that it asymptotically tends to the processing time corresponding to a CPT solution. In order to compare these results to the efficiency of refined theories some cases are distinguished and commented:

- Large number of layers: The number of layers in the structure will increase the size and the processing time of the WFEM analysis. However this accounts only for an insignificant fraction of the total solution. Moreover, the WFEM homogenization process results in a constant number of six DoF per node for the FE model, independently of the number of layers. In contrast, for LW approaches the number of DoF per node directly depends on the number of layers, making it prohibitive for structures with a large number of laminas. With regard to global ESL approaches, the number of DoF per node may be independent of the number of layers, however it is probable that a higher order theory should be used to account for layers with inhomogeneous characteristics. Considering that for an ESL theory of order p, the resulting number of DoF per node is equal to $3(p+2)$ it is clear that the accurate HSDT approaches will be considerably less efficient than the presented approach. Zig-zag theories have also the advantage of preserving a predefined number of DoF per node independently of the number of layers. However, as with the ESL theories a number of DoF per node larger than six is needed to accurately model a structure composed of many laminas. Mixed HSDT/zig-zag (see [Sulmoni et al., 2008]) theories are generally more efficient than HSDT theories, however they also require a large number of DoF per node in order to achieve good accuracy.
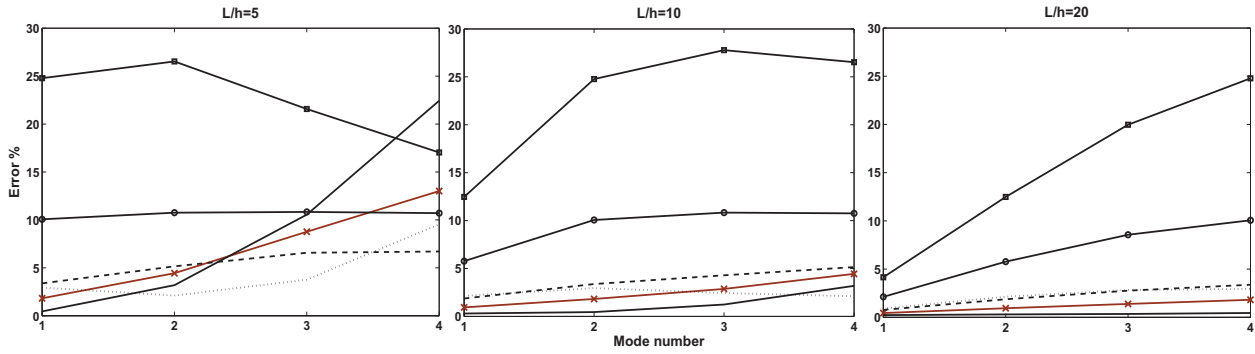
Figure 3.11: *Error of the prediction of the first four natural frequencies for the layered beam compared to the reference values: Present approach(-x-), GLHT ($\cdots$), ZZT (–), HSDT-19 (--), HSDT-11 (-o-), HSDT-3 ($-\square-$)*

- Large structure and/or high frequency analysis: Modelling a large aerospace panel and pushing the analysis at higher frequencies both result in increasing the total size of the model. Taking into account for the results presented in Table 3.3 and the aforementioned comments it is clear that all homogenization theories resulting in more than six DoF per node will become less efficient than the WFEM homogenization when increasing the size of the model.

- Large number of frequency steps: The additional time needed for the solution with the presented approach is proportional to the number of frequency steps of the analysis. As shown in Table 3.3, this additional time will become more evident when modelling particularly small panels having a small model size for a very large number of frequency steps, which is not very common for industrial cases. Even for these cases however, when a panel comprising a large number of laminas is to be modelled, the presented approach will probably be more efficient than LW and ESL theories.

Table 3.3: *Processing times for 100 frequency steps*

Model size	Procedure	Time (in sec)	Fraction of the total processing time
4875 DoF	WFEM matrix calculation (72 DoF), analysis and post-processing	1.1	1.8%
	FE CLPT solution	41	67.1%
	Additional time of the dynamic solution	19	31.1%
8355 DoF	WFEM matrix calculation (72 DoF), analysis and post-processing	1.1	0.6%
	FE CLPT solution	153	86.4%
	Additional time of the dynamic solution	23	13%
32115 DoF	WFEM matrix calculation (72 DoF), analysis and post-processing	1.1	0.2%
	FE CLPT solution	575	95.2%
	Additional time of the dynamic solution	28	4.6%

It can therefore generally be concluded that the WFEM homogenization becomes significantly more efficient than HSDT approaches, high order zig-zag theories and LW methods as the size of the model and the number of laminas for the structure increase.
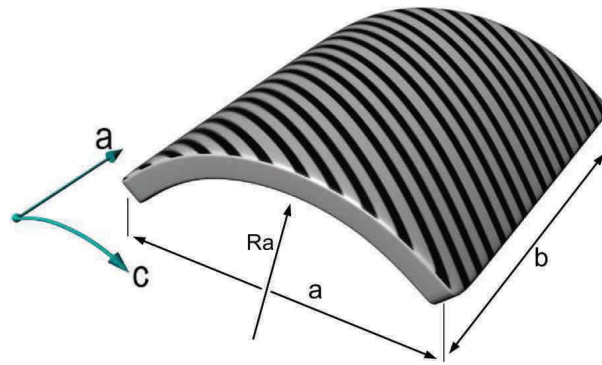
Figure 3.12: *A composite singly curved panel modelled within the current approach*

3.8 Application of the ESL approach to a shell structure

Following the modelling of a flat layered structure, the application of the dynamic stiffness approach on a layered shell will be investigated. A sandwich cylinder is used as an illustration example.

3.8.1 Homogenization procedure

A singly curved thick shell of arbitrary layering and anisotropy is hereby considered (see fig.4.2). Following the analysis in [Chronopoulos et al., 2012e], the homogenization procedure for curved structures would involve the computation of the wavenumbers propagating within the shell using the WFEM and subsequently the direct comparison of the computed wavenumbers to exact values for classic shell theories in order to determine the dynamic material characteristics of the ESL. Such an analysis would give accurate predictions on the purely circumferential modes of the shell, however with regard to the modelling of the stiffness effects below the ring frequency towards the axial direction the approach would encounter two major challenges:

- It is particularly difficult to encounter exact relationships between the axially propagating wavenumbers and the mechanical characteristics of the shell structure. Approximate solutions for the Donnell-Mushtari and the Flügge theories can be found in [Fuller and Fahy, 1982] and [Karczub, 2006] respectively. However, the flexural/axial coupling effects within a shell imply that the flexural wavenumber cannot be expressed merely as a function of the flexural stiffness and the mass of the structure, as is the case with flat panels. The use of such wavenumber relations would therefore imply a source of approximation and a significantly increased complexity of the problem.

- Even if a 'neat' expression of the wavenumbers as a function of the mechanical characteristics of the shell proves feasible, the application of the approach would be hindered by the geometric stiffening effects. In order to avoid such effects from disturbing the accuracy of the solution the modelled ESL should present the same ring frequency as the original layered shell.

Using the aforementioned considerations, the calculation of the dynamic mechanical properties for the ESL is conducted in the following section.

3.8.2 Expressions for the dynamic characteristics

The ESL structure should now have an equal flexural stiffness and surficial density as well as a ring frequency equal to the one of the original layered shell. Considering the relations of the three aforementioned quantities as a function of the mechanical characteristics for a Donnell-Mushtari type thin shell we have:

$$
\begin{aligned}
f_r &= \frac{1}{2\pi R}\sqrt{\frac{E_a}{\rho}} \\
\rho_s &= \rho h \\
D_{a,c} &= \frac{E_{a,c}h^3}{12(1-v^2)}
\end{aligned}
\tag{3.17}
$$

with f_r the ring frequency, $E_{a,c}$ the Young's modulus in the axial and circumferential directions, v the Poisson's ratio, h the thickness of the ESL, ρ its density and R the radius of the shell. Considering the equivalence between the Donnell-Mushtari and the Kirchhoff-Love theories it can be deduced that the axial and circumferential flexural stiffnesses should be related to the flexural wavenumbers by the relation:

$$
\hat{D}_{a,c} = \frac{\omega^2\rho_s}{\hat{k}_{f,WFE}^4}
\tag{3.18}
$$

with $\hat{k}_{f,WFE}$ the WFEM calculated flexural wavenumbers of the flat layered panel and ˆ represents the frequency dependence. Using eq.(3.17),(3.18) the equivalent mechanical characteristics for the ESL can be deduced as:

$$
\begin{aligned}
\hat{E}_a &= \sqrt{\frac{\rho_s^3}{12\hat{D}_a}}\omega_r^3 R^3(1-v^2) = \frac{\rho_s\hat{k}_{f,WFE,a}^2}{\sqrt{12}\omega}\omega_r^3 R^3(1-v^2) \\
\hat{E}_c &= \frac{12(1-v^2)\omega^2\rho_s}{\hat{k}_{f,WFE,c}^4\hat{h}^3} \\
\hat{\rho} &= \frac{\hat{E}_a}{\omega_r^2 R^2(1-v^2)} = \frac{\rho_s\hat{k}_{f,WFE,a}^2}{\sqrt{12}\omega}\omega_r R \\
\hat{h} &= \frac{\rho_s}{\hat{\rho}}
\end{aligned}
\tag{3.19}
$$

Using eq.(3.19) the dynamic stiffness and mass matrices of the ESL shell can be computed for every frequency value.

3.8.3 Numerical results

As an illustration the approach will be applied to a sandwich cylindrical shell. The radius of the shell is equal to R=679.5 mm. Its facesheets are made of material VI and have a thickness equal to 1 mm, while its core is made of material VII and has a thickness of 12.7 mm. The mechanical characteristics of the materials are exhibited in Table 3.1. The axis $(x = 0, y = 0)$ corresponds to the center axis of the shell. The cylinder is considered to be freely suspended at all sides.

The first natural frequencies (corresponding to out-of-plane non rigid modes) as predicted by a full 3D FE solid model and the equivalent ESL model of the cylinder are compared in fig.3.13. In the solid model, the cylinder's facesheets are modelled using shell elements which are attached to the solid elements representing the core.
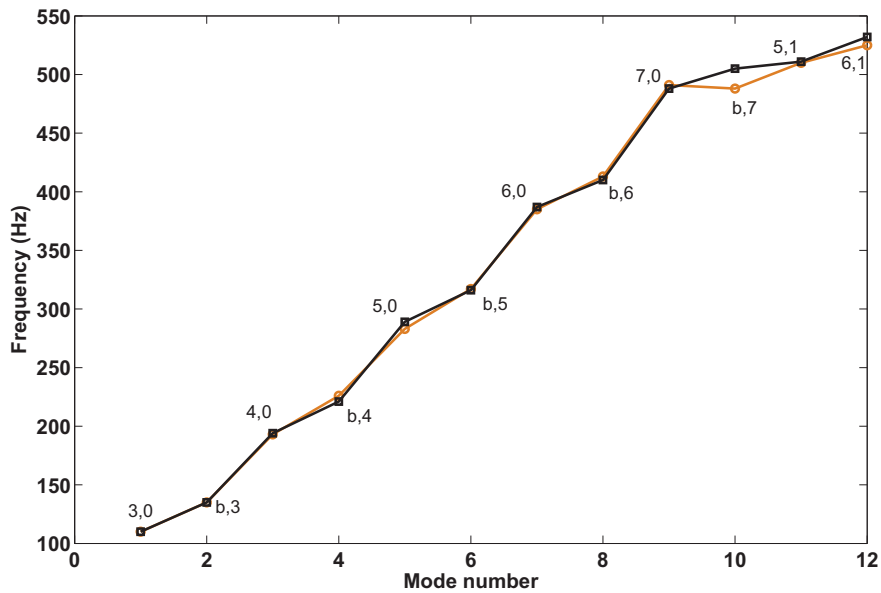
Figure 3.13: *Comparison of the predicted natural frequencies for the: 3D FE model (□) and the ESL model (O). Mode type is given aside.*

A very good agreement between the two models is observed for the circumferential, the breathing and the mixed flexural modes. The error of the first twelve predicted natural frequencies varies from 0.2% to a maximum of 2.3% for the breathing mode of order 7. For the sake of clarification, a circumferential flexural mode (5,0), the corresponding breathing mode and a flexural mode are presented in fig.3.14.

In order to give a global idea of the correlation of the response predictions of the two models the total energy level was calculated for an undamped cylinder with $\eta = 0$ as well as for the case in which the global loss factor of the structure is equal to $\eta = 1\%$. The results are exhibited in fig.3.15 and fig.3.16 respectively.

A very good correlation between the predictions of the 3D FE model and the ESL approach is generally observed. The frequency step of the solution was 2Hz for the 3D FE model and 1Hz for the ESL model. For the undamped case it is observed that the modal peaks of the ESL prediction
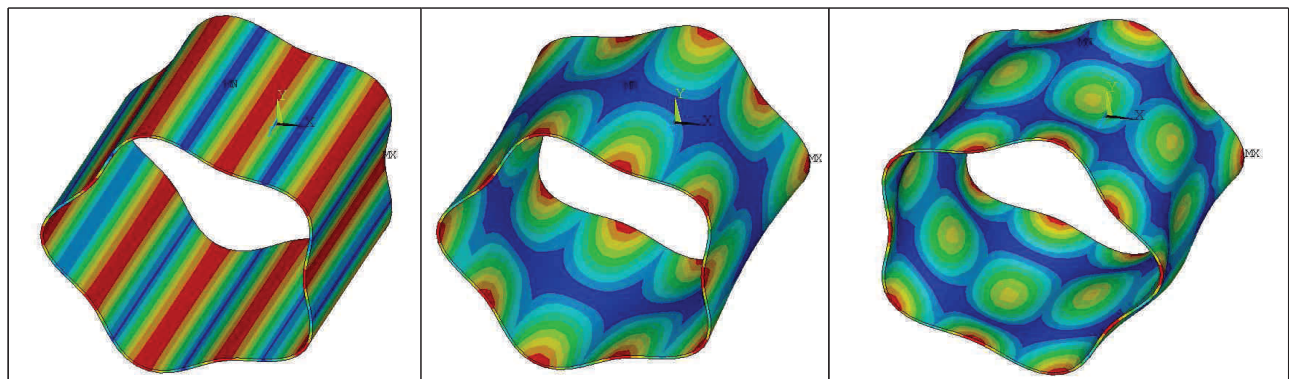
Figure 3.14: *The modes (5,0) (left), the breathing mode 5 (center) and the mode (5,1) for the modelled sandwich cylinder*
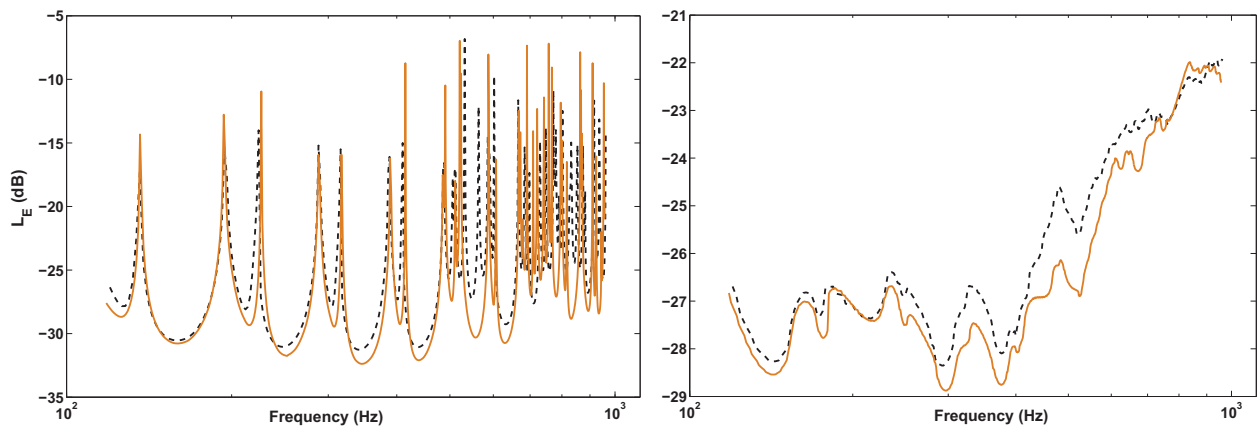
Figure 3.15: *Left: Comparison between the predicted total energy level of the layered cylinder with $\eta = 0$ by: the 3D FE modelling (--) and the ESL model (–). Right: 1/3 octave band averaged results.*
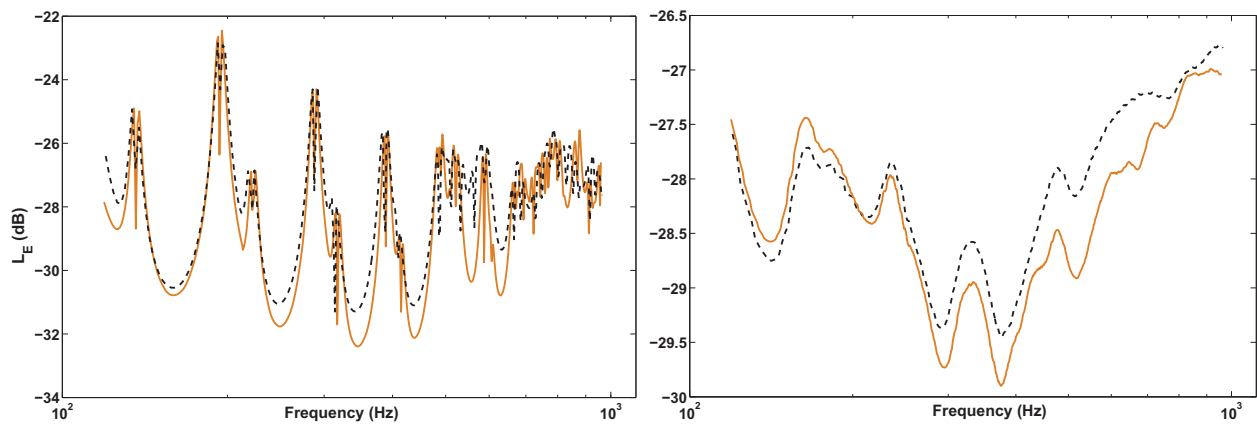
Figure 3.16: *Left: Comparison between the predicted total energy level of the layered cylinder with $\eta = 1\%$ by: the 3D FE modelling (--) and the ESL model (–). Right: 1/3 octave band averaged results.*

Table 3.4: *Calculation times for 410 frequency steps in sec*

	3D FE model	ESL model
WFEM homogenization (60 DoF)	0	4
FE solution	1890	822
Additional time for the dynamic FE matrices calculation	0	107
Total	1890	933

are in the most cases higher than the ones of the 3D FE model. This is due to the finer frequency resolution of the ESL solution. Excellent agreement is observed up to 500Hz. The exact prediction of resonances at higher frequencies is particularly sensitive to parametric and non parametric uncertainties. It is therefore more appropriate to describe the structural response using average values. In fig.3.15,3.16 1/3 octave band averaged results are also given for the total vibrational energy of the structure. For the undamped case, the averaged response of the ESL prediction remains within 1.5dB of the results of the 3D FE model throughout the frequency range. For the damped case an excellent correlation is also observed between the predictions with the averaged results presenting a maximum difference of 0.9dB.

3.8.4   Computational efficiency of the approach

The computation times for the 3D FE model as well as for the ESL model of the sandwich cylinder are shown in Table 3.2. It is observed that despite the fact that the FE matrices were calculated for every frequency step the ESL solution is significantly faster than the 3D FE model. As discussed in [Chronopoulos et al., 2012e] this reduction of the computational effort will be more significant -also compared to refined shell theories- for larger industrial structures and for structures comprising more layers through their thickness. In the presented example the 3D FE model comprised d_{3D}=24600 DOF while the ESL one comprised d_{ESL}=12300 DOF. For the modelling of a multi-layered shell using solid FE the ratio between the number of DoF for the two models will be equal to $d_{3D}/d_{ESL} = (n+1)$ with n the number of layers of the stratified shell, which will result in a much greater reduction of the computation time by the ESL.

3.9   Conclusions

In the presented work, a dynamic stiffness approach was adopted in order to compute the dynamic response of composite panels through an ESL method. The approach was also experimentally validated using a sandwich orthotropic panel which comprised a honeycomb core and carbon-epoxy type facesheets. Summarizing the most important points of the work: 1) Excellent correlation was observed between the experimental resonances and the ones predicted by the WFEM results for the sandwich panel. 2) In contrast, CLPT and FSDT approaches failed to correctly predict any resonance higher than the first one. A full three-dimensional modelling of the panel led to satisfactory results, however it would be prohibitive in terms of computational effort for larger industrial structures. 3) The propagating flexural wavenumbers predicted by the WFEM were successfully validated using the experimentally measured vibratory field of the panel. The results converged very fast with respect to frequency. 4) The dynamic response of the sandwich panel was successfully predicted at various points. Excellent correlation between the presented dynamic stiffness approach and the experimental results was observed for the low frequency range. At higher frequencies, the parametric uncertainties of the sandwich panel make the prediction of its precise response impossible. Despite these uncertainties however, the ESL approach is still able

to accurately predict the medium of the response for higher frequencies. 5) It was exhibited that while the WFEM homogenization can provide accurate results compared to higher order refined shell theories; 6) the presented approach is also significantly more efficient than them. 7) The suggested ESL approach was also successfully applied to a cylindrical sandwich shell.

Chapter 4

A unified approach for the broadband vibroacoustic response of composite shells

4.1   Abstract

A model for the prediction of the vibroacoustic performance of composite shells of various geometries within a Statistical Energy Analysis (SEA) approach is developed hereby. The dispersion characteristics of composite orthotropic shell structures of a variety of geometries, namely curved panels and cylindrical shells are predicted by a Wave Finite Element (WFE) method. The mass and stiffness matrices of a structural segment are computed by a conventional Finite Element (FE) modelling and the wave propagation characteristics are derived by forming a polynomial eigenproblem whose eigenvalues correspond to structural wavenumbers. The numerical issues concerning the formation and the solution of this nonlinear eigenproblem are discussed. The modal density and the radiation efficiency of the structure are then evaluated using its numerically extracted wave propagation characteristics. The broadband vibroacoustic response of each configuration under a reverberant field excitation can then be computed within an SEA approach.

4.2   Introduction

Composite closed and non-closed shell constructions, including curved panels and cylinders are often encountered in the modern aerospace and automotive industry, mainly due to their advantage of being light and their ability to suit the particular demands of each structure type and manufacturer. Nevertheless the poor acoustic performance of materials of that type induces high levels of noise transmission within the payload or passenger compartment. The prediction of the vibroacoustic behaviour of composite shell structures is therefore a field of extensive study and of high importance for the modern industrial needs. It is widely known that the knowledge of the wave dispersion characteristics of such structures is an important characteristic that can facilitate the prediction of the vibroacoustic behaviour of the structure.

Analytical formulas for the dispersion characteristics within curved and cylindrical shells can be found in the bibliography, either in the form of classical expressions for thin isotropic shells [Graff, 1991, Leissa, 1969], or various approximate theories [Langley, 1994c, Tyutekin, 2004]. Many modern studies are dedicated to the calculation of dispersion characteristics using numerical methods, such as spectral methods. The authors in [Xi et al., 2000] and [Mahapatra and Gopalakrishnan, 2003] used a spectral finite element method to predict the characteristic equations of composite cylindrical shells. The Semi-Analytical Finite Element (SAFE) method was used in [Finnveden, 2004] in order to predict the wave dispersion within curved structures.

In [Heron, 2002] the author conducts an SEA analysis of a composite curved member using a discrete layer model for the prediction of the dispersion characteristics within sandwich singly curved panels. It is supposed that the panel's facesheets behave only flexurally, while the core retains only its shear effects and bears no bending loads. More recently Ghinet*et al* developed a LW model based on Mindlin theory to predict the dispersion relations and the vibroacoustic behaviour of singly curved composite panels [Ghinet et al., 2005]. A similar model for the calculation of the dispersion characteristics for sandwich cylinders and the prediction of the cylinder's modal transmission coefficients under a diffused field was presented in [Ghinet et al., 2006]. The vibroacoustic response of composite curved sandwich panels was numerically calculated in [Klos et al., 2003, Buehrle et al., 2001] using an FEM model coupled with the boundary element method, however this approach is not appropriate for large scale structures as it requires much computational effort. A modal method was used in [Cunningham et al., 2003] for the calculation of the response of doubly curved panels sandwich panels to a random acoustic excitation.

The Wave Finite Element Method (WFEM) was introduced in [Mead, 1973] in order to nu-

merically predict the wave dispersion characteristics of elastic dissipative structures. The main underlying assumption of the method is the periodicity of the structure to be modelled. The Periodic Structure Theory (PST) is then coupled to the FEM. A wide variety of structures, including a vehicle's chassis [Houillon, 1999], and a stiffened plate [Ichchou et al., 2008c] has already been modelled using the WFEM. More recently, the WFEM was applied for composite curved and cylindrical 2-dimensional panels in [Manconi and Mace, 2009] and for the 1-dimensional case in [Zhou and Ichchou, 2010].

In this chapter, a robust approach is presented for the prediction of the vibroacoustic performance of composite structural shells of various geometries, namely curved panels and cylinders, within an SEA context. The main SEA quantities for the structures are calculated in a wave-context approach, following the computation of the dispersion characteristics of the structures by a WFEM. The main advantage of the present methodology is its ability to accurately model any kind of heterogeneous (in the sense of thickness), composite panels for a very wide frequency range.

The work presented in this paper is part of a research project which started in 2000 by EADS Astrium Space Transportation. The objective is the prediction of the vibration levels of the electronic equipment of the launch vehicle and of the payload at its mounting points within the mid-frequency range, under the severe and complex aeroacoustic environment embracing the launch vehicles during lift-off [Ichchou et al., 2009]. Indeed, electronic equipments usually have their first modes of vibration in the mid frequency domain. They are therefore particularly sensitive to these excitation bands. To achieve the prediction of mid-frequency response, an SEA-Like method was chosen by Astrium ST (see [Troclet et al., 1999, Troclet et al., 2009]). The results of the current work will eventually be used to improve the prediction of the developed approaches with regard to the response of composite structures.

The chapter is organized as follows: In sec.4.3 the WFEM main equations are presented for singly and doubly curved panels. The numerical issues that may occur in the case of very light and stiff composites are also discussed. In sec.4.4 the most important characteristics of the panels for conducting an SEA, namely their modal density and their radiation efficiency are calculated. The procedure in order to calculate the Sound Transmission Loss (STL) of the panels is also given. In sec.4.5 numerical examples are presented for the validation of the presented approach. The conclusions of the work are given in sec.4.6.

4.3 The WFEM for curved structures

4.3.1 Presentation of the method

The WFEM for two-dimensional flat composite panels was presented and validated in [Manconi and Mace, 2007, Inquiété, 2008]. Following the extraction of the mass and stiffness matrices $\mathbf{M}$ and $\mathbf{K}$ of a segment representing the periodic structure to be modelled, a polynomial eigenvalue problem can be formed as:

$$\left\{ \begin{array}{cccc} \mathbf{I} & \lambda_a^{-1}\mathbf{I} & \lambda_c^{-1}\mathbf{I} & \lambda_c^{-1}\lambda_a^{-1}\mathbf{I} \end{array} \right\} \mathbf{D} \left\{ \begin{array}{c} \mathbf{I} \\ \lambda_c\mathbf{I} \\ \lambda_a\mathbf{I} \\ \lambda_c\lambda_a\mathbf{I} \end{array} \right\} \mathbf{u_Q} = \mathbf{0} \tag{4.1}$$

with $\mathbf{D}$ the dynamic stiffness matrix of the modelled structure calculated as $\mathbf{D} = \left(\mathbf{K} \left(1 + \eta i \right) - \omega^2 \mathbf{M} \right)$, $\mathbf{u_Q}$ the displacements of the DoF of the reference edge Q and λ_c, λ_a the wavelengths of the waves
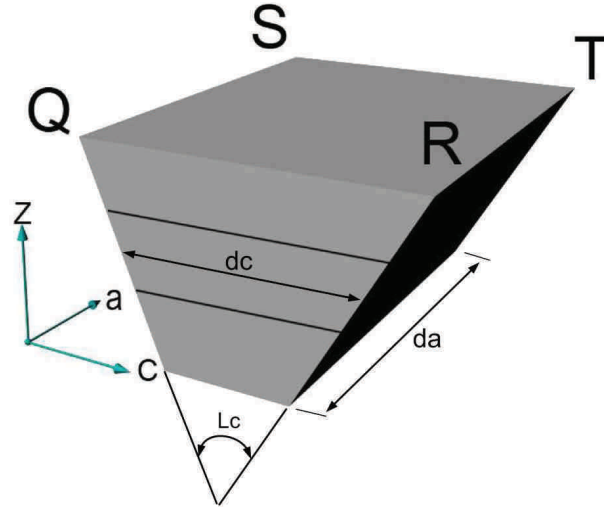
Figure 4.1: *An FE model of the trapezoid segment corresponding to the curved panel*
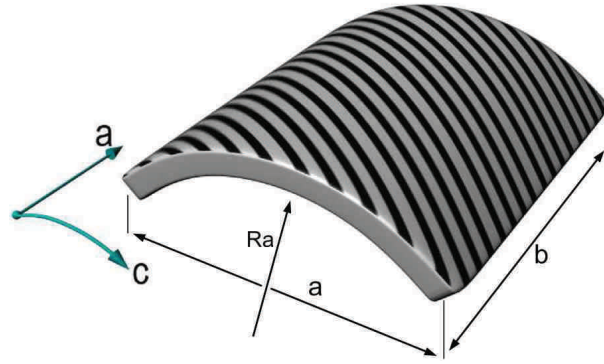
Figure 4.2: *A composite singly curved panel modelled within the current approach*

propagating in the c and a directions respectively. The dynamic stiffness matrix should be written as:

$$\mathbf{D} = \begin{bmatrix} \mathbf{D_{QQ}} & \mathbf{D_{QR}} & \mathbf{D_{QS}} & \mathbf{D_{QT}} \\ \mathbf{D_{RQ}} & \mathbf{D_{RR}} & \mathbf{D_{RS}} & \mathbf{D_{RT}} \\ \mathbf{D_{SQ}} & \mathbf{D_{SR}} & \mathbf{D_{SS}} & \mathbf{D_{ST}} \\ \mathbf{D_{TQ}} & \mathbf{D_{TR}} & \mathbf{D_{TS}} & \mathbf{D_{TT}} \end{bmatrix} \tag{4.2}$$

with Q, R, S and T the ensemble of the DoF laying on each of the four edges of the segment.

For the WFEM modelling of a periodic curved composite structure, a method similar to the one used in [Manconi and Mace, 2009] will be used. We consider a prismatic segment of the flat composite panel (see fig.4.1) to be modelled with mid-thickness dimensions d_c in the curvature direction and d_a in the axial direction, and whose properties may vary through the thickness direction. The extracted mass and stiffness matrices for the prismatic segment are $\mathbf{M_{flat}}$ and $\mathbf{K_{flat}}$ respectively. The mass and stiffness matrices for the corresponding singly curved structure (see fig.4.2) can then be written as:

$$\mathbf{M} = \mathbf{T}^T \mathbf{M_{flat}} \mathbf{T} \tag{4.3}$$
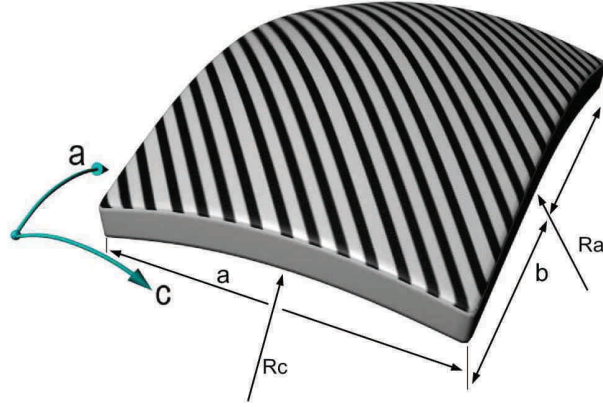
Figure 4.3: *A layered doubly curved panel*

$$\mathbf{K} = \mathbf{T}^T \mathbf{K_{flat}} \mathbf{T} \tag{4.4}$$

where the transformation matrix $\mathbf{T}$ is a block diagonal matrix produced by a repeated pattern of submatrices of type:

$$\begin{bmatrix} \cos L_a & 0 & -\sin L_a \\ 0 & 1 & 0 \\ \sin L_a & 0 & \cos L_a \end{bmatrix} \tag{4.5}$$

for the left-side nodes, and:

$$\begin{bmatrix} \cos L_a & 0 & \sin L_a \\ 0 & 1 & 0 \\ -\sin L_a & 0 & \cos L_a \end{bmatrix} \tag{4.6}$$

for the right-side nodes, where $L_a = \dfrac{d_c}{2R_a}$, with R_a the mid-thickness curvature radius around a axis of the curved structure. The analysis can then be conducted using the transformed matrices and following the same procedure as for the flat panels.

4.3.2 Calculation of doubly curved panels

For the analysis of a doubly curved shell of fixed radii (see fig.4.3), the trapezoid FE model segment should be modified to a pyramidal frustum and a second transformation matrix $\mathbf{T_c}$ should be applied to the mass and stiffness matrices to account for the double curvature of the shell. The matrix $\mathbf{T_c}$ will be a repeated pattern of submatrices of type:

$$\begin{bmatrix} 1 & 0 & 0 \\ 0 & \cos L_c & -\sin L_c \\ 0 & \sin L_c & \cos L_c \end{bmatrix} \tag{4.7}$$

for the lower-side nodes, and:

$$\begin{bmatrix} 1 & 0 & 0 \\ 0 & \cos L_c & \sin L_c \\ 0 & -\sin L_c & \cos L_c \end{bmatrix} \tag{4.8}$$

for the upper side nodes, where $L_c = \dfrac{d_a}{2R_c}$, with R_c the mid-thickness curvature radius around c axis of the curved structure. The new mass and stiffness matrices can be written as:

$$\mathbf{M} = \mathbf{T_c}^T \mathbf{T}^T \mathbf{M_{flat}} \mathbf{T} \mathbf{T_c} \tag{4.9}$$

$$\mathbf{K} = \mathbf{T_c}^T \mathbf{T}^T \mathbf{K_{flat}} \mathbf{T} \mathbf{T_c} \tag{4.10}$$

4.3.3   Numerical issues

When a stiff and light configuration (such as a sandwich material with stiff facesheets coupled to a light core) is to be modelled, care has to be taken for the discretization of the structural segment. A particularly small segment may result in the product $\omega^2 \mathbf{M}$ being much smaller than the stiffness matrix $\mathbf{K}$ and round-off errors may occur during the calculation of the dynamic stiffness matrix for low frequencies. In that case the numerical solver may be unable to compute the correct eigenvalues for the problem. This is the reason for which as large segments as possible should be chosen for low frequency calculations. On the other hand very large segments will result in poor accuracy of the solution for higher frequencies.

In order to get a large segment without sacrificing the accuracy of the calculation for higher frequencies, four piles of elements can be used and unified, resulting in a pile of mid-side nodded elements with internal nodes as shown in fig.4.4. However the eigenproblem to be solved can get excessively complex in this way. For that reason the relations given in [Manconi and Mace, 2007], introducing dependence of the mid-side nodes displacement with respect to the reference edge node Q will be used:

$$\mathbf{u_U} = \lambda_c^{0.5} \mathbf{u_Q}, \ \ \mathbf{u_V} = \lambda_a^{0.5} \mathbf{u_Q} \tag{4.11}$$

The errors introduced by this assumption seem to be negligible for the cases of interest. A validation of this assumption for curved structures will be presented in the section of numerical examples.

The internal nodes Y can be taken into account by a dynamic condensation method presented in [Inquiété, 2008]. The dynamic stiffness matrix will now be partitioned as:

$$\begin{bmatrix} \mathbf{D_{QQ}} & \mathbf{D_{QR}} & \mathbf{D_{QS}} & \mathbf{D_{QT}} & \mathbf{D_{QU}} & \mathbf{D_{QV}} & \mathbf{D_{QW}} & \mathbf{D_{QX}} \\ \mathbf{D_{RQ}} & \mathbf{D_{RR}} & \mathbf{D_{RS}} & \mathbf{D_{RT}} & \mathbf{D_{RU}} & \mathbf{D_{RV}} & \mathbf{D_{RW}} & \mathbf{D_{RX}} \\ \mathbf{D_{SQ}} & \mathbf{D_{SR}} & \mathbf{D_{SS}} & \mathbf{D_{ST}} & \mathbf{D_{SU}} & \mathbf{D_{SV}} & \mathbf{D_{SW}} & \mathbf{D_{SX}} \\ \mathbf{D_{TQ}} & \mathbf{D_{TR}} & \mathbf{D_{TS}} & \mathbf{D_{TT}} & \mathbf{D_{TU}} & \mathbf{D_{TV}} & \mathbf{D_{TW}} & \mathbf{D_{TX}} \\ \mathbf{D_{UQ}} & \mathbf{D_{UR}} & \mathbf{D_{US}} & \mathbf{D_{UT}} & \mathbf{D_{UU}} & \mathbf{D_{UV}} & \mathbf{D_{UW}} & \mathbf{D_{UX}} \\ \mathbf{D_{VQ}} & \mathbf{D_{VR}} & \mathbf{D_{VS}} & \mathbf{D_{VT}} & \mathbf{D_{VU}} & \mathbf{D_{VV}} & \mathbf{D_{VW}} & \mathbf{D_{VX}} \\ \mathbf{D_{WQ}} & \mathbf{D_{WR}} & \mathbf{D_{WS}} & \mathbf{D_{WT}} & \mathbf{D_{WU}} & \mathbf{D_{WV}} & \mathbf{D_{WW}} & \mathbf{D_{WX}} \\ \mathbf{D_{XQ}} & \mathbf{D_{XR}} & \mathbf{D_{XS}} & \mathbf{D_{XT}} & \mathbf{D_{XU}} & \mathbf{D_{XV}} & \mathbf{D_{XW}} & \mathbf{D_{XX}} \end{bmatrix} \tag{4.12}$$
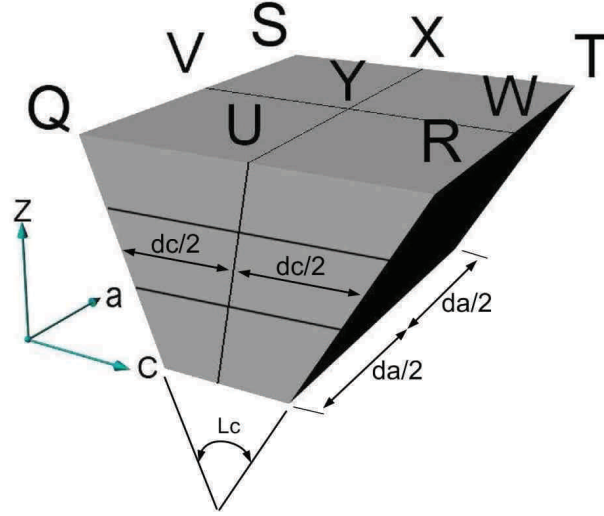
Figure 4.4: *A trapezoid FE model divided into four stacks of elements*

And the new eigenproblem will be given by the equation:

$$
\left\{ \begin{array}{cccccccc} \mathbf{I} & \lambda_c^{-1}\mathbf{I} & \lambda_a^{-1}\mathbf{I} & \lambda_c^{-1}\lambda_a^{-1}\mathbf{I} & \lambda_a^{-0.5}\mathbf{I} & \lambda_c^{-1}\lambda_a^{-0.5}\mathbf{I} & \lambda_c^{-0.5}\mathbf{I} & \lambda_a^{-1}\lambda_c^{-0.5}\mathbf{I} \end{array} \right\} \mathbf{D} \left\{ \begin{array}{c} \mathbf{I} \\ \lambda_c\mathbf{I} \\ \lambda_a\mathbf{I} \\ \lambda_c\lambda_a\mathbf{I} \\ \lambda_a^{0.5}\mathbf{I} \\ \lambda_c\lambda_a^{0.5}\mathbf{I} \\ \lambda_c^{0.5}\mathbf{I} \\ \lambda_a\lambda_c^{0.5}\mathbf{I} \end{array} \right\} \mathbf{u_Q} = \mathbf{0}
$$

(4.13)

which results in a fifth-degree polynomial eigenvalue problem considering that the frequency and the wavenumber in one direction are known (e.g wavenumber corresponding to a mode of the panel). Some ways for solving the present eigenproblem are presented in [Manconi and Mace, 2007] and [Inquiété, 2008]. It can be solved within a commercial mathematics software containing solution routines for non-linear eigenvalue problems. Once the solutions of the eigenproblem are known, the wavelengths corresponding to real, propagating in the structure waves are distinguished from evanescent waves and numerical artifacts by a process described in [Inquiété, 2008]. The calculated wavelengths can then be converted to wavenumbers for each wave type using eq.(4.14).

$$
\kappa_c = \frac{log\left(\lambda_c\right)}{-id_c} \quad \text{and} \quad \kappa_a = \frac{log\left(\lambda_a\right)}{-id_a}
$$

(4.14)

4.4 Calculation of the energy analysis properties for the structures

4.4.1 Calculation of the modal density

The Courant's approach presented in [Courant and Hilbert, 1989] has been adopted by many authors (see [Ghinet et al., 2005, Wilkinson, 1968, Hart and Shah, 1971]) for the modal density cal-
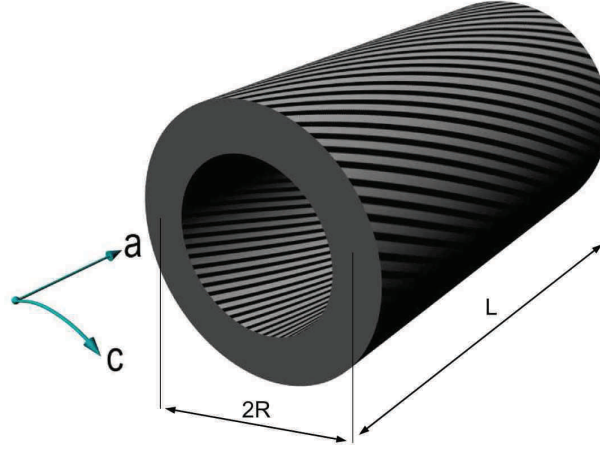
Figure 4.5: *A composite cylindrical shell modeled within the present approach*

culation of shallow shells. This formula can be written as a function of the propagating wavenumber for each angle ϕ and its corresponding group velocity c_g of each wave type:

$$n\left(\omega, \phi\right) = \frac{A \; \kappa\left(\omega, \phi\right)}{2\pi^2 \; |c_g\left(\omega, \phi\right)|} \tag{4.15}$$

where A is the area of the panel and the group velocity is expressed as:

$$c_g\left(\omega, \phi\right) = \frac{d\omega}{d\kappa\left(\omega, \phi\right)} \tag{4.16}$$

The modal density of the structure is eventually given as a function of frequency:

$$n\left(\omega\right) = \int_0^\pi n\left(\omega, \phi\right) d\phi \tag{4.17}$$

With regard to the composite cylindrical shells (see fig.4.5), it is known that [Manconi and Mace, 2009, Troclet, 2006b], the circumferential wavenumber can only take discrete values, namely: $k_c = n/R$, where n is an integer and R the cylinder's radius. Therefore, the entirety of the propagating axial wavenumbers k_a for each possible k_c in the frequency range considered, has to be calculated. The flexural waves are considered to carry the vast majority of energy for a vibroacoustic transmission, therefore they will be the only ones to be considered for the analysis. Once all the propagating wave types and their wavenumbers are calculated, the eigenfrequency for each mode can be computed, as it is known (see [Troclet, 2006b]), that for a simply supported cylinder each mode corresponds to an axial wavenumber of $k_a = m\pi/L$ with m an integer and L the cylinder's length. By knowing the resonance frequency for each mode, it is straightforward to count the number of modes in each frequency band and calculate the cylinder's modal density.

4.4.2 Calculation of the radiation efficiency

In order to calculate the radiation efficiency $\sigma\left(\kappa\left(\omega, \phi\right)\right)$ of shallow composite shells the asymptotic formulas presented in [Leppington et al., 1982] are used. Energy equipartition amongst the resonant

modes is assumed, so that the radiation efficiency is written as:

$$\sigma_{rad}(\omega) = \frac{1}{n(\omega)} \int_0^\pi \sigma(\kappa(\omega, \phi)) n(\omega, \phi) d\phi \tag{4.18}$$

The radiation efficiency for cylindrical shells can be estimated using the calculated axial and circumferential propagating wavenumbers for each mode of the cylinder, as described in [Szechenyi, 1971a]. The modes whose wavenumbers satisfy the relationship:

$$k^2 > k_c^2 + k_a^2 \tag{4.19}$$

-where k is the acoustic wavenumber- are considered to be acoustically fast (AF) modes, while the contrary is true for the acoustically slow (AS) modes. Following the same process used for flat plates, AS modes can be classified into edge modes and corner modes, whose definition can be found in [Maidanik, 1962] where it is derived that for a cylindrically shaped structure there is no corner mode radiation. An expression for the radiation efficiency for AS edge modes as a function of the flexural wavenumbers of each mode is presented in [Szechenyi, 1971a], and will be used within the current approach. Eventually, the averaged cylinder's radiation efficiency for a frequency band is considered as:

- $\sigma_{rad} = \dfrac{N_{AF}}{N}$ in the case of coexistence of AF and AS modes, where N_{AF} is the number of AF modes in the band and N the total number of modes in the band.

- $\sigma_{rad} = 1$ in the case that only AF modes exist in the frequency band, and

- $\sigma =_{rad} \dfrac{\sum \sigma_{AS}}{N}$ where σ_{AS} the radiation efficiency of each AS edge mode, in case only AS modes exist in the frequency band.

4.4.3 Calculation of the Sound Transmission Loss (STL)

A classical SEA approach is used in order to calculate the STL (or TL) of the curved panels under a reverberant sound field. The configuration to be modelled is presented in fig.4.6 and it comprises three subsystems. A source room (subsystem 1), the composite panel (subsystem 2) and a receiving room (subsystem 3).

Following SEA analysis [Lesueur et al., 1988] the Noise Reduction (NR) of the sound power level occurring inside the receiving room will be given by the relation:

$$NR = 10 \, log_{10} \left(\frac{\eta_{13} + \dfrac{n_2 \eta_{rad}^2}{n_1 (\eta_2 + 2\eta_{rad})}}{\eta_3 + \dfrac{n_1 \eta_{13}}{n_3} + \dfrac{n_2 \eta_{rad}}{n_3}} \right) \tag{4.20}$$

with $1, 2, 3$ the indices representing the source room, the composite panel and the receiving room respectively, η_{13} the non-resonant radiation loss factor, η_i the dissipation loss factor for each subsystem, η_{rad} the radiation loss factor of the panel, and n_i the modal density of each subsystem. In order to account for the finite dimensions of the panel, a spatial windowing correction technique will be used to correct the non-resonant transmission η_{13}. The method is detailed in [Ghinet and Atalla, 2001].
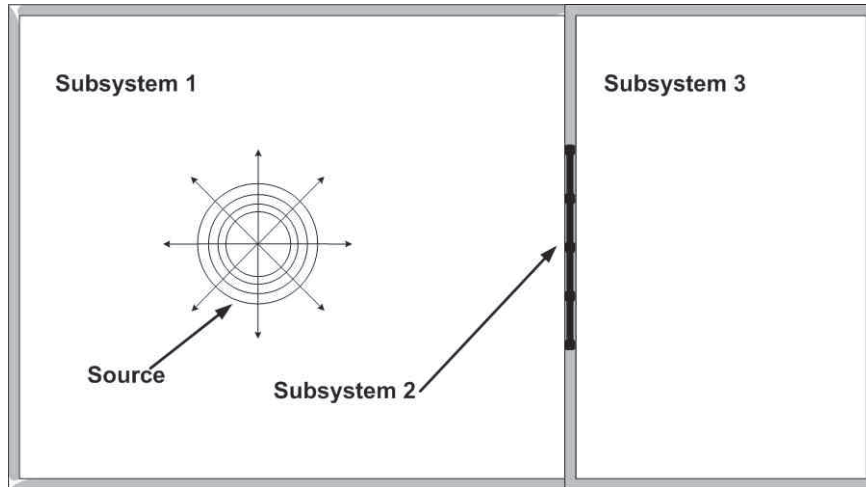
Figure 4.6: *The configuration to be modelled by SEA analysis*

Finally the TL of the structure can be calculated as:

$$STL = NR + 10 \, log_{10} \left(\frac{A}{\alpha A_3} \right) \tag{4.21}$$

where A is the area of the panel, α is the absorption coefficient of the receiving room and A_3 the total area of the receiving room.

For the resonant and non-resonant transmission within and outside a cylindrical shell the relations presented in [Szechenyi, 1971b] will be used. The non-resonant transmission coefficient above the shell's ring frequency is considered equal to the one for flat plates. For frequencies below the ring frequency the relation for the non-resonant transmission is corrected. As a statistical conception of the system is adopted, the accuracy of the given expressions depends on the modal density of the subsystems.

4.5   Numerical examples

In this section numerical applications of the approach described above will be presented. The examples include a curved sandwich panel as well as cylindrical shells for which the wavenumber, modal density, radiation efficiency, as well as the sound transmission loss under a reverberant sound field are calculated. The mechanical characteristics of each material used in the validation procedure are mentioned in Table 4.1. The directions c and a for a curved panel and a cylindrical shell are shown in fig.4.5. All validation runs were executed using ANSYS 12.1 software for the modelling and extraction of segments matrices and MATLAB 7.9.0 for the calculation of all presented results. All segments were modelled using ANSYS linear SOLID45 type elements, and all calculations were done with a 3.16GHz, double core processor using 8GB of RAM memory. The dimensions of each segment were chosen so that at least 10 elements exist per propagating wavelength. Details on the computation times for each substep of each validation case, as well as the number of DoF used to model each of the segments are given at the end of the section, in Table 4.2.

Table 4.1: *Mechanical properties of materials*

Material I	Material II	Material III	Material IV	Material V
ρ=1550 kg/m^3	ρ=110.44 kg/m^3	ρ=110.44 kg/m^3	ρ=7820 kg/m^3	ρ=9740 kg/m^3
$v_{ca} = 0.3$	$v_{ca} = 0.2$	$v_{ca} = 0.45$	$v_{ca} = 0.3$	$v_{ca} = 0.028$
$E_c = 48\ GPa$	$E_c = 0.1448\ GPa$	$E_c = 0.1448\ GPa$	$E_c = 210\ GPa$	$E_c = 2.024\ GPa$
$E_a = 48\ GPa$	$E_a = 0.1448\ GPa$	$E_a = 0.1448\ GPa$	$E_a = 210\ GPa$	$E_a = 3.138\ GPa$
$G_{ca} = 18.1\ GPa$	$G_{ca} = 0.05\ GPa$	$G_{ca} = 0.05\ GPa$	$G_{ca} = 80.77\ GPa$	$G_{ca} = 0.889\ GPa$
$G_{az} = 2.76\ GPa$	$G_{az} = 0.05\ GPa$	$G_{az} = 0.05\ GPa$	$G_{az} = 80.77\ GPa$	$G_{az} = 0.889\ GPa$
$G_{cz} = 2.76\ GPa$	$G_{cz} = 0.05\ GPa$	$G_{cz} = 0.05\ GPa$	$G_{cz} = 80.77\ GPa$	$G_{cz} = 0.889\ GPa$
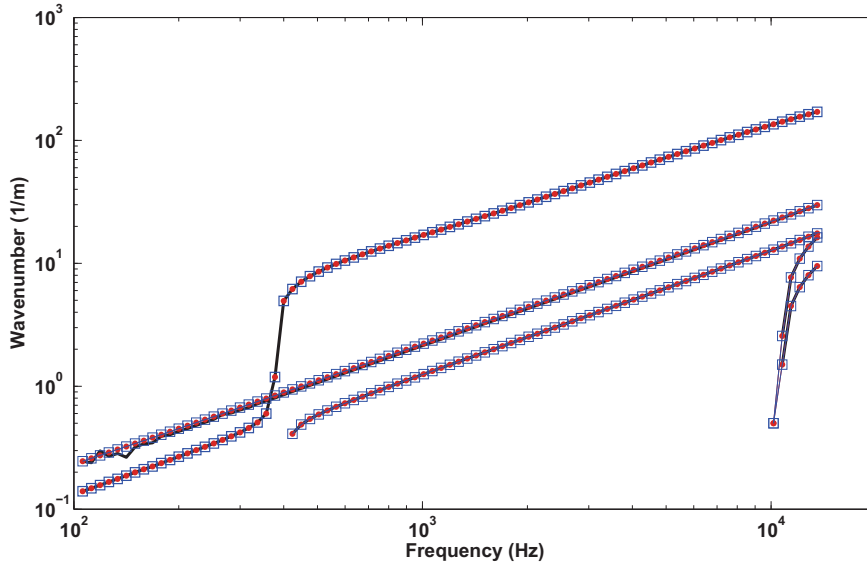
Figure 4.7: *Comparison of the WFEM calculated wavenumbers for the sandwich singly curved panel towards direction a (–) with model presented in [Ghinet et al., 2005] (bullets) and model presented in [Heron, 2002] (□)*

4.5.1   Validation of dispersion curve calculations

First and foremost the dispersion characteristics of a singly curved sandwich panel comprising facesheets made of material I and a core made of material II were computed. The thickness of each facesheet and of the core are 1.2mm and 12.7mm respectively. The panel has a curvature radius of 2m, and projected dimensions of 2.43m and 2.03m. The WFEM dispersion curves of the panel are presented in fig.4.7 and are compared to the results of a Mindlin type LW model presented in [Ghinet et al., 2005] and a discrete layer model for sandwich-type panels proposed in [Heron, 2002]. It is observed that the wavenumber results correlate excellently. Moreover the predicted ring frequencies of the panel are very much in agreement. Minor fluctuations are present for the low-frequency band of the shear wave type curve because of the numerical intricacies discussed in sec.4.3.3. This however will not affect the vibroacoustic response prediction, as in that case the flexural wave is the one transmitting the great majority of energy through the partitions.

   Next, in order to validate the assumption made for the dependence of the mid-side nodes displacement with respect to the reference node Q (see eq.(4.11)), the wavenumbers for the same structure as before will be calculated using a single pile of solid elements and will be compared to the above presented result, which was computed with a four pile segment comprising mid-nodes.
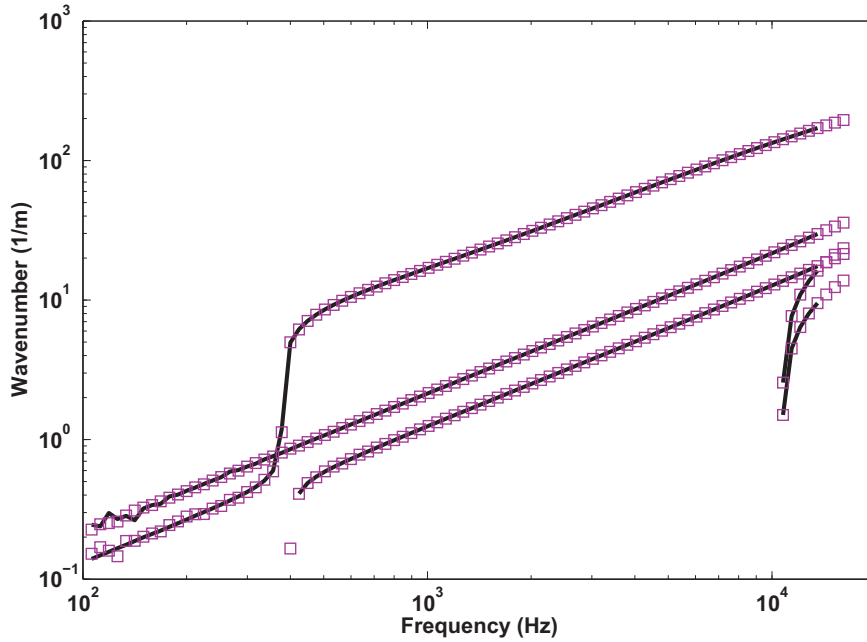
Figure 4.8: *Comparison of the WFEM calculated wavenumbers for the sandwich singly curved panel towards direction a using mid-side nodes (–) with a single pile element segment (□)*

The result is shown in fig.4.8. No significant differences are observed between the two results, validating the assumption made for the mid-side nodes displacements. As expected, the results of the flexural wavenumber calculated with a segment comprising a single pile of elements slightly fluctuate within the low frequency range due to the numerical issues described in sec.4.3.3.

The dispersion characteristics of a doubly curved sandwich panel are subsequently calculated. The panel has the same material characteristics and projected dimensions as the singly curved one. The two radii towards directions a and c are equal to 2m. The results are shown in fig.4.9 and are compared to the axial dispersion curves of the singly curved panels. It is firstly observed that the cut-on frequency of the first axial wave changes from about 400 Hz to about 700 Hz. This change shows the effect of the geometry parameters on the longitudinal propagation characteristics. However the frequency of the flexural behaviour transition towards a flat panel (where the flexural wavenumber suddenly increases to converge to the one of a flat plate), remains the same at about 380 Hz. It is also observed that the flexural wavenumber for the doubly curved panel below the transition frequency is greater that the one of the singly curved panel.

Subsequently, the WFEM will be applied to the segment of a cylindrical shell made of highly orthotropic material. As it was aforementioned in sec.4.4.1 the circumferential wavenumber for cylindrical shells can only take certain discrete values ($k_c = n/R$, $n = 0, 1, ...$). The axial wavenumbers can therefore be calculated for every discrete value of the circumferential wavenumber. In order to more properly illustrate the dispersion curves for a cylindrical shell, a 3D wavenumber surface is plotted. The cylinder is made up of material V. It has a radius curvature of 0.2515 m and a thickness of h=0.003 m. The resulting k-space figures are plotted as a function of frequency in fig.4.10. The observations are qualitatively in agreement to the diagrams presented in [Szechenyi, 1971a]. Up until the cylinder's ring frequency the frequency-constant wavenumber curves are beginning and terminating on the circumferential wavenumber axis. Beyond the ring frequency level, the curves are terminating on the axial wavenumber axis. We already know that each mode corresponds to an axial wavenumber of $k_a = m \, pi/L$ and a circumferential wavenumber of $k_c = n/R$. Therefore the corresponding frequency and wavenumbers for each mode of the structure can be
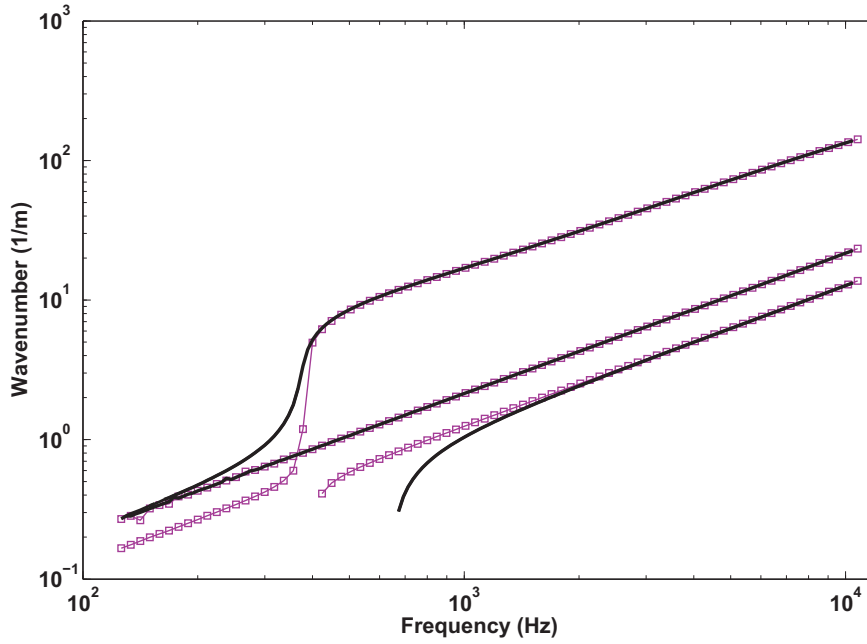
Figure 4.9: *Comparison of the WFEM calculated wavenumbers for the doubly curved sandwich panel (−) and the singly curved one towards direction a (□)*

found by interpolating on fig.4.10.

4.5.2   Validation of modal density calculations

Once the propagating wavenumbers for the sandwich curved panel are predicted, its modal density for the flexural modes can be estimated. The results are shown in fig.4.11 and are compared with the ones presented in [Ghinet et al., 2005]. The excellent agreement shown is due to the identical wavenumber prediction for the two models and the use of the same modal density derivation formula.

The modal density of flexural modes for the doubly curved panel is presented in fig.4.12 and compared to the modal density of the singly curved one. As it is expected from the observations
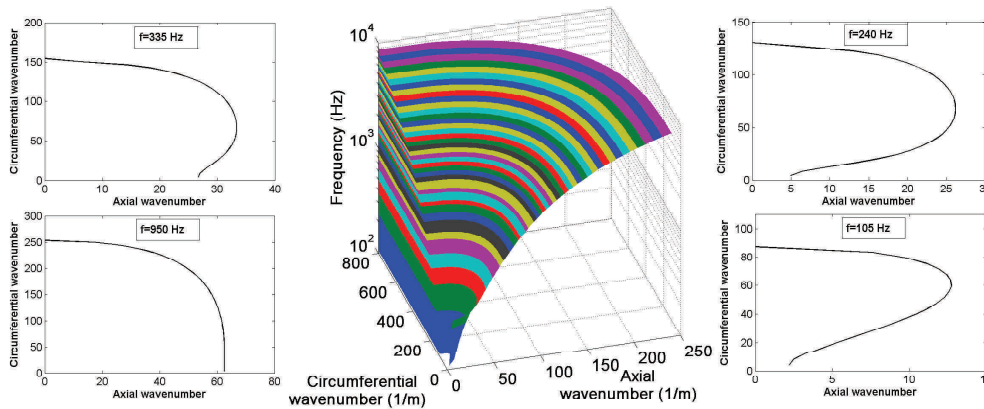
Figure 4.10: *A three-dimensional aspect of the flexural wavenumbers within a composite orthotropic cylinder, and four curves resulted from interpolation on the 3D diagram for constant frequencies.*
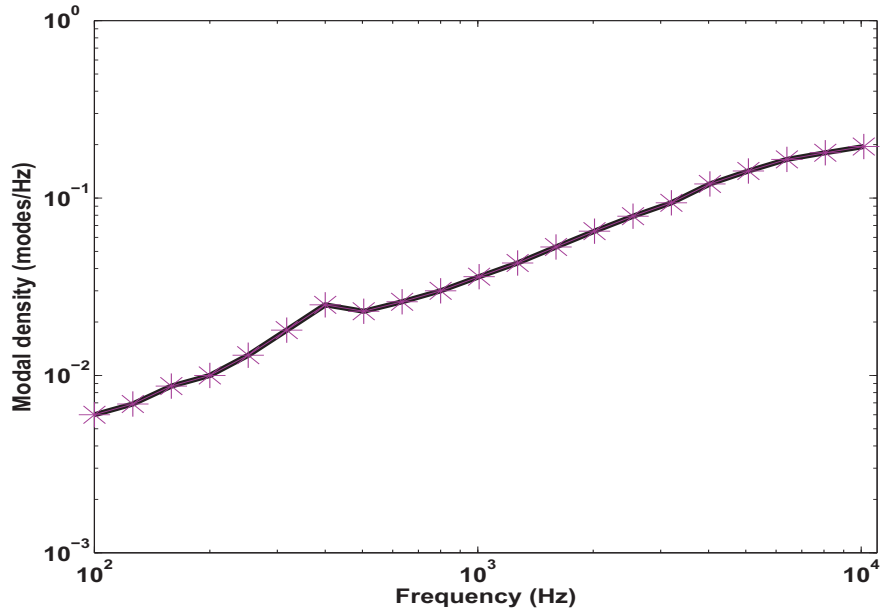
Figure 4.11: *Comparison of the modal density using the present approach (–) with results in [Ghinet et al., 2005] (*)*

regarding the wavenumbers, great differences considering the compared modal densities are presented below the flexural transition frequency (around 380 Hz), with the modal density of the doubly curved panel being much smaller that the one of the singly curved one. This observation implies that the first modes of the singly curved panel under its ring frequency are owed to the high flexural wavenumber towards its axial direction. It should be noted that the sudden increase of the modal density of the doubly curved panel is due to the fact that the flexural transition frequency occurs at the same frequency for all propagating directions (same wavenumbers for all directions of propagation). On the other hand, a singly curved panel has different transition frequencies for each propagating direction (see [Ghinet et al., 2005]) which means that the increase of the wavenumbers and of the modal density occurs progressively.

In order to validate the presented methodology for cylindrical shells a calculation for a metallic cylinder will firstly be presented due to lack of modal density and radiation efficiency results for composite cylinders in the open bibliography to the author's best knowledge. The cylindrical shell is made of material IV. It has a length equal to L=0.63m, a radius equal to R=0.2515m, and a thickness of h=0.003 m. The frequency averaged modal density for the cylinder is shown in fig.4.13. The calculated modal density is compared to the models presented in [Ramachandran and Narayanan, 2007] and [Langley, 1994b]. Excellent agreement is observed between the compared results. It is also shown that the ring frequency of the cylinder is very well predicted. Some fluctuations are present due to the different frequency bands considered in each model.

4.5.3   Validation of radiation efficiency calculations

The radiation efficiency of the curved sandwich is calculated using the Leppington's asymptotic formulas; the result is shown in fig.4.14 and it is in accordance with the results presented in [Ghinet et al., 2005]. Minor differences in the pre-coincidence region are obviously due to the complexity of the numerical implementation of the Leppington's asymptotic and transition formulas. The individual modal radiation efficiencies are also calculated using the formulas given in [Wallace,
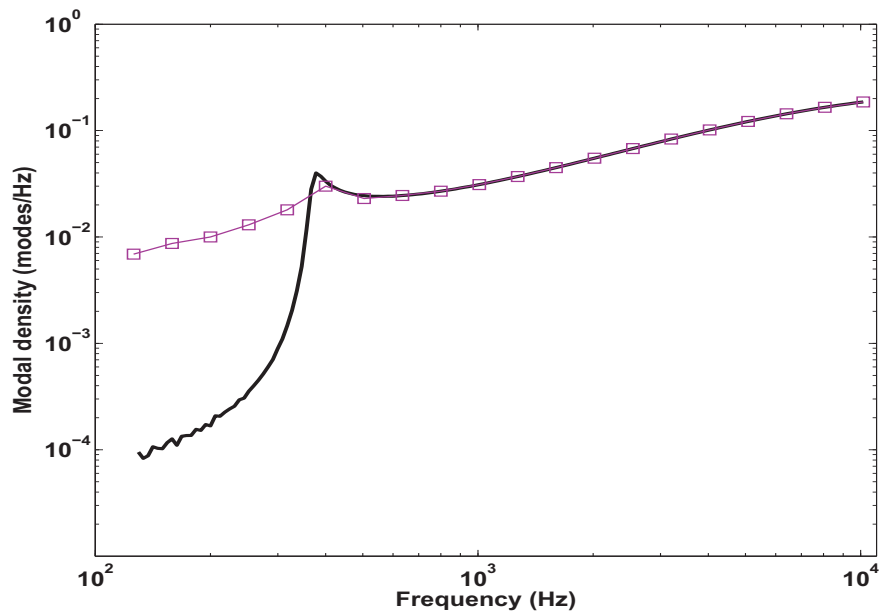
Figure 4.12: *Comparison of the modal densities of a doubly curved (–) and a singly curved panel (□)*
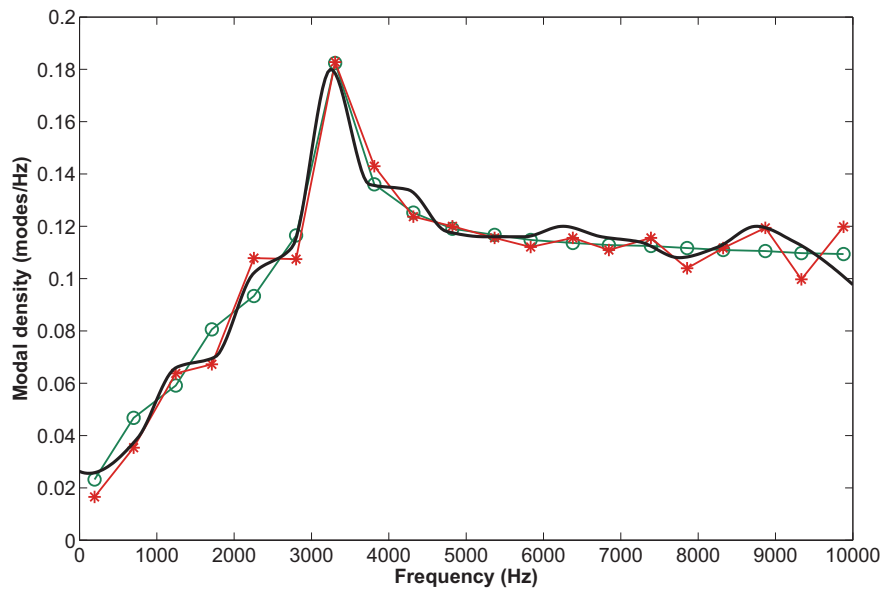
Figure 4.13: *Modal density of the cylindrical shell: present methodology(–), model presented in [Ramachandran and Narayanan, 2007] (∗), model presented in [Langley, 1994b] (o)*
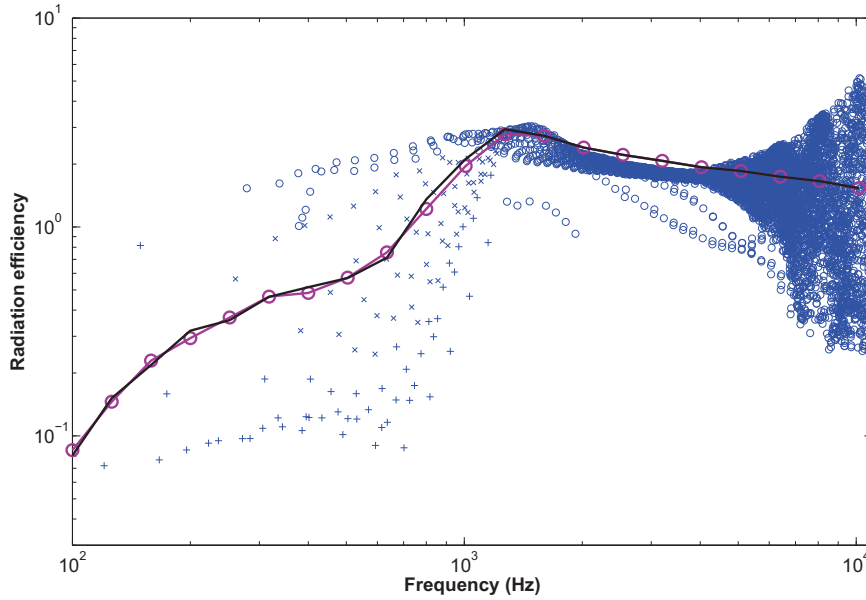
Figure 4.14: *Comparison of the radiation efficiency of a sandwich panel using: the present methodology (−), results in [Ghinet et al., 2005] (o), modal radiation formulas in [Wallace, 1972] (surface modes 'o', x-edge modes '+', x-y edge modes 'x')*

1972] and presented in the same figure. Each mode is separately attributed to different categories as shown in [Anderson and Bratos-Anderson, 2005]. For frequencies up to 1 kHz the used formulas seems to provide a fair average radiation efficiency by passing through the modal values for each frequency. In the post-coincidence region, the modal radiation values seem to gradually diverge probably due to the untruthful estimations of the modal radiation expressions which are originally given for the region where the acoustic wavelength is much greater than the panel's trace wavelength (see [Fahy and Gardonio, 2007]).

The computed radiation efficiency of the metallic cylinder is presented in fig.4.15 and is compared to the ones predicted by the models proposed in [Ramachandran and Narayanan, 2007] and [Miller and Faulkner, 1981]. Good agreement is observed between the different models. It should be noted that the model presented in [Ramachandran and Narayanan, 2007] considers AF modes with a radiation efficiency higher than unity, in contrast to the other two models where the radiation efficiency of AF modes is considered equal to unity.

4.5.4   Validation of transmission loss estimations

With the main SEA quantities being calculated, the calculation of the TL is a straightforward procedure using the equations presented in sec.4.4.3. The TL is one of the most important non-dimensional vibroacoustic indicators for a structure.

A sandwich curved panel whose facesheets were made up of material I and its core of material III was tested to measure its TL, and the experimental results are presented in [Ghinet et al., 2006]. The panel has a projected area of 1.37m x 1.65m, its facesheets have a thickness of 1.47mm and its core a thickness of 12.7mm. The TL predicted by the current approach is presented in fig.4.16 and it is observed that the results correlate very well. The effect of the ring frequency region on the TL of the panel is correctly predicted. The coincidence region, one of the most important frequency bands to predict was also very well modelled both in terms of the coincidence frequency range and the TL level. Small discrepancies within the coincidence range are probably due to the frequency
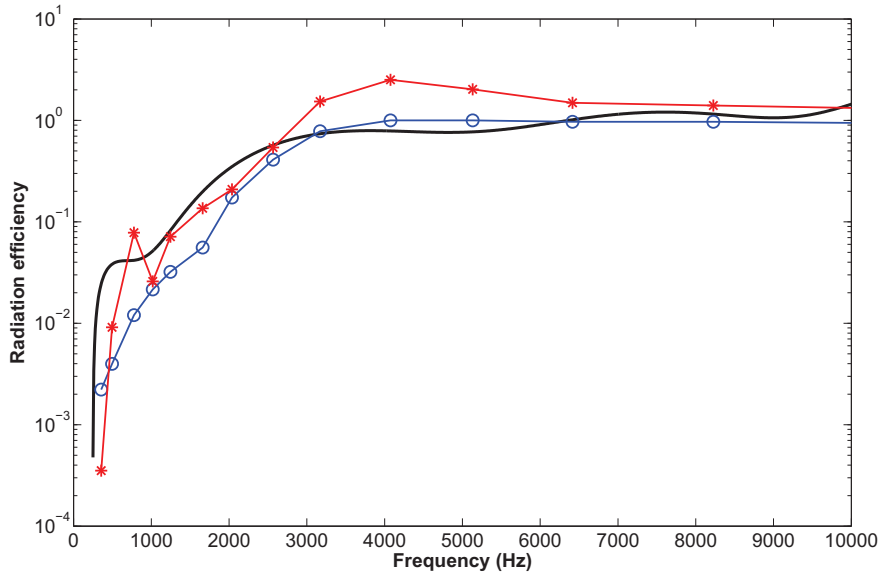
Figure 4.15: *Radiation efficiency of the cylindrical shell: present methodology (–), model presented in [Ramachandran and Narayanan, 2007] (∗), model presented in [Miller and Faulkner, 1981] (o)*

dependent damping of the structure. In the post-coincident region the presented approach is also in perfect agreement with the experimental results. The current model is very much in accordance with the one presented in [Ghinet et al., 2005].

Subsequently the TL of the doubly curved panel is calculated using the same approach as for the singly curved one and is presented in fig.4.17. It is shown that the two results are similar above the ring frequency, as the two panels have similar flexural wavenumbers (converged to a flat plate flexural wavenumber) above this frequency. Below the ring frequency, the much lower modal density of the doubly curved wavenumber implies that its resonant transmission coefficient will also be much lower, therefore its TL will be much higher than the one of the singly curved panel. The sudden fall of the doubly curved panel TL is due to the sudden rise of its modal density at the corresponding frequency range. It should be noted that a much lower modal density suggests a much lower modal overlap factor for the doubly curved panel below the ring frequency. This means that care should be taken, as the number of modes dominating the response of the structure could still be too low for an SEA approach to be accurately applied.

The TL within a sandwich type cylinder for a diffused external acoustic field is then calculated and shown in fig.4.18. The cylinder has facesheets made of material I with a thickness of $1.2mm$ and a core made up of material III with its thickness equal to $12.7mm$. The radius of the cylindrical shell is equal to $2m$. The result is compared with the model presented in [Ghinet et al., 2006], where the TL in the cylinder is calculated by computing its mechanical impedance. An excellent agreement is observed between the two models with regard to the prediction of the occurrence of the ring frequency and the coincidence region and their impact on the TL. For lower frequencies, a small difference between the predictions is observed, probably due to the different ways in which the two models account for the non-resonant transmission effects. It is worth reminding that the model in [Ghinet et al., 2006] assumes cylinders of infinite length with non-resonant acoustic interior. Moreover the acoustic transmission is considered as a forced solution problem and thus frequencies for which the propagating wavenumber in the structure exceeds the acoustic wavenumber are not considered. On the other hand, within the current approach the relations given in [Szechenyi, 1971b] for the non-resonant transmission are used. The non-resonant transmission above the
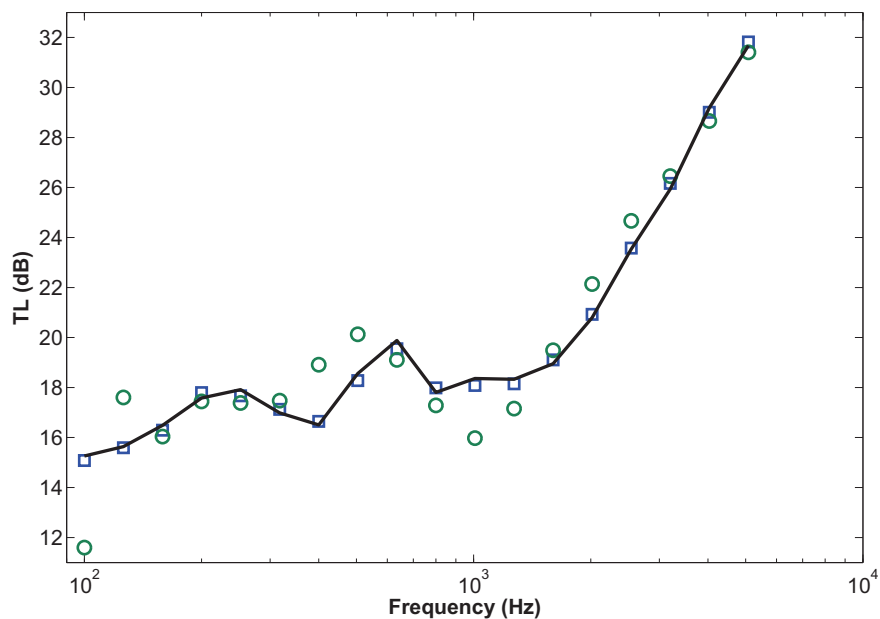
Figure 4.16: *Comparison of the transmission loss for the singly curved panel: present approach (−), experimental results in [Ghinet et al., 2006] (o), model presented in [Ghinet et al., 2005] (□)*
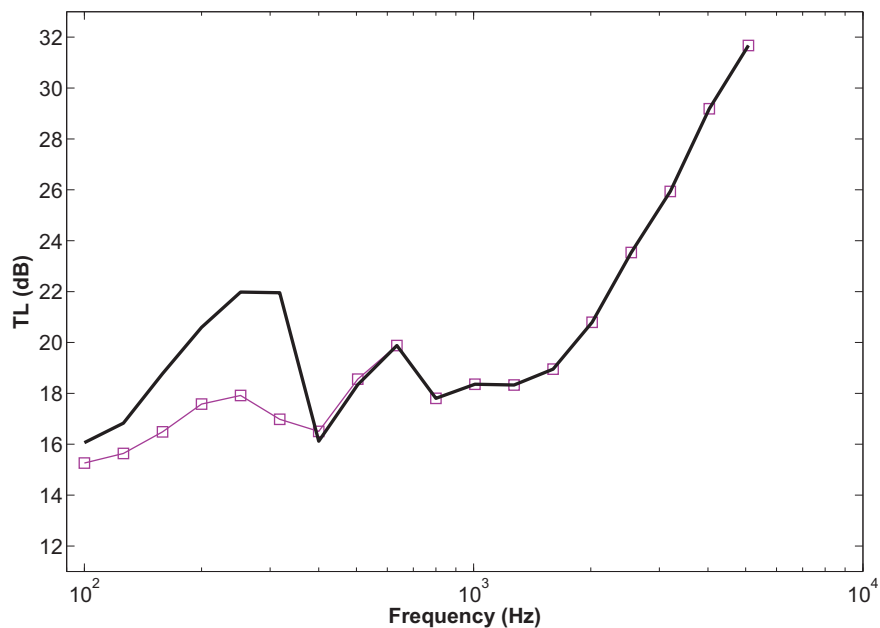
Figure 4.17: *Comparison of the transmission loss for the doubly and the singly curved panels: doubly curved panel (−), singly curved panel (□)*
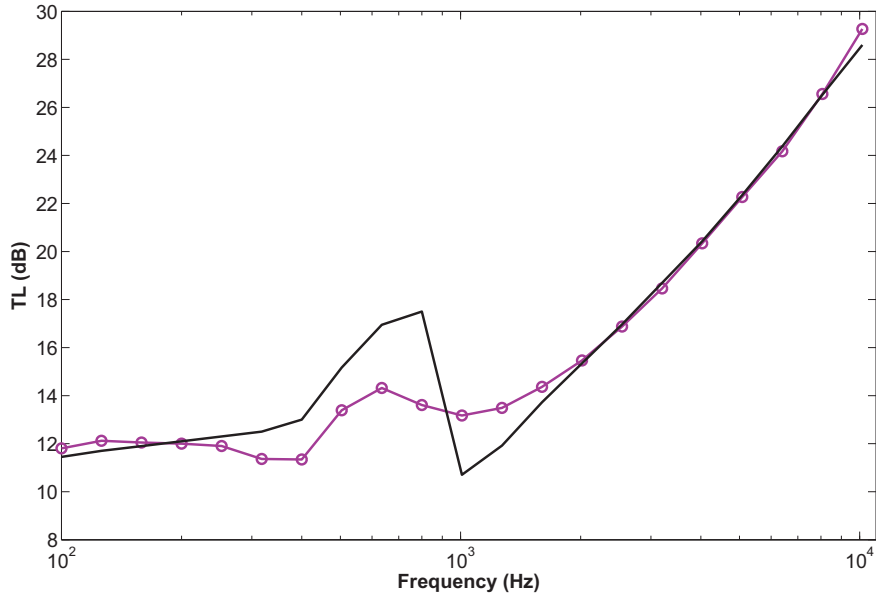
Figure 4.18: *Comparison of the diffused field TL in the cylinder: present approach (–), model presented in ref [Ghinet et al., 2006] (o)*

ring frequency of the cylinder in considered equal to the one for flat plates, while below the ring frequency the expression is corrected to take into account for the proportions of the acoustic wavenumber bands that fall into the sub- and super-coincident regions.

The computation times needed for each substep of the validation process as well as the number of DoF for the segments used in each case, are presented in Table 4.2. It is worth commenting that calculating a doubly curved panel is slightly more expensive than a singly curved one due to the extra time needed for the double transformation process. The largest percentage of calculation time for all types of structures is consumed for the computation of dispersion characteristics for each desired frequency and direction. Last but not least, the fastest calculation occurs for the cylindrical shell, mainly due to the fact that the radiation efficiency formulas that are used in this case are less expensive.

4.6   Conclusions

A robust unified-approach model for the prediction of the vibroacoustic performance of composite structural shells of various geometries within an SEA wave context approach was presented in the current work. More precisely: 1) The WFEM was used in order to predict the dispersion characteristics of arbitrarily layered composite closed and non-closed shells. The wave propagation characteristics agree very well with results presented in the literature. The ring frequencies of the curved structures are also successfully predicted. 2) The numerical issues that may arise for the low-frequency predictions when modelling exotic, light composites are discussed and an effective solution for increasing the size of the modelled segment without losing the precision at higher frequencies was proposed. 3) The main energy analysis properties, namely the modal density and the radiation efficiency of the shells were predicted following the calculation of their dispersion characteristics. The calculation was done using analytic and asymptotic formulas in a wave context. The results present a very good correlation between a variety of models presented in the literature and the current approach, validating the robustness of the later. 4) For the

Table 4.2: *Computation times for validation steps (in seconds)*

	Singly curved sandwich (mat. I,II)	Doubly curved sandwich (mat. I,II)	Sandwich cylinder (mat. I,III)
Number of segment DoF	156 DoF	156 DoF	168 DoF
Matrices extraction and transformation	3.1	5.4	3.5
Dispersion characteristics calculation (for 37 directions and 1/3 octave bands)	113.4	113.5	121.7
Modal density calculation	1.9	1.9	7.1
Radiation efficiency calculation	7.4	7.4	2.8
Calculation of the finite size correction integral	19.3	19.3	–
STL calculation	4.4	4.3	3.5
Total	149.5	151.8	138.6

calculation of the STL of the shells a classic SEA approach was adopted. A validated model was also used to take into account for the finite dimensions of the panel and to correct the non-resonant transmission coefficient. 5) For the non-closed shells, a generally very good agreement between the experimental measurements and the prediction of the presented method was observed. Small discrepancies within the coincidence range are probably due to the frequency dependent dissipation factor of the composite shell. 6) The results of the current approach for a cylindrical composite shell are successfully compared to the prediction of a 3D elasticity model. The effectiveness and robustness of the current approach is therefore demonstrated.

Chapter 5

Reducing a composite structural-acoustic system subject to random distributed excitations in the low and the mid-frequency range

5.1 Abstract

The problem of the dynamic response of a structural-acoustic system in the mid-frequency range is considered in this work. The structure is a composite panel of arbitrary thickness and anisotropy. The dissipation characteristics for both, the structure and the cavity are taken into account. The system is initially modelled using finite elements, and is subsequently reduced using the Second Order Arnoldi Reduction method (SOAR) which does not require inversion of large matrices for every computed frequency, thus resulting in more efficient calculation times. The fully coupled system is modelled using a Statistical Energy Analysis like (SEA-like) approach, and the energetic characteristics for each subsystem are computed and compared to the direct FEM solution. The error of the reduced model calculations for each frequency band is presented and the limits of the reliability of the reduction are explored. Different strategies concerning the reduction process parameters are investigated in order to optimize the accuracy with respect to time efficiency. The loading applied to the model comprises typical random distributed excitations, such as a 'rain-on-the-roof' excitation, a diffused sound field and a Turbulent Boundary Layer (TBL) excitation.

5.2 Introduction

Structural acoustic interactions in a broadband frequency range are a regular problem in modern aerospace and automotive industry. The level of noise induced by structural vibration in a cavity has to be predicted, in order to optimize the acoustic transparency of a system, such as a payload cavity of a launch vehicle, or a passenger cavity for a car. The structural loading usually includes random, distributed excitations, such as diffused acoustic fields and aerodynamic excitations. The structures are often made of composite non-isotropic materials, complicating the modelling of the structural response. Moreover, the size of the cavities is often too large, which makes deterministic techniques such as Finite Elements (FE) excessively expensive in terms of computational time at higher frequencies [Desmet, 2002]. Statistical methods such as Statistical Energy Analysis (SEA) are often considered more suitable for the medium frequency range but have limited accuracy, particularly when the modal overlap of the system is low [Mace et al., 2005]. It is therefore a vital task, the development of a robust approach for the calculation of the response of large systems, in that range where deterministic methods are too costly and statistical methods too inaccurate.

Numerous authors have investigated the fluid-structure interaction in the broadband frequency domain. In the low-frequency range, the system is typically modelled using FE or Boundary Elements (BE) as in [Maluski and Gibbs, 2000]. A Component Mode Synthesis (CMS) was used in [Magalhaes and Ferguson, 2003] in order to predict the low-frequency one-dimension fluid-structure interaction. The authors in [Pan and Bies, 1990] gave an energetic description of a panel-cavity coupled system in the mid-frequency range, by considering the modes of each uncoupled subsystem. The work was extended by Rochambeau et al. using an SEA-like approach in [de Rochambeau et al., 2011, Rochambeau et al., 2008], in order to give an accurate description of the fluid-structure interaction problem in the mid-frequency range. The method was initially introduced and studied by the authors in [Mace et al., 2005, Mace, 2005b, Fredö, 1997, Troclet et al., 2009]. The impact of the strength of coupling between the structure and the fluid on the accuracy of the prediction is investigated in [de Rochambeau et al., 2011]. Strong coupling means that taking into account for the uncoupled modes of the subsystems will lead to inaccurate results especially for the low frequency range. Furthermore the assumption of analytical expressions of the modal data of the subsystems used in [Rochambeau et al., 2008] restricts the applicability of the method to rectangular thin isotropic structures and rectangular cavities.

In order to reduce the computational effort required to resolve a structural-acoustic system, several reduction methods have been introduced. Modal reduction techniques have been successfully applied in [de Rochambeau et al., 2011, Peretti and Dowell, 1992, Ferguson et al., 2002], but they usually require analytical expressions of the modal data of the subsystems which are not always available (e.g for composite structures of arbitrary geometry). Recently, the moment matching approaches for the reduction of large scale second order systems have received much attention [Antoulas, 2005, Willcox et al., 2001, Han et al., 2005, Srinivasan Puri et al., 2009]. The method consists in finding a reduced Krylov subspace to project the initial system and was successfully applied to a fully coupled structural-acoustic system in the low-frequency range in [Srinivasan Puri et al., 2009]. Bai and Su in [Bai and Su, 2005] introduced the second-order Krylov subspace and the Second Order Arnoldi procedure (SOAR) in order for the reduced system to maintain the second order form of the initial one.

The modelling of pragmatic aerodynamic loads have been a long-term challenge. The author in [Corcos, 1963] presented one of the first models for a Turbulent Boundary Layer (TBL) excitation. Other models derived from Corcos expression were then suggested by Chase and Efimstov in order to improve the predictions for the low-frequency range [Chase, 1980, Efimtsov, 1982]. In order for such loads to be integrated in an SEA type method, δ-correlated equivalent expressions for the excitations are required. Maidanik was the first to give such an expression, with the spatial-extent approach in [Maidanik, 1961]. Recently, equivalent approaches were suggested based on a wavenumber expression of the excitation. The author in [Finnveden, 2004] modelled a TBL excitation using an asymptotic approach for the wavenumber transform of the spatial coherence function. In [Ichchou et al., 2009], the authors applied the equivalent δ-correlated excitation method on a rectangular panel and proposed an equivalent model for a TBL excitation.

The main novelty of the work hereby presented is the use of a second order moment matching method in order to reduce a fully coupled structural-acoustic system, subject to realistic aerodynamic distributed excitations, in a broadband frequency range. An expression for the TBL equivalent coherence function when applied on an orthotropic plate is given. A dynamic scheme for the number of moments that are taken into account in each frequency range is also presented in an attempt to optimize the computational efficiency of the approach. The approach is generic and robust. It drastically reduces the computation time. Moreover the advantages of an FE modelling are maintained. This implies that the system can have an arbitrary geometry and the structure can be made of an arbitrary composite material. The coupling between the subsystems can also be of arbitrary nature.

The chapter is organized as follows: In sec.5.3 the concept of a hybrid FE/SEA method for a structural acoustic coupling is presented. In sec.5.4 the equivalence relations between a purely δ-correlated excitation and realistic aeroacoustic excitations are discussed. A reverberant sound field, as well as a TBL excitation are modelled. In sec.5.5 the reduction of the vibroacoustic system using a second order Krylov subspace method, along with a dynamic scheme for increased computational efficiency are presented. Finally, in sec.5.6 numerical examples for the validation of the above presented models are given.

5.3   Modelling a structural-acoustic system with a hybrid FE/SEA method

A vibroacoustic system as the one presented in fig.5.1 is to be modelled. In the mid-frequency domain FE modelling becomes greatly costly in terms of computational times. On the other hand, the conditions for forming a proper SEA matrix are not always satisfied, mainly because of the
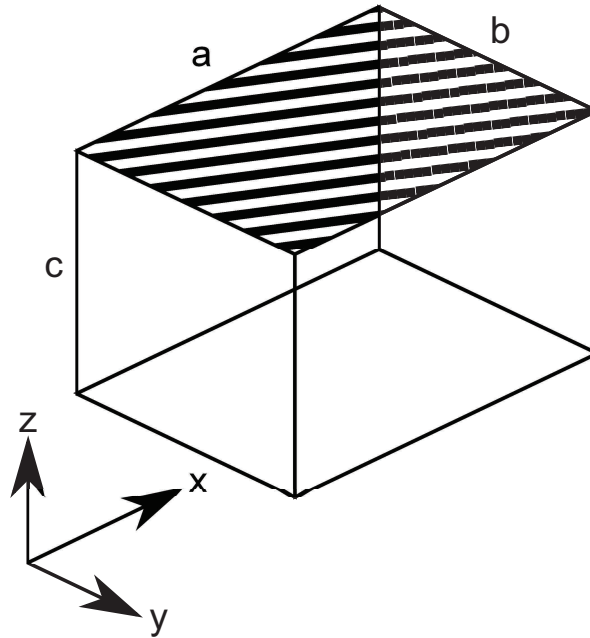
Figure 5.1: *View of the modelled configuration*

fact that the weak coupling condition between the subsystems is not satisfied and because of the indirect coupling between substructures that cannot be neglected. Moreover, in the mid-frequency range the intrinsic damping of the substructures has a great role on energetic transfer between them. Consequently, damping cannot be separated from the Coupling Loss Factors (CLF), as it is in SEA equations.

The Energy Influence Coefficient (EIC) method was presented in [Guyader et al., 1982]. As in SEA, the system is discretized in distinct n interconnected subsystems. Assuming that the loads applied to different subsystems are uncorrelated, and that the loads applied to each subsystem are δ-correlated, the column matrix of subsystems kinetic energies can be written as the product of the EIC matrix with the matrix of Power Spectral Densities (PSD) of the loads applied to the subsystems:

$$
\left\{
\begin{array}{c}
E_1 \\
E_2 \\
... \\
E_n
\end{array}
\right\}
=
\left[
\begin{array}{cccc}
A_{11} & A_{12} & ... & A_{1n} \\
A_{21} & A_{22} & ... & A_{2n} \\
... & ... & ... & ... \\
A_{n1} & A_{n2} & ... & A_{nn}
\end{array}
\right]
\left\{
\begin{array}{c}
P_1 \\
P_2 \\
... \\
P_n
\end{array}
\right\}
$$

The SEA-like method used in [Mace, 2005b, Fredö, 1997, Troclet et al., 2009], is very similar to the EIC method, with the sole difference being that the kinetic energy of the subsystems is replaced by their total energy. By exciting the subsystems one by one, the above relation can be

written as:

$$
\begin{bmatrix}
\langle E_{11}\rangle & \langle E_{12}\rangle & ... & \langle E_{1n}\rangle \\
\langle E_{21}\rangle & \langle E_{22}\rangle & ... & \langle E_{2n}\rangle \\
... & ... & ... & ... \\
\langle E_{n1}\rangle & \langle E_{n2}\rangle & ... & \langle E_{nn}\rangle
\end{bmatrix}
=
\begin{bmatrix}
A_{11} & A_{12} & ... & A_{1n} \\
A_{21} & A_{22} & ... & A_{2n} \\
... & ... & ... & ... \\
A_{n1} & A_{n2} & ... & A_{nn}
\end{bmatrix}
\mathbf{I}
$$

where

$$
\langle E_{ij}\rangle = \frac{E_{ij}}{P_j} \tag{5.3}
$$

with E_{ij} the total energy of subsystem i when subsystem j is excited and P_j the PSD injected in subsystem j. Finally, the EIC matrix can be written as:

$$
\begin{bmatrix}
A_{11} & A_{12} & ... & A_{1n} \\
A_{21} & A_{22} & ... & A_{2n} \\
... & ... & ... & ... \\
A_{n1} & A_{n2} & ... & A_{nn}
\end{bmatrix}
=
\begin{bmatrix}
\langle E_{11}\rangle & \langle E_{12}\rangle & ... & \langle E_{1n}\rangle \\
\langle E_{21}\rangle & \langle E_{22}\rangle & ... & \langle E_{2n}\rangle \\
... & ... & ... & ... \\
\langle E_{n1}\rangle & \langle E_{n2}\rangle & ... & \langle E_{nn}\rangle
\end{bmatrix}
$$

The injected power as well as the subsystem energies can be computed, by an FE modelling. The spatially averaged calculated values will then be used to estimate the energy of each subsystem and the energy exchange between them. Classic FE models as in [Everstine, 1997] will be used for the structural acoustic coupling. The total energy of an acoustic subsystem comprising N nodes can be written as:

$$
E_{ac}(\omega) = \frac{\langle p_i^2\rangle V}{\rho_0 c_0^2} \tag{5.5}
$$

with $\langle p_i^2\rangle$ the mean-square sound pressure of subsystem i, V the volume of the cavity, ρ_0 the density of the acoustic medium and c_0 the celerity of the medium. The total energy of a structural subsystem can be written as:

$$
E_{str}(\omega) = \rho_s S \langle \tilde{v}_i^2\rangle \tag{5.6}
$$

assuming that the potential and kinetic energies in both types of subsystems are equal. In eq.(5.6), $\langle \tilde{v}_i^2\rangle$ is the mean-square velocity of subsystem i, ρ_s is the surface density of the structure and S is the total area of the structural component.

5.4 Random distributed excitations

As mentioned in sec.5.3, in order to calculate the EIC of a system using the SEA-like method, a δ-correlated 'Rain-On-the-Roof' (ROR) excitation has to be applied on the subsystems. Moreover, the excitations applied to different subsystems have to be uncorrelated. Unluckily however, ROR does not represent real world excitations.

The most commonly encountered random aeroacoustic excitations in the aerospace and automotive fields are either diffused acoustic fields, or TBL excited vibration during high speed cruising.

In [de Rochambeau et al., 2011] it is shown that the following relationships between an aeroacoustic excitation and a ROR one are valid:

$$E_{s,s}^{aer}(\omega) \approx \frac{C_{eq}(\omega)}{\rho_s} E_{s,s}^{ror}(\omega)$$

$$E_{a,s}^{aer}(\omega) \approx \frac{C_{eq}(\omega)}{\rho_s} E_{a,s}^{ror}(\omega) \tag{5.7}$$

$$P_s^{aer}(\omega) \approx \frac{C_{eq}(\omega)}{\rho_s} P_s^{ror}(\omega)$$

in which s stands for the structure and a for the acoustic medium. Therefore:

$$A_{s,s}^{aer} \approx A_{s,s}^{ror}$$
$$A_{a,s}^{aer} \approx A_{a,s}^{ror} \tag{5.8}$$

Where $C_{eq}(\omega)$ is the equivalent coherence function of the aeroacoustic excitation. The great advantage of this formulation, is based on the fact that by calculating the energy exchange properties of the system under a ROR excitation, an aeroacoustic excitation can be simulated through its equivalent coherence function. Therefore only one simulation is needed for the prediction of the response of a system, under several simultaneously applied aerodynamic excitations.

5.4.1 Equivalent function for a diffused sound field

An incident diffused sound field comprises an infinite number of uncorrelated plane waves with incidence angles uniformly distributed over a half space. The equivalence correlation function of a diffused sound field can be written as in [de Rochambeau et al., 2011]:

$$C_{diff}(\omega) = \left(\frac{\pi}{k_0}\right)^2 \sigma_{rad}(\omega) \tag{5.9}$$

Where k_0 is the acoustic wavenumber given by $k_0 = \omega/c_0$. The radiation efficiency $\sigma_{rad}(\omega)$ for an orthotropic panel having finite dimensions can be calculated using expressions such as the set of asymptotic formulas given in [Leppington et al., 1982], or the one given in [Cotoni et al., 2008].

5.4.2 Equivalent function for a TBL excitation

Following the wavenumber space equivalence approach presented in [Ichchou et al., 2009], an equivalent ROR excitation can be calculated. The equivalent correlation function can be expressed in the wavenumber space as:

$$C_{eq}(k_x, k_y, \omega) = \frac{C_{eq}(\omega)}{4\pi^2} \tag{5.10}$$

Comparing the wavenumber-frequency spectrum of the studied excitation with the one of the equivalent ROR excitation, C_{eq} can be written in cartesian coordinates as:

$$\int_{k_{x1}}^{k_{x2}} \int_{k_{y1}}^{k_{y2}} C_{eq}(k_x, k_y, \omega)\, dk_y dk_x = \int_{k_{x1}}^{k_{x2}} \int_{k_{y1}}^{k_{y2}} C(k_x, k_y, \omega)\, dk_y dk_x \tag{5.11}$$

Substituting eq.(5.10) in eq.(5.11) implies that for an orthotropic panel C_{eq} can be written as:

$$C_{eq}(\omega) = \frac{4\pi^2}{(k_{x2} - k_{x1})(k_{y2} - k_{y1})} \int_{k_{x1}}^{k_{x2}} \int_{k_{y1}}^{k_{y2}} C(k_x, k_y, \omega)\, dk_y dk_x \qquad (5.12)$$

A classic model presented in [Corcos, 1963] will be used hereby, according to which the coherence function for a TBL excitation propagating in the x direction is given as:

$$C_{TBL}(\zeta, \eta, \omega) = e^{-\alpha_x \frac{\omega|\zeta|}{U_c}} e^{-\alpha_y \frac{\omega|\eta|}{U_c}} e^{\frac{i\omega\zeta}{U_c}} \qquad (5.13)$$

where $\zeta = x - x'$ and $\eta = y - y'$. The above expression can be written in the wavenumber space (see [de Rochambeau et al., 2011]) as:

$$C_{TBL}(k_x, k_y, \omega) = \frac{\alpha_x \alpha_y k_c^2}{\pi^2 (\alpha_x^2 k_c^2 + (k_x - k_c)^2)(a_y^2 k_c^2 + k_y^2)} \qquad (5.14)$$

Eventually, substituting eq.(5.14) in eq.(5.12) the equivalent coherence function of the TBL excitation can be obtained:

$$C_{eq}(\omega) = \frac{4\pi^2}{(k_{x2} - k_{x1})(k_{y2} - k_{y1})} \int_{k_{x1}}^{k_{x2}} \int_{k_{y1}}^{k_{y2}} \frac{\alpha_x \alpha_y k_c^2}{\pi^2 (\alpha_x^2 k_c^2 + (k_x - k_c)^2)(a_y^2 k_c^2 + k_y^2)} dk_y dk_x \qquad (5.15)$$

In the above equations a_x, a_y are empirical coefficients depending on the nature of the TBL excitation, U_c is the convection velocity and $k_c = \omega/U_c$ is the convection wavenumber.

5.5   Reduction using a second order moment matching method

Following classical FE formulation for structural-acoustic coupled subsystems [Everstine, 1997, Craggs, 1971], the discretized system can be written as a system of second order ordinary differential equations as:

$$\mathbf{M} \left\{ \begin{array}{c} \ddot{\tilde{x}}(t) \\ \ddot{\tilde{p}}(t) \end{array} \right\} + \mathbf{C} \left\{ \begin{array}{c} \dot{\tilde{x}}(t) \\ \dot{\tilde{p}}(t) \end{array} \right\} + \mathbf{K} \left\{ \begin{array}{c} \tilde{x}(t) \\ \tilde{p}(t) \end{array} \right\} = \mathbf{F_{sa}} \tilde{u}(t)$$
$$\tilde{y}(t) = \ell^t \left\{ \begin{array}{c} \tilde{x}(t) \\ \tilde{p}(t) \end{array} \right\} \qquad (5.16)$$

For a system with N DoF, $\mathbf{M}$, $\mathbf{C}$, $\mathbf{K} \in \Re^{N \times N}$ are the non-symmetric mass, damping and stiffness matrices, $\tilde{x}(t)$ stands for the structural displacement vector, $\tilde{p}(t)$ denotes the nodal pressure vector in the acoustic fluid, $\mathbf{F_{sa}}$ is the input matrix, $\tilde{u}(t)$ signifies the load vector of the system and ℓ^t is the transposed output matrix.

5.5.1   The Second Order ARnoldi (SOAR) process

The objective of a model order reduction process is the calculation of a subspace $\mathbf{S} \in \mathbb{C}^{N \times m}$ with m the size of the reduced model, for which the solution of the original system is written as:

$$\left\{ \begin{array}{c} \tilde{x} \\ \tilde{p} \end{array} \right\} = \mathbf{S}\tilde{b} + \tilde{\epsilon} \qquad (5.17)$$

with $\tilde{b} \in \Re^m$ and $\tilde{\epsilon}$ the error of the approximation process. Both m and $\tilde{\epsilon}$ have to be minimized, for the computational cost and the error of the reduced solution to be acceptable. Assuming harmonic excitation, the system of equations can be written after a Laplace transform as:

$$s^2 \mathbf{M} \left\{ \begin{array}{c} \tilde{x} \\ \tilde{p} \end{array} \right\} + s\mathbf{C} \left\{ \begin{array}{c} \tilde{x} \\ \tilde{p} \end{array} \right\} + \mathbf{K} \left\{ \begin{array}{c} \tilde{x} \\ \tilde{p} \end{array} \right\} = \tilde{F}$$
$$\tilde{y} = \ell^t \left\{ \begin{array}{c} \tilde{x} \\ \tilde{p} \end{array} \right\} \tag{5.18}$$

After some algebraic manipulation of the above system the variable vector is eliminated and the transfer function can be written as:

$$\tilde{h}(s) = \ell^t \left(s^2 \mathbf{M} + s\mathbf{C} + \mathbf{K} \right)^{-1} \tilde{F} \tag{5.19}$$

With $s = i\omega$, $\omega > 0$. Assuming $\mathbf{K}$ non-singular the system has a Taylor series expansion which around $s = 0$ can be written as in [de Villemagne and Skelton, 1987]:

$$\tilde{h}(s) = \tilde{m}_0 + \tilde{m}_1 s + \tilde{m}_2 s^2 + ... = \sum_{i=1}^{\infty} \tilde{m}_i s^i \tag{5.20}$$

with $\tilde{m}_i$ the leading moments. The idea of a moment matching method is to find a reduced system of dimension m, whose transfer function matches as many leading moments of the original system as possible. The second order Krylov subspace was introduced for this reason in [Su and Craig Jr., 1991]. It is defined as the subspace, spanned by the vector sequence $\tilde{q}_i$, denoted as:

$$\mathcal{K}_m \left(\mathbf{A}, \mathbf{B}, \tilde{q}_0 \right) = span \left(\tilde{q}_0, \tilde{q}_1, ..., \tilde{q}_{m-1} \right) \tag{5.21}$$

with the vector sequence $\tilde{q}_i$:

$$\tilde{q}_i = \left\{ \begin{array}{c} \tilde{q}_0 \\ \mathbf{A}\tilde{q}_0 \\ \mathbf{A}\tilde{q}_{i-1} + \mathbf{B}\tilde{q}_{i-2} \quad \text{for } i \geq 2 \end{array} \right. \tag{5.22}$$

Vector $\tilde{q}_0$ is called the starting vector, while vectors $\tilde{q}_i$ for $i > 0$ are called basic vectors. It is shown, [Lampe and Voss, 2005] that for $\mathbf{A} = -\mathbf{K}^{-1}\mathbf{C}$, $\mathbf{B} = -\mathbf{K}^{-1}\mathbf{M}$, and $\tilde{q}_0 = \mathbf{K}^{-1}\tilde{F}$, the moments of the system can be written with respect to the above vector sequence as:

$$\tilde{m}_i = \ell^t \tilde{q}_i \tag{5.23}$$

Assuming an orthogonal basis $\mathbf{S}$ of $\mathcal{K}_m$ and projecting the initial system on this basis we get the reduced second order system:

$$s^2 \mathbf{M_r}\tilde{b} + s\mathbf{C_r}\tilde{b} + \mathbf{K_r}\tilde{b} = \tilde{F}_r$$
$$\tilde{y}_r = \ell_r^t \tilde{b} \tag{5.24}$$

with

$$\mathbf{M_r} = \mathbf{S}^t\mathbf{MS}, \ \mathbf{C_r} = \mathbf{S}^t\mathbf{CS}, \ \mathbf{K_r} = \mathbf{S}^t\mathbf{KS}, \ \tilde{F}_r = \mathbf{S}^t\tilde{F}, \ \ell_r^t = \ell^t\mathbf{S} \tag{5.25}$$

In [Salimbahrami and Lohmann, 2006] it is shown that if a matrix $\mathbf{S}$ is a basis of the second-order Krylov subspace $\mathcal{K}_m \left(-\mathbf{K}^{-1}\mathbf{C}, -\mathbf{K}^{-1}\mathbf{M}, \mathbf{K}^{-1}\tilde{F} \right)$ and $\mathbf{K_r}$ is non-singular, then the first m leading moments of the original and the reduced-order models are matched. The iterative process followed for finding an orthogonal basis $\mathbf{S}$ of the second order Krylov matrix was presented in [Bai and Su, 2005], and is called a Second Order ARnoldi reduction (SOAR). The main advantage of SOAR compared to the Arnoldi reduction is the preservation of the nature of a second order system. It is therefore expected to be at least as accurate as the first order Arnoldi process [Yue and Meerbergen, 2010].

5.5.2 Expansion about $s_0 \neq 0$

If the expansion series of the system's transfer function is to be calculated around a point $s_0 \neq 0$, eq.(5.19) can be written as:

$$\tilde{h}(s) = \ell^t \left((s + s_0)^2 \mathbf{M} + (s + s_0)\mathbf{C} + \mathbf{K} \right)^{-1} \tilde{F}$$
$$= \ell^t \left(s^2\mathbf{M} + s(\mathbf{C} + 2s_0\mathbf{M}) + (\mathbf{K} + s_0\mathbf{C} + s_0^2\mathbf{M}) \right)^{-1} \tilde{F} \tag{5.26}$$

By comparing eq.(5.19) to eq.(5.26), it can be seen that we can calculate the transfer function of a system around s_0 by substituting $\mathbf{K}$ with $\mathbf{K} + s_0\mathbf{C} + s_0^2\mathbf{M}$ and $\mathbf{C}$ with $\mathbf{C} + 2s_0\mathbf{M}$ in eq.(5.19). The modified Krylov subspace can therefore be written as:

$$\mathcal{K}_m^{s_0} =$$
$$\mathcal{K}_m \left((\mathbf{K} + s_0\mathbf{C} + s_0^2\mathbf{M})^{-1}(\mathbf{C} + 2s_0\mathbf{M}), (\mathbf{K} + s_0\mathbf{C} + s_0^2\mathbf{M})^{-1}\mathbf{M}, (\mathbf{K} + s_0\mathbf{C} + s_0^2\mathbf{M})^{-1}\tilde{F} \right) \tag{5.27}$$

and the modified reduced system matrices will be calculated by projecting the initial system's matrices to an orthogonal basis of the modified Krylov subspace.

5.5.3 Dynamic dimensioning and sampling processes

As aforementioned the response of the reduced system can be calculated using the reduced transfer function:

$$\tilde{h}_r(s) = \ell_r^t \left(s^2\mathbf{M_r} + s\mathbf{C_r} + \mathbf{K_r} \right)^{-1} \tilde{F}_r \tag{5.28}$$

The accuracy of the reduced model depends highly on the number of moments m that are matched. It is observed [Antoulas, 2005, Srinivasan Puri et al., 2009], that $\tilde{\epsilon}$ increases with frequency. It can therefore be concluded that the number of matched moments needed to approximate a system with a certain $\tilde{\epsilon}$ also increases with frequency.

To the best of the authors knowledge, there exist no method for the *a priori* estimation of the error bounds for a Krylov subspace reduction process. Hereby, m_h is introduced as the minimum number of matched moments, so that $\tilde{\epsilon}$ is acceptable for the highest desired frequency band to be calculated. In the same sense, the minimum number of moments needed for the approximation error $\tilde{\epsilon}$ to be acceptable for the lowest frequency band is denoted as m_l. To minimize the computational time of the solution, a linear relation is proposed hereby, in order to decide the number of moments

Table 5.1: *Mechanical properties of materials*

Material I	Material II
ρ=9740 kg/m^3	ρ=3500 kg/m^3
$E_x = 2023.7\ GPa$	$E_x = 70\ GPa$
$E_y = 31375\ GPa$	$E_y = 70\ GPa$
$v_{xy} = 0.028$	$v_{xy} = 0.25$
$v_{xz} = 0$	$v_{xz} = 0.25$
$v_{yz} = 0.434$	$v_{yz} = 0.25$
$G_{xy} = 888.79\ GPa$	$G_{xy} = 28\ GPa$
$G_{yz} = 888.79\ GPa$	$G_{yz} = 28\ GPa$
$G_{xz} = 888.79\ GPa$	$G_{xz} = 28\ GPa$

(and therefore the size of the reduced model) m_ω that will be taken into account for the calculation at each ω :

$$m_\omega = m_l + \frac{(\omega - \omega_{min})(m_h - m_l)}{\omega_{max} - \omega_{min}} \qquad (5.29)$$

with $\omega_{min}, \omega_{max}$ respectively the minimum and the maximum angular frequencies of the analysis.

Another computational advantage of the Krylov subspace reduction methods is the possibility of extracting the solution exclusively for the desired DoF, by truncating the rows of ℓ^t that correspond to the discarded DoF. Taking into account that for an SEA-like calculation, it is the spatially averaged displacement and pressure that are required and in order to further reduce the calculation burden, a random sampling of the DoF to be calculated can be made. The impacts on accuracy as well as the computational advantages of this approach will be exhibited in sec.5.6.

5.6 Numerical examples

In this section, numerical applications for the models presented in sec.5.3 to sec.5.5 are exhibited.

5.6.1 ROR excitation

The configuration shown in fig.5.1 is to be modelled. The dimensions a, b and c are 0.7m, 0.6m and 0.5m respectively. The structure is a layered, highly orthotropic panel made of Material I (see Table 5.1), with a thickness of 0.5mm . The damping of the system is considered to be Rayleigh proportional.

The structural-acoustic system is modelled by coupling Mindlin-Reissner type two-dimensional finite elements for the panel, to three-dimensional acoustic elements for the cavity. The resulting FE model comprises 3186 structural DOF and 17832 acoustic pressure DoF. A ROR excitation is initially applied to the structural panel, using loads of equal magnitude and of random phase and position. In order to excite the entirety of the subsystem modes in each frequency band (necessary condition for a ROR excitation), the Influence Circle approach exhibited in [Troclet et al., 2009] will be used to decide the number of applied loads. The error $\epsilon\left(\omega\right)$ between the FE direct solution
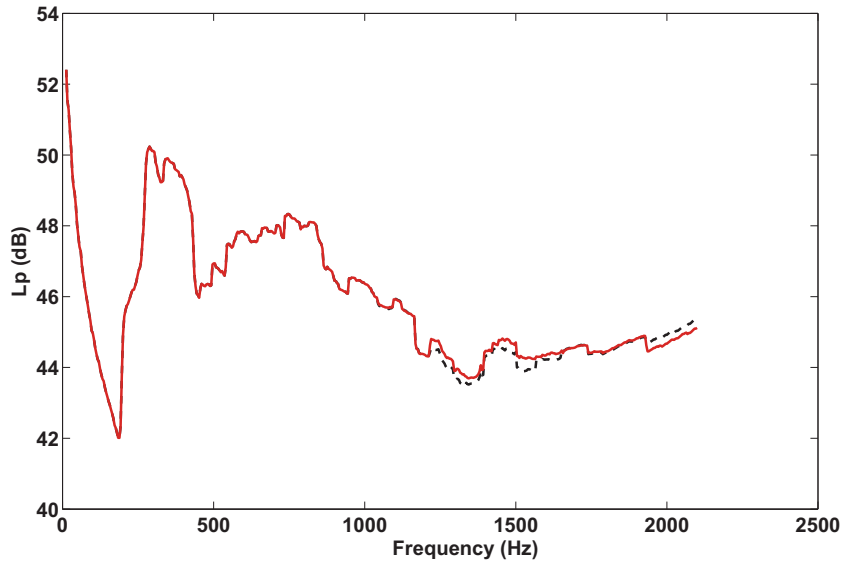
Figure 5.2: *Noise transfer function for a central acoustic DoF under a ROR excitation: FE direct solution (--), SOAR method (–)*

and the estimation of the reduced model is computed as:

$$\tilde{\epsilon}(\omega) = \frac{\left|\tilde{h}_r(\omega) - \tilde{h}(\omega)\right|}{\left|\tilde{h}(\omega)\right|} \tag{5.30}$$

Firstly, the noise transfer function for a central cavity node is calculated in order to validate the ability of the SOAR method to accurately predict the response of a single DoF. The node coordinates are (0.2m,0.325m,0.072m). The reference pressure is $p_{ref} = 20\mu$Pa. The acoustic medium's density is $\rho_0 = 1.3$ kg/m^3, its celerity is c_0=343m/sec, and the admittance of the cavity's boundaries is considered Y=0.1. The resulting Frequency Response Function (FRF) is shown in fig.5.2. The size of the reduced model is m =2000 and the expansion point of the reduced transfer function is s_0=13200rad/sec for all the results shown below, unless if differently noted. The results are averaged over one-third octave frequency bands.

Excellent agreement is observed in the low-frequency range of the response prediction. It is noted that the cavity's modal overlap M_c is equal to 1 for $f = 780$Hz. The error for this frequency band is $2.1e^{-6}$. It is observed that the error becomes noticeable only after $f = 1200$Hz. The largest divergence of the approximation occurs for the highest frequency band and is equal to 0.3dB.

The transfer function of the displacement amplitude of a structural DoF is then calculated using the same procedure. The nodal coordinates of the DoF are (0.275m,0.075m). The reference displacement is considered as $d_{ref} = 5e^{-8}$m. The results are averaged in the same way as before and are shown in fig.5.3

Again excellent agreement is observed in the low-frequency range of the prediction. The panel's modal overlap M_p is equal to 1 for $f = 985$Hz, where the error of the reduced system calculation is equal to $2.9e^{-5}$. The error becomes perceptible for frequencies higher than $f = 1440$Hz, where a cut-off frequency is observed. Just beyond this cut-off frequency, ϵ increases from 0.0087 to 0.043. The sudden increase is apparently due to the lack of higher order moments which contain information for the solution above that frequency. The largest difference between the approximated and the FE solutions occurs at the highest frequency band and is equal to 0.15dB.
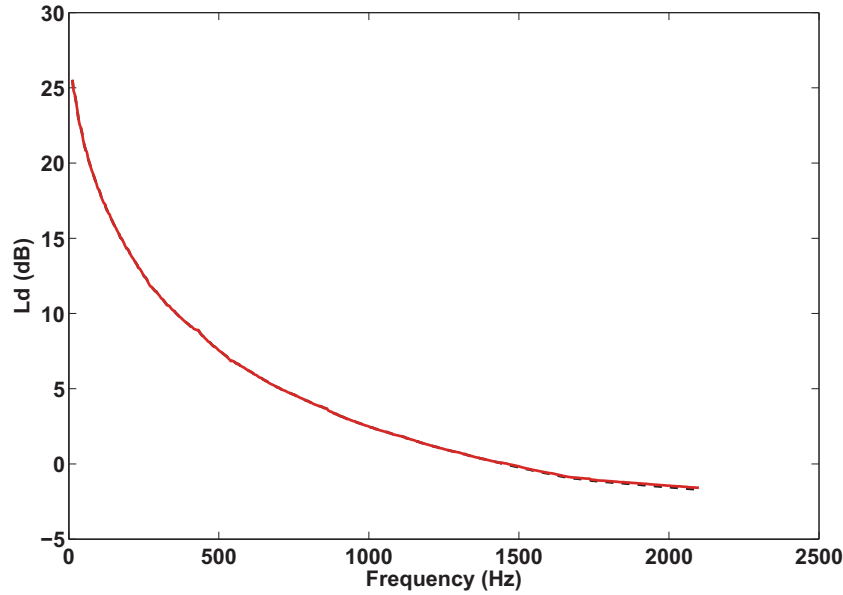
Figure 5.3: *Displacement transfer function for a structural DoF of the panel for an ROR excitation: FE direct solution (--), SOAR method (–)*

5.6.2 Influence of the calculation parameters on the reduced model accuracy

The most important parameters related to the reduced model are the dimension of the reduced model m and the expansion point s_0. In order to investigate the effect of m on the accuracy of the reduced model prediction, the error of the noise transfer function presented in fig.5.2 is calculated for different values of m. The results are presented in fig.5.4 The expansion point is s_0=2200rad/sec for all calculations.

It is observed that the accuracy of the approximation is generally increasing with the dimension of the reduced model. The extension of m from 250 to 500, reduces ϵ by almost six orders of magnitude in the low-frequency range. Further extension of m may not be so effective, however it reduces the error. It is observed that the cut-off frequency (occurring when ϵ increases by several orders of magnitude in a short frequency range) of the prediction increases with m. Several cut-off frequencies are observed for $m = 1000$ and $m = 2000$. It is observed that higher order moments contain information on the response of the system in the entire frequency range.

The influence of the choice of the expansion point s_0 is then investigated. The results of the error between the reduced transfer function and the FE calculated one for various expansion points are shown in fig.5.5. The reduced model dimension is $m = 500$ for all four cases.

It is observed that solving for s_0=1000Hz reduces the error around this region but results in larger error for higher frequencies. For a very high s_0=7000Hz, the error is large in the low frequency range, however it progressively reduces in the higher frequency range. For an s_0 at the end of the analysis range, a high cut-off frequency is observed. The curve for s_0=3500Hz presents a lower cut-off frequency, however it seems to be more precise than the other predictions for higher frequencies. For the rest of the analysis, an s_0 at the end of the analysis range is chosen (s_0=13200rad/sec).
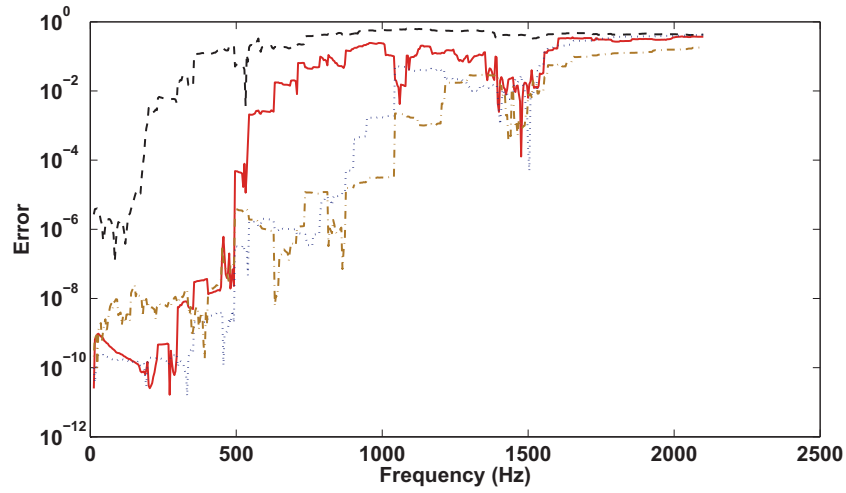
Figure 5.4: *Error of the reduced model estimation with respect to its dimension m: m=250(--), m=500(–), m=1000(· · ·), m=2000(-∗-)*
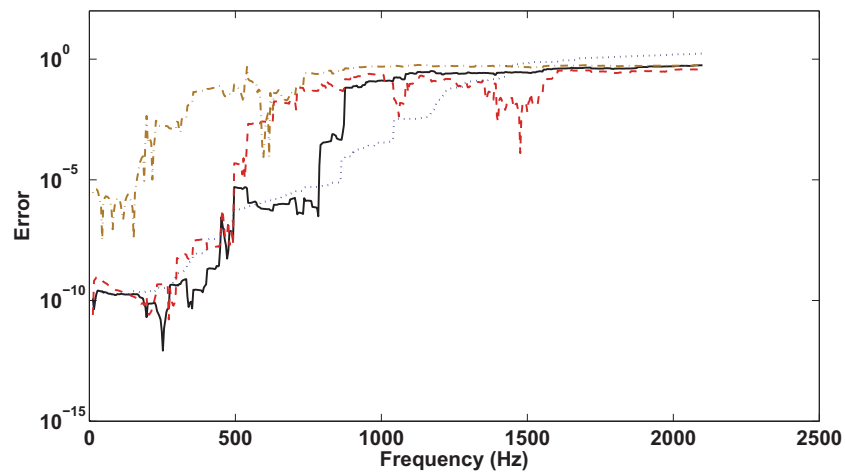
Figure 5.5: *Error of the reduced model estimation with respect to the expansion point of the reduced transfer function: s_0=1000 Hz(· · ·), s_0=2100 Hz(–), s_0=3500 Hz(--), s_0=7000 Hz(-∗-)*
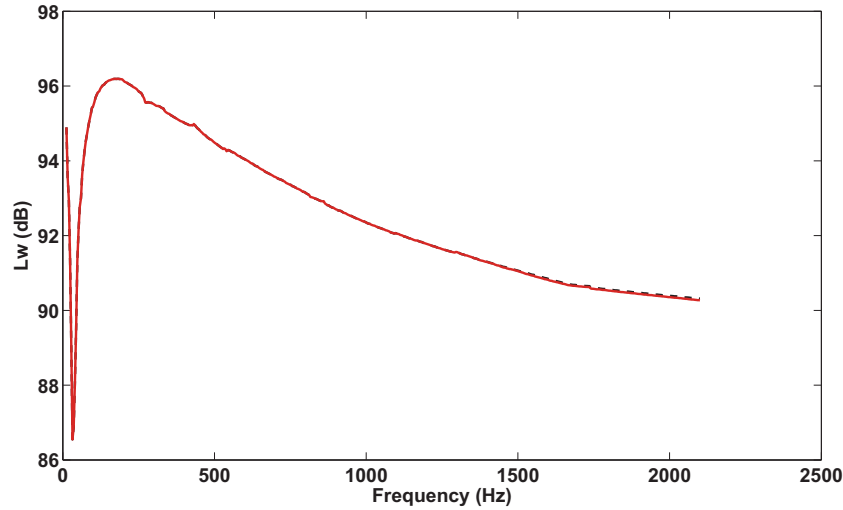
Figure 5.6: *Injected power in the system by an ROR excitation: FE direct solution (--), SOAR method (–)*
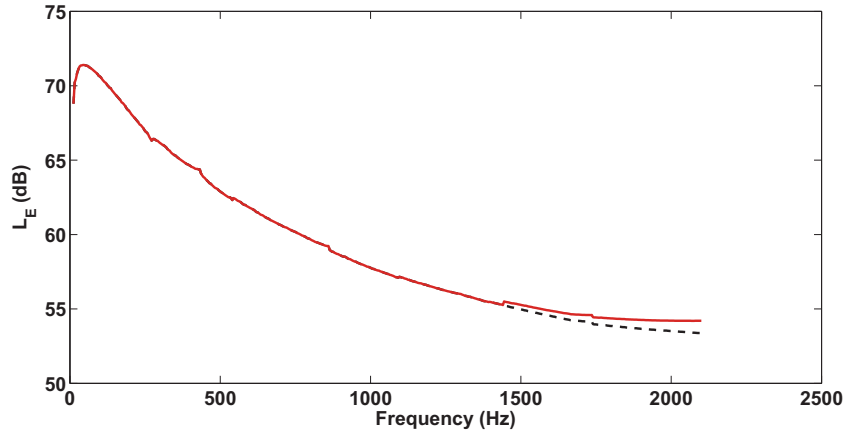
Figure 5.7: *Energy of the panel subsystem under an ROR excitation: FE direct solution (--), SOAR method (–)*

5.6.3   SEA-like analysis for a ROR excitation

An SEA-like analysis of the vibroacoustic system is conducted. The panel is excited with a ROR load. The resulted injected power is shown in fig.5.6. The reference power is considered to be $P_{ref} = 10^{-12}$W. All results are averaged over one-third octave frequency bands.

The results of the direct FE solution and the SOAR estimation present an excellent correlation throughout analysis range. The lowest of the curve is due to the low structural admittance in the stiffness controlled region of the panel. The effect of considering a damped system, as well as averaging the results does not allow the visualization of each mode separately in the low frequency range. No cut-off frequency is observed. The largest deviation between the two predictions is 0.05dB for f=2100Hz.

The steady-state total energy of the composite panel is presented in fig.5.7. The reference energy is considered to be $E_{ref} = 10^{-12}$J.

The results are in excellent agreement up until f=1440Hz. Contrary to fig.5.6 a cut-off fre-
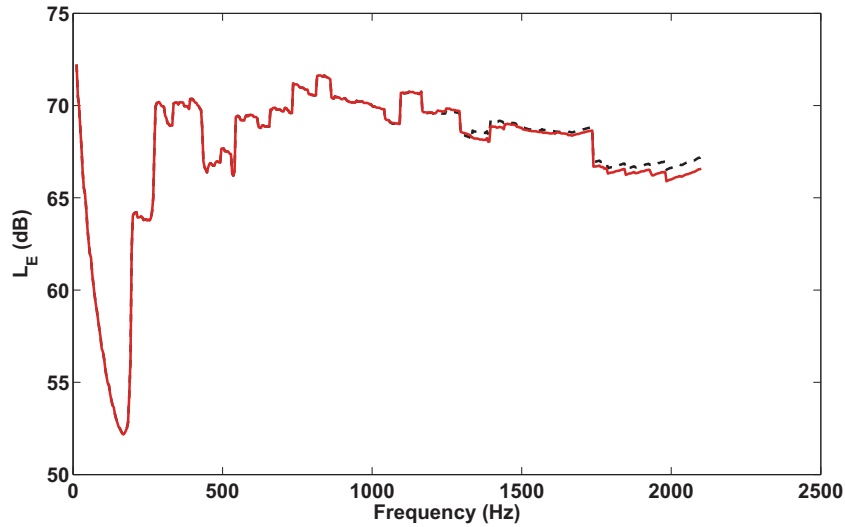
Figure 5.8: *Energy of the cavity subsystem under an ROR excitation: FE direct solution (--), SOAR method (–)*

quency is observed at that point and the error drastically increases. The largest difference between the two predictions is here 0.8dB for f=2100Hz.

The energy transmitted from the vibrating panel to the cavity under a ROR excitation is calculated using eq.(5.5) and is presented in fig.5.8.

Once again in the low frequency range no significant discrepancies are observed between the reduced solution and the FE model. In the medium and higher frequency ranges the SOAR approach seems to be slightly underestimating the cavity energy with the maximum difference between the two models being 0.6dB for f=2100Hz.

The EIC under a ROR excitation are presented for the structural and the cavity subsystems is fig.5.9,5.10. It is noted that A_{ss} stands for the structural EIC when the structure is excited, while A_{cs} is the EIC for the cavity when the structure is excited. The EIC used as reference is $EIC_{ref} = 10^{-12}$sec.

Similar behaviour as in fig.5.7 is observed for the panel behaviour. The error seems to increase dramatically after the cut-off frequency, reaching 1.05dB at the end of the analysis range. The peak of the curve at the very low frequency range is due to the increased impedance of the panel in that range. For the cavity subsystem the two predictions are very much in accordance with the maximum divergence being 0.3dB for f=1390Hz.

5.6.4 Diffused field excitation

The results of an SEA-like analysis with the panel excited by a reverberant field on its dry side are presented hereby. As stated in sec.5.4, a new FE simulation is not needed for the response of the system to be predicted. The energy quantities of the subsystems under a diffused field excitation, are directly related to the ones for a ROR (of an equal Power Spectral Density (PSD)) through the equivalence function presented in eq.(5.9). The radiation efficiency of the panel is computed using the Leppington's set of asymptotic formulas, accounting for the finite dimensions, as well as the orthotropy of the panel. The resulting levels of energy L_E for the subsystems are presented in fig.5.11,5.12.
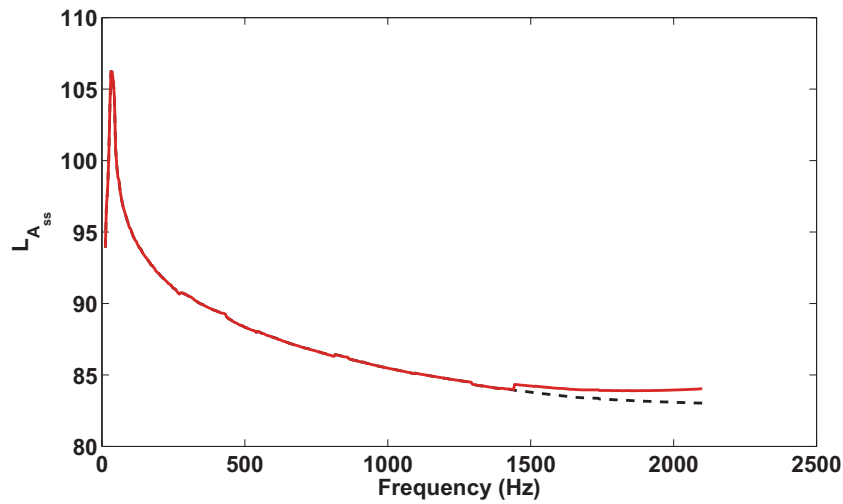
Figure 5.9: *EIC for the structural subsystem under a ROR excitation: FE direct solution (--), SOAR method (–)*
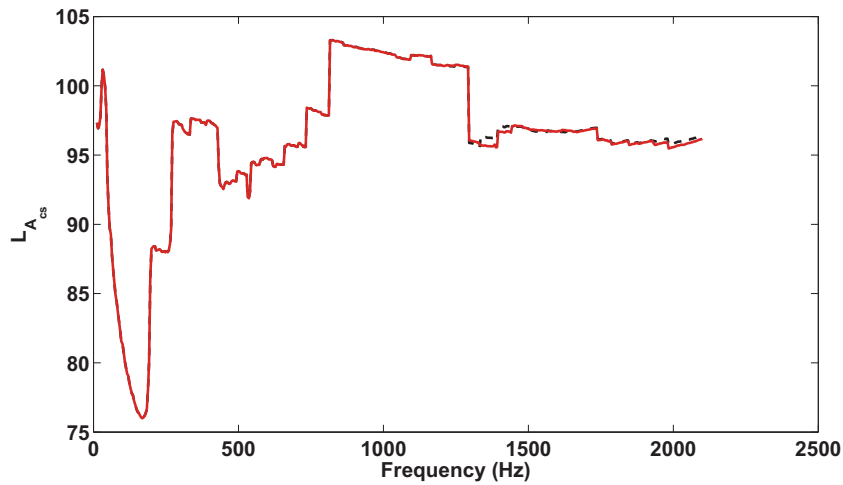
Figure 5.10: *EIC for the acoustic subsystem under a ROR excitation: FE direct solution (--), SOAR method (–)*
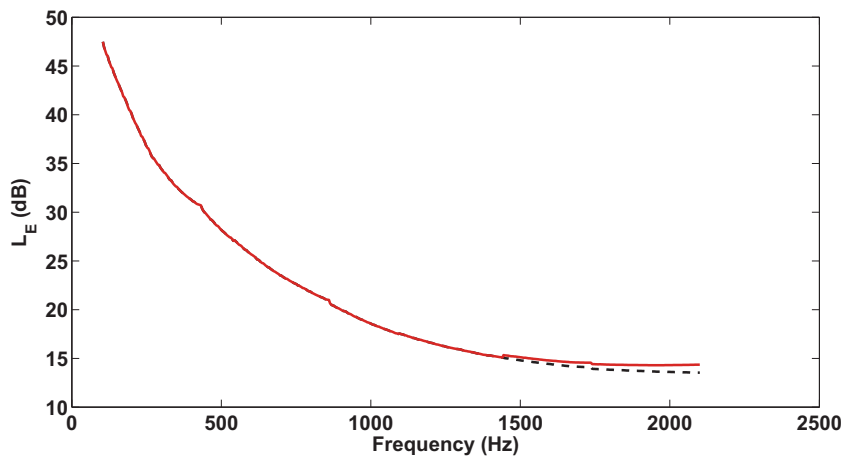
Figure 5.11: *Steady-state energy for the structural subsystem under a reverberant field excitation: FE direct solution (--), SOAR method (–)*
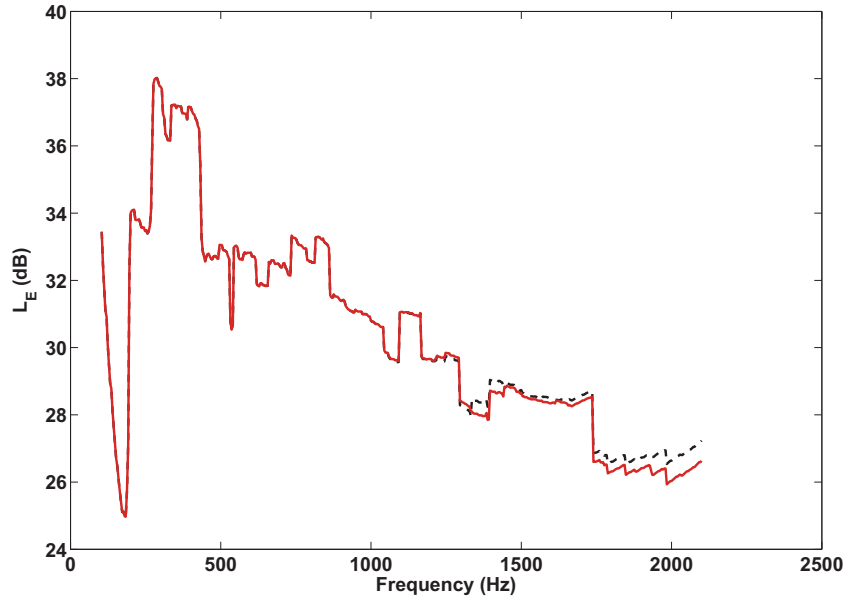
Figure 5.12: *Steady-state energy for the acoustic subsystem under a reverberant field excitation: FE direct solution (--), SOAR method (–)*

The comparison between the FE and SOAR methods are in very good agreement for the entire frequency range. The maximum difference between the predictions occurs at the end of the analysis range for both subsystems and is equal to 0.9dB for the panel's and 0.7dB for the cavity's energy level.

5.6.5   TBL excitation

A TBL excitation with empirical values corresponding to U_c =0.9 Mach which is a typical convection velocity for an aerospace structure, will be modelled using its equivalent coherence function presented in eq.(5.15). A stream propagating in x, as well as in y direction is hereby modelled. The resulting acoustic energy inside the cavity subsystem is shown in fig.5.13.

It is shown that the FE results are in a very good agreement with the ones obtained after the SOAR reduction. The largest discrepancy for both results is 0.6dB at $f = 2100$Hz. The different resulting energies for the two propagation directions are due to the orthotropic characteristics of the panel. The higher induced energy for the stream propagating towards y direction implies that the convective wavenumber is closer to the panel's structural wavenumber in this direction, resulting in better coupling and more efficient energy transmission.

5.6.6   Modelling a stiffened double panel

In order to exhibit the ability of the presented approach to deal with the modelling of complex systems, the thin panel presented above is replaced with a double, stiffened panel. The panel is presented in fig.5.14. The dimensions of the cavity subsystem a, b and c are now $0.86m$, $0.6m$ and $0.55m$ respectively. The double panel structure comprises Π-shaped stiffeners in between the facesheets.

The thickness of the facesheets and the stiffening structures is equal to $h = 1$mm. The distance between the facesheets is $d = 0.02$m. The panel comprises five vertical stiffeners with a periodic
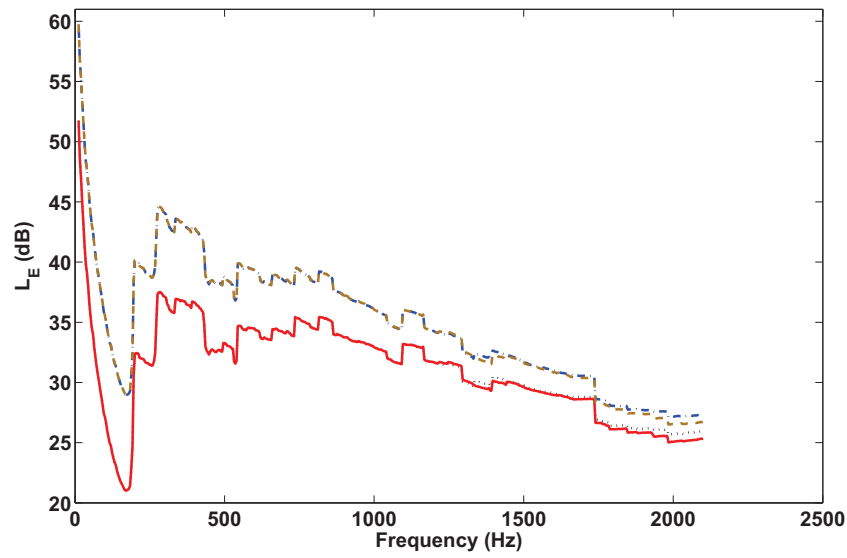
Figure 5.13: *Energy of the cavity subsystem under a TBL excitation of 0.9 Mach applied on the panel: Layer propagating towards x: FE direct solution ($\cdots$), SOAR method (–), Layer propagating towards y: FE direct solution ($\cdot - -\cdot$), SOAR method (--)*
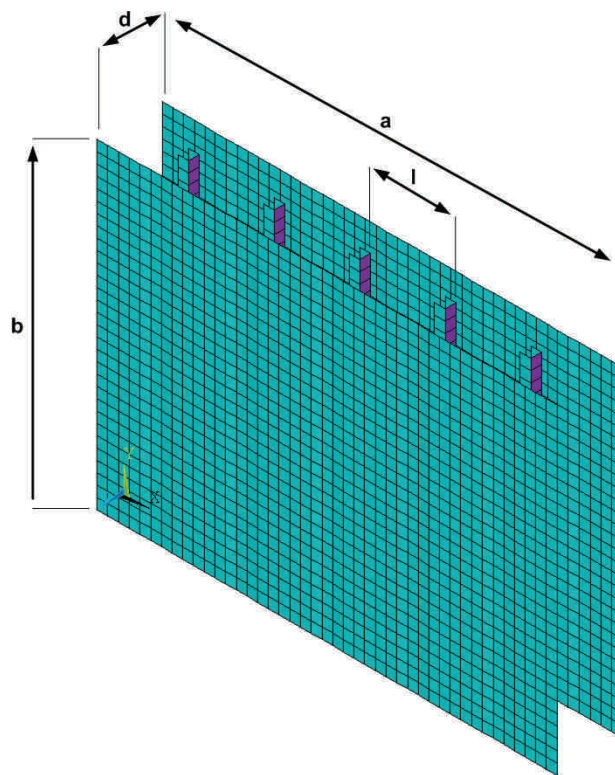
Figure 5.14: *The modelled stiffened double panel*
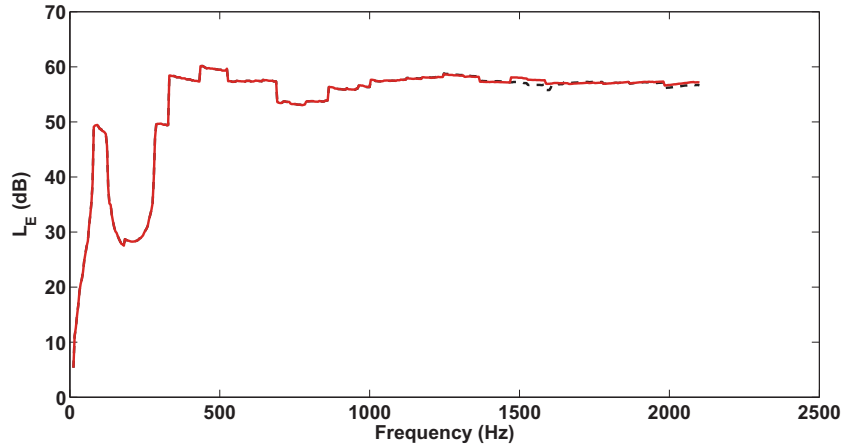
Figure 5.15: *Energy of the cavity subsystem under an ROR excitation applied on the double panel: FE direct solution (--), SOAR method (–)*

distance of $l = 0.16$m. The panel is made of material II. The damping of the system is considered to be Rayleigh proportional with 0.03 and 0.01 the mass and stiffness matrix multipliers respectively.

As with the previous example, the structural-acoustic system is modelled by coupling Mindlin-Reissner type two-dimensional finite elements for the panel, and three-dimensional linear acoustic elements for the cavity. The FE model comprises 13707 structural DoF and 38467 pressure DoF. A δ-correlated (ROR) excitation is initially applied on the dry side of the structural panel, using loads of equal magnitude and of random phase and position. The dimension of the reduced system is equal to $m = 800$. The resulting acoustic energy inside the cavity subsystem is shown in fig.5.15.

Excellent correlation between the results is observed until approximately $f = 1450$ Hz. The maximum divergence of the solution from the FE prediction occurs at approximately $f = 1600$Hz and is equal to 1.3 dB.

5.6.7   Discussion on the computational efficiency of the approach

The ability of the SOAR reduction method to accurately model a structural acoustic system was exhibited in the above presented results. However, calculation efficiency is also of essential importance. For this reason the dynamic scheme presented in sec.5.5.3 is applied hereby. Moreover, a sampling is applied over the cavity nodes for which the pressure solution is calculated. The structural-acoustic system system comprising the monolithic orthotropic panel is firstly considered. A sampling of 10% over the calculated DoF is applied. The results are presented in fig.5.16.

For a 10% sampling the results seem to be in excellent correlation with both the FE and the full (constant m=2000) SOAR solutions until about f=1440Hz. An interesting observation is that in the high frequency range the full reduced model underestimates the energy level, while the sampled one overestimates it. This is apparently due to the chosen sampling pattern. The presented result involves spatial randomization of the solved acoustic DoF for every frequency range. The maximum divergence of the dynamic scheme estimation is 1.3dB, while the one of the full calculation is 0.7dB at the highest frequency band of the analysis.

For the case of the double stiffened panel, the result obtained by the dynamic reduction and sampling scheme for the acoustic energy level inside the cavity when a ROR excitation is applied on the panel, is shown in fig. 5.17.

Excellent correlation between the results is observed until about $f = 1100$ Hz. The maximum
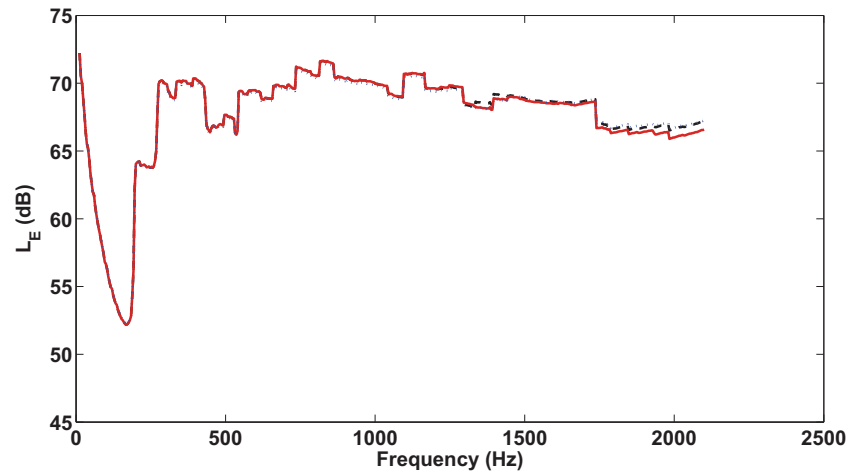
Figure 5.16: *Energy of the cavity estimated by averaging over 10% of the cavity nodes: FE direct solution (--), SOAR full (–), dynamic scheme (···)*
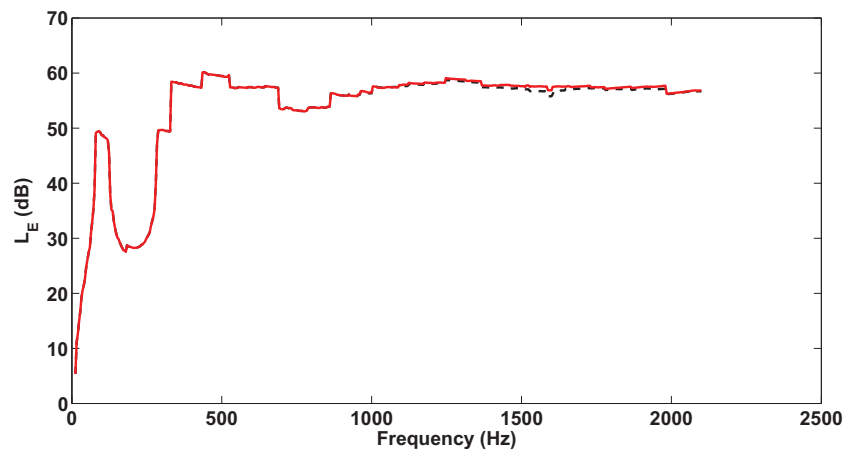
Figure 5.17: *Energy of the cavity subsystem for the double panel system, when the dynamic reduction scheme is used: FE direct solution (--), SOAR method (–)*

Table 5.2: *Calculation times*

	Orthotropic panel (m=2000)	Double panel (m=800)
Full FE solution	204 min	709 min
Calculation of the Krylov subspace + full solution	109 min	113 min
Calculation of the Krylov subspace + dynamic dimensioning	28 min	
Calculation of the Krylov subspace + dynamic dimensioning + 10% sampling	23 min	38 min

divergence of the solution from the FE prediction occurs at approximately $f = 1600$Hz and is equal to 1.3 dB. It is observed that compared to the full SOAR solution (when using constantly $m = 800$), the low frequency range prediction is slightly affected (discrepancies of 0.03 to 0.8 dB are exhibited). On the other hand, for the high frequency range where m converges to the one used for the full solution, the results are hardly affected.

The calculation time for each of the above exhibited calculations is presented in Table 5.2. It can therefore be concluded that the approach can drastically reduce the computation time while not having an important impact on the accuracy of the prediction. The total number of computed frequencies is 523. All calculations were done using a server of two, quadruple core Xeon E5343 processors, with 8Gb of RAM memory available. The direct FEM solution was done using a Lanczos algorithm within the software ANSYS 12.1, while the calculation of the Krylov subspace and the reduced solution was done using MATLAB 7.9.0. It is observed that the SOAR method reduces the demanded calculation time by almost 47% if the solution for all DoF is computed. In the case of a dynamic dimensioning of the reduced model, coupled with a 10% sampling of the solved acoustic DoF, the time reduction is almost 89%. For the case of the double stiffened panel, it is exhibited that the SOAR solution for a full solution of $m = 800$ reduces the calculation time by almost 84%. In the case of a dynamic dimensioning of the reduced model, the time reduction is 95%. This time reduction is expected to be even greater for larger industrial systems.

5.7   Conclusions

Concluding on the presented work, a structural acoustic system modelled with FE was reduced using the SOAR approach, and its broadband response to distributed aeroacoustic loads was calculated. The energy levels of the subsystems were calculated within an SEA-like approach. Summarizing the most important concluding points: 1) The approach can be used independently of the geometry and the structural acoustic coupling nature of the system as there is no need for analytical expressions of the dynamic characteristics of the subsystems. The structure may be composite and complex. The advantages of a FE modelling are therefore preserved. 2) Excellent agreement is observed in the low-frequency range for the SOAR estimation and the direct FE solution. The error of the approximation generally increases with respect to frequency. More vectors should therefore be added in the Krylov subspace in order to retain the error in a given level. A dynamic scheme for dimensioning the reduced system in each frequency band was proposed. The maximum divergence of the reduced model predictions from the FE solution were generally reported at the highest frequency of the calculation. 3) The approach was also verified for a double stiffened panel coupled with an acoustic cavity. It was shown that complex systems with regard to materials and geometry can successfully be modelled and reduced using the presented approach. 4) A cut-off

frequency range was observed, during which the error of the reduced system approximation raises by several orders of magnitude. Increasing the dimension of the reduced model can delay the appearance of this cut-off frequency. 5) The calculation times are drastically reduced when the proposed dynamic dimensioning of the reduced system is used. Moreover, further reduction can be achieved by sampling over the acoustic DoF that are calculated for the application of the SEA-like approach.

Chapter 6

Industrial validation on a layered cone-cylinder-cone shell structure

6.1 Abstract

The structural response of an industrial layered structure composed of a combination of conical and cylindrical shells is hereby modelled. In the low and the mid-frequency ranges a dynamic stiffness ESL approach coupled to FE analysis is used in order to predict the response of the shell configuration. The results are validated by experimental measurements on a composite mock-up of the SYLDA structure, as well as by a full 3D FE modelling. In the high frequency range where SEA predictions are valid, the WFEM is used in order to revisit the CLF calculation for structural transmission between the composite shells that are individually considered as SEA subsystems. Finally the energy ratios between the subsystems is computed and validated by experimental measurements conducted on the aforementioned industrial structure. The robustness of an SEA approach is then questioned.

6.2 Introduction

Structures made of composite materials and having complex geometric characteristics are extensively used in the modern aerospace industry. More precisely, composite conical-cylindrical combinations of shells are often used as protective payload structures (SYLDA structure of Ariane 5), rocket booster parts, and fuselage components. Modelling the vibroacoustic behaviour of cylindrical and conical shell structures as well as of their combinations is thus essential during the design process of modern aerospace products.

The vibrational modelling of coupled conical-cylindrical systems consists a relatively new area of research. Numerical techniques such as the FEM are still considered as the most pertinent approach for modelling coupled composite systems of complex geometries. With regard to the rest of the available models, a number of approaches have been recently published, being roughly divided into modal approaches which aim to predict the free vibration natural frequencies and mode shapes of the system and wave approaches which aim to predict the wave dispersion and transmission between parts of the system that have homogeneous characteristics. The former type of models is usually used when an accurate description of the global modes of the system is essential for predicting its vibrational behaviour that is mainly for the low frequency range. On the other hand, modelling the system in a wave context is more suitable for calculating the SEA coupling loss factors between subsystems which is more accurate in the high frequency range.

One of the first investigations on the effect of discontinuities on the vibration of thin connected shells is made in [Kalnins, 1964]. Some years later, in [Hu and Raney, 1967] experimental and analytical results were given for a truncated cylinder-cone configuration. In [Irie et al., 1984] the authors modelled a thin conical-cylindrical shell configuration by implementing the Flügge's equations of motion in a transfer matrix approach. More recently in [Patel et al., 2000] the problem was solved using a shell FE for which the variational quantities were calculated using the Mindlin theory. In [El Damatty et al., 2005] the FE derived results for a thin conical-cylindrical shell combination were verified through experimental measurements. In [Efraim and Eisenberger, 2006] a power series solution was applied for the calculation of the natural frequencies of segmented axisymmetric shells. Moreover in [Caresta and Kessissoglou, 2010] the authors analyzed the free vibration of thin coupled shells, also by using a power series method to model the displacement field within the conical part. Both Donnell-Mushtari and Flügge equations of motion were considered. More recently in [Kang, 2012] the free vibration characteristics of a conical-cylindrical section of variable thickness were computed through a Ritz method. The structure was however assumed to be homogeneous through its thickness.

With regard to modelling the behaviour of coupled shells in a wave-context, the bibliography is not so broad. In [Rose et al., 1973], the authors included transverse-shear, radial and rotary inertia effects in a bending theory in order to analyze the wave propagation in cylindrical-conical-cylindrical shell configuration. Experimental verification of the results was also provided. In [Langley, 1994a] the coupling loss factors of orthotropic curved panels are calculated using a wave dynamic stiffness matrix approach initially introduced in [Langley and Heron, 1990].

In this chapter, the WFEM will be employed in order to model the vibroacoustic response of an industrial composite conical-cylindrical-conical shell structure. In the low frequency range the dynamic stiffness approach exhibited in Chapter 3 of this thesis is used within an FE context for predicting the spatial response of the structure. In the higher frequency range the influence of the global modes on the response is considered as insignificant and the shell configuration is modelled in a wave-context SEA approach. The WFEM results are again used in order to revisit the calculation of the CLF between the layered shells. Experimental results are presented for the verification of the entirety of the numerical models.

The chapter is organized as follows: In sec.6.3 the industrial composite SYLDA structure to be tested and modelled is presented. In sec.6.4 the WFEM results are used to form an ESL of the layered SYLDA shell within an FE analysis. The predictions are compared to experimental results. In sec.6.5 each shell is individually considered as an SEA subsystem. The WFEM results are used in order to calculate the CLF of the shell combination which are used in order to form the SEA coefficients matrix. Conclusions on the presented work are exhibited in sec.6.6.

6.3 Presentation of the SYLDA structure

In this section the industrial composite structure to be experimentally and numerically modelled is exhibited. The configuration to be vibroacoustically analyzed is the SYLDA structure, its name standing for the french acronym of SYstéme de Lancement Double d'Ariane 5. The SYLDA is located inside the launcher fairing (see fig.6.1) and allows for multiple payloads to be simultaneously launched.

The SYLDA structure is roughly an assembly of two cones and a cylindrical central part (see fig.6.2). The employed materials are of sandwich type with a honeycomb aluminium core and carbon/epoxy made facesheets. Those parts are either bonded together or connected through pyrotechnic cordons which allow the expulsion of the SYLDA parts before placing the payload in orbit. Other connecting elements include springs and Carbon Fibre Reinforced Polymer (CFRP) rings. The structure also includes holes throughout its circumference for giving access to the payload and allowing the atmospheric air to escape during the flight of the vehicle towards the exosphere. All the details regarding the SYLDA structure and its subparts are presented in [EADS Astrium, 2003].

In order to conduct an experimental validation on the SYLDA and due to the prohibitive cost of testing an identical to the real SYLDA model, a mock-up of the composite cone-cylinder-cone structure was acquired (see fig.6.3). To make the application of deterministic methods such as the FE feasible, the mock-up structure is a 1/4 scale reproduction of the real one. The exact dimensions of the inner cavity surrounded by the tested structure are shown in fig.6.5. All dimensions are in mm. The materials used are of sandwich type; employing 1mm thick carbon/epoxy made facesheets (Material I) and a 12.7mm thick Nomex honeycomb core (Material II). The material characteristics are given in Table 6.1, with coordinate a coinciding with the axial direction of the shell, c with the circumferential direction and r with the radial one. No holes and no stiffeners are included in order to simplify the numerical modelling.
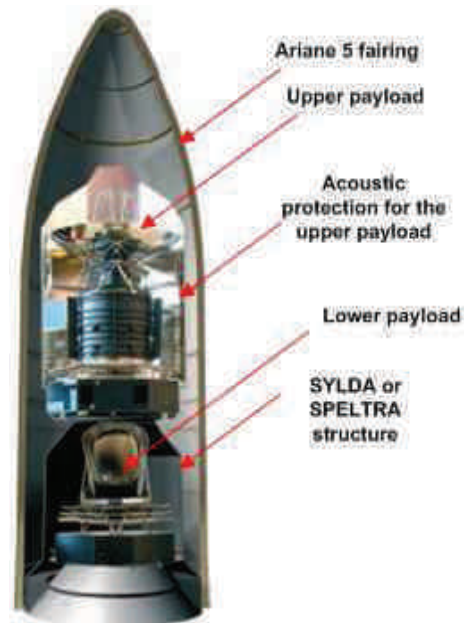
Figure 6.1: *An illustration of the Ariane 5 spacecraft*

Figure 6.2: *A caption of the real SYLDA structure*

Figure 6.3: *A caption of the SYLDA mock-up used for experimental manipulation*
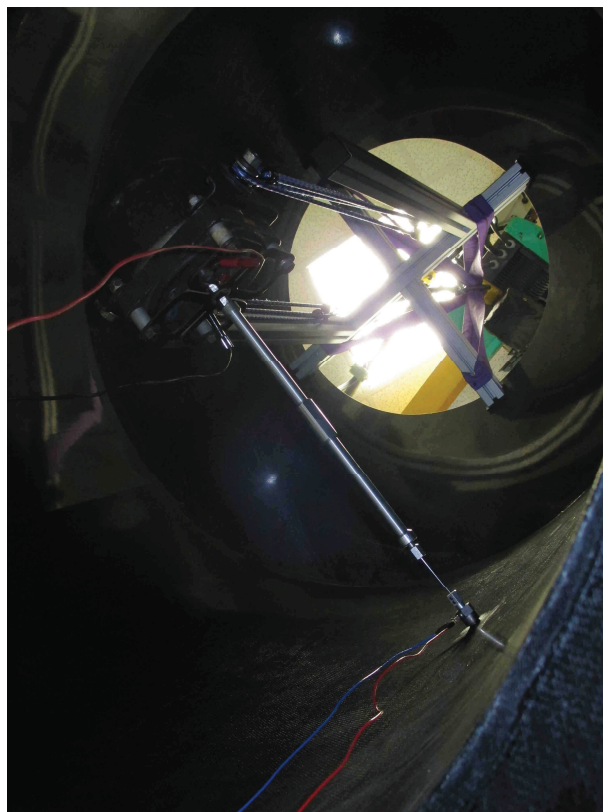
Figure 6.4: *A caption of the excitation configuration inside the shell*
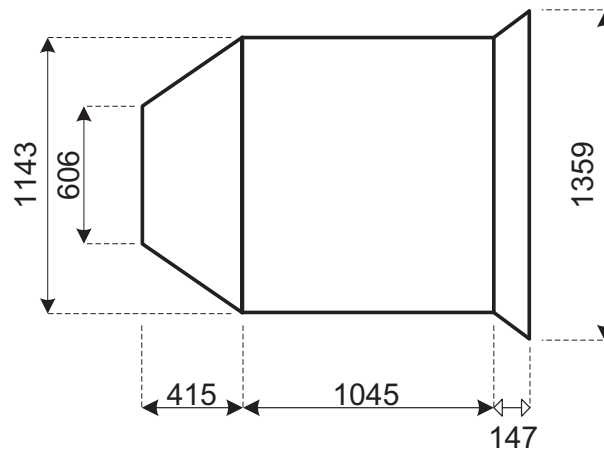
Figure 6.5: *Dimensions of the SYLDA mock-up configuration*

Table 6.1: *Mechanical properties of materials*

Material I	Material II
$\rho = 1530$ kg/m^3	$\rho = 63$ kg/m^3
$E_a = 47$ GPa	$E_a = 78$ MPa
$E_c = 47$ GPa	$E_c = 78$ MPa
$v_{ac} = 0.1$	$v_{ac} = 0.2$
$G_{ac} = 7.4$ GPa	$-$
$-$	$G_{ra} = 49$ MPa
$-$	$G_{rc} = 28$ MPa

The system to be modelled comprises the SYLDA structure coupled with its inner and outer acoustic cavities. The structure is freely suspended throughout the considered experimental testing. The SYLDA is suspended through a metallic cross section which is mounted on a lifting apparatus. The excitor lays inside the shell's cavity and is mounted on the same cross section that supports the shell (see fig.6.4). In order to avoid a simultaneous rigid motion of the excitor device, a heavy excitor weighting 19kg was chosen. Furthermore, in order to avoid slight revolutions of the structure during the testing process, part of the structure's weight was borne by polyurethane made supports to produce friction with the floor. The analysis is separated into two main parts: i) A low to mid-frequency deterministic modelling and ii) a high to mid-frequency SEA modelling approach.

6.4 Low to mid-frequency range modelling

6.4.1 Introduction

In this section, a deterministic numerical modelling of the dynamic response of the SYLDA structure is attempted. Initially, a full FE model comprising shell elements for the facesheets coupled to solid elements representing the core is elaborated. The results are compared to experimental outcomes in order to observe the limits of accuracy of a 3D FE modelling, as well as the impact of inevitable parametric uncertainties of the manufactured shell on its dynamic response. Subsequently, an application of the dynamic stiffness approach presented in Chapter 3 is attempted. The peculiarities of the conical substructures are discussed and envisaged by considering the structure
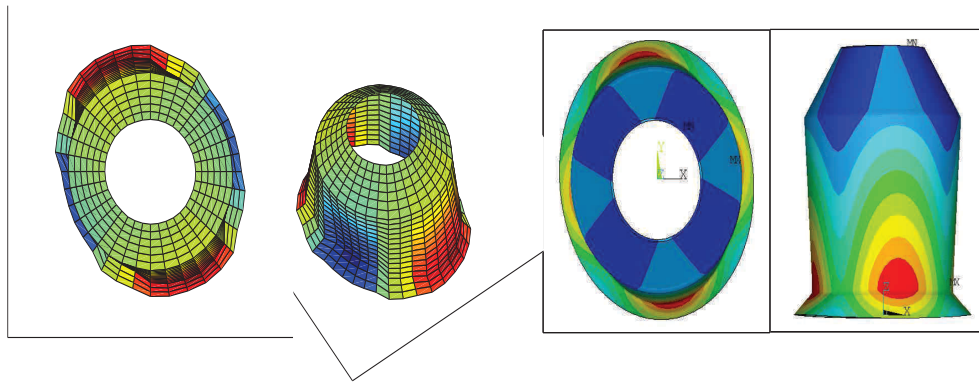
Figure 6.6: *The global circumferential mode of order 2: Measured (left) at 61.2 Hz, FE prediction (right) at 55.3 Hz*
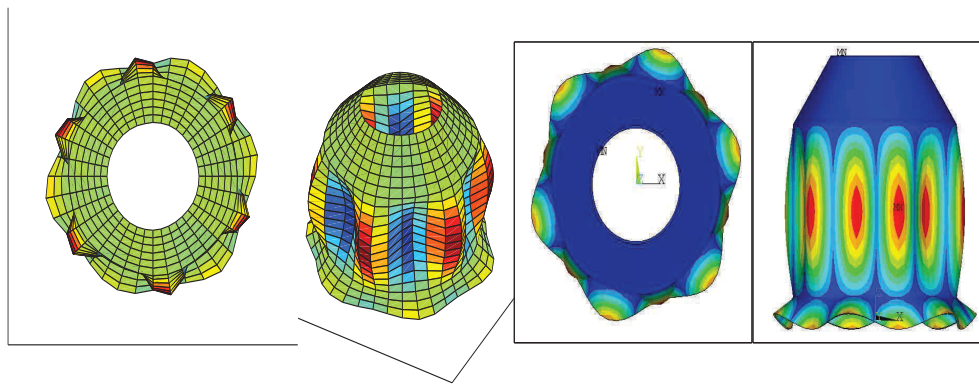
Figure 6.7: *The global circumferential mode of order 6: Measured (left) at 387.5 Hz, FE prediction (right) at 386.7 Hz*

to be locally cylindrical. The results of the dynamic stiffness ESL are compared to the full 3D modelling results and the pros and cons of the approach are commented.

6.4.2   Numerical modelling using FE

The SYLDA structure is firstly numerically modelled by a full 3D FE mesh. The mesh comprises 6048 shell elements for the facesheets, coupled to 3024 solid elements which are used to model the core of the sandwich material. Perfect continuous connections are assumed at the interfaces of the conical and the cylindrical substructures. A modal numerical analysis of the composite shell structure is firstly conducted.

Using the experimentally obtained complex FRF of 792 measured points on the SYLDA, the vibrational motion of the structure was illustrated for each frequency and phase using polar coordinates in MATLAB. By investigating the obtained FRF, the experimentally measured natural frequencies in the low and mid-frequency ranges were detected and plotted for comparison to the numerically predicted ones. Some representative natural frequencies along with their mode shapes are compared in figs.6.6-6.11.

In figs.6.6-6.9 the circumferential global modes of order 2,6,8 and 10 are exhibited. As it is observed by the FRF curves (see below) these are the most 'responsive' modes and therefore the most important ones to be predicted. It can be seen that an excellent agreement exists between
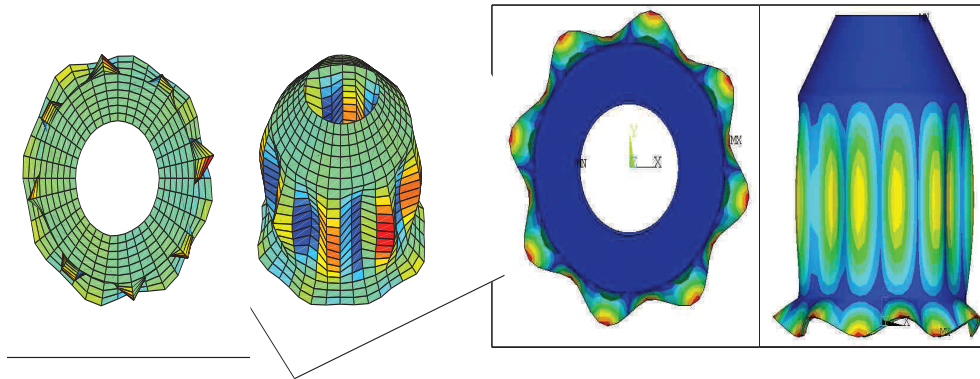
Figure 6.8: *The global circumferential mode of order 8: Measured (left) at 561.2 Hz, FE prediction (right) at 562.7 Hz*
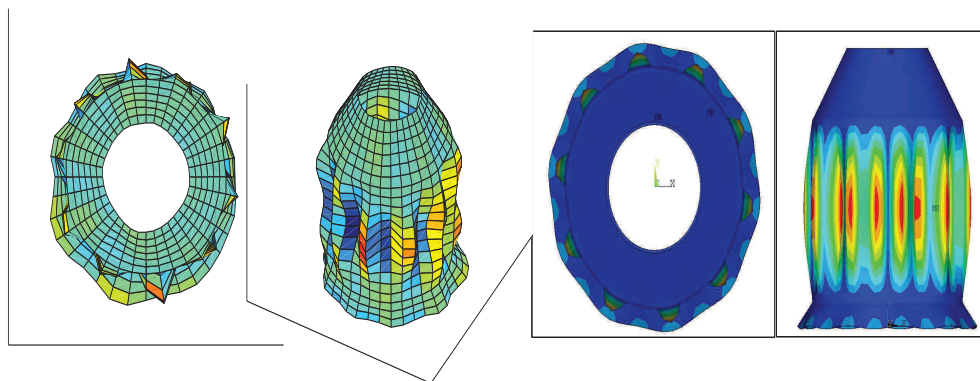
Figure 6.9: *The global circumferential mode of order 10: Measured (left) at 741.5 Hz, FE prediction (right) at 732.2 Hz*
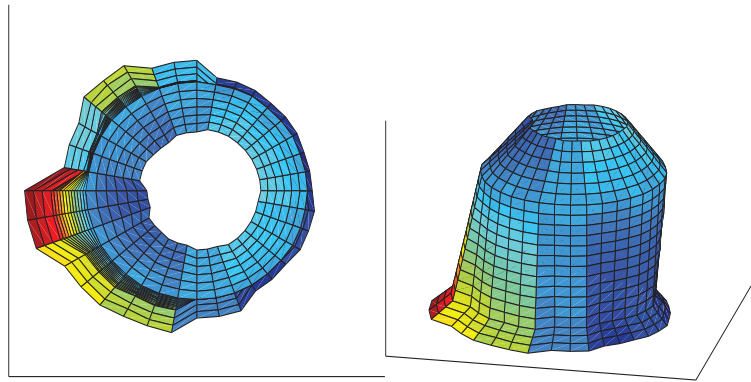
Figure 6.10: *The numerically non predicted fundamental mode of order 1: Measured at 8.8 Hz*
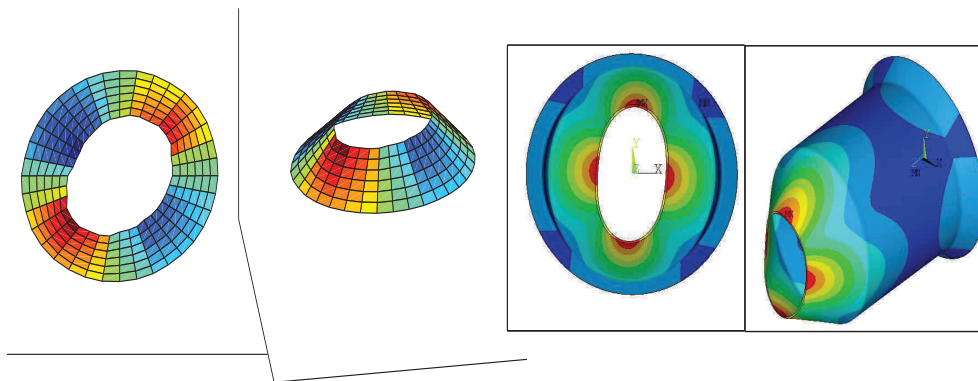
Figure 6.11: *The local circumferential mode of order 2 for the coupled upper cone subsystem: Measured (left) at 97.1 Hz, FE prediction (right) at 90.3 Hz*

the predicted and the measured natural frequencies, with the relative difference being less than 1,5% at all cases except the mode of order 2. The difference in the latter case can be attributed to the fact that the experimental boundary conditions of the structure were not perfectly free as assumed for the numerical model. Regarding the mode shapes of the natural frequencies, an excellent correlation is also observed between the predicted and the measured deformations. It can also be observed that while the cylindrical part of the structure along with the lower conical part seem to have a common global motion for all modal displacements, the upper conical part does not participate in this global structural motion. Thus the upper part presents a local subsystem behaviour already in the low frequency range.

In fig.(6.10) the circumferential mode resulted by the passage of a single circumferential bending wave (therefore of order 1) is presented. The particularly responsive fundamental mode is experimentally observed however it is not numerically predicted by the FE model. This difference in the fundamental frequency prediction can be crucial for low frequency excitations. The fundamental frequency prediction by analytical models usually raises with the thickness ratio of the shells and is discussed in [Qatu, 2004]. The fundamental local mode of the upper conical substructure is exhibited in fig.(6.11).

Following the modal analysis, a harmonic analysis was numerically conducted. In cylindrical coordinates, the excitation force is fixed at $(\theta, z)=(0^o, 494\text{mm})$ position of the cylindrical part. The resulting velocity FRF at arbitrary points of the three substructures are presented in figs.6.12-6.17.

The measured and the FE predicted velocity FRF at two arbitrary points of the cylindrical
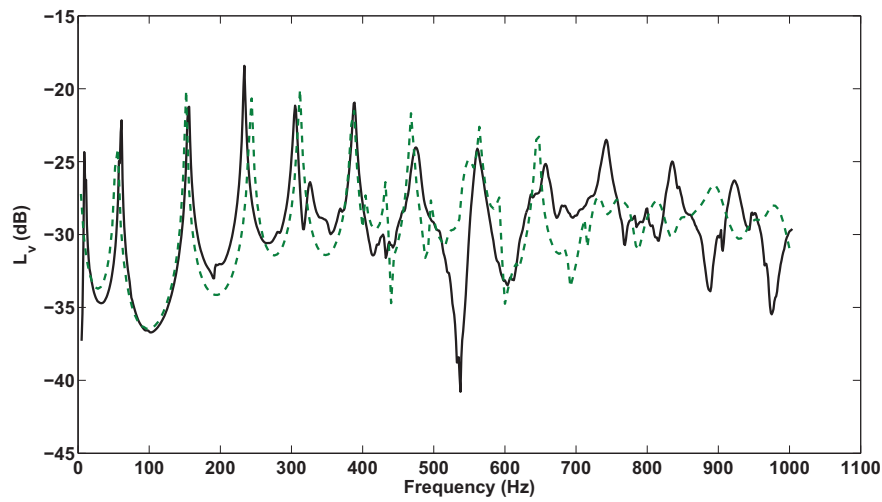
Figure 6.12: *Velocity FRF level comparison at (180º,508mm) of the cylindrical part: Experimental results (–), FEM results (- -)*
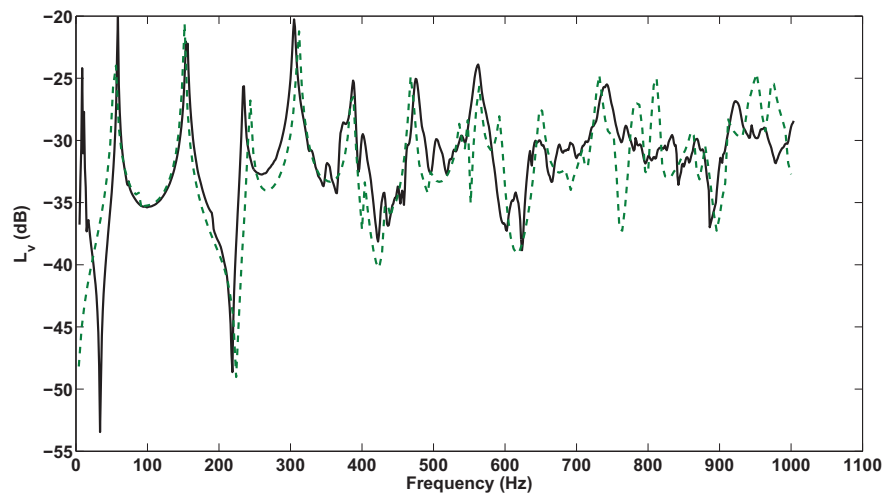
Figure 6.13: *Velocity FRF level comparison at (250º,263mm) of the cylindrical part: Experimental results (–), FEM results (- -)*
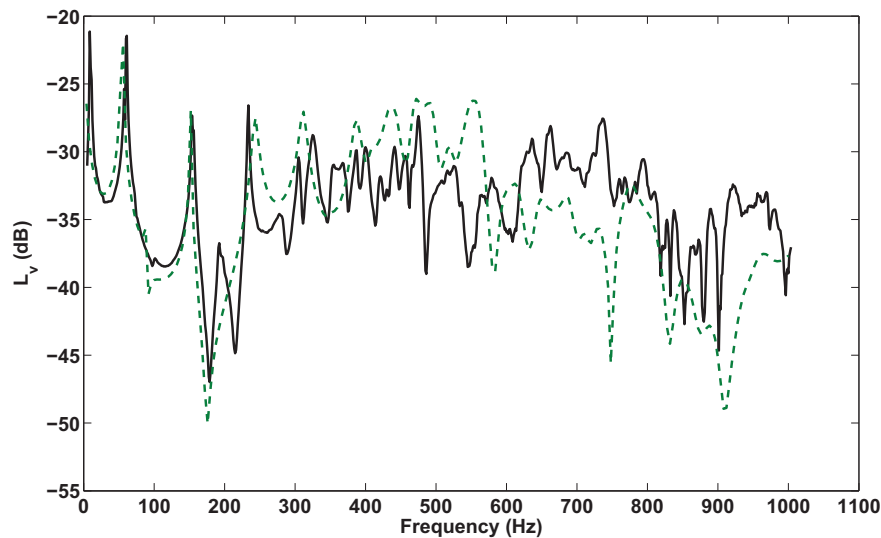
Figure 6.14: *Velocity FRF level comparison at (180º,50mm) of the lower conical part: Experimental results (–), FEM results (- -)*

section are presented in figs.6.12,6.13. An excellent agreement between the experimental results and the numerical predictions is observed within the low frequency range. With the exception of the fundamental frequency (as discussed above), the entirety of the global modal behaviour of the structure is very well predicted throughout the presented frequency range. Experimental values were used for the structural damping loss factor which were measured as discussed in chapter 3. The modal peaks corresponding to peripheral modes of the cylinder tend to be the most responsive ones. The impact of the local modes of the conical subsystems is observable at some positions (e.g around 320 Hz for fig.6.12), while this effect is not observable with regard to the FE results.

The measured and the FE predicted velocity FRF at arbitrary points of the lower conical section are presented in figs.6.14,6.15 and for the upper conical part in figs.6.16,6.17. For the lower conical part a fairly good agreement of the response is observed up until 500 Hz with the predicted resonances and anti-resonances being well correlated with the measured ones. For higher frequencies however the velocities of both the presented points seem to be underestimated by the FEM, implying a coupling greater than the one predicted. Observing the high number of peaks of the experimental curve in this frequency range, this can be attributed to the effect of local modes of other substructures on the response of the lower cone, including indirect coupling with the upper cone modes. With regard to the upper conical structure, the response also seems to be generally well predicted by the FE model with the exception of a frequency range around 600 Hz where the response seems to have been underestimated. Comparing the FRF of the cylindrical part to the ones obtained on the conical parts, it is seen that the later contain many more peaks, despite the fact that conical parts are substantially smaller than the cylindrical one. This stresses the impact of coupled structures modes on the response of the considered conical shell and indicates the complicated nature of waves travelling in a conical structure.

In order to get a more global idea of how the predicted response compares to measurements, the total energy of each subsystem was calculated using the force normalized measured and predicted velocities. The results are presented in figs.6.18,6.19,6.20, with the subscripts 1,2,3 standing for the upper cone, the cylinder and the lower cone respectively.

Regarding the cylindrical part is it observed that the FE predicted subsystem energy is very much in accordance with the measured one throughout the considered frequency band. As afore-
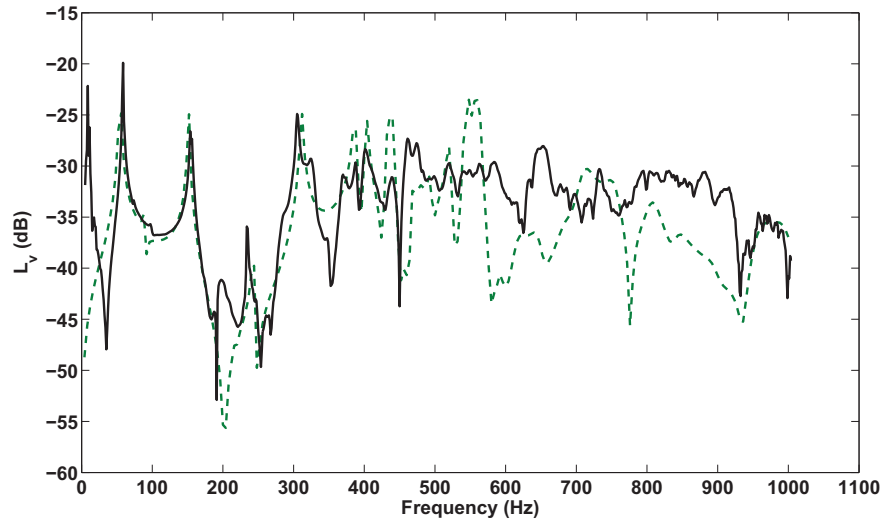
Figure 6.15: *Velocity FRF level comparison at (245º,110mm) of the lower conical part: Experimental results (–), FEM results (- -)*
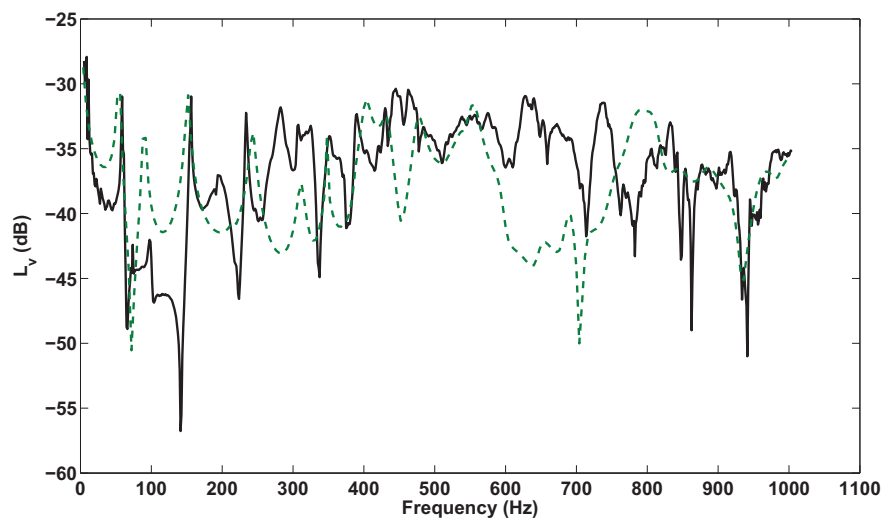
Figure 6.16: *Velocity FRF level comparison at (180º,204mm) of the upper conical part: Experimental results (–), FEM results (- -)*
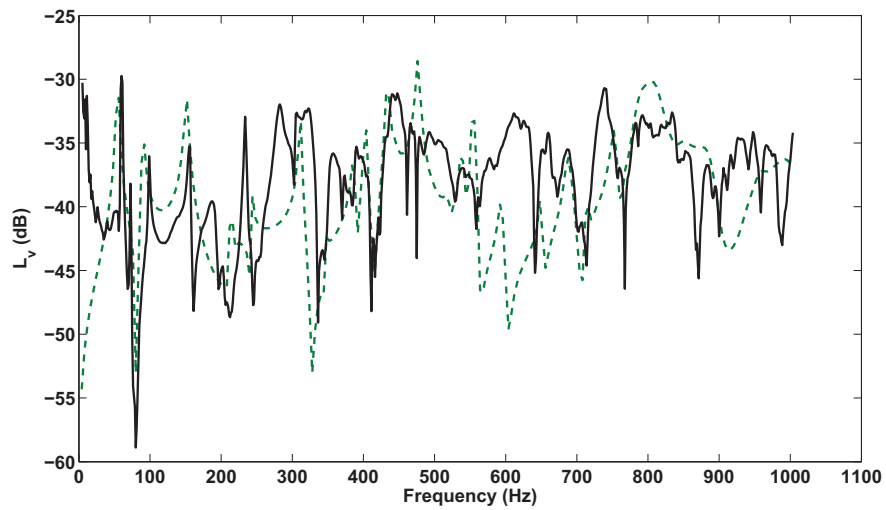
Figure 6.17: *Velocity FRF level comparison at (250º,219mm) of the upper conical part: Experimental results (–), FEM results (- -)*
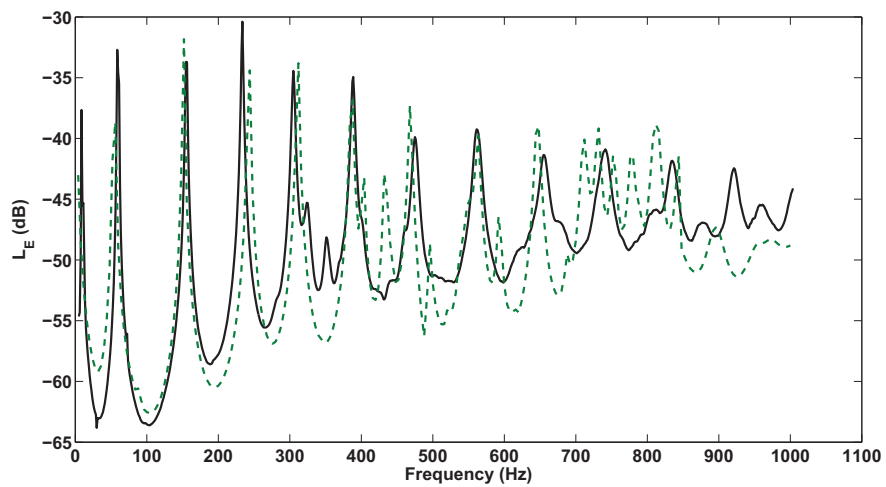
Figure 6.18: *Total energy level of the cylindrical subsystem: Experimental results (–), FEM results (- -)*
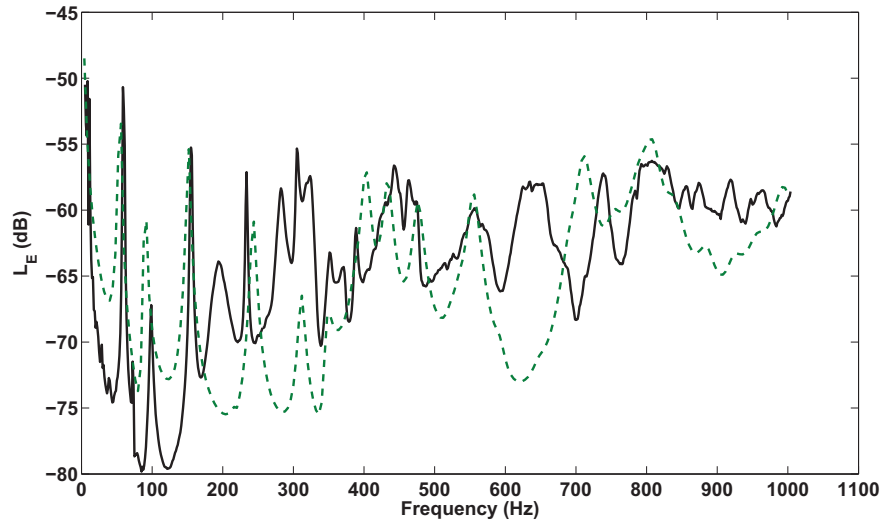
Figure 6.19: *Total energy level of the upper conical subsystem: Experimental results (–), FEM results (- -)*
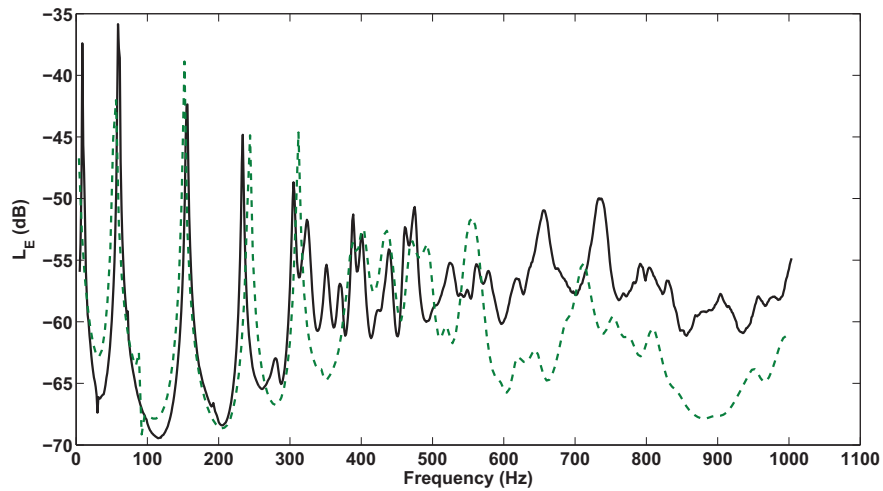
Figure 6.20: *Total energy level of the lower conical subsystem: Experimental results (–), FEM results (- -)*
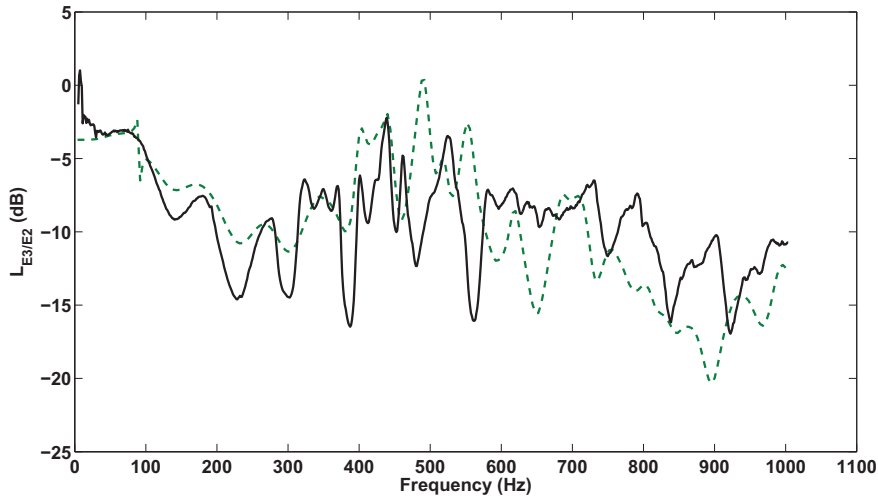
Figure 6.21: *Level of energy ratio E3/E2: Experimental results (−), FEM results (- -)*
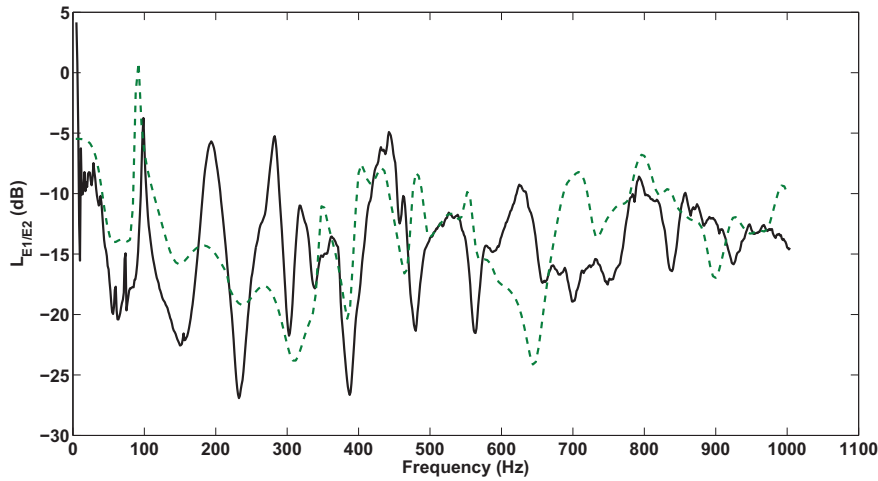
Figure 6.22: *Level of energy ratio E1/E2: Experimental results (−), FEM results (- -)*

mentioned, the FEM seems to be underestimating the effect of local modes of the conical parts on the energy of the cylindrical part, especially for frequencies between the resonances where this effect becomes evident. The energy of the upper conical part (along with the impact of the upper cone local modes) seems to be overestimated up to 150Hz and afterwards underestimated until 400Hz. It is noted as an example that despite the fact that the upper cone local mode of order 3 is well predicted by the FE modal analysis at 217 Hz, in fig.6.19 this mode is not observable. Better correlation is observed for higher frequencies. With regard to the upper conical part, it can be seen that it follows a global modal behaviour, influenced by the modes of the cylindrical part up until 300 Hz. While beyond this frequency the cylindrical modes are apparent on the energy function, a number of local modes can also be observed, resulting in a local-global behaviour. At higher frequencies the coupling of the lower cone to the rest of the structure is underestimated by the FE predictions.

In order to get an idea of the coupling strength between the substructures, the energies of the three subsystems divided by their mass were considered. In fig.6.21, the ratio of the lower cone energy divided by the one of the excited cylinder is presented. In the low frequency range the ratio approaches 1, implying a global response of the system. Local modes hit in for higher frequencies.

Figure 6.23: *Division of the conical substructures into sections of different material characteristics*

For frequencies above 700Hz, the coupling of the two subsystems is underestimated as commented about fig.6.20. In fig.6.22 a similar quantity, this time considering the energy of the upper cone is given. It is seen that for the low frequency range, while the peaks are frequency wise well predicted, the impact of local modes to the upper subsystem's energy is strongly underestimated. On the other hand, the energy transmission to the conical subsystem during resonances of the cylindrical system is overestimated as can be seen at approximately 150 Hz and 230 Hz. For higher frequencies, results are better correlated.

6.4.3 Numerical modelling using a dynamic stiffness ESL approach

An attempt to predict the response of the SYLDA structure using the ESL approach exhibited in Chapter 3 is hereby conducted through an FE modelling. The equivalence relations between a layered cylindrical structure and a Donnell-Mushtari single layer model as given in eq.(3.19) will be employed.

In order to apply the technique to a conical-cylindrical shell combination the structure was divided into layers each of which was considered cylindrical for the application of eq.(3.19) with a mean radius equal to $R = (R_{min} + R_{max})/2$. The number of layers N was selected so that the difference of the ring frequencies of two consecutive layers is approximately 5%. Better accuracy can effectively be achieved by increasing the number of divisions. The division of the SYLDA structure into layers of the same material and thickness is illustrated in fig.6.23. The ring frequency for each of the modelled layers of the composite shell with N=18 is shown in fig.6.24.

It is straightforward to write the dynamic stiffness matrix of the ESL model by adding the stiffness matrices of each layer as:

$$\mathbf{K} = \begin{bmatrix} \mathbf{K}_{1,LL} & \mathbf{K}_{1,LR} & & & & \\ \mathbf{K}_{1,RL} & \mathbf{K}_{1,RR} + \mathbf{K}_{2,LL} & \mathbf{K}_{2,LR} & & & \\ & \mathbf{K}_{2,RL} & \mathbf{K}_{2,RR} + \mathbf{K}_{3,LL} & \mathbf{K}_{3,LR} & & \\ & & \mathbf{K}_{3,RL} & \mathbf{K}_{3,RR} + \mathbf{K}_{4,LL} & \ldots & \\ & & & & \ldots & \\ & & & & \mathbf{K}_{N-1,RR} + \mathbf{K}_{N,LL} & \mathbf{K}_{N,LR} \\ & & & & \mathbf{K}_{N,RL} & \mathbf{K}_{N,RR} \end{bmatrix} \tag{6.1}$$

The response of the shell is subsequently calculated under an harmonic load. The results are

Figure 6.24: *Relation between the radius and the ring frequency of the modelled curved segment*

Figure 6.25: *Displacement FRF level comparison at (180º,508mm) of the cylindrical part: 3D FEM results (–), dynamic stiffness modelling (- -)*

Figure 6.26: *Displacement FRF level comparison at (13°,292mm) of the upper conical part: 3D FEM results (−), dynamic stiffness modelling (- -)*

compared to the 3D FE results in fig.6.25, 6.26 and 6.27. The response at an arbitrary point on each of the three subsystems is exhibited.

Very good correlation is observed between the ESL and the 3D FE model in the low frequency range (up to 400Hz) for all three subsystems, with the resonances and the antiresonances being well predicted both in terms of frequency and displacement level. The local modes of both the cylindrical and the upper conical shell seem to be well predicted. This fact also suggests that the coupling strength between the subsystems is also well reproduced by the ESL approach. In the mid-frequency range (above 500Hz) the prediction of the response of the subsystems becomes very sensitive to the characteristics attributed to each layer. Regarding the response average however, it can be observed that the ESL approach is very much in correlation with the 3D FE model.

In order to compare the predictions considering the coupling strength between the two conical shells and the excited cylindrical substructure, the total vibrational energy of each subsystem is calculated and the results are presented in figs.6.28, 6.29 and 6.30.

It is observed that the prediction of the energies of the cylindrical and the lower conical sub-systems is in very good correlation between the two models. In the low frequency range the peaks and the lows are according to each other both in terms of frequency and energy level. At higher frequencies discrepancies are observed but the average predictions are very well correlated. The coupling strength is therefore very well predicted. With regard to the upper conical shell the results are in good correlation in the low frequency range, where the local modes of the conical shell are well predicted. Discrepancies between the two models are occurring between 350 and 500Hz probably due to a global/local behaviour of the composite cone which is not always well predicted by the ESL model. At higher frequencies -where the behaviour of the conical shell apparently becomes more 'local'- the average response predictions are again in good agreement.
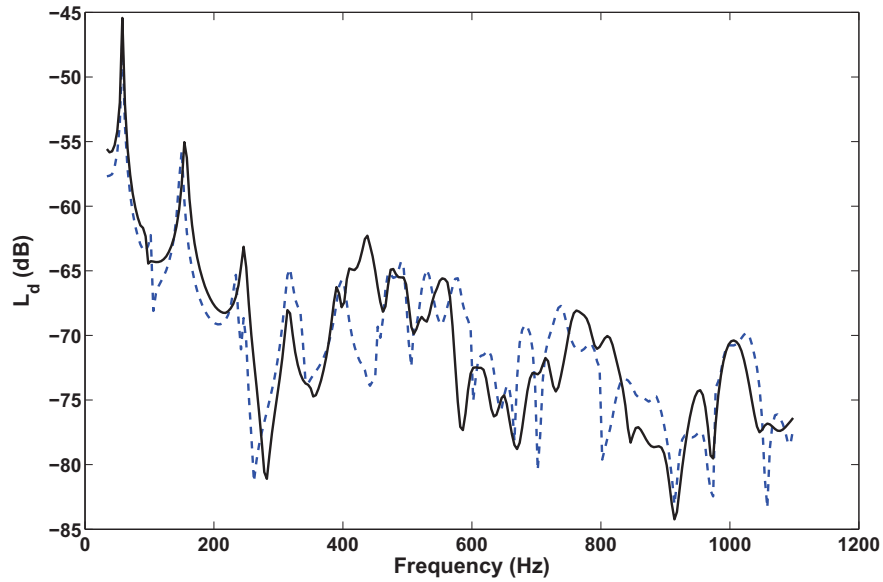
Figure 6.27: *Displacement FRF level comparison at (205º,56mm) of the lower conical part: 3D FEM results (−), dynamic stiffness modelling (- -)*
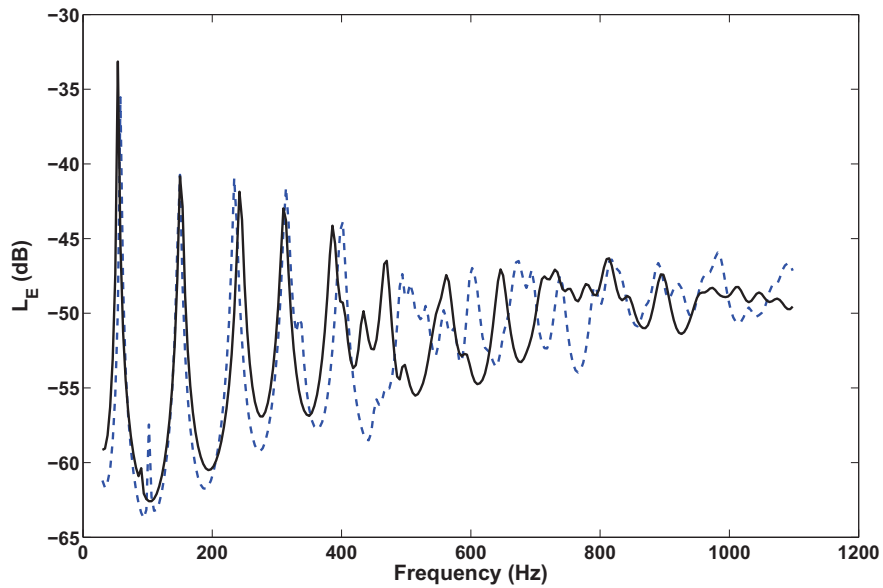
Figure 6.28: *Energy level comparison for the cylindrical part: 3D FEM results (−), dynamic stiffness modelling (- -)*
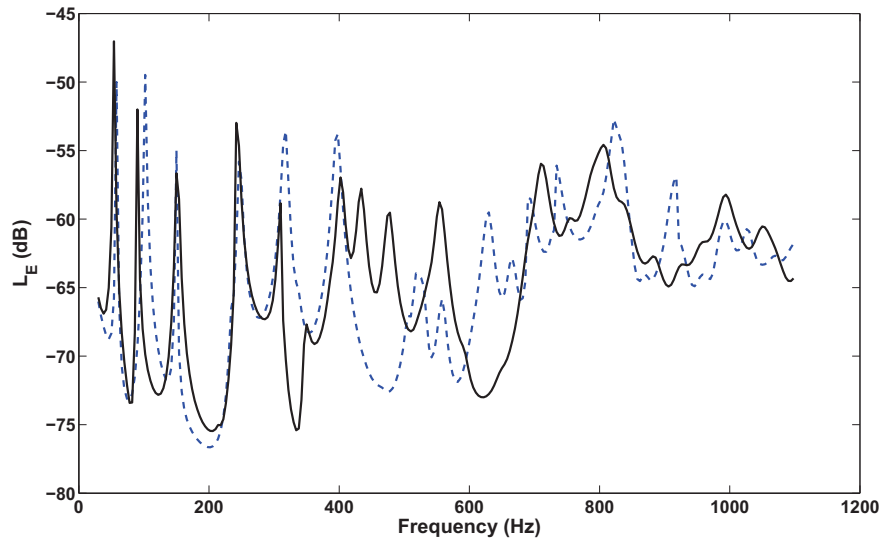
Figure 6.29: *Energy level comparison for the upper conical part: 3D FEM results (–), dynamic stiffness modelling (- -)*
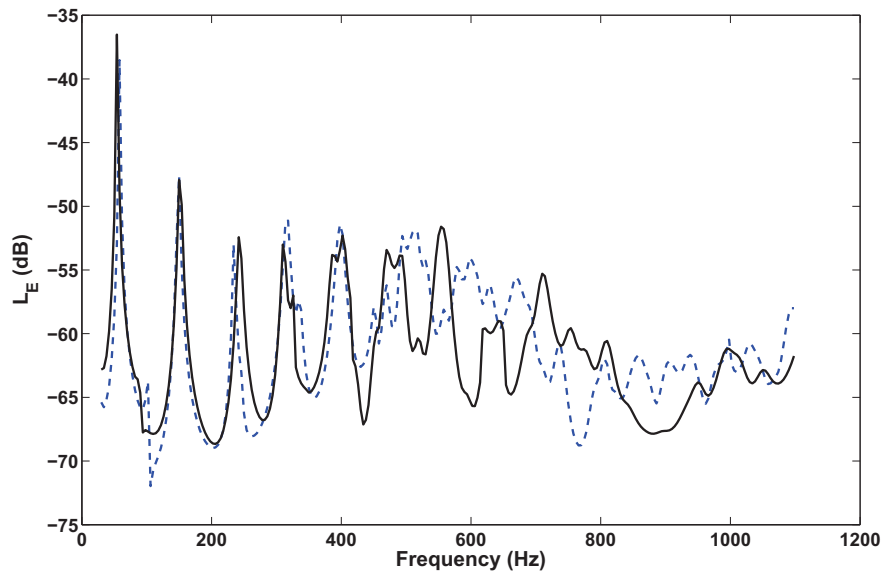
Figure 6.30: *Energy level comparison for the lower conical part: 3D FEM results (–), dynamic stiffness modelling (- -)*

6.5 Statistical Energy Analysis modelling of a composite shell assembly

6.5.1 Introduction

In the high frequency range where the modal overlap of the structural response of a component is high - mainly due to the increasing modal density of a sandwich structure and the increase of radiation damping - the response can effectively be represented by medium energy quantities. The SEA has been traditionally used for the response prediction in the high frequency domain and is to a large extent based on the accurate calculation of the Coupling Loss Factors (CLF) between the considered subsystems. In Chapter 2 the WFEM was used to calculate the CLF for a vibroacoustic system comprising two rooms divided by a layered panel. Hereby, the WFEM will be used in order to revisit the calculation of the CLF between structural composite subsystems. The experimental results obtained on the SYLDA structure will be used to validate the developed models.

6.5.2 Coupling Loss Factors calculation for a layered beam assembly

The considered system comprises two layered structural 1D waveguides (see fig.6.31) connected through a joint. The approach hereby adopted is presented to a large extent in [Mencik and Ichchou, 2005] in order to calculate the transmission and diffusion coefficients for connected 1D waveguides. More recently it was also adopted by [Renno and Mace, 2012] for the calculation of the transmission efficiency and the response of an ensemble of waveguides. The modelled parts in fig.6.31 include the excited waveguide 1 and the receiver waveguide 2 as well as the connecting component. A WFEM/FE analysis is therefore adopted in order to predict the transmission coefficients between the waveguides.

The wave dispersion characteristics within the semi-infinite waveguides are modelled with the WFEM as described in sec.1.2.5. The resulting $2n$ eigenvalues can be associated with n incident waves $\lambda_{inc,1...n}$ and n reflected waves $\lambda_{ref,n+1...2n}$ with n the number of DoF on each side of the modelled segment and the eigenvalues of the same wave type being related as: $\lambda_{ref,i} = 1/\lambda_{inc,i}$. Along with the eigenvalues, the obtained eigenvectors can be classified as:

$$\mathbf{\Phi} = \begin{bmatrix} \mathbf{\Phi}_q^{inc} & \mathbf{\Phi}_q^{ref} \\ \mathbf{\Phi}_f^{inc} & \mathbf{\Phi}_f^{ref} \end{bmatrix} \text{ with } \mathbf{\Phi}_q^{inc} = \begin{bmatrix} \phi_{q,1}^{inc} & \phi_{q,2}^{inc} & ... & \phi_{q,n}^{inc} \end{bmatrix} \tag{6.2}$$

where the subscripts q, f and $1:n$ correspond to the displacement vectors the force vectors and the wave type respectively. Similar expressions hold for $\mathbf{\Phi}_q^{ref}$, $\mathbf{\Phi}_f^{inc}$ and $\mathbf{\Phi}_f^{ref}$.

The connecting component (surrounded by the dashed line in fig.6.31) can be modelled using conventional FE. It is hereby assumed that the DoF of the joint FE model are compatible with the ones of the WFEM models. The harmonic response of the joint segment can be described as:

$$\begin{bmatrix} \mathbf{D}_{j11} & \mathbf{D}_{j12} & \mathbf{D}_{j1I} \\ \mathbf{D}_{j21} & \mathbf{D}_{j22} & \mathbf{D}_{j2I} \\ \mathbf{D}_{jI1} & \mathbf{D}_{jI2} & \mathbf{D}_{jII} \end{bmatrix} \begin{Bmatrix} \mathbf{q}_j^1 \\ \mathbf{q}_j^2 \\ \mathbf{q}_j^I \end{Bmatrix} = \begin{Bmatrix} \mathbf{f}_j^1 \\ \mathbf{f}_j^2 \\ \mathbf{f}_j^I \end{Bmatrix} \tag{6.3}$$

with the subscripts L,R and I corresponding to left-side, right-side and internal nodes respec-
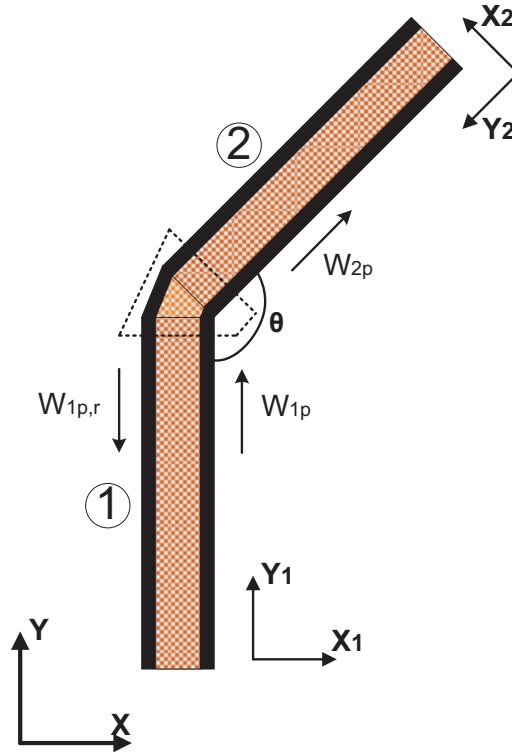
Figure 6.31: *Assembly of two layered 1D waveguides. FE modelled segment surrounded by the dashed line.*

tively. Using classical condensation techniques the system of eq.(6.3) is written as:

$$
\begin{bmatrix}
\mathbf{D}_{j11} - \mathbf{D}_{j1I}\mathbf{D}_{jII}^{-1}\mathbf{D}_{jI1} & \mathbf{D}_{j12} - \mathbf{D}_{j1I}\mathbf{D}_{jII}^{-1}\mathbf{D}_{jI2} \\
\mathbf{D}_{j21} - \mathbf{D}_{j2I}\mathbf{D}_{jII}^{-1}\mathbf{D}_{jI1} & \mathbf{D}_{j22} - \mathbf{D}_{j2I}\mathbf{D}_{jII}^{-1}\mathbf{D}_{jI2}
\end{bmatrix}
\left\{
\begin{array}{c}
\mathbf{q}_j^1 \\
\mathbf{q}_j^2
\end{array}
\right\}
=
\left\{
\begin{array}{c}
\mathbf{f}_j^1 \\
\mathbf{f}_j^2
\end{array}
\right\}
\tag{6.4}
$$

Concerning the structural response of the waveguides, it is shown in [Zhong and Williams, 1995] that the state vectors $\mathbf{q}_R^1, \mathbf{f}_R^1, \mathbf{q}_L^2, \mathbf{f}_L^2$ can be written as a superposition function of the wave

eigenvectors and the corresponding wave amplitudes $\mathbf{Q}^{inc,i}, \mathbf{Q}^{ref,i}$ as:

$$
\left\{ \begin{array}{c} \mathbf{q}_R^1 \\ \mathbf{f}_R^1 \end{array} \right\} = \left[\begin{array}{cc} \mathbf{\Phi}_q^{inc,1} & \mathbf{\Phi}_q^{ref,1} \\ \mathbf{\Phi}_f^{inc,1} & \mathbf{\Phi}_f^{ref,1} \end{array} \right] \left\{ \begin{array}{c} \mathbf{Q}^{inc,1} \\ \mathbf{Q}^{ref,1} \end{array} \right\}
$$

$$
\left\{ \begin{array}{c} \mathbf{q}_L^2 \\ \mathbf{f}_L^2 \end{array} \right\} = \left[\begin{array}{cc} \mathbf{\Phi}_q^{inc,2} & \mathbf{\Phi}_q^{ref,2} \\ \mathbf{\Phi}_f^{inc,2} & \mathbf{\Phi}_f^{ref,2} \end{array} \right] \left\{ \begin{array}{c} \mathbf{Q}^{inc,2} \\ \mathbf{Q}^{ref,2} \end{array} \right\}
$$

(6.5)

The continuity conditions at the interfaces of the joint with the waveguides as well as the equilibrium of the system impose that:

$$
\left\{ \begin{array}{c} \mathbf{q}_j^1 \\ \mathbf{q}_j^2 \end{array} \right\} = \left[\begin{array}{cc} \mathbf{R_1} & \mathbf{0} \\ \mathbf{0} & \mathbf{R_2} \end{array} \right] \left\{ \begin{array}{c} \mathbf{q}_R^1 \\ \mathbf{q}_L^2 \end{array} \right\}
$$

$$
\left\{ \begin{array}{c} \mathbf{f}_j^1 \\ \mathbf{f}_j^2 \end{array} \right\} = \left[\begin{array}{cc} \mathbf{R_1} & \mathbf{0} \\ \mathbf{0} & \mathbf{R_2} \end{array} \right] \left\{ \begin{array}{c} \mathbf{f}_R^1 \\ \mathbf{f}_L^2 \end{array} \right\}
$$

(6.6)

with $\mathbf{R_1}, \mathbf{R_2}$ the transformation matrices for the waveguides 1 and 2 respectively. Using the systems in eq.(6.4),(6.5),(6.6) the matrix containing the transmission and reflection coefficients for each wave type is written as in [Mencik and Ichchou, 2005]:

$$
\mathcal{C} = -[\mathbf{R}\mathbf{\Phi}_f^{ref} - \mathbf{D}_j\mathbf{R}\mathbf{\Phi}_q^{ref}]^{-1}[\mathbf{R}\mathbf{\Phi}_f^{inc} - \mathbf{D}_j\mathbf{R}\mathbf{\Phi}_q^{inc}] \tag{6.7}
$$

with $\mathbf{R} = \left[\begin{array}{cc} \mathbf{R_1} & \mathbf{0} \\ \mathbf{0} & \mathbf{R_2} \end{array} \right]$, $\mathbf{\Phi}_f^{ref} = \left[\begin{array}{cc} \mathbf{\Phi}_f^{ref,1} & \mathbf{0} \\ \mathbf{0} & \mathbf{\Phi}_f^{ref,2} \end{array} \right]$, $\mathbf{\Phi}_q^{ref} = \left[\begin{array}{cc} \mathbf{\Phi}_q^{ref,1} & \mathbf{0} \\ \mathbf{0} & \mathbf{\Phi}_q^{ref,2} \end{array} \right]$, $\mathbf{\Phi}_f^{inc} =$

$\left[\begin{array}{cc} \mathbf{\Phi}_f^{inc,1} & \mathbf{0} \\ \mathbf{0} & \mathbf{\Phi}_f^{inc,2} \end{array} \right]$, $\mathbf{\Phi}_q^{inc} = \left[\begin{array}{cc} \mathbf{\Phi}_q^{inc,1} & \mathbf{0} \\ \mathbf{0} & \mathbf{\Phi}_q^{inc,2} \end{array} \right]$ and $\mathbf{D}_j = \left[\begin{array}{cc} \mathbf{D}_{j11} - \mathbf{D}_{j1I}\mathbf{D}_{jII}^{-1}\mathbf{D}_{jI1} & \mathbf{D}_{j12} - \mathbf{D}_{j1I}\mathbf{D}_{jII}^{-1}\mathbf{D}_{jI2} \\ \mathbf{D}_{j21} - \mathbf{D}_{j2I}\mathbf{D}_{jII}^{-1}\mathbf{D}_{jI1} & \mathbf{D}_{j22} - \mathbf{D}_{j2I}\mathbf{D}_{jII}^{-1}\mathbf{D}_{jI2} \end{array} \right]$.

The CLF between wave type p in the waveguide 1 and wave type z propagating in waveguide 2 can be computed using the classical relation:

$$
\eta_{p_1,z_2} = \frac{\tau_{p_1,z_2} c_{g,p_1}}{2\omega L_1} \tag{6.8}
$$

with L_1 the length of waveguide 1, c_{g,p_1} the group velocity of the incident wave and τ_{p_1,z_2} the transmission efficiency between the two wave types expressed as:

$$
\tau_{p_1,z_2} = \frac{P_{T,z_2}}{P_{I,p_1}} \tag{6.9}
$$

with P_{T,z_2} the transmitted power in waveguide 2 and P_{I,p_1} the incident power in waveguide 1. Using the expressions presented in [Ichchou et al., 2007] the energy densities for a waveguide

within which a wave z is propagating are written as:

$$E_{K,z}^{inc} = \frac{\omega^2}{4L_s} Re \left(\left\{ \begin{array}{c} \mathbf{\Phi}_{q,z}^{inc} \\ \lambda_z^{inc} \mathbf{\Phi}_{q,z}^{inc} \end{array} \right\}^H \mathbf{M}_s \left\{ \begin{array}{c} \mathbf{\Phi}_{q,z}^{inc} \\ \lambda_z^{inc} \mathbf{\Phi}_{q,z}^{inc} \end{array} \right\} \right)$$

$$E_{P,z}^{inc} = \frac{1}{4L_s} Re \left(\left\{ \begin{array}{c} \mathbf{\Phi}_{q,z}^{inc} \\ \lambda_z^{inc} \mathbf{\Phi}_{q,z}^{inc} \end{array} \right\}^H \mathbf{K}_s \left\{ \begin{array}{c} \mathbf{\Phi}_{q,z}^{inc} \\ \lambda_z^{inc} \mathbf{\Phi}_{q,z}^{inc} \end{array} \right\} \right) \tag{6.10}$$

$$E_{T,z}^{inc} = E_{K,z}^{inc} + E_{P,z}^{inc}$$

with $E_{K,z}, E_{P,z}, E_{T,z}$ the kinetic, potential and total energy densities and $\mathbf{M}_s, \mathbf{K}_s$ the mass and stiffness matrices of the modelled segment of the waveguide. The power due to the passage of a wave z propagating within a waveguide can be written as:

$$P_{I,z}^{inc} = \frac{1}{2} Re \left(i\omega (Q_z^{inc})^H \left\{ \mathbf{\Phi}_{f,z}^{inc} \right\}^H \mathbf{\Phi}_{q,z}^{inc} Q_z^{inc} \right) \tag{6.11}$$

The transmission efficiency between the two waves can therefore be written as:

$$\tau_{p_1,z_2} = \frac{Re \left(i\omega (Q_{z_2}^{ref})^H \left\{ \mathbf{\Phi}_{f,z_2}^{ref} \right\}^H \mathbf{\Phi}_{q,z_2}^{ref} Q_{z_2}^{ref} \right)}{Re \left(i\omega (Q_{p_1}^{inc})^H \left\{ \mathbf{\Phi}_{f,p_1}^{inc} \right\}^H \mathbf{\Phi}_{q,p_1}^{inc} Q_{p_1}^{inc} \right)} \tag{6.12}$$

however the ratio of the amplitudes of the two waves can be found in matrix $\mathcal{C}$, therefore eq.(6.12) becomes:

$$\tau_{p_1,z_2} = \frac{Re \left(i\omega \left\{ \mathbf{\Phi}_{f,z_2}^{ref} \right\}^H \mathbf{\Phi}_{q,z_2}^{ref} \right) |\mathcal{C}_{p_1,z_2}|^2}{Re \left(i\omega \left\{ \mathbf{\Phi}_{f,p_1}^{inc} \right\}^H \mathbf{\Phi}_{q,p_1}^{inc} \right)} \tag{6.13}$$

The group velocity of the wavetype is written as in [Ichchou et al., 2007]:

$$c_{g,z}^{inc} = \frac{P_{I,z}^{inc}}{E_{T,z}^{inc}} \tag{6.14}$$

Therefore by introducing eq.(6.13),(6.14) into (6.8) it is straightforward to calculate the CLF between two waves propagating in the layered 1D waveguides.

6.5.3   Coupling Loss Factors calculation for coupled layered 2D panels

Two layered panels are assumed to be connected through a joint (see fig.6.32). The diffused field CLF between the two panels are to be calculated. Compared to the methodology described in sec.6.5.2 the analysis now differs.

A 2D WFE analysis is initially conducted for the two panels. As described in sec.1.2.5 the wavenumbers propagating in parallel to the joint (say k_x) as well as the frequency can be fixed for the nonlinear eigenproblem. The 3D wavenumber maps (as the one shown in fig.2.5) for the
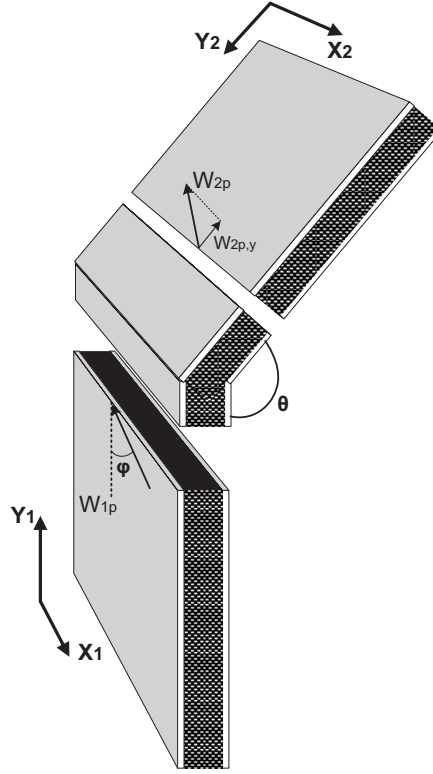
Figure 6.32: *Assembly of two layered plates in an angle; descritized into the excited panel (subsystem 1), the 2D joint and the inclined panel (subsystem 2).*

two connected panels can be plotted. By interpolating on these maps the wavenumber k for every angle of incidence ϕ is therefore known.

The diffused field CLF for two anisotropic panels is taken as in [Langley, 1994a]:

$$\eta_{p_1,z_2} = \frac{L_{12}}{2\pi^2 n_{p_1}} \int\limits_{\phi_{min}}^{\phi_{max}} \frac{c_{gx,p_1}\tau_{p_1,z_2}}{c_{p_1} c_{g,p_1}} d\phi \tag{6.15}$$

with L_{12}, n_{p_1} the connection length of the two panels and the modal density of p wave type in panel 1, c_{p_1}, c_{g,p_1} the phase and group velocities of p wave type in panel 1 and τ_{p_1,z_2} the angle dependent transmission efficiency of p wave type in panel 1 to the z wave type in panel 2. Once the wavenumbers k_x, k_y for every ϕ are known the problem can be considered as an 1D problem described in sec.6.5.2, with the wave mode shapes in waveguide 1 now equal to:

$$\mathbf{\Phi}_{q,f}^{inc,1} = \mathbf{R}_\phi \mathbf{\Phi}_{q,f}^{inc,1,2D} \tag{6.16}$$

With $\mathbf{\Phi}_{q,f}^{inc,1,2D}$ the wave mode shapes as predicted by the 2D WFEM and $\mathbf{R}_\phi$ a transformation matrix applied to account for the angle of incidence ϕ. The transmission and reflection coefficients can therefore be computed as before:

$$\mathcal{C}(\phi) = -[\mathbf{R}\mathbf{\Phi}_f^{ref} - \mathbf{D}_j\mathbf{R}\mathbf{\Phi}_q^{ref}]^{-1}[\mathbf{R}\mathbf{\Phi}_f^{inc} - \mathbf{D}_j\mathbf{R}\mathbf{\Phi}_q^{inc}] \tag{6.17}$$
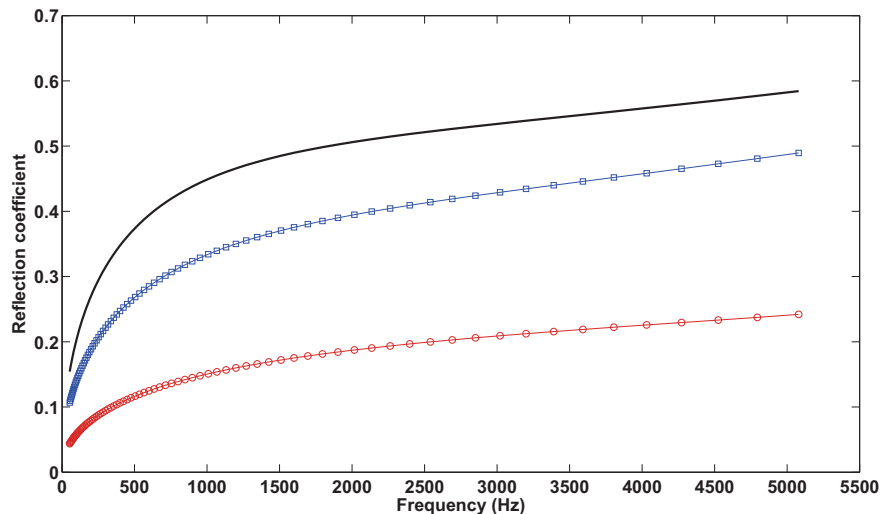
Figure 6.33: *Transmission coefficients for a flexural/flexural coupling of the layered panels with $\theta=32,9^o$ and $\phi=0$ (–), $\phi=30$ ($\square$), $\phi=60$ (o)*

this time with $\mathbf{R} = \begin{bmatrix} \mathbf{R_{1,\theta}R_{1,\phi}} & \mathbf{0} \\ \mathbf{0} & \mathbf{R_{2,\theta}} \end{bmatrix}$.

The ϕ dependent transmission efficiency can therefore be calculated and by introducing it into eq.(6.15) the diffused field CLF can be predicted. Is is noted that anisotropic panels may actually carry energy away from the connecting interface. Therefore the integration in eq.(6.15) should be conducted only for angles for which the c_{gx,p_1} quantity is positive.

Numerical examples of the described approach are then exhibited. The approach is applied to two layered panels coupled with an angle $\theta=32,9^o$ (corresponding to the connecting angle of the upper conical shell) and having the same characteristics as the sandwich material of the SYLDA model, with directions x and y coinciding with directions c and a respectively. The transmission coefficients for a flexural/flexural wave coupling are shown in fig.6.33.

The results are qualitatively in agreement with analytical solutions for thin isotropic structures (see [Cremer et al., 2005]) that suggest that the transmission coefficient increases with frequency and decreases when increasing the angle of attack. Analytical solutions for coupled layered thick structures are particularly difficult, if not impossible to find. The reflection coefficients for the same type of coupling are exhibited in fig.6.34. The same comments apply for the reflection coefficients for being qualitatively in correlation with analytical results.

6.5.4 SEA analysis of the SYLDA

An SEA analysis of the SYLDA structure is hereby conducted in order to compute the structural response of each substructure. The three layered shells are considered as separate subsystems. A qualitative presentation of the power exchange between the subsystems is given in fig.6.35.
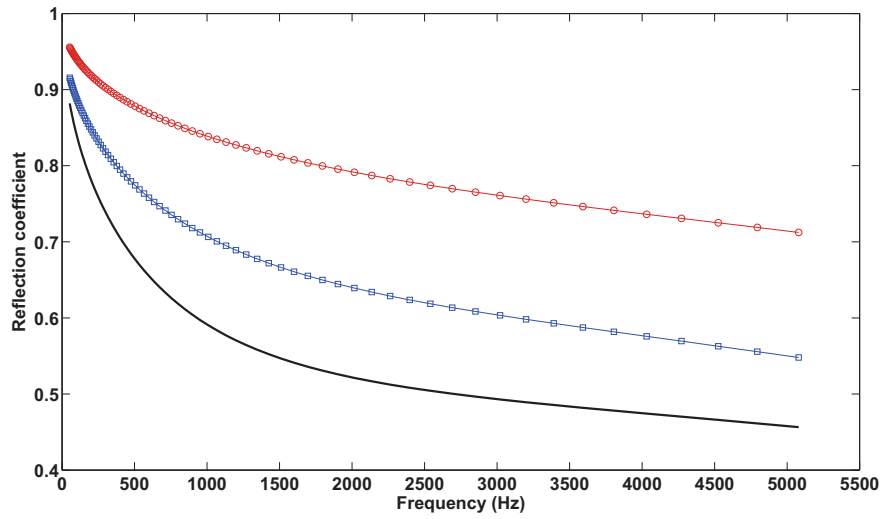
Figure 6.34: *Reflection coefficients for a flexural/flexural coupling of the layered panels with θ=32,9°* *and φ=0 (−), φ=30 (□), φ=60 (o)*
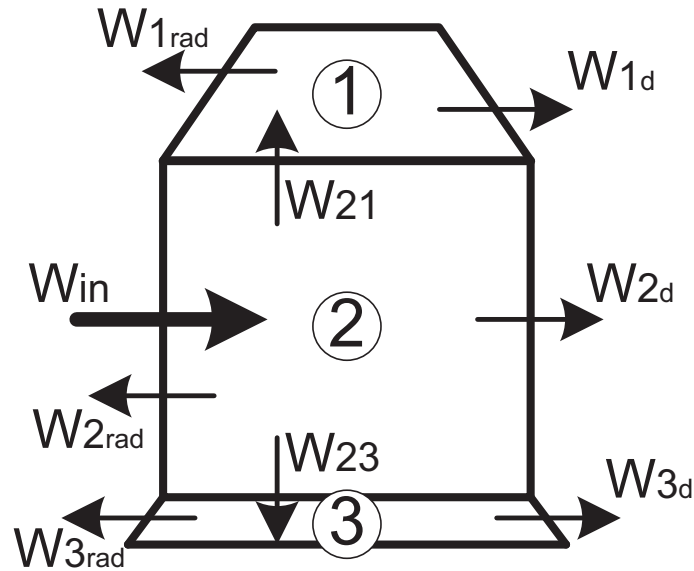
Figure 6.35: *Power exchange between the subsystems, considered for the SEA analysis of the SYLDA.*

The SEA system of equations is formulated as:

$$
\begin{bmatrix}
\eta_{d,1} + \eta_{12} + \eta_{rad,1} & -\eta_{21} & 0 \\
-\eta_{12} & \eta_{d,2} + \eta_{21} + \eta_{23} + \eta_{rad,2} & -\eta_{32} \\
0 & -\eta_{23} & \eta_{d,3} + \eta_{32} + \eta_{rad,3}
\end{bmatrix}
\begin{Bmatrix} E_1 \\ E_2 \\ E_3 \end{Bmatrix}
=
\begin{Bmatrix} 0 \\ \dfrac{W_{2,inj}}{\omega} \\ 0 \end{Bmatrix}
\tag{6.18}
$$

with E_i the spatially averaged total energy of subsystem i, $W_{2,inj}$ the power injected in subsystem 2, $\eta_{rad,i}$ the Radiation Loss Factor (RLF) of subsystem i and $\eta_{d,i}$ the Dissipation Loss Factor (DLF) of subsystem i. Writing the solution of the system as:

$$
\begin{Bmatrix}
\dfrac{\omega E_1}{W_{2,inj}} \\[2mm]
\dfrac{\omega E_2}{W_{2,inj}} \\[2mm]
\dfrac{\omega E_3}{W_{2,inj}}
\end{Bmatrix}
= \mathbf{A}^{-1}
\begin{Bmatrix} 0 \\ 1 \\ 0 \end{Bmatrix}
\tag{6.19}
$$

with $\mathbf{A} = \begin{bmatrix}
\eta_{d,1} + \eta_{12} + \eta_{rad,1} & -\eta_{21} & 0 \\
-\eta_{12} & \eta_{d,2} + \eta_{21} + \eta_{23} + \eta_{rad,2} & -\eta_{32} \\
0 & -\eta_{23} & \eta_{d,3} + \eta_{32} + \eta_{rad,3}
\end{bmatrix}$, it is now straight-

forward that the energy ratios will be equal to:

$$
\frac{E_1}{E_2} = \frac{\mathbf{B}_{1,1}}{\mathbf{B}_{2,1}}
$$

$$
\frac{E_3}{E_2} = \frac{\mathbf{B}_{3,1}}{\mathbf{B}_{2,1}}
\tag{6.20}
$$

with $\mathbf{B} = \mathbf{A}^{-1} \begin{Bmatrix} 0 \\ 1 \\ 0 \end{Bmatrix}$. The CLF are calculated as described above, with the assumption

that the shells are behaving as flat panels above their maximum ring frequency. It is noted that the analysis is conducted for a flexural/flexural wave transmission between the structures, as this produces the vast majority of the out of plane vibration of the shells. Once η_{21} and η_{23} are known, η_{12} and η_{32} can be calculated using the reciprocity relationship:

$$
\frac{\eta_{ij}}{\eta_{ji}} = \frac{n_j}{n_i}
\tag{6.21}
$$

The modal density of the cylindrical shell is calculated as described in Chapter 4. With regard to the conical shells the wavenumbers calculated by a WFEM considering their mean radius $(R_{max} + R_{min})/2$ were used to calculate their modal density given by the relation [Godzevich, 1966]:

$$
n = \frac{dN}{df} = \frac{d\dfrac{\iint dkx\ dky}{\Delta kx\ \Delta ky}}{df}
\tag{6.22}
$$

The radiation efficiency for the cylindrical shell is calculated by separating the modes into acoustically fast and acoustically slow as done in Chapter 4. For the conical shells the same approach is used, with the assumption that their radius R is equal to their mean radius.

Figure 6.36: *Energy ratio predictions E_1/E_2:experimental measurements (1/6 octave averaged) (–), WFEM/SEA approach ($\square$). Energy ratio predictions E_3/E_2: experimental measurements (1/6 octave averaged) (- -), WFEM/SEA approach (o)*

Comparison of experimental and numerical results

The experimentally measured energy ratios are post-processed as in sec.6.4.3. The predictions of the WFEM derived CLF approach are then compared to the experimental values in fig.6.36.

As expected, the experimental results present large fluctuations in the low frequency range where the coupling between the systems varies intensely with the number and type of modes. An SEA approach can therefore not accurately model the system's response under these circumstances. For higher frequencies however, regarding the upper cone's response the WFEM/SEA approach is in very good correlation with the experimental results with the discrepancies varying from 0.9 to 1.6 dB above 1500 Hz. The numerical approach seems to underestimate the energy ratio probably due to parametric uncertainties that are not taken into account and possibly due to the assumptions adopted in the calculation of the radiation efficiency and the modal density of the conical shells. With regard to the prediction of the lower cone's response, discrepancies between 3 and 5 dB are observed above 1500 Hz. The experimental response of the shell presents intense fluctuations throughout the frequency range of measurements. This fact suggests that the shell can not be considered as weakly coupled to the cylindrical structure. As aforementioned the 'weak coupling' assumption is central to the robustness of the SEA approach. A deterministic approach that takes into account for the individual modal coupling between the subsystems (such as the SEA-like method) would therefore be more suitable for modelling the response of subsystem 3.

Comparison to SEALASCAR predictions

The results obtained by the numerical WFEM/SEA approach are now compared to the predictions directly obtained by the SEALASCAR software in fig.6.37. It is noted that the software computes the CLF between thin and layered structures using analytical models.

It is evident that the energy ratios E_1/E_2 and E_3/E_2 are overestimated by SEALASCAR. Therefore, while analytical approaches are suitable for modelling the coupling of thin structures they do not succeed in accurately predicting the modal density and the CLF between layered shells.
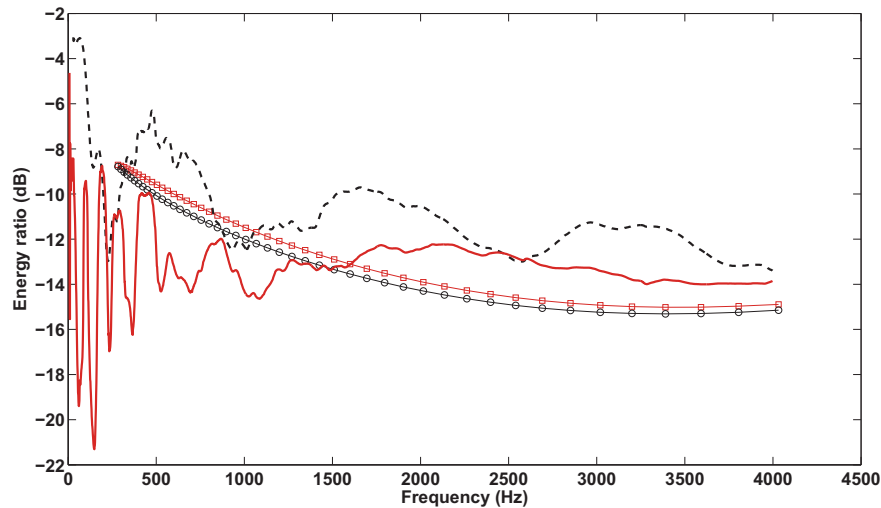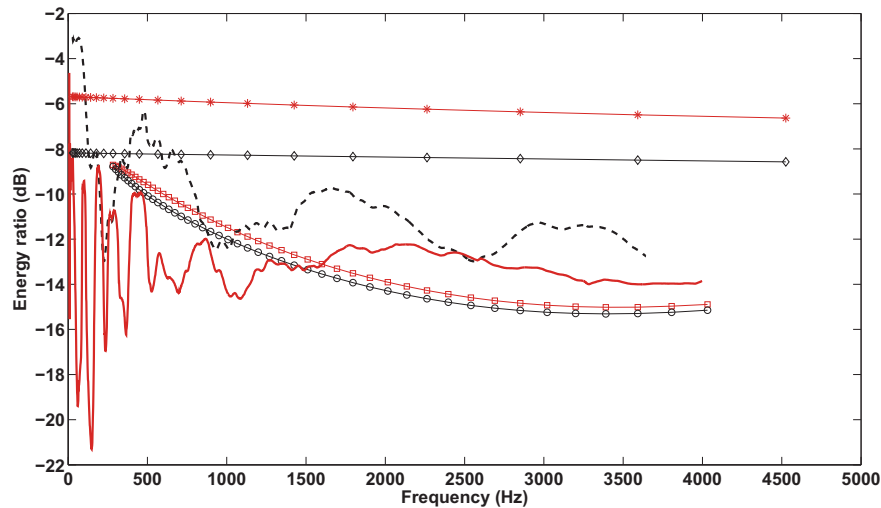
Figure 6.37: *Energy ratio predictions E_1/E_2: experimental measurements (1/6 octave averaged) (–), WFEM/SEA approach (□), SEALASCAR (*). Energy ratio predictions E_3/E_2: experimental measurements (1/6 octave averaged) (- -), WFEM/SEA approach (o), SEALASCAR (⋄)*

6.6 Conclusions

To summarize the most important points of the presented work: 1) With respect to the modal analysis of the SYLDA model the numerical results were in very good correlation with the experimental measurements for at least up to the first 15 modes of the structure. This suggests that the parametric uncertainties of a real structure do not influence dramatically its dynamic behaviour in the low frequency range. 2) The FE modelling failed to predict the first circumferential mode of the structure. 3) In the mid and the higher frequency ranges, an accurate prediction of the modal peaks of the structural response by an FE model is no longer feasible and importance is given to the correct prediction of the medium of the response. 4) A dynamic stiffness ESL approach coupled to an FE modelling was successfully used in order to predict the dynamic response of the structure. The conical shells were considered to be divided into locally cylindrical parts in order for the technique to be applied. The approach can be described as satisfactorily accurate while being particularly efficient and simple to be applied. 5) In the high frequency range the WFEM was used in order to revisit the calculation of structural CLF between the shells and the system was modelled within an SEA approach. The predictions seem to be in very good agreement with the experimental results for high frequencies. 6) The coupling between the cylindrical and the lower conical subsystems seems to remain high for a very broad frequency range. The robustness of an SEA analysis in this range is therefore questioned as the weak coupling assumption seems not satisfied. 7) The WFEM revisited prediction presented a significant improvement compared to the predictions of the SEA software nowadays used within EADS Astrium.

Chapter 7

Conclusions and perspective work

Concluding remarks on the conducted research and the industrial contribution

The main findings and contributions of the conducted work are summarized below. The benefits that these findings could have for the design of industrial products are also briefly mentioned:

- The efficient calculation of the response of composite structures of arbitrary layering and thicknesses. The approach was used to extend the application of FE modelling of layered structures to higher frequencies. By coupling WFEM and FE analyses the resulting ESL approach proves to be particularly efficient and accurate compared to 3D FE modelling and other refined ESL approaches. At the same time the FE modelling preserves the advantage of modelling structures of arbitrary geometries and damping characteristics. Simplicity is also an important benefit of the approach as no complicated numerical solutions are employed. The similar natures of the FE and the WFEM methods is also an advantage concerning the applicability of the technique in the industrial world.

- The calculation of the CLF for composite configurations. The CLF were revisited using the WFEM in order to model the vibroacoustic as well as the structural coupling of various industrial configurations. A great variety of geometries was considered, including flat, singly curved and doubly curved panels as well as cylindrical shells. Despite the fact that the CLF of an SEA analysis are generally valid in the high frequency range, the results were also in excellent agreement with experimental results of the bibliography for lower frequencies. The results of the current approach are substantially improved compared to the predictions of the SEA software currently used within EADS Astrium.

- Experimental analyses were conducted for the validation of a number of the presented approaches. Experimental results that are generally difficult to find in open bibliography were initially given in order to validate the dynamic ESL modelling approach. Furthermore an industrial composite shell structure -SYLDA- was tested in order to measure the coupling nature of connected shell components over a wide frequency range. This was the first time that such an experimental work was conducted within EADS Astrium. Compared to these results the developed approaches proved to be robust and accurate, while a number of issues were determined were further work is needed. Last but not least, experimental work was conducted on sandwich structures concerning their temperature dependent characteristics. This parametric survey unveiled the importance of considering the operating temperature

and altitude of layered structures as parameters of a vibroacoustic analysis of the industrial product.

- The use of a Krylov subspace approach for reducing a structural acoustic system in a broadband frequency range. Besides the dynamic stiffness ESL modelling another approach for reducing a composite vibroacoustic system was used; this time based on direct mathematical treatment of the system of second order differential equations. Distributed TBL and diffused field acoustic excitations were applied to the system and various techniques were discussed in order to reduce the dimensions of the reduced model. The versatility of such a reduction technique that can model systems of arbitrary geometry, configuration and damping characteristics can prove to be very interesting for the industrial world.

Perspective work

The conducted work has the potential to serve as a basis to the development and the extension of a number of emerging noise and vibration prediction techniques. It would be impossible to present an exhaustive list of such probable perspective works, however the author attempts to foresee a number of them below, hoping that they will serve as ideas in the future.

- The inclusion of all propagating and possibly evanescent WFEM wave solutions to the updated ESL approach. This is a straightforward extension that would allow for the full and accurate vibrational (in and out of plane) response prediction of structures having arbitrary geometries and fuzzy configurations. The efficiency of such an approach would be very interesting for the industrial world. The extension of the approach for conducting modal and transient analyses while retaining its efficiency would also be of great interest.

- The calculation of the radiation efficiency of composite conical shells and arbitrary composite shells of revolution. The knowledge of wave propagation and modal behaviour of composite shell structures could directly lead to the prediction of the efficiency of their coupling to the surrounding acoustic medium. If the development of a WFEM wave propagation prediction for conical structures proves impossible, the shell could be treated as locally cylindrical. This would be of great interest for the accurate prediction of the CLF in the high frequency range. The accurate prediction of the modal characteristics of such complicated structures would also allow for the accurate calculation of the EIC within an SEA-like analysis, much more robust in the mid-frequency range.

- The dynamic stiffness ESL modelling implemented within an FE approach can lead to efficient calculation of stiffened multilayered structures of various geometries and boundary conditions. Moreover, the calculation of the reflection coefficients at structural discontinuities by an FE/WFEM approach can lead to a wave description of the local modes of a stiffened structure, resulting in a complete wave based prediction of the modal global/local behaviour of the stiffened structure in a very wide frequency range. A similar approach can be used in order to reduce composite fuzzy components at their interface with the master structure resulting in more efficient computation.

- Model the parametric and non-parametric uncertainties in the wave dispersion characteristics of a structure. Parametric uncertainties would typically include statistical distributions of the mechanical and geometric characteristics of the modelled structure and some researchers have already attempted to model them in various ways. Non-parametric uncertainties such as bounding the pollution errors of the WFEM modelling are also of great importance.

- Approaches such as the ESL modelling or the calculation of the transmission and reflection coefficients at structural discontinuities can find straightforward applications at engineering fields such as the Structural Health Monitoring (SHM), control and design of smart structures. The versatility and robustness of an FE based approach coupled with the efficiency offered by the wave context quantities would be of great interest for the industrial world.

Bibliography

[Adhikari, 2000] Adhikari, S. (2000). Damping models for structural vibration. *PhD Thesis, Cambridge University.*

[Aitharaju and Averill, 1999] Aitharaju, V. R. and Averill, R. C. (1999). C^0 zig-zag finite element for analysis of laminated composite beams. *Journal of Engineering Mechanics*, 125(3):323–330.

[Akrout, 2005] Akrout, S. (2005). *Comportement dynamique déterministe et large bande des structures guidées.* PhD thesis, École Centrale de Lyon.

[Allard, 1993] Allard, J. F. (1993). Propagation of sound in porous media: Modeling sound absorbing materials.

[Anderson and Bratos-Anderson, 2005] Anderson, J. S. and Bratos-Anderson, M. (2005). Radiation efficiency of rectangular orthotropic plates. *Acta Acustica united with Acustica*, 91(1):61–76.

[Angell, 1988] Angell, C. A. (1988). Perspective on the glass transition. *Journal of Physics and Chemistry of Solids*, 49(8):863–871.

[Antoulas, 2005] Antoulas, A. C. (2005). Approximation of large-scale dynamical systems.

[Armenakas, 1970] Armenakas, A. (1970). Propagation of harmonic waves in composite circular-cylindrical rods. *Journal of the Acoustical Society of America*, 47(3):822–837.

[Babuska et al., 1997] Babuska, I., Strouboulis, T., Gangaraj, S. K., and Upadhyay, C. S. (1997). Pollution error in the h-version of the finite element method and the local quality of the recovered derivatives. *Computer Methods in Applied Mechanics and Engineering*, 140(1-2):1–37.

[Bai and Su, 2005] Bai, Z. and Su, Y. (2005). SOAR: A second-order Arnoldi method for the solution of the quadratic eigenvalue problem. *SIAM Journal on Matrix Analysis and Applications*, 26(3):640–659.

[Berthaut et al., 2005] Berthaut, J., Ichchou, M. N., and Jezequel, L. (2005). K-space identification of apparent structural behaviour. *Journal of Sound and Vibration*, 280(3-5):1125–1131.

[Bies and Hamid, 1980] Bies, D. and Hamid, S. (1980). In situ determination of loss and coupling loss factors by the power injection method. *Journal of Sound and Vibration*, 70(2):187 – 204.

[Blake, 1986] Blake, W. K. (1986). Mechanics of flow-induced sound and vibration. Volume 1: General concepts and elementary sources. *App.Math. Mech., Int.Ser.Monographs*, 17:ISBN 0–12–103501–8/–.

[Boisson et al., 1985] Boisson, C., Guyader, J., and Lesueur, C. (1985). Etude numérique de la transmission d'énergie vibratoire entre structures assemblées: cas d'assemblages en L, T et +. *Acustica*, 58:221–233.

[Boisson et al., 1982] Boisson, C., Guyader, J., Millot, P., and Lesueur, C. (1982). Energy transmission in finite coupled plates, part II: Application to an L shaped structure. *Journal of Sound and Vibration*, 81(1):93 – 105.

[Bolton et al., 1998] Bolton, J. S., Song, H. J., and Kim, Y. K. (1998). The wavenumber decomposition approach to the analysis of tire vibration. *Proceedings of the Noise-Conference '98*, 97.

[Buehrle et al., 2001] Buehrle, R. D., Robinson, J. H., and Grosveld, F. W. (2001). Vibroacoustic model validation for a curved honeycomb composite panel. In *Collection of Technical Papers - AIAA/ASME/ASCE/AHS/ASC Structures, Structural Dynamics and Materials Conference*, volume 4, pages 2988–2996.

[Caresta and Kessissoglou, 2010] Caresta, M. and Kessissoglou, N. J. (2010). Free vibrational characteristics of isotropic coupled cylindrical-conical shells. *Journal of Sound and Vibration*, 329(6):733–751.

[Carrera, 2000] Carrera, E. (2000). An assessment of mixed and classical theories on global and local response of multilayered orthotropic plates. *Composite Structures*, 50(2):183–198.

[Carrera, 2003] Carrera, E. (2003). Historical review of zig-zag theories for multilayered plates and shells. *Applied Mechanics Reviews*, 56(3):287–308.

[Chandiramini, 1978] Chandiramini, K. (1978). Some simple models describing the transition from weak to strong coupling in statistical energy analysis. *Journal of the Acoustical Society of America*, 63(4):1081–1083.

[Chase, 1980] Chase, D. M. (1980). Modeling the wavevector-frequency spectrum of turbulent boundary layer wall pressure. *Journal of Sound and Vibration*, 70(1):29–67.

[Cho and Parmerter, 1993] Cho, M. and Parmerter, R. R. (1993). Efficient higher order composite plate theory for general lamination configurations. *AIAA Journal*, 31(7):1299–1306.

[Chronopoulos et al., 2011a] Chronopoulos, D., Ichchou, M., and Troclet, B. (2011a). Caractérisation du comportement vibroacoustique des panneaux composites par la méthode des éléments finis ondulatoire. In *Proceedings of the CFM2011*, Besancon, France.

[Chronopoulos et al., 2011b] Chronopoulos, D., Ichchou, M., and Troclet, B. (2011b). On the calculation of energy properties of carbon composite curved panels by a wave finite element. In *Proceedings of the ICC3*, Arcachon, France.

[Chronopoulos et al., 2012a] Chronopoulos, D., Ichchou, M., and Troclet, B. (2012a). Efficient calculation of the acoustic radiation of a stiffened double panel in a cavity using a SOAR reduction for the mid-frequency range. In *Proceedings of the NOVEM2012*, Sorrento, Italy.

[Chronopoulos et al., 2012b] Chronopoulos, D., Ichchou, M., and Troclet, B. (2012b). Predicting the dynamic response of sandwich panels using a wave finite element method: Experimental validation. In *Proceedings of the DYNACOMP2012*, Arcachon, France.

[Chronopoulos et al., 2012c] Chronopoulos, D., Ichchou, M., and Troclet, B. (2012c). The vibroacoustic response of aerospace sandwich structures: Bridging the gap between experimental and numerical results. In *Proceedings of the ISMA2012*, Leuven, Belgium.

Bibliography

[Chronopoulos et al., 2012d] Chronopoulos, D., Ichchou, M., Troclet, B., and Bareille, O. (2012d). Efficient prediction of the response of layered shells by a dynamic stiffness approach. *Composite Structures*, http://dx.doi.org/10.1016/j.compstruct.2012.10.012.

[Chronopoulos et al., 2012e] Chronopoulos, D., Troclet, B., Bareille, O., and Ichchou, M. (2012e). Modelling the response of composite panels by a dynamic stiffness approach. *Composite Structures*, http://dx.doi.org/10.1016/j.compstruct.2012.08.047.

[Chronopoulos et al., 2012f] Chronopoulos, D., Troclet, B., Ichchou, M., and Lainé, J. P. (2012f). A unified approach for the broadband vibroacoustic response of composite shells. *Composites Part B: Engineering*, 43(4):1837–1846.

[Clarkson and Ranky, 1983] Clarkson, B. L. and Ranky, M. F. (1983). Modal density of honeycomb plates. *Journal of Sound and Vibration*, 91(1):103–118.

[Corcos, 1964] Corcos, G. (1964). The structure of the turbulent pressure field in boundary layer flows. *Journal of Fluid Mechanics*, 18(3):353–378.

[Corcos, 1963] Corcos, G. M. (1963). Resolution of pressure in turbulence. *Journal of the Acoustical Society of America*, 35(2):192–199.

[Cotoni et al., 2008] Cotoni, V., Langley, R. S., and Shorter, P. J. (2008). A statistical energy analysis subsystem formulation using finite element and periodic structure theory. *Journal of Sound and Vibration*, 318(4-5):1077–1108.

[Courant and Hilbert, 1989] Courant, R. and Hilbert, D. (1989). Methods of mathematical physics, vol. 1. *New York: John Wiley*.

[Craggs, 1971] Craggs, A. (1971). The transient response of a coupled plate-acoustic system using plate and acoustic finite elements. *Journal of Sound and Vibration*, 15(4):509–528.

[Cremer et al., 2005] Cremer, L., Heckl, M., and Petersson, B. A. T. (2005). *Structure-borne sound: Structural vibrations and sound radiation at audio frequencies*, 3:54–55.

[Crocker and Price, 1969] Crocker, M. J. and Price, A. J. (1969). Sound transmission using statistical energy analysis. *Journal of Sound and Vibration*, 9(3):469–486.

[Cunningham et al., 2003] Cunningham, P. R., Langley, R. S., and White, R. G. (2003). Dynamic response of doubly curved honeycomb sandwich panels to random acoustic excitation. Part 2: Theoretical study. *Journal of Sound and Vibration*, 264(3):605–637.

[Davis, 1999] Davis, E. B. (1999). Designing honeycomb panels for noise control. *AIAA-99-1917*.

[de Rochambeau, 2010] de Rochambeau, M. (2010). *Analyse des interactions fluide-structure en moyennes fréquences sous chargement aérodynamique*. PhD thesis, École Centrale de Lyon.

[de Rochambeau et al., 2011] de Rochambeau, M., Ichchou, M., and Troclet, B. (2011). Modeling of random aerodynamic loads applied on fluid-structure coupled systems using rain-on-the-roof equivalent excitation. *Engineering Computations (Swansea, Wales)*, 28(4):472–491.

[de Villemagne and Skelton, 1987] de Villemagne, C. and Skelton, R. E. (1987). Model reductions using a projection formulation. *International Journal of Control*, 46(6):2141–2169.

[Desmet, 1998] Desmet, W. (1998). *A wave based prediction technique for coupled vibro-acoustic analysis*. PhD thesis, KU Leuven.

Bibliography

[Desmet, 2002] Desmet, W. (2002). Mid-frequency vibro-acoustic modelling: Challenges and potential solutions. In *Proceedings of the 2002 International Conference on Noise and Vibration Engineering, ISMA*, pages 835–862.

[Desmet et al., 2000] Desmet, W., Sas, P., and Vandepitte, D. (2000). Trefftz-based prediction technique for the steady-state dynamic analysis of coupled plates. *Shock and Vibration Digest*, 32(1):46.

[Desmet et al., 2001] Desmet, W., Sas, P., and Vandepitte, D. (2001). An indirect Trefftz method for the steady-state dynamic analysis of coupled vibro-acoustic systems. *Computer Assisted Mechanics and Engineering Sciences*, 8(2-3):271–288.

[Desmet et al., 2002] Desmet, W., Van Hal, B., Sas, P., and Vandepitte, D. (2002). A computationally efficient prediction technique for the steady-state dynamic analysis of coupled vibro-acoustic systems. *Advances in Engineering Software*, 33(7-10):527–540.

[Dong and Nelson, 1972] Dong, S. B. and Nelson, R. B. (1972). On natural vibrations and waves in laminated orthotropic plates. *Journal of Applied Mechanics, Transactions ASME*, 39 Ser E(3):739–745.

[Dym and Lang, 1974] Dym, C. L. and Lang, M. A. (1974). Transmission of sound through sandwich panels. *Journal of the Acoustical Society of America*, 56(5):1523–1532.

[EADS Astrium, 2003] EADS Astrium, . (2003). Functional File for SYLDA5 EGA PA2 configuration. *Internal Document Ref: TE911 No:149804*.

[Efimtsov, 1982] Efimtsov, B. M. (1982). Characteristics of the field of turbulent wall pressure fluctuations at large Reynolds numbers. *Soviet Physics Acoustics*, 28(4):289–292.

[Efraim and Eisenberger, 2006] Efraim, E. and Eisenberger, M. (2006). Exact vibration frequencies of segmented axisymmetric shells. *Thin-Walled Structures*, 44(3):281–289.

[El Damatty et al., 2005] El Damatty, A. A., Saafan, M. S., and Sweedan, A. M. I. (2005). Dynamic characteristics of combined conical-cylindrical shells. *Thin-Walled Structures*, 43(9):1380–1397.

[Everest, 1994] Everest, F. A. (1994). The master handbook of acoustics. *McGrawHill*.

[Everstine, 1997] Everstine, G. C. (1997). Finite element formulatons of structural acoustics problems. *Computers and Structures*, 65(3):307–321.

[Ewins, 2000] Ewins, D. J. (2000). Modal Testing: Theory, Practice and Application.

[Fahy and Gardonio, 2007] Fahy, F. and Gardonio, P. (2007). Sound and structural vibration:radiation, transmission and response. *Academic Press*.

[Ferguson et al., 2002] Ferguson, N. S., Halkyard, C. R., Mace, B. R., and Heron, K. H. (2002). The estimation of wavenumbers in two-dimensional structures. In *Proceedings of the 2002 International Conference on Noise and Vibration Engineering, ISMA*, pages 799–806.

[Finnveden, 1995] Finnveden, S. (1995). Ensemble averaged vibration energy flows in a three-element structure. *Journal of Sound and Vibration*, 187(3):495 – 529.

[Finnveden, 2004] Finnveden, S. (2004). Evaluation of modal density and group velocity by a finite element method. *Journal of Sound and Vibration*, 273(1-2):51–75.

Bibliography

[Ford et al., 1967] Ford, R. D., Lord, P., and Walker, A. W. (1967). Sound transmission through sandwich constructions. *Journal of Sound and Vibration*, 5(1):9–21.

[Fredö, 1997] Fredö, C. (1997). A SEA-like approach for the derivation of energy flow coefficients with a finite element model. *Journal of Sound and Vibration*, 199(4):645–666.

[Frostig and Thomsen, 2004] Frostig, Y. and Thomsen, O. (2004). Higher-order free vibration of sandwich panels with a flexible core. *Int J Solids Struct*, 41:1697–1724.

[Fuller and Fahy, 1982] Fuller, C. R. and Fahy, F. J. (1982). Characteristics of wave propagation and energy distributions in cylindrical elastic shells filled with fluid. *Journal of Sound and Vibration*, 81(4):501–518.

[Ghinet and Atalla, 2001] Ghinet, S. and Atalla, N. (2001). Sound transmission loss of insulating complex structures. *Canadian Acoustics - Acoustique Canadienne*, 29(3):26–27.

[Ghinet and Atalla, 2006] Ghinet, S. and Atalla, N. (2006). Vibro-acoustic behaviors of flat sandwich composite panels. *Transactions of the Canadian Society for Mechanical Engineering*, 30(4):473–493.

[Ghinet and Atalla, 2011] Ghinet, S. and Atalla, N. (2011). Modeling thick composite laminate and sandwich structures with linear viscoelastic damping. *Computers and Structures*, 89(15-16).

[Ghinet et al., 2005] Ghinet, S., Atalla, N., and Osman, H. (2005). The transmission loss of curved laminates and sandwich composite panels. *Journal of the Acoustical Society of America*, 118(2):774–790.

[Ghinet et al., 2006] Ghinet, S., Atalla, N., and Osman, H. (2006). Diffuse field transmission into infinite sandwich composite and laminate composite cylinders. *Journal of Sound and Vibration*, 289(4-5):745–778.

[Godzevich, 1966] Godzevich, V. G. (1966). Free vibrations of circular conic shells. *NASA technical report*.

[Graff, 1991] Graff, K. F. (1991). Wave motion in elastic solids. *Dover Publications, Inc.*

[Grosh and Williams, 1993] Grosh, K. and Williams, E. G. (1993). Complex wave-number decomposition of structural vibrations. *Journal of the Acoustical Society of America*, 93(2):836–848.

[Guyader et al., 1982] Guyader, J., Boisson, C., and Lesueur, C. (1982). Energy transmission in finite coupled plates, part I: Theory. *Journal of Sound and Vibration*, 81(1):81–92.

[Hambric et al., 2004] Hambric, S., Hwang, Y., and Bonness, W. (2004). Vibrations of plates with clamped and free edges excited by low-speed turbulent boundary layer flow. *Journal of Fluids and Structures*, 19:93–110.

[Han et al., 2005] Han, J. S., Rudnyi, E. B., and Korvink, J. G. (2005). Efficient optimization of transient dynamic problems in MEMS devices using model order reduction. *Journal of Micromechanics and Microengineering*, 15(4):822–832.

[Hart and Shah, 1971] Hart, F. and Shah, K. (1971). Compendium of modal densities for structures. *NASA Contractor Reports*.

[Heron, 2002] Heron, K. H. (2002). Curved laminates and sandwich panels within predictive SEA. *Proceedings of the Second International AutoSEA Users Conference*.

Bibliography

[Hiverniau, 2006] Hiverniau, B. (2006). *Transmissions solidiennes : méthodologie de prévision vibroacoustique moyennes et hautes fréquences sous excitations aéroacoustiques.* PhD thesis, École Centrale de Lyon.

[Houillon, 1999] Houillon, L. (1999). Modélisation vibratoire des carrosseries automobiles en moyennes et hautes fréquences, (Vibrational modelling of automotive chassis, for medium and high frequenceis). *PhD Thesis, Ecole Centrale de Lyon.*

[Hu and Raney, 1967] Hu, W. C. L. and Raney, J. P. (1967). Experimental and analytical study of vibrations of joined shells. *Am.Inst.Aeronautics Astronautics J.*, 5:976–980.

[Ichchou et al., 2007] Ichchou, M., Akrout, S., and Mencik, J. (2007). Guided waves group and energy velocities via finite elements. *Journal of Sound and Vibration*, 305(4-5):931–944.

[Ichchou et al., 2009] Ichchou, M., Hiverniau, B., and Troclet, B. (2009). Equivalent 'rain on the roof' loads for random spatially correlated excitations in the mid-high frequency range. *Journal of Sound and Vibration*, 322(4-5):926 – 940.

[Ichchou et al., 2008a] Ichchou, M. N., Bareille, O., and Berthaut, J. (2008a). Identification of effective sandwich structural properties via an inverse wave approach. *Engineering Structures*, 30(10):2591–2604.

[Ichchou et al., 2008b] Ichchou, M. N., Berthaut, J., and Collet, M. (2008b). Multi-mode wave propagation in ribbed plates: Part I, wavenumber-space characteristics. *International Journal of Solids and Structures*, 45(5):1179–1195.

[Ichchou et al., 2008c] Ichchou, M. N., Berthaut, J., and Collet, M. (2008c). Multi-mode wave propagation in ribbed plates: Part II: Predictions and comparisons. *International Journal of Solids and Structures*, 45(5):1196–1216.

[Ichchou et al., 2011] Ichchou, M. N., Bouchoucha, F., Ben Souf, M. A., Dessombz, O., and Haddar, M. (2011). Stochastic wave finite element for random periodic media through first-order perturbation. *Computer Methods in Applied Mechanics and Engineering*, 200(41-44):2805–2813.

[Inquiété, 2008] Inquiété, G. (2008). Simulation numérique de la propagation des ondes dans les structures composites stratifiées, (Numerical simulation of wave propagation in composite layered structures). *PhD Thesis, Ecole Centrale de Lyon.*

[Irie et al., 1984] Irie, T., Yamada, G., and Muramoto, Y. (1984). Free vibration of joined conical-cylindrical shells. *Journal of Sound and Vibration*, 95(1):31–39.

[Kalnins, 1964] Kalnins, A. (1964). Free vibration of rotationally symmetric shells. *Journal of the Acoustical Society of America*, 36(7):1355–1365.

[Kang, 2012] Kang, J. (2012). Three-dimensional vibration analysis of joined thick conical - cylindrical shells of revolution with variable thickness. *Journal of Sound and Vibration*, 331(18):4187–4198.

[Kant and Swaminathan, 2001] Kant, T. and Swaminathan, K. (2001). Free vibration of isotropic, orthotropic, and multilayer plates based on higher order refined theories. *Journal of Sound and Vibration*, 241(2):319–327.

[Kapuria et al., 2004] Kapuria, S., Dumir, P. C., and Jain, N. K. (2004). Assessment of zig-zag theory for static loading, buckling, free and forced response of composite and sandwich beams. *Composite Structures*, 64(3-4):317–327.

Bibliography

[Karczub, 2006] Karczub, D. G. (2006). Expressions for direct evaluation of wave number in cylindrical shell vibration studies using the Flügge equations of motion. *Journal of the Acoustical Society of America*, 119(6):3553–3557.

[Klos et al., 2003] Klos, J., Robinson, J., and Buehrle, R. (2003). Sound transmission through a curved honeycomb composite panel. *J AIAA*, pages 2003–3157.

[Kurtze and Watters, 1959] Kurtze, G. and Watters, B. G. (1959). New wall design for high transmission loss or high damping. *J.Acoust.Soc.Am.*, 31(6):739–748.

[Lampe and Voss, 2005] Lampe, J. and Voss, H. (2005). Second-order Arnoldi: Reduction application to some engineering problems. *Proceedings of the XVI-th Summer School on Software and Algorithms of Numerical Mathematics*, pages 153–173.

[Langley, 1989] Langley, R. (1989). A general derivation of the statistical energy analysis equations for coupled dynamic systems. *Journal of Sound and Vibration*, 135(3):499–508.

[Langley, 1990] Langley, R. (1990). A derivation of the coupling loss factors used in statistical energy analysis. *Journal of Sound and Vibration*, 141(2):207–219.

[Langley, 1994a] Langley, R. S. (1994a). Elastic wave transmission coefficients and coupling loss factors for structural junctions between curved panels. *Journal of Sound and Vibration*, 169(3):297–317.

[Langley, 1994b] Langley, R. S. (1994b). The modal density and mode count of thin cylinders and curved panels. *Journal of Sound and Vibration*, 169(1):43–53.

[Langley, 1994c] Langley, R. S. (1994c). Wave motion and energy flow in cylindrical shells. *Journal of Sound and Vibration*, 169(1):29–42.

[Langley, 1997] Langley, R. S. (1997). Some perspectives on wave-mode duality in SEA. *IUTAM Symposium on Statistical Energy Analysis*, pages 1–12.

[Langley and Heron, 1990] Langley, R. S. and Heron, K. H. (1990). Elastic wave transmission through plate/beam junctions. *Journal of Sound and Vibration*, 143(2):241–253.

[Lee et al., 1990] Lee, K. H., Senthilnathan, N. R., Lim, S. P., and Chow, S. T. (1990). An improved zig-zag model for the bending of laminated composite plates. *Composite Structures*, 15(2):137–148.

[Leissa, 1969] Leissa, A. W. (1969). Vibration of plates.

[Leppington, 1988] Leppington, F. (1988). The transmission of sound through anisotropic rectangular plates. *Proc. R. Soc. Lond.*, 416:199–215.

[Leppington et al., 1982] Leppington, F. G., Broadbent, E. G., and Heron, K. H. (1982). Acoustic radiation efficiency of rectangular panels. In *Proceedings of The Royal Society of London, Series A: Mathematical and Physical Sciences*, volume 382, pages 245–271.

[Leppington et al., 2002] Leppington, F. G., Heron, K. H., and Broadbent, E. G. (2002). Resonant and non-resonant transmission of random noise through complex plates. *Proceedings of the Royal Society A: Mathematical, Physical and Engineering Sciences*, 458(2019):683–704.

[Lesueur et al., 1988] Lesueur, C., Heckl, M., and Delcambre, J. (1988). *Rayonnement acoustique des structures*. Ed. Eyrolles.

Bibliography

[Li and Liu, 1997] Li, X. and Liu, D. (1997). Generalized laminate theories based on double superposition hypothesis. *International Journal for Numerical Methods in Engineering*, 40(7):1197–1212.

[Liu and Achenbach, 1994] Liu, G. R. and Achenbach, J. D. (1994). Strip element method for stress analysis of anisotropic linearly elastic solids. *Journal of Applied Mechanics, Transactions ASME*, 61(2):270–277.

[Liu et al., 1991] Liu, G. R., Tani, J., Ohyoshi, T., and Watanabe, K. (1991). Characteristic wave surfaces in anisotropic laminated plates. *Journal of vibration, acoustics, stress, and reliability in design*, 113(3):279–285.

[Lyon and DeJong, 1995] Lyon, R. and DeJong, R. (1995). *Theory and application of Statistical Energy Analysis*. Butterworth-Heinemann.

[Lysmer, 1970] Lysmer, J. (1970). Lumped mass method for Rayleigh waves. *Bulletin of the Seismological Society of America*, 60(1):89–104.

[Mace, 2003] Mace, B. (2003). Statistical energy analysis, energy distribution models and system modes. *Journal of Sound and Vibration*, 264(2):391–409.

[Mace, 2005a] Mace, B. (2005a). Statistical energy analysis: coupling loss factor, indirect coupling and system modes. *Journal of Sound and Vibration*, 279(1-2):141–170.

[Mace and Shorter, 2000] Mace, B. and Shorter, P. (2000). Energy flow models from finite element analysis. *Journal of Sound and Vibration*, 233(3):369–389.

[Mace, 2005b] Mace, B. R. (2005b). Statistical energy analysis: Coupling loss factors, indirect coupling and system modes. *Journal of Sound and Vibration*, 279(1-2):141–170.

[Mace et al., 2005] Mace, B. R., Duhamel, D., Brennan, M. J., and Hinke, L. (2005). Finite element prediction of wave motion in structural waveguides. *Journal of the Acoustical Society of America*, 117(5):2835–2843.

[Mace and Manconi, 2008] Mace, B. R. and Manconi, E. (2008). Modelling wave propagation in two-dimensional structures using finite element analysis. *Journal of Sound and Vibration*, 318(4-5):884–902.

[Magalhaes and Ferguson, 2003] Magalhaes, M. D. C. and Ferguson, N. S. (2003). Acoustic-structural interaction analysis using the component mode synthesis method. *Applied Acoustics*, 64(11):1049–1067.

[Mahapatra and Gopalakrishnan, 2003] Mahapatra, D. R. and Gopalakrishnan, S. (2003). A spectral finite element for analysis of wave propagation in uniform composite tubes. *Journal of Sound and Vibration*, 268(3):429–463.

[Maidanik, 1961] Maidanik, G. (1961). Use of delta function for the correlations of pressure fields. *Journal of the Acoustical Society of America*, 33(11):1598–1609.

[Maidanik, 1962] Maidanik, G. (1962). Response of ribbed panels to the reverberant acoustic fields. *Journal of the Acoustical Society of America*, 34(6):809–826.

[Maluski and Gibbs, 2000] Maluski, S. P. S. and Gibbs, B. M. (2000). Application of a finite-element model to low-frequency sound insulation in dwellings. *Journal of the Acoustical Society of America*, 108(4):1741–1751.

Bibliography

[Manconi and Mace, 2007] Manconi, E. and Mace, B. R. (2007). Modelling wave propagation in two-dimensional structures using a wave/finite element technique. *ISVR Technical Memorandum*, (966).

[Manconi and Mace, 2009] Manconi, E. and Mace, B. R. (2009). Wave characterization of cylindrical and curved panels using a finite element method. *Journal of the Acoustical Society of America*, 125(1):154–163.

[Manconi and Mace, 2010] Manconi, E. and Mace, B. R. (2010). Estimation of the loss factor of viscoelastic laminated panels from finite element analysis. *Journal of Sound and Vibration*, 329(19):3928–3939.

[Markus and Mead, 1995] Markus, S. and Mead, D. J. (1995). Wave motion in a three-layered, orthotropic-isotropic-orthotropic, composite shell. *Journal of Sound and Vibration*, 181(1):149–167.

[Matsunaga, 2001] Matsunaga, H. (2001). Vibration and buckling of multilayered composite beams according to higher order deformation theories. *Journal of Sound and Vibration*, 246(1):47–62.

[McDaniel and Shepard Jr., 2000] McDaniel, J. G. and Shepard Jr., W. S. (2000). Estimation of structural wave numbers from spatially sparse response measurements. *Journal of the Acoustical Society of America*, 108(4):1674–1682.

[Mead, 1973] Mead, D. J. (1973). A general theory of harmonic wave propagation in linear periodic systems with multiple coupling. *Journal of Sound and Vibration*, 27(2):235–260.

[Mencik and Ichchou, 2005] Mencik, J. . and Ichchou, M. N. (2005). Multi-mode propagation and diffusion in structures through finite elements. *European Journal of Mechanics, A/Solids*, 24(5):877–898.

[Meunier and Shenoi, 2001] Meunier, M. and Shenoi, R. (2001). Dynamic analysis of composite sandwich plates with damping modeled using high-order shear deformation theory. *Journal of Composite Structures*, 54:243–254.

[Miller and Faulkner, 1981] Miller, V. R. and Faulkner, L. L. (1981). Prediction of aircraft interior noise using the statistical energy analysis method. *Proceedings of Design Engineering Technical Conference*, pages 235–244.

[Mindlin, 1951] Mindlin, R. D. (1951). Influence of rotatory inertia and shear on flexural vibrations of isotropic, elastic plates. *Journal of Applied Mechanics*, 18.

[Mindlin and Medick, 1959] Mindlin, R. D. and Medick, M. A. (1959). Extensional vibrations of elastic plates. *J.Appl.Mech.*, 26:561–569.

[Moore and Lyon, 1991] Moore, J. A. and Lyon, R. H. (1991). Sound transmission loss characteristics of sandwich panel constructions. *Journal of the Acoustical Society of America*, 89(2):777–791.

[Muller and Touratier, 1995] Muller and Touratier, M. (1995). On the so-called variational consistency of plate models, I. Indefinite plates: Evaluation of dispersive behavior. *J.Sound Vibration*, 188(4):517–527.

[Narayanan and Shanbhag, 1982] Narayanan, S. and Shanbhag, R. L. (1982). Sound transmission through a damped sandwich panel. *Journal of Sound and Vibration*, 80(3):315–327.

Bibliography

[Nayfeh, 1995] Nayfeh, A. H. (1995). Wave propagation in layered anisotropic media with applications to composites. *Applied Mathematics and Mechanics*, 39.

[Pan and Bies, 1990] Pan, J. and Bies, D. A. (1990). The effect of fluid-structural coupling on sound waves in an enclosure - Theoretical part. *Journal of the Acoustical Society of America*, 87(2):691–707.

[Patel et al., 2000] Patel, B. P., Ganapathi, M., and Kamat, S. (2000). Free vibration characteristics of laminated composite joined conical-cylindrical shells. *Journal of Sound and Vibration*, 237(5):920–930.

[Peretti and Dowell, 1992] Peretti, L. and Dowell, E. (1992). Asymptotic modal analysis of a rectangular acoustic cavity excited by wall vibration. *AIAA Journal*, 30(5):1191–1198.

[Petyt, 1990] Petyt, M. (1990). Introduction to finite element vibration analysis.

[Prel, 1999] Prel, Y. (1999). Composite materials on Ariane 5 launcher. *SAMPE Journal*, 35(5):13–17.

[Prosser and Gorman, 1994] Prosser, W. H. and Gorman, M. R. (1994). Plate mode velocities in graphite/epoxy plates. *Journal of the Acoustical Society of America*, 96(2):902–907.

[Qatu, 2004] Qatu, M. S. (2004). Vibration of laminated shells and plates.

[Ramachandran and Narayanan, 2007] Ramachandran, P. and Narayanan, S. (2007). Evaluation of modal density, radiation efficiency and acoustic response of longitudinally stiffened cylindrical shell. *Journal of Sound and Vibration*, 304(1-2):154–174.

[Reddy, 1997] Reddy, J. (1997). Mechanics of laminated composite plates: theory and analysis.

[Reddy, 1984] Reddy, J. N. (1984). A simple higher order theories for laminated composites plates. *ASME J.Appl.Mech.*, 51:742–745.

[Reddy, 2004] Reddy, J. N. (2004). Mechanics of laminated composite plates and shells: Theory and Analysis.

[Remillat, 1997] Remillat, C. (1997). Modélisation, identification des propriétés de coeur et optimisation de structures sandwiches á ame viscoélastique, (modeling, identification of core properties and optimization of viscoelastic core sandwich structures). *PhD Thesis, Ecole Centrale de Lyon*.

[Renji et al., 1997] Renji, K., Nair, P. S., and Narayanan, S. (1997). Critical and coincidence frequencies of flat panels. *Journal of Sound and Vibration*, 205(1):19–32.

[Renno and Mace, 2012] Renno, J. and Mace, B. (2012). Calculation of reflection and transmission coefficients of joints using a hybrid finite element/wave and finite element approach. *Journal of Sound and Vibration*. Article in Press.

[Rochambeau et al., 2008] Rochambeau, M. D., Ichchou, M., Jezequel, L., and Troclet, B. (2008). Fluid-structure interaction in the mid-frequency domain. *Mecanique et Industries*, 9(6):551–557.

[Rose et al., 1973] Rose, J. L., Mortimer, R. W., and Blum, A. (1973). Elastic-wave propagation in a joined cylindrical-conical-cylindrical shell. *Experimental Mechanics*, 13(4):150–156.

[Salimbahrami and Lohmann, 2006] Salimbahrami, B. and Lohmann, B. (2006). Order reduction of large scale second-order systems using Krylov subspace methods. *Linear Algebra and Its Applications*, 415(2-3):385–405.

Bibliography

[Schwab, 1998] Schwab, C. (1998). p- and hp- finite element methods.

[Shah and Datta, 1982] Shah, A. H. and Datta, S. K. (1982). Harmonic waves in a periodically laminated medium. *International Journal of Solids and Structures*, 18(5):397–410.

[Shorter and Mace, 1998] Shorter, P. and Mace, B. (1998). Stochastic energy flow models. In *proceedings Internoise98*, Christchurch, New Zealand.

[Soedel, 1993] Soedel, W. (1993). Vibrations of shells and plates.

[Soize, 1987] Soize, C. (1987). Analyse energétique statistique (SEA). *Etude Bibliographique 1975-1986, Tomes I and II.*

[Sokolinsky and Nutt, 2004] Sokolinsky, V. and Nutt, S. (2004). Consistent higher-order dynamic equations for soft-core sandwich beams. *AIAA J*, 42(2):374–382.

[Srinivasan Puri et al., 2009] Srinivasan Puri, R., Morrey, D., Bell, A. J., Durodola, J. F., Rudnyi, E. B., and Korvink, J. G. (2009). Reduced order fully coupled structural-acoustic analysis via implicit moment matching. *Applied Mathematical Modelling*, 33(11):4097–4119.

[Stavsky, 1961] Stavsky, Y. (1961). Bending and stretching of laminated aelotropic plates. *Proc.Am.Soc.Civil Engrs.*, 87(EM6):31–56.

[Su and Craig Jr., 1991] Su, T.-J. and Craig Jr., R. R. (1991). Model reduction and control of flexible structures using Krylov vectors. *Journal of Guidance, Control, and Dynamics*, 14(2):260–267.

[Sulmoni et al., 2008] Sulmoni, M., Gmür, T., Cugnoni, J., and Matter, M. (2008). Modal validation of sandwich shell finite elements based on a p-order shear deformation theory including zig-zag terms. *International Journal for Numerical Methods in Engineering*, 75(11):1301–1319.

[Sun and Liao, 1990] Sun, C. T. and Liao, W. C. (1990). Analysis of thick section composite laminates using effective moduli. *J.Compos.Mater.*, 24:977–993. Cited By (since 1996): 14.

[Sun et al., 1996] Sun, C. T., Luo, J., and McCoy, R. W. (1996). Analysis of wave propagation in thick-section composite laminates using effective moduli. *Composites Part B: Engineering*, 27(6 SPEC. ISS.):613–621.

[Szechenyi, 1971a] Szechenyi, E. (1971a). Modal densities and radiation efficiencies of unstiffened cylinders using statistical methods. *Journal of Sound and Vibration*, 19(1):65–81.

[Szechenyi, 1971b] Szechenyi, E. (1971b). Sound transmission through cylinder walls using statistical considerations. *Journal of Sound and Vibration*, 19(1):83–94.

[Tisseur and Meerbergen, 2001] Tisseur, F. and Meerbergen, K. (2001). The quadratic eigenvalue problem. *SIAM Review*, 43(2):235–286.

[Torvik, 2011] Torvik, P. J. (2011). On estimating system damping from frequency response bandwidths. *Journal of Sound and Vibration*, 330(25):6088–6097.

[Troclet, 2006a] Troclet, B. (2006a). Logiciel SEALASCAR - Prévision de la réponse vibroacoustique haute fréquence des structures au bruit aérodynamique et au bruit rasant - Manuel théorique. Note EADS ST TE35 145225.

[Troclet, 2006b] Troclet, B. (2006b). Manuel Théorique du logiciel SEALASCAR. *EADS Astrium.*

Bibliography

[Troclet, 2007] Troclet, B. (2007). Analyse énergétique des vibrations sous sollicitations aéroacoustiques et validation dans l'industrie spatiale. *Mémoire d'Habilitation à Diriger des Recherches.*

[Troclet et al., 1999] Troclet, B., Hiverniau, B., Ichchou, M. N., and Jezequel, L. (1999). Analyse vibroacoustique des lanceurs, (Vibroacoustic analysis of launch vehicles). *Giens 2007. Volume X - n° x/2007.*

[Troclet et al., 2009] Troclet, B., Hiverniau, B., Ichchou, M. N., Jezequel, L., Kayvantash, K., and Bekkour, T. (2009). FEM / SEA hybrid method for predicting mid and high frequency structure-borne transmission. *The Open Acoustics Journal,*, 2:45–60.

[Tyutekin, 2004] Tyutekin, V. V. (2004). Helical waves of an elastic cylindrical shell. *Acoustical Physics*, 50(3).

[Van Genechten et al., 2011] Van Genechten, B., Vandepitte, D., and Desmet, W. (2011). A direct hybrid finite element - wave based modelling technique for efficient coupled vibro-acoustic analysis. *Computer Methods in Applied Mechanics and Engineering*, 200(5-8):742–764.

[Vinson and Sierakowski, 2002] Vinson, J. R. and Sierakowski, R. L. (2002). Vibration of composite beams. The behaviour of structures composed of composite materials. *Kluwer Academic Publishers.*

[Waki et al., 2009] Waki, Y., Mace, B. R., and Brennan, M. J. (2009). Numerical issues concerning the wave and finite element method for free and forced vibrations of waveguides. *Journal of Sound and Vibration*, 327(1-2):92–108.

[Wallace, 1972] Wallace, C. E. (1972). Radiation resistance of a rectangular panel. *Journal of the Acoustical Society of America*, 51(3 Part 2):946–952.

[Wang et al., 2010] Wang, T., Li, S., Rajaram, S., and Nutt, S. R. (2010). Predicting the sound transmission loss of sandwich panels by statistical energy analysis approach. *Journal of Vibration and Acoustics, Transactions of the ASME*, 132(1):0110041–0110047.

[Wang et al., 2008] Wang, T., Sokolinsky, V., Rajaram, S., and Nutt, S. R. (2008). Consistent higher-order free vibration analysis of composite sandwich plates. *Composite Structures*, 82(4):609–621.

[Wang et al., 2005] Wang, T., Sokolinsky, V. S., Rajaram, S., and Nutt, S. R. (2005). Assessment of sandwich models for the prediction of sound transmission loss in unidirectional sandwich panels. *Applied Acoustics*, 66(3):245–262.

[Wester and Mace, 1996] Wester, E. and Mace, B. (1996). Statistical energy analysis of two edge-coupled rectangular plates : ensemble averages. *Journal of Sound and Vibration*, 193(4):793–822.

[Whitney and Pagano, 1970] Whitney, J. and Pagano, N. (1970). Shear deformation in heterogeneous anisotropic plates. *A Appl Mech Trans ASME*, 37 Ser E(4):1031–1036.

[Wilkinson, 1968] Wilkinson, J. P. D. (1968). Modal densities of certain shallow structural elements. *Journal of the Acoustical Society of America*, 43(2):245–251.

[Willcox et al., 2001] Willcox, K., Peraire, J., and White, J. (2001). An Arnoldi approach for generation of reduced-order models for turbomachinery. *Computers and Fluids*, 31(3):369–389.

[Xi et al., 2000] Xi, Z. C., Liu, G. R., Lam, K. Y., and Shang, H. M. (2000). Dispersion and characteristic surfaces of waves in laminated composite circular cylindrical shells. *Journal of the Acoustical Society of America*, 108(5 I):2179–2186.

Bibliography

[Xie et al., 2004] Xie, G., Thompson, D. J., and Jones, C. J. C. (2004). Mode count and modal density of structural systems: Relationships with boundary conditions. *Journal of Sound and Vibration*, 274(3-5):621–651.

[Yuan and Hsieh, 1998] Yuan, F. G. and Hsieh, C. C. (1998). Three-dimensional wave propagation in composite cylindrical shells. *Composite Structures*, 42(2):153–167.

[Yue and Meerbergen, 2010] Yue, Y. and Meerbergen, K. (2010). Using model order reduction for design optimization of structures and vibrations. *TW Reports TW566, Department of Computer Science*.

[Zhen and Wanji, 2008] Zhen, W. and Wanji, C. (2008). An assessment of several displacement-based theories for the vibration and stability analysis of laminated composite and sandwich beams. *Composite Structures*, 84(4):337–349.

[Zhong and Williams, 1995] Zhong, W. X. and Williams, F. W. (1995). On the direct solution of wave propagation for repetitive structures. *Journal of Sound and Vibration*, 181(3):485–501.

[Zhou and Crocker, 2010] Zhou, R. and Crocker, M. J. (2010). Sound transmission loss of foam-filled honeycomb sandwich panels using statistical energy analysis and theoretical and measured dynamic properties. *Journal of Sound and Vibration*, 329(6):673–686.

[Zhou and Ichchou, 2010] Zhou, W. J. and Ichchou, M. N. (2010). Wave propagation in mechanical waveguide with curved members using wave finite element solution. *Computer Methods in Applied Mechanics and Engineering*, 199(33-36):2099–2109.

AUTORISATION DE SOUTENANCE

Vu les dispositions de l'arrêté du 7 août 2006,

Vu la demande du Directeur de Thèse

Monsieur M. ICHCHOU

et les rapports de

Monsieur D. DUHAMEL
Professeur - Ecole Nationale des Ponts et Chaussées -Laboratoire NAVIER - 6/8 avenue Blaise Pascal
Champs-sur-Marne - 77455 MARNE LA VALLEE cedex 2

Et de

Monsieur F. GAUTIER
Professeur - Université du Maine - Laboratoire d'Acoustique (UMR CNRS 6613)
Ecole Nationale Supérieure d'Ingénieurs du Mans - Rue Aristote - 72085 LE MANS cedex 9

Monsieur CHRONOPOULOS Dimitrios

est autorisé à soutenir une thèse pour l'obtention du grade de **DOCTEUR**

Ecole doctorale MECANIQUE, ENERGETIQUE, GENIE CIVIL ET ACOUSTIQUE

Fait à Ecully, le 22 novembre 2012

P/Le directeur de l'E.C.L.
La directrice des Etudes

M-A. GALLAND